Werner clathrates: structure and selectivity

MERRILL WICHT

Thesis presented for the degree of

DOCTOR OF PHILOSOPHY

In the Department of Chemistry

University of Cape Town

November 2016

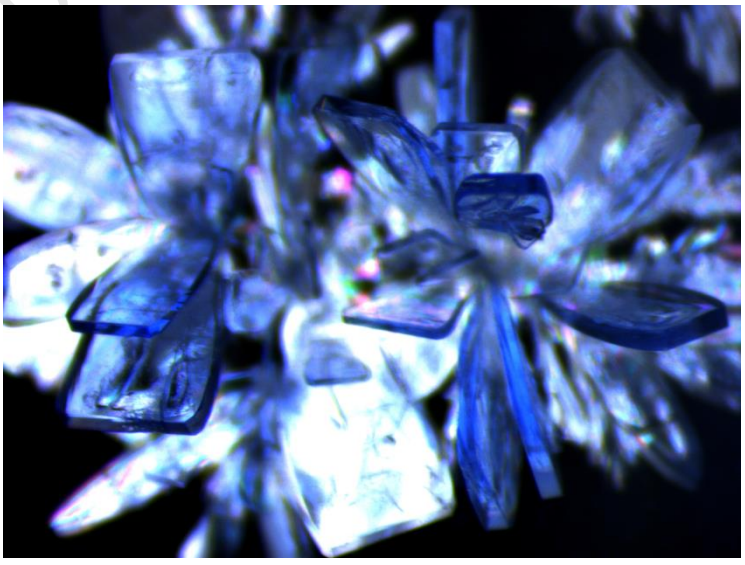

In a goal-less caucus race,

Atoms rush through empty space

Or a lunatic dervish dance

From whose whirling, by mere chance

Order somehow comes to birth-

Sky and stars, and this green earth.

Living forms of every kind,

Till at length emergent mind

Gleams for a little while, and then

Things collapse to chaos again.

Old Democritus, how he laughed –

Scheme that's both sublime and daft.

from Laughing Philosopher / Weeping Philosopher

By John Heath-Stubbs

Acknowledgements

- My Supervisors, Professor Luigi R. Nassimbeni, for his expert supervision and encouragement; and Dr Nikoletta B. Báthori, for her excellent promotion of ideas and her patience during the course of my doctoral studies.

- Dr Hong Su for her assistance on single crystal X-ray diffraction data collection.

- David Kok and Peter Roberts for technical assistance in their laboratories.

- Members of the Supramolecular Chemistry research group and Dr Clive L. Oliver for their welcome support and friendship.

- The National Research Foundation (NRF) and Cape Peninsula University of Technology for financial support

- To my family for their interest and encouragement and friends for keeping me on the straight and narrow path.

- Lastly, to my husband, Kevin, for your support every step of the way. I dedicate this thesis to you. Thank you.

Publications and Conferences

Parts of this thesis have been published:

1. Merrill M. Wicht, Nikoletta B. Báthori and Luigi R. Nassimbeni, Isoquinoline-based Werner clathrates with xylene isomers: Aromatic interactions vs. molecular flexibility, *Dalton Trans.*, **2015**, 44, 6863 – 6870. DOI: 10.1039/c5dt00084j

2. Merrill M. Wicht, Hong Su, Nikoletta B. Báthori and Luigi R. Nassimbeni, Werner clathrate formation with polyaromatic hydrocarbons: comparison of different crystallisation methods, *CrystEngComm*, **2016**, 18, 2509 – 2519. DOI: 10.1039/c5ce02185e

3. Merrill M. Wicht, Nikoletta B. Báthori and Luigi R. Nassimbeni, Enhanced selectivity towards xylene isomers of mixed ligand Ni(II) thiocyanato complex, *Polyhedron*, **2016**, 119, 127-133. DOI:10.1016/j.poly.2016.08.022

Parts of this thesis have been presented at the following conferences:

4. U6 Consortium 2nd International Conference, Cape Town, South Africa, 2 – 10 September 2014.
   Title: Selectivity of a Werner complex towards aromatic guest isomers (Oral presentation).

5. Pan African and South African Meeting of the International Year of Crystallography - IYCr2014 Africa, Bloemfontein, South Africa, 15 – 17 October 2015.
   Title: Selectivity of a Werner complex towards aromatic guest isomers (Poster presentation).

6. The 29th European Crystallographic Meeting (ECM29), Rovinj, Croatia, 23 – 27 August 2015.
   Title: Isoquinoline-based Werner clathrates with xylene isomers: Aromatic interactions vs. molecular flexibility (Poster presentation).

7. 15th International Seminar on Inclusion Compounds, Warsaw, Poland, 16 – 20 August 2015.
   Title: Isoquinoline-based Werner clathrates with xylene isomers: Aromatic interactions vs. molecular flexibility (Poster presentation).

Abstract

The development of enhanced selectivity of a host towards (aromatic) isomers continues to be an important feature in supramolecular studies. In this thesis, several nickel Werner complexes have been synthesised and used as crystallographic hosts with inclusions of aromatic isomers, polycyclic aromatic hydrocarbons, alcohols or ketones. Thermogravimetric methods were used to confirm the composition of the host-guest complexes and were employed to analyse their thermal behaviour. Structural features of the inclusion compounds were investigated using single crystal X-ray analysis and X-ray powder diffraction. Selectivity of the host towards binary or tertiary mixtures of guests has been scrutinised and the response determined by gas chromatography and nuclear magnetic resonance spectroscopy.

The characteristics of the pyridine derivative ligands co-ordinated to the metal ion in the Werner complexes are instrumental in the behaviour of the inclusion compound. When the host $Ni(NCS)_2(isoquinoline)_4$ (**H1**) was exposed to xylene isomers the selectivity of the rigid isoquinoline ligand was investigated and compared to the more pliable 4-phenylpyridine. The flexibility of torsion angles in a range of pyridine derivative ligands was investigated to substantiate the findings for lack of selectivity with **H1**. Selectivity of **H1** for the xylene isomers was determined for both the liquid and vapour phase binary mixtures of the guests using headspace gas chromatography for analysis. This was pursued with a mixed-ligand complex of both isoquinoline and 4-phenylpyridine to form the host $Ni(NCS)_2(isoquinoline)_2(4\text{-phenylpyridine})_2$, **H4**. The crystal structures of this host with the three xylene isomers, ortho, meta and para-xylene (**ox**, **mx** and **px**, respectively) were analysed and the packing scrutinised. The arrangement of the ligands gave the new host flexibility to pack **mx** more intimately than the other two isomers hence the preferred selectivity outcome , i.e. **mx**>**ox**>**px** of this study.

The single crystal structures of the Werner host, bis-isothiocyanato tetrakis-vinylpyridine nickel (II), **H3**, with seven polyaromatic hydrocarbons (PAHs), indene (**IND**), naphthalane (**NAP**), azulene

(**AZU**), fluorene (**FLU**), anthracene (**ANT**), phenanthrene (**PHE**) and pyrene (**PYR**) were interpreted. Structural analysis revealed two types of crystal arrangements. The enhancement of green chemistry in the form of grinding, which avoids the use of solvents, slurrying and melt procedures was investigated. The success of inclusion compound formation by grinding was dependent on diffusion and the rate constant and half-life of the enclathration reaction were determined for the reactions between the host with two of the guests. The outcome of the crystallisation reaction and the grinding with this selected Werner host was the same; hence the preparation of these compounds via a more environmentally friendly solvent free or low solvent method has high potential.

Werner hosts were designed and synthesized with so called 'sticky ligands', *viz.* coordinated aromatic groups with hydrogen bonding functionalities, with the aim to explore their inclusion formation properties. The synthesis of $Ni(NCS)_2(nicotinamide)_4$, **H5**, $Ni(NCS)_2(isonicotinamide)_4$, **H6**, and $Ni(NCS)_2(nicotinamide)_2(isonicotinamide)_2$, **H7**, whose functional groups form amide synthons, generated specific packing patterns which were examined in this thesis. Guests such as amides, alcohols and ketones were located in positions, either in voids or in layers, between the host sheets. Three dimensional packing arrangements were observed and are discussed in the **H6** and **H7** structures.

The thesis is aimed to present and discuss the selected Werner complexes and their inclusion formation properties. The obtained supramolecular systems have shown a great variety of structural features which can be altered on a systematic manner.

Abbreviations and compound codes

TGA	Thermogravimetric analysis
PXRD	Powder X-ray diffraction
GC	Gas chromatography
^{1}H NMR	Proton nuclear magnetic resonance
PAH	Polyaromatic hydrocarbon
H1	$Ni(NCS)_2(isoquinoline)_4$
H2	$Ni(NCS)_2(4\text{-}phenylpyridine)_4$
H3	$Ni(NCS)_2(4\text{-}vinylpyridine)_4$
H4	$Ni(NCS)_2(isoquinoline)_2(4\text{-}phenylpyridine)_2$
H5	$Ni(NCS)_2(nicotinamide)_4$
H6	$Ni(NCS)_2(isonicotinamide)_4$
H7	$Ni(NCS)_2(nicotinamide)_2(isonicotinamide)_2$

Colour Scheme

The following colour scheme was used for the representation of atoms in the molecular diagrams

HYDROGEN

SULPHUR

OXYGEN

NITROGEN

CARBON

NICKEL

Table of Contents

Chapter 1

Introduction

Short histories of Crystal Engineering and Alfred Werner's insights into coordination chemistry are presented in this chapter. Metal-organic hosts enclathrating aromatic guests illustrate a range of different non-covalent interactions. Mixed ligand formations and the use of attractive ligands in these host compounds gave variety in the types of selectivity and packing architecture. Green chemistry methods of crystal formation are described and evaluated.

Crystal Engineering

The earliest correlation between crystal and molecular properties were first addressed by W.H. Bragg in 1921.[1] The principle of close-packing and the consideration of size and shape were stated by Kitaigorodskii in his thoughts about the molecule to crystal formation and the design thereof.[2] The design of both pure organic and metal-organic crystalline solids belongs to the subject of crystal engineering which has been defined by Desiraju in the following words: "Crystal engineering is the understanding of intermolecular interactions in the context of crystal packing and the utilisation of such understanding in the design of new solids with desired physical and chemical properties."[3] The question often asked is how molecules recognise one another from the early stages of connection toward nucleation and final crystallisation. Aliphatic or aromatic hydrocarbon portions of a molecule are effective supramolecular functional groups and intermolecular interactions result in molecular recognition which leads to the design of a crystal. Crystallisation is a purification technique or segregation mechanism which allows particles to come together in an ordered three-dimensional array.[4] Crystal properties are usually anisotropic. They grow and dissolve in different directions and at different rates. Properties such as refractive indices, electrical conductivity and thermal expansion coefficients, may vary with direction. Regular packing of constituent atoms, ions or molecules forms a crystalline three-dimensional array. A space group represents the group of the symmetry elements, which are applied to the asymmetric unit (ASU) to generate the whole crystal. Organic, inorganic and organometallic chemistries are drawn together in the context of crystal engineering through the visualisation of crystal structures as networks.

Inclusion Chemistry

Inclusion compounds were discovered in 1811 by Humphrey Davy when he was working with chlorine clathrate hydrate, a compound formed between Cl_2 gas and water-ice.[5] In 1823, Michael Faraday investigated this species, but it was only shown by von Stackelberg[6] in 1949 to be a cage inclusion compound with water as the host. The introduction of X-ray crystal structure analysis by

von Laue in 1912 developed a tempestuous phase in the evolution of 'inclusion chemistry'.[7] Emil Fischer described enzyme-substrate action as the lock-and-key principle in 1894[8] and more than 100 years later this metaphor has become more refined and developed with modern technology. Supramolecular chemistry, defined by Jean-Marie Lehn,[9] as the 'chemistry of molecular assemblies and of the intermolecular bond' is also expressed as 'chemistry beyond the molecule'. Originally it was defined in terms of non-covalent interactions between a 'host' and a 'guest'. It is also based on the theme of mutual recognition of molecules. The recognition process is characterised through a complex combination of geometrical and chemical factors. The interacting molecules recognise one another effectively and efficiently through their dissimilarities.[3] A "supermolecule", also known as a "supramolecular assembly" is a well-defined complex of molecules held together by non-covalent interactions. Lehn prepared cryptands in the late 1960s and shaped many developments in the field of supramolecular chemistry. In his Nobel lecture of 1987 he refers to the partners in the supramolecular species as the *molecular receptor* and the *substrate* which is the smaller compound and seeks to be bound.[10]

In 1952 Cramer[11] described an 'inclusion compound' as one which has the ability to incorporate suitably sized molecules into cavities between their molecules by physical imprisonment. He recognised that the cavity-containing structure need not be stable, but would form only on the incorporation of the guest substance/s. For this to occur, the space must be sufficient for this enclosure to happen. Many naturally occurring inorganic compounds possess cavities in their crystal structures, hence may have importance industrially. Examples of these inclusions are known for zeolites, uranium mica, graphite and alumino-silicate clay minerals.

Coordination Chemistry

The fundamentals of supramolecular chemistry date back to the late 19th century when in 1893 Alfred Werner[12] developed the idea of coordination chemistry.[13] In 1913, Werner received the Nobel Prize in

Chemistry for his theory on coordination chemistry. One of his colleagues commented that his coordination theory was "an ingenious impudence" and it has been said that the inspiration came to him in a flash of genius.[14] Although an organic chemist, Werner's research interests turned towards coordination compounds in which ammonia or organic amines were bound to metal centres. The fundamental step towards his coordination theory was his identification of two types of "valence", the primary or ionisable valence (*Hauptvalenz*) and the secondary or non-ionisable valence (*Nebenvalenz*). Conceptually a fixed coordination number for a specific element is observed in a distinct oxidation state.[15,16] Supramolecular complexes of metal cations constitute the coordination of relatively labile metal ions and commensurate chelating ligands. Ligands are generally ions or molecules which are Lewis bases or electron donors, often lone pair donors.[17] Bonding in coordination complexes ranges from ionic ion-dipole to entirely covalent. The metal's charge and size and the properties of the ligand determine the degree of covalence. The coordination number and geometry of the complex is dependent on the size and shape of the ligands. Transition metals with unfilled sub-shells tend to form covalent complexes with well-defined coordination geometries.

Supramolecular chemistry involves non-covalent binding: a molecule or 'host' binds another smaller molecule or 'guest' to produce a 'host-guest' complex. A molecular complex is based on the host-guest relationship, which involves a complementary arrangement of the binding sites in the host and guest. The host component is defined as an organic molecule or ion whose binding sites converge in the complex such as Lewis basic donor atoms or hydrogen bond donors. The guest component is any molecule or ion whose binding sites, such as hydrogen bond acceptor anions, diverge in the complex. Hosts require design and synthesis whereas guests are relatively abundant.

Clathrate chemistry

The term 'clathrate' was one of the first descriptions of a supramolecular cage-like host-guest structure. In 1948 H.M. Powell[18] defined this as a kind of inclusion compound in which two or more

components enclose a set of molecules in a suitable structure. A feature of clathrates is a thermodynamically unstable host lattice[19] which is stabilised by the inclusion of a second component bound by forces similar to intermolecular forces in liquids. A clathrate compound is regarded as a "solid solution of the second component in the (meta-stable) host lattice". Molecules which fit into the host lattice are able to stabilise its structure, although a smaller amount of the guest may be sufficient to produce a thermodynamically stable crystal. Gas hydrates crystallise in structures with gas molecules occupying the cavities formed by the water molecules linked together by hydrogen bonds.[20] This leads to the nonstoichiometric composition of gas hydrates.

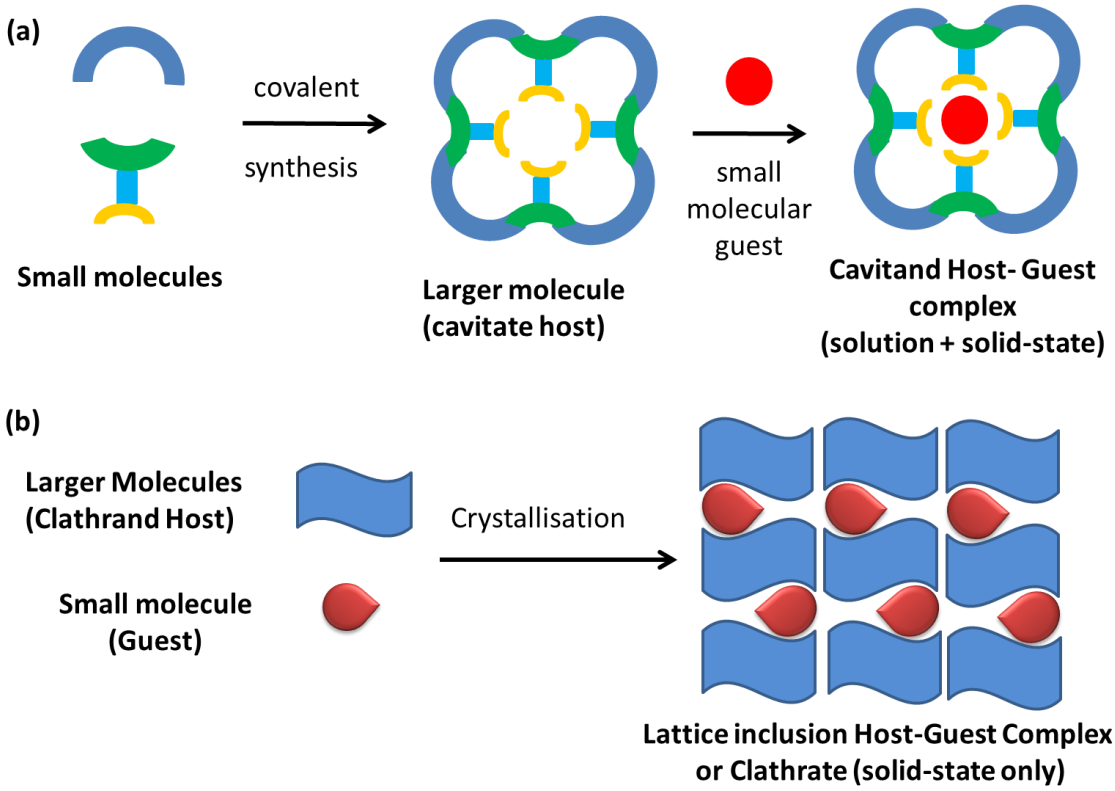

Figure 1.1 (a) Synthesis and conversion of a cavitand into a cavitate by inclusion of a guest into the cavity of the host molecule; (b) Inclusion of guest molecules in cavities formed between the host molecules in the lattice resulting in conversion from a clathrand into a clathrate.

Clathrates are relatively easily prepared and are important for technical processes. Application of inclusion compounds includes the separation of isomer mixtures and racemates, 'solidification' of gases or liquids, stabilization of sensitive or toxic substances, polymerisation inside inclusion

channels (topochemistry) and battery systems and organic conductors.[7] Host compounds are divided into two major classes, *cavitands* and *clathrands*.[21] The former refers to a host possessing permanent intramolecular cavities which are available in both the solution and solid states; and the latter hosts have extrinsic cavities (gap between two or more host molecules) relevant only in the crystalline state. A cavitand forms a *cavitate* host-guest aggregate as shown in Figure 1.1(a) and a clathrand forms a *clathrate* shown in Figure 1.1(b).

The process of inclusion compound synthesis may be described in general as

$$H_{(s,\alpha)} + nG_{(l)/(g)} \rightarrow H{\bullet}G_{n(s,\beta)}$$

where α depicts the non-porous phase of the pure host H or the apohost and the phase of the host-guest compound with guest:host ratio *n* is described by *β*.[22] Figure 1.2 illustrates the general scheme for the formation and decomposition of an inclusion compound. After dissolving the apohost in the liquid guest (step *a*), the solution is allowed to concentrate until the host-guest complex is formed as the *β*-phase crystals (step *b*). Decomposition of the *β*-phase on heating may occur in different ways. Step *c* shows the reversion to the original *α*-phase:

$$H{\bullet}G_{n(s,\beta)} \rightarrow H_{(s,\alpha)} + nG_{(g)} \uparrow$$

Partial decomposition (step *d*) may take place with the introduction of a new *γ*-phase:

$$H{\bullet}G_{n(s,\beta)} \rightarrow H{\bullet}_{G(n-m)(s,\gamma)} + mG_{(g)}$$

In step *e*, in which the compound maintains its structure, while the guest is lost, the "empty" clathrate or β_0 phase is formed. This rare phenomenon, which is similar to that observed for zeolites, has occurred in the gossypol-dichloromethane clathrate[23] and other molecular compounds, for example, the calixarene compound, 1,2-dimethoxy-*p*-tert-butylcalix(4)dihydroquinone.[24]

The topology of the *β*-phase inclusion compounds is likely to change based on the crystallisation temperature, and these are shown in Figure 1.3. In *cryptates* or *clathrates* the guest is completely surrounded or 'entombed' as in a crypt. The name originates from the Greek *kryptos* meaning 'hidden'. In some compounds, the guest is found in one dimensional channels or tubes in the host structure and the system is termed *tubulate*. In the layer or *intercalate* type the guest is sandwiched by the host in layers as is found in graphite which has a slippery feel because oxygen is intercalated between layers of carbon. Intercalation of the guests is reversible hence layered solids will more likely retain their host structure throughout intercalation and de-intercalation steps. Note that the host to guest ratios differ between cryptates, tubulates and intercalates, with cryptates having a low guest:host ratio whereas the intercalate ratio is much higher.[25,26]

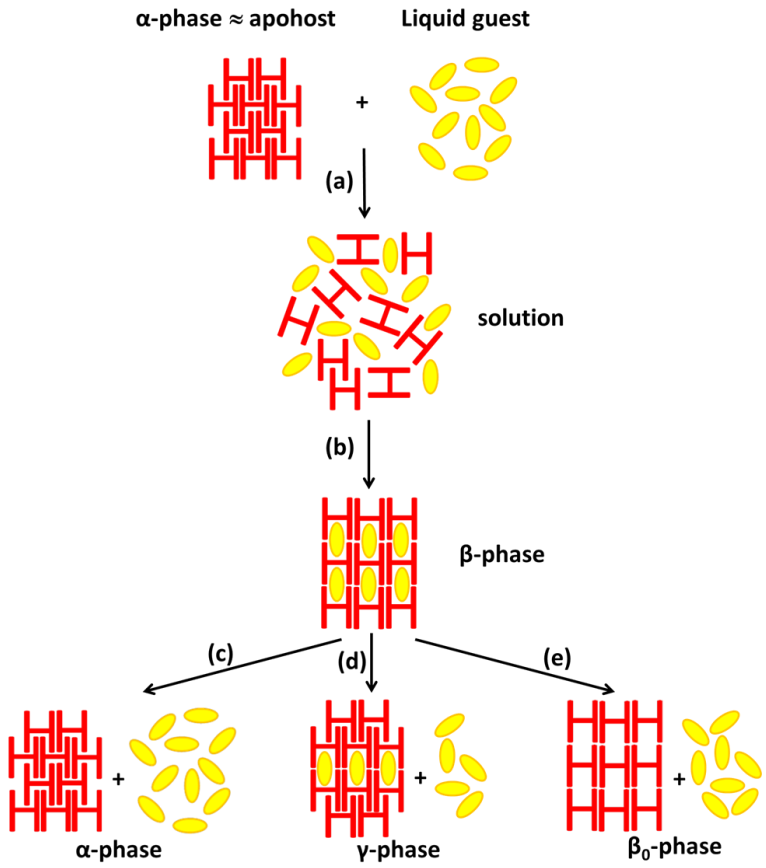

Figure 1.2 Schematics of the formation by crystallisation and the three forms of decomposition of an inclusion compound

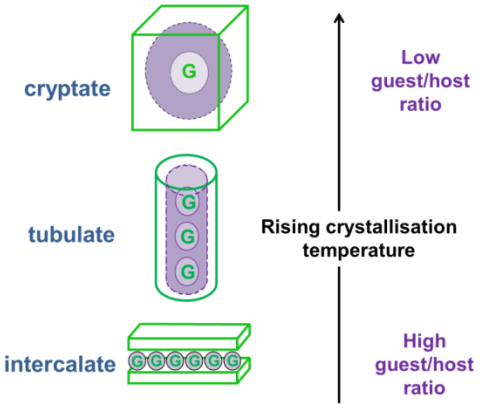

Figure 1.3 Change in host-guest topology with crystallization temperature
(Adapted from L.R. Nassimbeni, Acc. Chem. Res. **2003,** 36, 631)

As the crystallisation temperature increases, the guest/host ratio decreases and the topology alters from low temperature to high temperature in the formats: intercalate, tubulate, cryptate then apohost.

The forces between host and guest determine whether the aggregate is a complex in which primarily electrostatic interactions which include hydrogen bonding, ion-dipole, dipole-dipole, or similar interactions occur; or a clathrate or cavitate with less specific and often weaker non-directional interactions such as van der Waals, hydrophobic, or crystal close-packing effects is the case.

Host : guest interactions

The main specific interactions formed between host and guest are hydrogen bonding, CH···π interaction, van der Waals interactions, dipole-dipole interactions and halogen bonding. 'Noncovalent' interactions comprise a number of attractive and repulsive forces, all of which relate to the host and guest and their surroundings. The different types are listed below:[27]

Ion-ion interactions, such as the ionic solid sodium chloride, have bonds with strength similar to covalent bonding of 100 – 350 kJ mol^{-1}.

Ion-dipole interactions are apparent in complexes of metal cations with crown ethers and their strengths varies between 50 – 200 kJ mol^{-1}. The ether oxygen lone pairs are attracted to the cation positive charge. These interactions also include electrostatic coordinative bonds.

Dipole-dipole interactions result when two interacting dipoles are orientated relative to each other giving bond strengths of 5 – 50 kJ mol^{-1}.

Hydrogen bonding is a dipole-dipole interaction in which a hydrogen atom attached to an electronegative atom is attracted to a neighbouring dipole on an adjacent molecule or functional group.[28] Hydrogen bonding is described as the 'masterkey interaction in supramolecular chemistry'[29] because it is comparatively strong and has a nature which is eminently directional. They are found in a wide range of strengths, lengths and geometries. Strong hydrogen bonds with binding energies between 60 -120 kJ mol^{-1} and heteroatom-heteroatom distances between 2.2 and 2.5 Å, for example O-H···O and N-H···O; moderate hydrogen bonds (15 – 60 kJ mol^{-1}; 2.5 – 3.2 Å, e.g. C-H···O and O-H···π); and weak hydrogen bonds which occur between soft acids and soft bases (binding energy < 15 kJ mol^{-1} a long donor-acceptor distance of up to 4 Å such as C-H···π).[22] Strong hydrogen bonds are principally covalent in nature and have narrow hydrogen bond angles of 175° to 180°; while moderate and weak hydrogen bonds have electrostatic character and bond angles of 130°-180° and 90°-150° respectively. Strong H bonds offer exceptional spatial control, whereas moderate and weak H bonds are more flexible. The strongest hydrogen bond known is F-H···F^-, between charged molecules and with an energy of 160 kJ mol^{-1}.

Cation-π interactions (5 – 80 kJ mol^{-1}) occur when transition metal cations form complexes with olefinic and aromatic hydrocarbons. The bonding is strong, but is not considered to be noncovalent because it is closely linked with the incomplete *d*-orbitals of the metals. Alkaline and alkaline earth metals interact with C=C double bonds with a more noncovalent weak interaction, portraying a vital function in biological systems.

π-π stacking is based on weak electrostatic interactions that occur between aromatic rings, one being electron rich and the other electron poor with a stabilisation energy in the range 8 – 40 kJ mol^{-1}. Charge assistance ($\pi^{+}\cdots\pi$) provides stability to these interactions. Planar chelate rings with delocalised π electron density in metal complexes have considerable aromatic nature and often provide $\pi\cdots\pi$ stacking interactions.[30] The three types of π-stacking are face-to-face (eclipsed or *β*-motif) stacking which gives graphite a slippery feel and lubricant qualities, edge-to-face (T-shaped or edge-on) interactions and offset face-to-face (slipped or skewed) (Figure 1.4(a), (b) and (c)) with the electron rich and poor aromatic rings giving repulsions and attractions as shown in (d), (e) and (f).

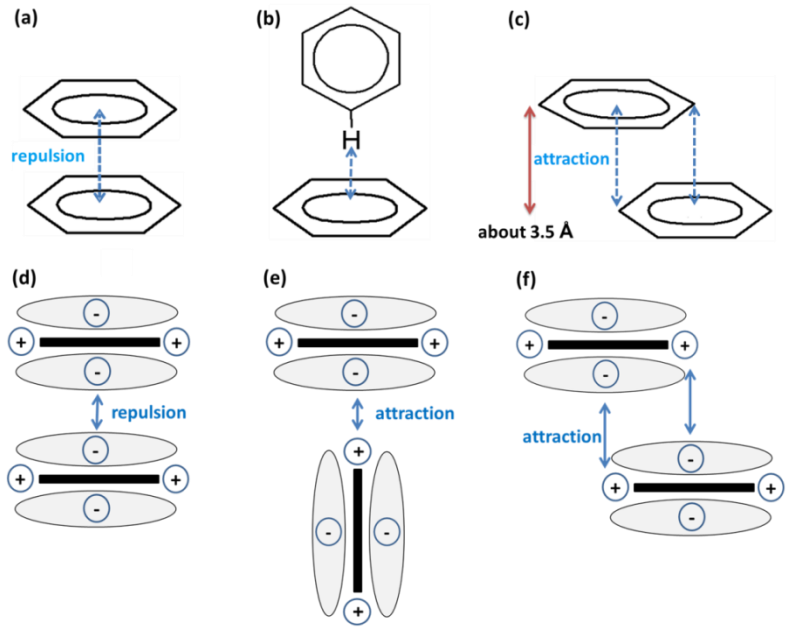

Figure 1.4 Types of π-π interactions:(a) face-to-face direct overlap (repulsion); (b) edge-to-face interaction which can be up to 5 Å long; and (c) face-to-face offset mode (attraction) with the matching attractions and repulsions due to the electron rich and poor aromatic rings in (d), (e) and (f)

The correlation between molecular structure and crystal structure of polynuclear aromatic hydrocarbons (PAHs) and their classification was performed by J. M. Robertson[31,32] in the 1940s. They crystallise in four different structural patterns, of which three are illustrated in Figure 1.5. Herringbone design, found in various areas such as fabrics, brick paving (Fig 1.5(a)) and weaving [33] is common in crystal structures of small aromatic hydrocarbons such as naphthalene and benzene (Fig 1.5(b)).[34] The latter interactions are regarded as weak forms of hydrogen bonds between slightly electron deficient hydrogen atoms of one aromatic ring and the electron rich π-cloud of another. The electrostatic repulsions between the two negatively charged π-systems determine the relative orientation of the two interacting molecules.[35] Plane separation for face-to-face and offset face-to-face interactions is 3.3 – 3.8 Å, whereas in edge-to-face interactions, the centroid-to-centroid distance up to 5 Å is acceptable.[36] Offset stacking and edge-to-face interactions are observed in the sandwich-herringbone motif found in perylene[37] and pyrene (Fig 1.5(c)) and the gamma-structures which are rich in C···C interactions are found in pyridazine and coronene (Fig 1.5(d)). Loots and Barbour[38] also considered N-derivatives of benzene, naphthalene and anthracene such as pyridine, quinoline and phenazine respectively, whose similar packing motif is combined with the effect of the molecular dipoles.

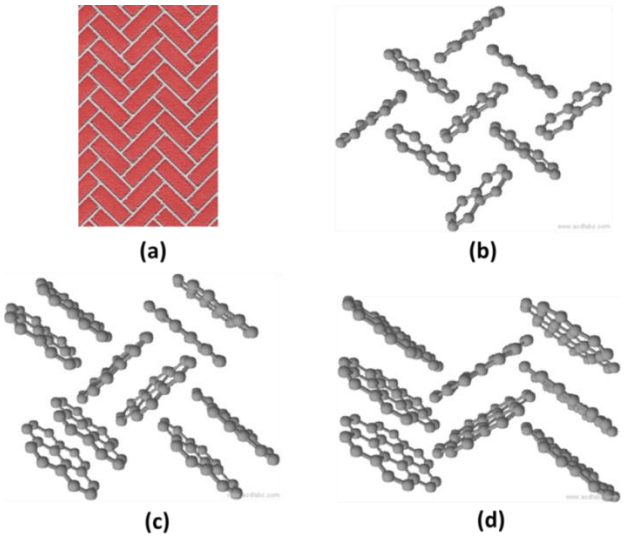

Figure 1.5 Diagrammatic representation of (a) brick paving, (b) naphthalene herringbone design, (c) sandwich herringbone of pyrene and (d) gamma (γ) motif of coronene
(Drawn using ChemSketch)[39]

Van der Waals forces arise from the interaction of an electron cloud polarised by an adjacent nucleus. They are weak (< 5kJ mol^{-1}) and nondirectional, providing general attractive interactions for 'soft' (polarisable) species. They are important in formation of inclusion compounds of small organic molecules within crystalline frameworks or molecular cavities.

Despite the recognition of **halogen bonding** in the 1950's[40], our interest towards these interactions continues to evolve. A Lewis base (D) interacts noncovalently with an electrophilic halogen (X). This compliments the activity of halogens in hydrogen-bonding interactions.[41]

According to Kitaigorodskii's packing theory,[2] molecules undergo shape simplification as they progress towards dimers, trimers, higher oligomers and finally crystals. A dovetail is formed between one molecule and the indentations of its neighbours reaching a maximum number of intermolecular contacts. Solid-state structures show a negligible amount of 'empty' space.

Werner clathrates

The design of supramolecular systems with a host compound forming a cage or channel with guest molecules trapped in the cavities as a stable inclusion compound is one of the main challenges of crystal engineering. Two types of inclusion compounds, the Hoffman- and Werner-type complexes, result from the assembly of inorganic coordination compounds. They border on either side between network solids and clathrates, with Hoffman inclusion compounds representative of infinite coordination polymers and Werner clathrates discrete coordination compounds.[42] Werner clathrates are formed by a wide range of Werner-type metal coordination complexes represented by the general formula MX_2A_4 where M is usually a divalent transition metal such as Fe^{2+}, Co^{2+}, Cr^{2+}, Ni^{2+}, Cu^{2+}, Zn^{2+}, Cd^{2+}, Mn^{2+} or Hg^{2+}; X is an anionic ligand such as NCS^-, NCO^-, NO_3^-, NO_2^-, Cl^-, Br^- or I^- and A is a neutral amine donor ligand such as pyridine or a derivative thereof. Due to the strong clathrate-

forming ability of many of these hosts the preparation of a pure, non-clathrated crystalline form is often difficult. The success of clathrate formation rests with two conditions, that is, that the central ion is a transition d-series element and the ligand prevents close packing of the complex molecules due to steric hindrance in the crystal lattice.[43] Simple pyridine ligands are suitable to form Werner-type clathrates.

Apart from the relatively simple structures of metals, of interest are also the structures of organic molecules, as alluded to earlier in the discussion of the structural patterns found in polycyclic aromatic hydrocarbons (Figure 1.5). This leads to the discussion of transition metal complexes (Werner complexes) as hosts in inclusion compounds and the properties of these compounds as they are altered by exchanging ligands, using mixed-ligand formation or providing other types of interactions between the host and the guest.

Schaffer *et al.*[44] showed that coordination complexes of transition metals are able to absorb organic compounds in a reversible but selective way. These guest molecules may be entrapped by the MX_2A_4 crystalline host lattice ranging from noble gases to condensed aromatic hydrocarbons.[45] The lattice void arises from the presence of the wide, flat pyridyl ligands.[9] Simple preparative procedures such as crystallisation of the host in the presence of the guest, contacting the solid host with liquid or dissolved guest or even direct uptake of the guest from a vapour phase can be used for formation of the inclusion compound. Since no evidence for chemical bonding between the guest and host components in the crystalline compounds was apparent, they were considered as clathrate-type complexes. These ‘Werner clathrates’, originally classified as ‘solid solutions’, comply with their behaviour as studied by Lipkowski and summarised in reviews dealing with their selectivity, crystal structures, and the thermodynamics of sorption and kinetics of desorption.[46, 47]

The structure of a Werner host complex, in most cases, demonstrates a *trans* octahedral coordination with the two anionic ligands in *trans* positions to each other. There are generally two typical configurations of the ligands, viz. 'four-blade propeller' and 'centrosymmetric' structures. In the propeller structure, the ligand arrangement minimizes the energy of nonbonded interactions; slightly higher repulsive interligand interactions are found in the centrosymmetric structure. The arrangement of pyridine ligands is unlikely to be coplanar due to the steric hindrance between them and the anions. The best compromise is thus the 'propeller' arrangement (as shown in Figure 1.8). The shape of these molecules may be either asymmetric or may adopt twofold axial symmetry. This type of conformation has been demonstrated for the crystalline α-Ni(NCS)$_2$(4-MePy)$_4$ molecule[48] as well as by Bond *et al.*[49] for Ni(NCS)$_2$(4-MePy)$_2$(4-PhPy)$_2$ in its 1:1 inclusion compound containing methylcellosolve as guest. The prediction of the centrosymmetric arrangement would be more likely if the metal ion were larger and / or the anion smaller such as Cd^{2+} and ONO^-.

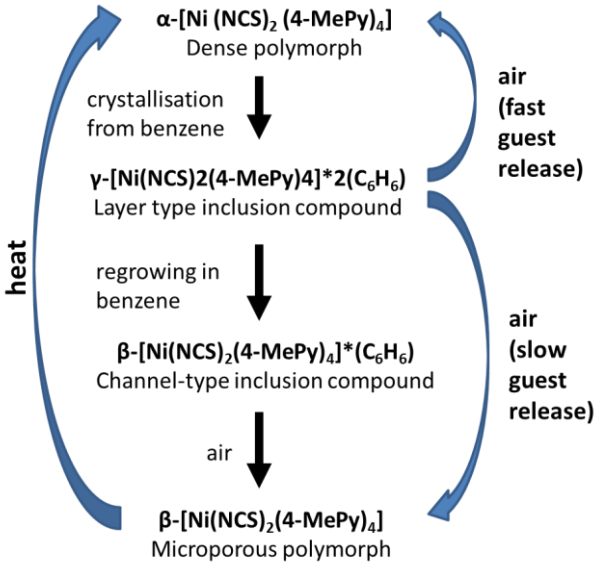

Figure 1.6 Schematic representation of the α, β and γ phases of the Werner host Ni(NCS)$_2$(4-MePy)$_4$ (Adapted from D.V. Soldatov, G.D. Enright and J.A. Ripmeester, *Cryst. Growth Des.*, **2004**, 4, 1185.)

Host [Ni(NCS)$_2$(4-methylpyridine)$_4$] is the original Werner host. It can form two kinds of inclusion compounds (Figure 1.6); the channel structure β-phase with a host:guest ratio ranging from 1:0.5 to 1:2 and a layer structure γ-phase with a 1:2 host guest ratio.[50] The pure α-phase can be obtained from

nitromethane or ethanol while the γ-phase is formed by crystallisation from benzene. Over time it slowly transforms into the β-phase. Both these materials collapse into the pure dense α-phase on guest removal.

These inorganic clathrate complexes are worthy for their ruggedness and uniform structural characteristics. In the solid state the complex is unable to pack efficiently due to its shape and a conveniently sized solvent or other molecule present during crystallisation will act as a guest. Werner clathrates are described by the term *organic zeolite*[51,52] as they provide stable and convenient model systems for methodical studies. They are truly porous and in [$Ni(NCS)_2$(4-methylpyridine)$_4$], slow removal of the benzene can result in the formation of a microporous guest-free apohost β_0-phase. The guest release can be followed by thermogravimetric analysis (TGA) shown schematically in Fig. 1.7, which is a common manner of assessing stability and stoichiometry of inclusion compounds. This divulges the 'clathrate-like' behaviour of the γ-phase which contrasts significantly with the zeolite behaviour of the microporous β-phase. The mass loss stages after initial wetting in benzene are as follows:

(1) evaporation of excess solvent; (2) release of guest benzene; (3) release of first 4-methylpyridine ligand; (4) release of second 4-methylpyridine ligand; and (5) release of remaining two 4-methylpyridine ligands to give $Ni(NCS)_2$.

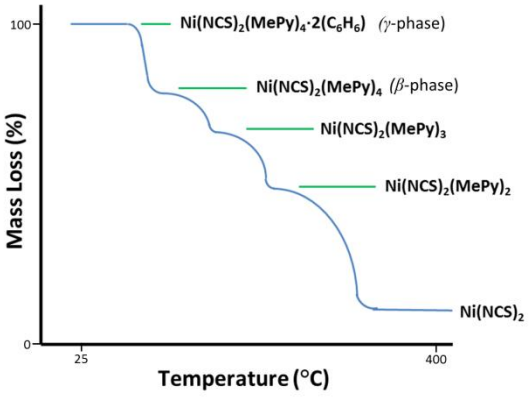

Figure 1.7 Sketch of a TGA curve to show stages (2) to (4) of the decomposition of $Ni(NCS)_2(MePy)_4{\cdot}2(C_6H_6)$ resulting in $Ni(NCS)_2$

The guest release in step 2 is the important part. In the clathrate γ-form this process occurs over a narrow temperature range bracketed by two plateaux representing the initial (γ) and final (α) phases. The guest release from the β-phase is continuous over the entire temperature range until the β-phase has decomposed. This characteristic desolvation behaviour, in which the guests slowly exit from a channel, is typical of zeolites.[23]

Noted in these studies is the dependence of lattice expansion on the volume and shape of the guest molecules. In most cases the host:guest ratio is 1:1. Physical properties of these structures are dependent on both the packing of the hosts as well as the properties of the guest. The enthalpy of clathration is related to the cavities in the host lattice. Soldatov[47] revisited the host compound [$Ni(NCS)_2$(4-methylpyridine)$_4$] and determined three crystal structures: the apohost (α), non-porous phase and the clathrates (β and γ). The adaptability of this host towards guest compounds is attributed to the fact that its β-phase volume expands by 5 – 14% upon guest inclusion. Recently there has been renewed interest in Werner clathrates[53,54] and Lusi and Barbour[55] have described polymorphism associated with an order-disorder phase transition of the guest in the [$Ni(NCS)_2$(4-phenylpyridine)$_4$] clathrate dependent on the thermal range investigated. The host preferentially discriminated in favour of one of the three isomers of xylene in solid-vapour competition experiments[56] and Barbour and co-workers[57] explored the preparation of phases by mechanochemical techniques which resulted in a series of solid solutions. Different sorption properties were exhibited by these solid solutions compared with the pure Werner complexes. Recently the structures of three Werner complexes have been analysed in terms of their packing, and the results of crystal densities were justified by Hirshfeld surface analysis and density functional theory calculations.[58]

When performing a kinetic study on a reaction there are two different ways in which it may be measured, viz. the measurement of α, the extent of reaction, as a function of time, *t*, at constant temperature; or as a function of temperature, *T*, which in increased according to a linear heating

programme, ϕ = dT/dt. The first method is an isothermal procedure, which corresponds to the conventional concentration vs t curve of homogeneous kinetics. The second method is the basis of a dynamic thermal analysis which is a measurement of α *vs* T.[59]

On the heating of a solid sample, decomposition is one of the possible changes which it may undergo. For the heterogeneous reaction A(s) → B(s) + C(g), the progress of the reaction is measured in terms of the change in mass of the sample. This is the fractional reaction, $\alpha = (m_0 - m_t) / (m_0 - m_f)$ where m_0 is the initial mass, m_t is the mass at time t and m_f the mass of the sample when the reaction is complete. Variations in anisotropic properties of the crystal structure as well as the presence of impurities and structural defects have effects on the thermal stability of solid samples. Decomposition of solid reactants is initiated at defective regions of the crystal with the formation of nuclei of the solid product as the gaseous product escapes. Strain on the neighbouring regions results in growth of the nuclei. The geometry of the nucleation and growth processes leads to predictions of the rate at which the gas product is evolved and the rate of decomposition are affected by chemical reactions and physical processes.

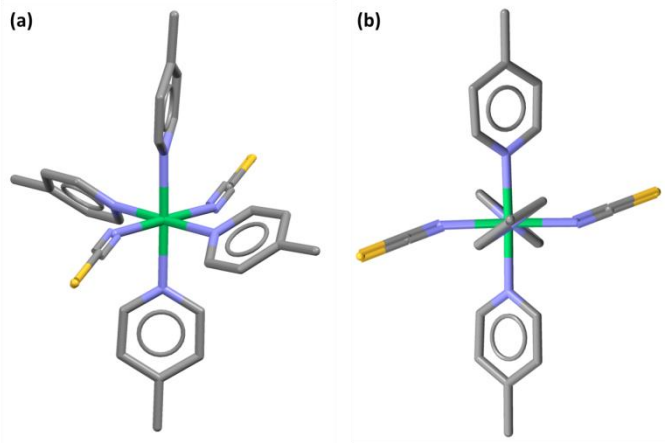

Figure 1.8 (a) General view of the Werner complex, $Ni(NCS)_2(4\text{-methylpyridine})_4$ followed by (b) the view along the ligands showing the propeller conformation

Werner clathrates have the ability to demonstrate versatility in the range of guests they capture due to the rotational freedom of the substituted pyridine ligands about their Ni-N bonds. A diagram of Werner complex, $Ni(NCS)_2(4\text{-methylpyridine})_4$, is shown in Fig. 1.8, illustrating the propeller conformation of the ligands. A variety of guests, differing in shape and size, can be included within the host molecules. The torsional configurations have been demonstrated by Moore *et al.*[60] with the host molecule $Ni(NCS)_2(4\text{-vinylpyridine})_4$. In the compounds studied, similar values were found for the four torsion angles, resulting in a ++++ conformation as found by Lipkowski[61] in his report on similar structures, frequently forming clathrates in the tetragonal space group $I4_1/a$. The host compound $Ni(NCS)_2(4\text{-phenylpyridine})_4$ has displayed a wide variety in packing, crystallising in a number of space groups such as $P2_1/n$ and $C2/c$. Two different sets of rotational freedom are observed, that is, torsion around Ni-N bonds and secondly, rotation of the phenyl rings with respect to their parent pyridines.[62] The pyridine torsion angles, consistent with the ++++ propeller conformation, all lie in the range of 19 - 46°. However, the ring systems twist in order to accommodate the guests, with the torsion angles assuming positive or negative torsion angles, without a discernible pattern.

Selectivity towards guest isomers by Werner hosts

In the TGA experiment, the mass of a solid sample is recorded as a function of steadily increasing temperature. The sample mass is expressed as a percentage of the initial mass. This results in a trace that shows one or more plateaux separated by a slope which corresponds to the loss of guest molecules at various temperatures. If the formula mass of the host and guest is known, then the host-guest ratio may be obtained by comparison of calculated and observed weight loss for various stoichiometries. The stability of the host-guest complex is indicated by the temperature at which the guest loss occurs. A flowing gas stream (usually dry N_2) carries away the weight-loss products.[63]

Some correlation between the conformational angle of the pyridine ligand around its metal-nitrogen coordination bond and the bond length observed by X-ray crystallography has been noted. The

minimum of the bond length corresponds to a conformational angle of ~45°. As calculated using empirical force field methods, this is in agreement with the minimum of the interligand repulsive energy of nonbonded interactions. A correlation also exists between the detailed structure of the coordination sphere of the host and the visible spectrum of the solid. In a plot of the spectral shift of the solid against the axial : equatorial ratio of the coordination bond lengths this effect can be seen.[38] Well-established separation methods which are capable of highly efficient separations are distillation, solvent extraction, precipitation and reverse osmosis. These methods rely on the difference in physical properties such as boiling points and density of these compounds. Isomers are difficult to separate as their properties are very similar.

Since the entrapment by a host can occur in a selective way, this gives a simple strategy for the separation of mixtures which are otherwise difficult to separate by normal experimental means such as distillation. This has been discussed at length when the separation of the three xylene isomers was carried out by selective sorption with a single substrate.[53] *Ortho*-, *meta*- and *para*-xylene as well as ethylbenzene constitute the C8 aromatic compounds from crude oil which are used in the production of polymers, plastics, resins and fungicides.[64] Xylenes are added to motor fuel as an anti-knocking agent.[65] Due to the similar physical properties of these compounds, separation by normal means becomes an expensive and inefficient undertaking. During the investigation into solid-vapour reactions between the xylene isomers and $Ni(NCS)_2$(*para*-phenylpyridine)$_4$, the extent of guest uptake was recorded gravimetrically as a function of time. During competition experiments the host compound was exposed to the vapours from liquid mixtures of the xylene isomers. Analyses of the products in each case were performed by a range of relevant PXRD, single crystal X-ray diffraction, kinetics studies and gas chromatography in hexane using a Flame Ionisation detector. In this case, discrimination in favour of *ortho*-xylene in the presence of *meta*- and *para*-xylenes was considerable; and favoured *meta*- over *para*-xylene in the absence of *ortho*-xylene.

This possible aspect in the use of Werner clathrates for selective separation of isomers, such as the above C8 aromatic compounds, is an area which still needs to be further explored. As mentioned in the review article by Santos *et al.*[66] the adsorption processes of the xylene isomers on zeolites and zeolite membranes have been considered by a number of researchers. The zeolite membranes are formed by preparing a layer of zeolite on the surface of a porous support and beta zeolite was used to give limited separation of *meta*-xylene from the other isomers. The use of molecular sieves such as modified faujasites X and Y with 10-13 Å pore diameter was considered efficient in the separation of *ortho*-xylene from its isomers, although the low selectivity values undermine the commercial availability. New research opportunities for dealing with the challenge of improving separation of pure isomers could follow the trend of developing new materials such as metal organic frameworks (MOFs).

Selectivity towards the xylene isomers and ethylbenzene, has formed an important part of this thesis. Xylenes are dimethyl benzenes and are used as solvents in industries such as printing, rubber and perfumes and are found in household products such as aerosol paints and lacquers and, due to their volatility, can impair the human respiratory system with air levels above the exposure limit.[57] Despite their similar physical and structural properties, xylene isomers have different industrial applications and their discrimination is therefore essential. Separation by the normal classical distillation process is extremely difficult since their boiling points are very close together and faujasite separation is based on their kinetic diameters (see Table 1.1). Adsorption and separation of xylene isomer vapours on a porous chromium material[67] showed a preference for *para*-xylene, but *meta*-xylene's interactions were weaker and only *ortho*-xylene could be clearly separated by the chromatographic column. Selective detection and discrimination of xylene isomers was developed with a field-effect transistor (FET) sensor based on an ambipolar semiconducting polymer.[68] Multiple sensing parameters were generated by the FET in electron and hole conduction toward xylene isomers. Chemically and structurally similar xylene isomers as well as binary and tertiary xylene mixtures were identified using pattern-recognition combined with multiple sensing parameters from a single ambipolar FET. Density

functional theory (DFT) calculations showed that energy levels of the polymer increase with the amount of adsorbed xylene isomer, indicating that structurally similar chemicals and their mixtures can be selectively detected.

Table 1.1 Physical properties of the aromatic C8 compounds

	***o*-xylene**	***m*-xylene**	***p*-xylene**	**ethylbenzene**
Boiling point/°C	144.4	138.85	138.35	136.2
Dipole moment/D	0.62	0.37	0.07	0.58
Kinetic diameter/nm	0.74	0.71	0.67	
Density at 25°C/g cm^{-3}	0.876	0.861	0.858	0.868
Vapour Pressure/mmHg	7	9	9	10

Separations by inclusion follow the methodology illustrated in Fig. 1.9 and 1.10. The process relies on molecular recognition between host and guest compounds, and typically consists of dissolving the host in a mixture of the guests (guest1 and guest2), using a non-competitive solvent where necessary. Should differentiation take place, the crystalline inclusion product will be enriched with a particular guest. The guest mixture can be released from the crystalline compound by dissolution or gentle warming. Analysis follows using analytical methods such as chromatography or NMR. The host compound is recovered and recycled.

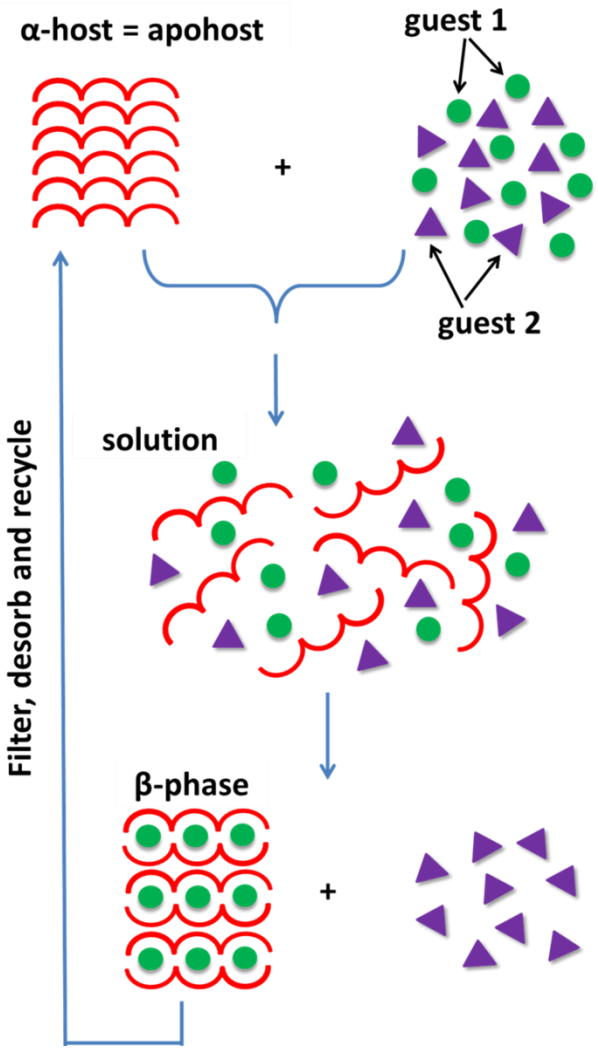

Figure 1.9 Schematic representation of selective inclusion

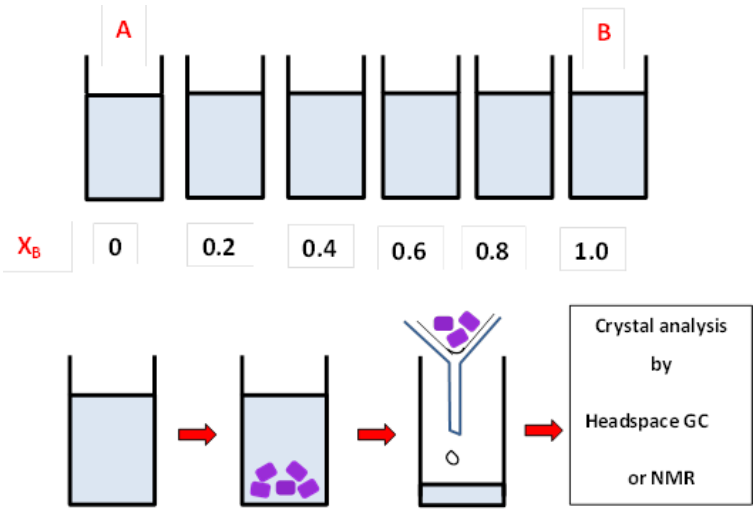

Figure 1.10 Crystallisation followed by analysis using headspace GC or NMR spectroscopy

When a host compound is crystallised from a mixture of two guests A and B to form a crystal containing a ratio of the two guests (H•nA•mB), the selectivity coefficient of this competition experiment can be determined from the formula

$$K_{(A:B)} = (K_{(B:A)})^{-1} = Z_A / Z_B * X_B / X_A \qquad (X_A + X_B = 1)$$

where X_A, X_B are the mole fractions of the guests in the mother liquor and Z_A, Z_B are their mole fractions in the crystal.[69] The selectivity falls into four categories which can be demonstrated by their coefficients. If there is no preference for one of the two guests, then $K_{A:B} = 1$, which is presented in Fig 1.11(a). Fig 1.11(b), shows preferential enclathration for the A guest over the B guest with the selectivity coefficient reaching a value of close to 10. Fig 1.11(c) illustrates concentration dependence and (d) a situation where the guest with the smaller concentration is preferred over that with the higher concentration. The latter is an unusual occurrence.

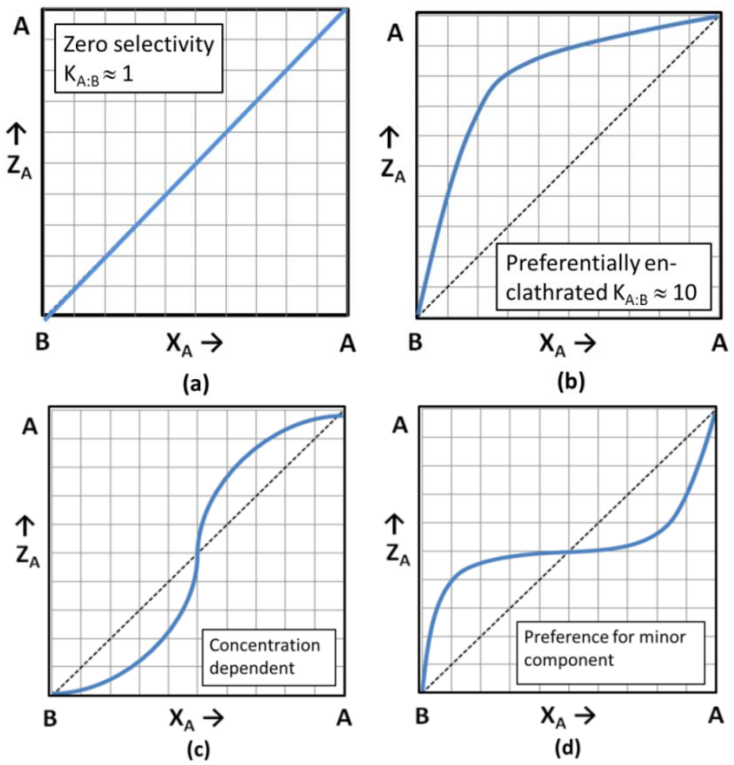

Figure 1.11 Examples of four selectivity curves showing (a) zero selectivity; (b) preference for one guest; (c) dependence on concentration and (d) preference for the minor component

In some cases the 2-component competition experiments were extended to analyse simultaneous competition between three guests. The results were presented as shown in Fig. 1.12 with each apex representing pure (100%) guest components **A**, **B** and **C**. If composition of the starting mixture was selected with an equimolar ratio, the green circle represents its position. The figure illustrates that the selectivity profiles for the three guests **A**, **B** and **C** gave $\mathbf{K_{A:B}} = 5$, $\mathbf{K_{B:C}} \approx 1$ and $\mathbf{K_{A:C}}$ concentration dependent. As shown in the inner triangle, **A** will be the preferred guest in the ternary competition experiment, with the result falling where the red triangle lies in the figure. Should the concentrations change to favour **C**, the findings will be different with the result moving towards the **C** corner as shown in purple in Fig 1.12.

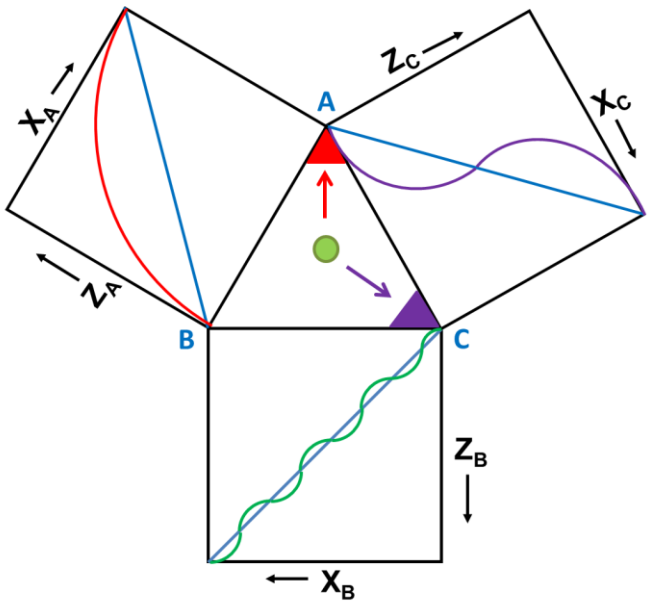

Figure 1.12 Selectivity profiles for a ternary mixture of guests **A**, **B** and **C**

Novel homochiral heterometallic coordination polymers have been studied by Lewinski *et al.*[70] In this research, the increasing demand for materials to selectively catalyse and separate enantiomers has been considered. The polymers were generated using chiral multifunctional ligands as linkers and

metal ion nodes with specific coordination geometry. These complexes act as chiral, semi-rigid building units for polymer construction.

The most distinctive feature in nature is the presence of chirality in organic molecules. Amplification of the same chiral phase would occur if the reaction results in a crystal which induces crystallization of the same chiral phase.[8] Several aspects of molecular recognition and self-assembly, such as lock-and-key mechanisms at crystal surfaces to reduce formation of mixed crystals or the effect of the solvent at the crystal-solution interface on crystal shape and growth, have been studied. The process known as 'total asymmetric transformation of the second type' is the generation of one-handed crystals from nonchiral molecules.[8] The conformational chirality in the crystal is converted into stable molecular chirality by a topochemical reaction in the solid phase, generating materials enriched with one enantiomer. Crystal nucleation can be controlled by using enantioselective inhibition. The solvent plays an important role in determining the size and structures of the nuclei. The solvent, being a 'tailor-made' additive, interacts differently with nonsymmetry-related faces of a growing crystal and with the facets of crystal nuclei. Certain enantiomers can be resolved using additives designed to enantioselectively bind to homochiral clusters of structures preventing them from crystallising but allowing the opposite chiral compound to grow into macroscopic crystals.

Design of Werner hosts for enhancement of properties

The "pores" in noncovalent frameworks are created during assembly of the crystalline inclusion compound but are generally only sustainable when occupied by guest molecules. Werner complexes are amenable to chemical modification which may provide a route to effective optimization of separation or selectivity.[71] Mixed ligand construction is one of the more recent or common ways of redesigning a host compound in order to provide adjustments to its properties.

The creation of new crystalline solids has considered the class of hybrid materials, existing as lattices of metal ions with organic ligand scaffolds. Structural complexity is reached by combining two different ligands to portray a combination of both acid and base ligands within the same system.[72] In many of these cases, the current advances consider coordination polymer systems which bridge via mixed ligands. Biological activity against human cancer cell lines were enhanced by the Cu(II) salicaldehyde-4-methyl-3-thiosemicarbazone mixed-ligand complex with imidazole and benzimidazole.[73] Two new three-dimensional porous structures of cadmium and cobalt demonstrated selective gas adsorption of CO_2 with flexible mixed ligands and rigid organic ligands containing different linear trinuclear metal carboxylate cores.[74] In a third example, an increase in fluorescence emission was observed following zinc coordination not seen in the free ligand.[75] This technique was considered in Chapter 5 where two ligands, one flexible and one rigid, were combined in a Werner host to demonstrate enhanced selectivity of one of the xylene isomers.

Common to Werner hosts is the lack of attractive chemical functionality that would allow the use of hydrogen bonding concepts. The pyridine or pyridine derivative ligands in these hosts usually form interactions with the guests via C-H$\cdots\pi$ or $\pi\cdots\pi$ interactions in the packing of aromatic molecules in crystals. These interactions occur when the attractive interactions between π-electrons and the σ-framework eclipse the adverse provision of π-electron repulsion.[76] The application of supramolecular chemistry in the creation of crystalline host-guest materials can demonstrate high shape specificity on clathration. Although molecular host-guest complexes may not be as sturdy as natural zeolites, they do have the benefit of adjusting their pore nature and size to attune to the guest requirements.[77]

In fact, Werner was the first to suggest that hydrogen was not monovalent when, in 1902, he indicated secondary valence (*Nebenvalenz*),[78] which proposed that the proton of the ammonium salts was linked to both ammonia and the anion according to the system $(H_3N\cdots H)X$. The concept that a hydrogen nucleus being held between two octets forms a *weak bond* was first discussed by Latimer and Rodebush[79] eighteen years later. In 1931, Pauling[80] used the term *hydrogen bond* for the first time.

Without the role played by H-bonding our understanding of many ideas in nature such as the shaping of DNA into genes and polypeptide chains into hair or muscles would be lacking. This makes it the single most powerful determinant of the composition of the ecosphere. [81]

"Sticky" or attractive ligands were considered in the Werner hosts and their structural characteristics have been studied in Chapter 6. The concept of CH···O hydrogen bonds was first alluded to by Sutor in the sixties,[82,83] followed by Taylor in 1982[84] and Desiraju in the 1990's. Donahue[85] contested the interest shown in molecular crystal engineering which supported the C-H···O bonds and his derision promoted structural chemist's rebuttal of the idea that a C-H group could form a hydrogen bond with electronegative atoms.[86] Taylor recently substantiated that X···H interactions stabilise crystal packing arrangements, even when the interactions are longer than the sum of the van der Waal's radii of the interacting atoms.[87] Of importance are the X···H contacts with X the halogen F or Cl where the driving force for the packing arrangement is the attractive nature of this contact and the repulsive nature of any alternative contacts.

Carboxylic acid and amide groups were considered to be similar with regard to the electron densities around the carbonyl and alkyl groups.[88] Hydrogen bonding now becomes an important interaction between ligand-ligand (or host-host) and ligand-guest with ligands such as nicotinamide and isonicotinamide. This is noticed in clathrate formation with guests such as alcohols, ketones or amides, all with functional groups which may provide interactions with proton donors or acceptors in those of the ligands. Structural aspects of the hosts and selectivity towards these guests were considered and are reported in Chapter 6.

Pattern predictions

Crystal engineering is the field that utilises the knowledge of intermolecular interactions and molecular architecture to synthesise new crystalline materials with specific chemical and physical properties. Retrosynthesis, a strategy of working backwards from the product to the reactant, is a powerful technique in organic synthesis. Using this approach, E.J. Corey[89] suggested the name *synthon* for smaller components representative of a target. *Supramolecular synthons* are spatial compositions of intermolecular interactions between complementary functional groups with molecules,[90] termed *tectons*,[91] interacting *via* the formation of non-covalent bonds. In crystal engineering, the term is used to describe the structural units used in coherent design of crystalline compounds with explicit properties.[92]

Representative synthons entail a few functional groups which are held together by directional interactions which can be strong. The molecular synthons are responsible for producing predictable patterns in the structure. A typical example is the carboxyl dimer found in acids such as benzoic acid. Related to this example is that of the primary amide N-H···O which, due to its 'extra' hydrogen atom, can be extended into a linear tape. This primary amide synthon as well as many other synthons are significant in the recognition events through which molecules assemble into supermolecules.

A few examples of the patterns which can be formed by molecular interactions representative of the synthons in the structure are shown in Fig 1.13. The 1:1 binary crystal of 4-nitrobenzoic acid and 4-(N,N-dimethylamino) benzoic acid forms a linear chain (Fig 1.13(a)) while isophthalic acid forms a zig-zag ribbon (Fig 1.13(b)). In both cases, the synthon connects phenyl rings to give two different linear arrays of the molecules.[93] A three point recognition pattern is found in the 1:1 molecular complex formed between cyanuric acid and melamine with interactions by one N-H···N and two N-H···O functional groups (Fig 1.13(c)). Due to its similarity to that of rose petals it is called a rosette.

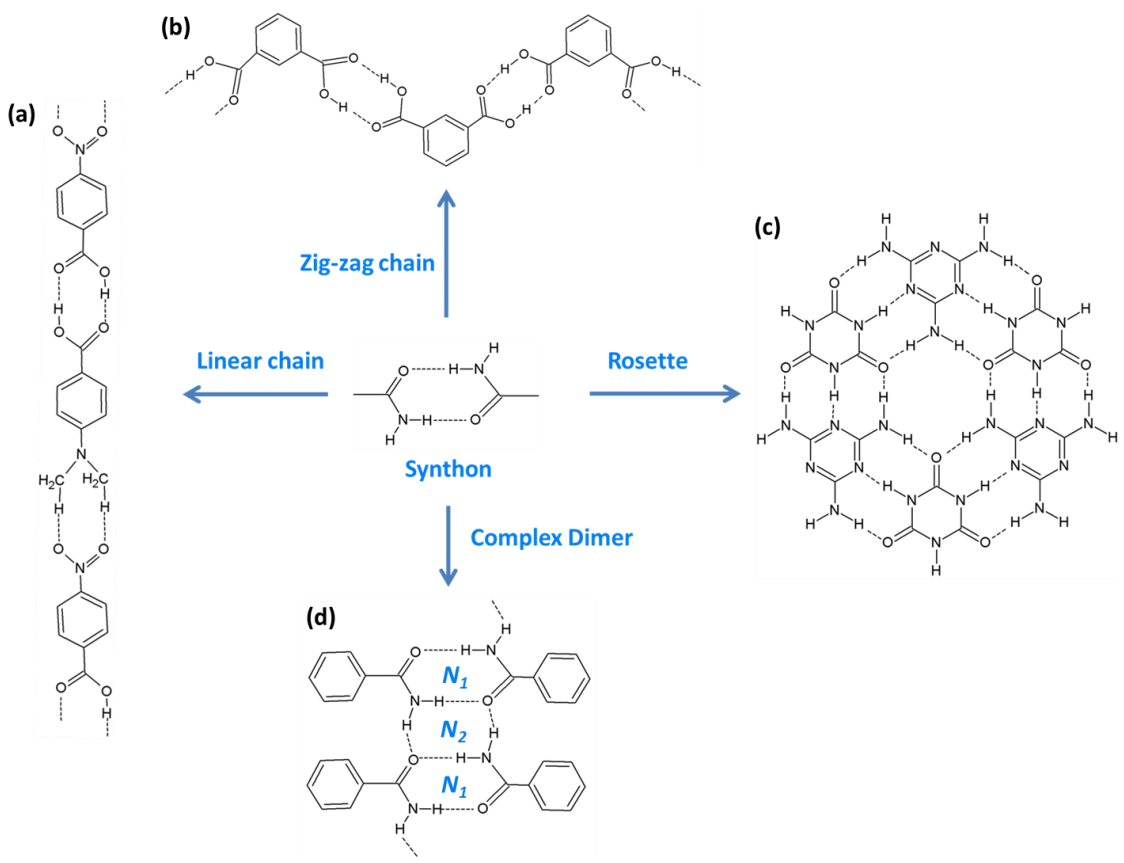

Figure 1.13 The production of different patterns from a synthon resulting in (a) a linear chain, (b) a zig-zag tape, (c) a rosette and (d) a combination of dimers

The encoding of hydrogen-bond patterns was developed by Etter and co-workers[94,95] and it was shown that pattern-preference can be established by functional groups. Graph sets which are used to describe the pattern of hydrogen bonding can involve higher-level sets, as shown in Fig 1.13(d). This compound contains two unique hydrogen bonds and there are two first-level graph sets, labelled N_1 and a second-level graph set, N_2, is created on combining the two unique hydrogen bonds within the structure.[96] The graph set is specified with a pattern designator (G), its degree (n), and the number of donors (d) and acceptors (a) in the form $G_d^a(n)$. In Fig 1.13(d), the two graph sets are N_1=$R_2^2(8)$ and N_2=$R_4^2(8)$, with R indicating an intermolecular ring.

The importance of looking at the 'chemistry beyond the molecule'[9] by identifying new synthons will produce control over molecular orientation, packing patterns and lattice dimensions and will provide the ability to fine-tune physical properties which are determined by the structure.[97] An example of this has been shown by Aakeröy *et al*.[98] where metal complexes were assembled to form porous materials with a variety of patterns to allow for inclusion of guests.

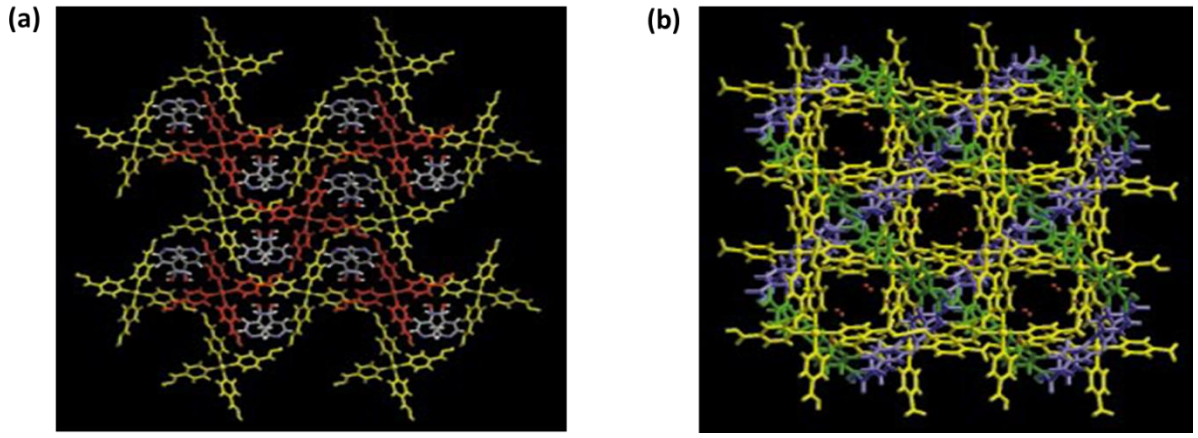

Figure 1.14 Patterns in the structure of two metal complexes showing (a) two interpenetrating hydrogen-bonded nets (in red and yellow) in a metal complex with guest 4-aldoximepyridine enclathrated by hydrogen bonds; and (b) three mutually perpendicular nets which interpenetrate via hydrogen bonding and shown in blue, green and yellow.
(C.B. Aakeröy, A.M. Beatty, and D.S. Leinen, *Angew. Chem. Int. Ed.* **1999**, 38, 12, 1815; Figures 2 and 5.)

The strategy of engineering the arrangement of the crystal structure was found in the compounds shown in Fig 1.14 which were formed by a nickel Werner complex. The oxime synthon allowed sheets to be formed with a 3D network with axially coordinated water molecules and bromide counterions. An inclusion compound, with the guest 4-aldoximepyridine captured in the channels by hydrogen bonds, is shown in Fig 1.14(a) with interpenetrating hydrogen-bonded nets depicted in red and yellow. In Fig 1.14(b), a metal complex is assembled through carboxylate – carboxylic acid hydrogen bonds to form a crystal structure with interpenetrating nets in three perpendicular planes. The nets are shown in blue, green and yellow in Fig 1.14(b). A true prediction of the pattern was made by the functional groups in the structure.

Comparison of different crystallisation and analytical methods

Environmentally friendly processes lead to the exploration of different modes of molecular self-assembly. These mechanochemical reactions are the result of milling or grinding the reactants together in a neat or dry grind in a mortar and pestle or using a ball mill.[99] Extraordinary success in the creation of non-covalent interactions as well as metal-ligand coordination bonds and the development of liquid-assisted grinding (LAG, also known as kneading or solvent-drop grinding) has provided a means of systematic study in a solvent-free environment.[100] Hasa *et al.*[101] provided evidence that the concept "one liquid for one specific polymorphic form" for LAG reactions is not always true, by producing more than one polymorphic form in 11 out of 15 crystal systems. Mechanochemical methods as well as slurrying and melt crystallisation were considered in Chapter 4 of this thesis using polycyclic aromatic hydrocarbons (PAHs) as guests and successful outcomes were reached for a number of these guests with the host $Ni(NCS)_2(4\text{-vinylpyridine})_4$. Powder X-ray diffraction (PXRD) analysis was used to compare the grinding outcome with that of the crystal structure synthesised using solution methods of formation.

Techniques previously used for the identification of guest molecules in host-guest crystalline materials include a wide range dependent on the form and solubility of the crystal. For instance, ^{1}H Nuclear Magnetic Resonance or gas chromatography was used if the crystal was soluble in a suitable solvent; headspace removal of the guest followed by GCMS analyses for non-soluble crystals or metal-organic structures; a combination of TGA and DSC for host/guest ratio in competition reactions and UV-Vis absorption for a metal organic framework MOF substances. However, in certain situations, guest identification by thermogravimetric analysis (TGA) is difficult without ready access to tandem TGA/GCMS equipment. A method involving solid phase microextraction (SPME) has been proposed by Beatty and Fischer.[102] Recent modifications to the SPME fibres show the inclusion of a metal organic framework (MOF) in the fibres which broadens the absorption to include benzene derivatives, organochlorine pesticides and other analytes of interest. It was found that the SPME

sampling could be used effectively, without creating noise and is a good identification method for disordered guest molecules.

The determination of the drug warfarin which is administered as a racemic mixture of the (R)- and (S)-warfarin forms was required to determine whether the (S)-warfarin's anticoagulant effect was more potent than that of the (R)- enantiomer. In a study by Malakova *et al.*[103] a LC method was developed and validated using chiral separation on a glycopeptide-based stationary phase with fluorescence detection.

This project encompasses the synthesis of Werner host complexes, a study of the structural features of their inclusion compounds and their ability for selectivity towards a mixture of isomers or guests with similar physical properties. The following objectives are presented in this thesis:

1. The synthesis of nickel thiocyanato Werner host complexes whose structures produce different physical and chemical properties.
2. The preparation of novel Werner clathrates with these hosts and a selection of guest isomers, polyaromatic hydrocarbons, alcohols or carbonyl compounds.
3. The full characterisation of compounds through X-ray diffraction and thermal analysis techniques.
4. The enhancement of the selectivity of the host towards one guest from a mixture of guests and the analysis thereof.
5. The investigation of other methods of crystallisation which addresses environmentally friendly methods such as grinding and slurrying.
6. The exploration of functional groups with the promotion of hydrogen bonding to characterise the patterns formed in the crystal packing.

References

[1] W. H. Bragg, *Proc. Phys. Soc.*, **1921**, 34, 33.

[2] A. I. Kitaigorodskii, *Molecular Crystals and Molecules*; 1973, Academic Press: New York.

[3] G.R. Desiraju, Crystal Engineering: From Molecule to Crystal, *J. Am. Chem. Soc.*, **2013,** 135, 9952

[4] R. Davey and J. Garside, in *From Molecules to Crystallizers: An Introduction to Crystallization*, Oxford University Press, **2000**

[5] H. Davy, *Phil. Trans. R. Soc. Lond.*,**1811,** 101, 155

[6] M. von Stackelberg, *Natuurwissenschaften*, **1949**, 86, 359

[7] F. Vogtle, *Supramolecular Chemistry*, John Wiley & Sons, **1991**, 171

[8] J-P. Behr, *The Lock and Key Principle: The State of the Art - 100 Years on*, John Wiley & Sons, **1994**, 1

[9] J-M. Lehn, *Supramolecular chemistry and self-assembly special feature: Toward complex matter: Supramolecular chemistry and self-organisation. Proc. Nat. Acad. Sci. USA*, **2002**, 99, 4763

[10] J-M. Lehn, *Supramoleular Chemistry - Scope and Perspectives. Molecules - Supermolecules - Molecular Devices*, **1987**, Nobel Lecture.

[11] F. Cramer, *Angew. Chem.*, **1952**, 64, 437

[12] A. Werner, *Justus Liegig Ann. Chem*., **1902**, 322, 261

[13] G.B. Kauffman, in *Alfred Werner Founder of Coordination Chemistry*, **1966**, Springer-Verlag Berlin Heidelberg GmbH

[14] G.B. Kauffman, *J.Chem.Ed.*, **1976**, 53 (7), 445

[15] E.C. Constable and C.E. Housecroft, *Chem.Soc.Rev.*, **2013**, 42(4):1429

[16] C.A. Schalley, *Analytical Methods in Supramolecular Chemistry*, **2007,** Wiley-VCH

[17] J.W. Steed and J.L. Atwood, in *Supramolecular Chemistry*, 2nd Edition, Wiley, **2009**, 106

[18] H.M. Powell, *J. Chem. Soc.*, **1948**, Vol. 61

[19] J.H. van der Waals and J.C. Platteeuw, *Advances in Chemical Physics*, **1959**, 2, 1

[20] J.H. van der Waals, *Trans. Faraday Soc.*, **1956**, 52, 184

[21] J.W. Steed and J.L. Atwood, in *Supramolecular Chemistry*, 2nd Edition, Wiley, **2009**, 6

[22] L.R. Nassimbeni, *Acc. Chem. Res.*, **2003**, 36, 631.

[23] B.T. Ibragimov, S.A. Talipov and T.F. Aripov, *J. Inclusion Phenom. Mol. Recognit. Chem.*, **1994**, 17, 317.

[24] C. Tedesco, L. Erra, M. Brunelli, V. Cipoletti, C. Gaeta, A.N. Fitch, J.L. Atwood and P. Neri, *Chem. Eur. J.*, **2010**, 42, 2371

[25] G.R. Desiraju, J.J. Vittal, and A. Ramanan, *Crystal Engineering: A Textbook*, World Scientific Publishing, **2011**, 132

[26] J.W. Steed and J.L. Atwood, in *Supramolecular Chemistry*, 2nd Edition, Wiley, **2009**, 27

[27] J.W. Steed and J.L. Atwood, in *Supramolecular Chemistry.* 2nd Edition, Wiley, **2009**, 556

[28] G.A. Jeffrey, in *An Introduction to Hydrogen Bonding*, **1997**, Oxford University Press: Oxford

[29] J-M. Lehn, *Supramolecular Chemistry*, **1995**, 1st Edition, VCH: Weinheim

[30] E.R.T. Tiekink, in *Supramolecular Chemistry: From Molecules to Nanomaterials*, **2012**, Vol 6, 2799

[31] J.M. Robertson, *J. Sci. Instrum.*, **1943**, 20, 175

[32] J.M. Roberston and H.M.M. Shearer, *Nature*, **1956**, 177, 885

[33] L.J. Barbour, D. Das, T. Jacobs, G.O. Lloyd and V.J. Smith, in *Supramolecular Chemistry: From Molecules to Nanomaterials*, **2012**, Vol 6, 2884

[34] L. Loots and L.J. Barbour, in *The Importance of Pi-interactions in Crystal* Engineering, **2012**, 112

[35] C.A. Hunter and J.K.M. Sanders, The Nature of pi-pi Interactions, *J. Am. Chem. Soc*., **1990**, 112, 5525

[36] J. Zukerman-Schpector and E.R.T. Tiekink [ed.]., *The Importance of Pi-interactions in Crystal Engineering: Frontiers in Crystal Engineering*. John Wiley & Sons Ltd., **2012,** 41 - 46 and 109-124

[37] L. Zhang, S.M. Fakhouri, F. Liu, J.C. Timmons, N.A. Ran and A.L. Briseno, *J. Mater. Chem.*, **2011**, 21, 1329

[38] L. Loots and L.J. Barbour, *CrystEngComm*, **2012,** 14, 300

[39] ACD/Labs/ChemSketch., v.11.00, Advanced Chemistry Development, Inc., Toronto, On, Canada

[40] R.L. Collin, *Acta Cryst.*, **1952**, 5, 431

[41] G.R. Desiraju and T. Steiner, in *The Weak Hydrogen Bond In Structural Chemistry and Biology*, **1999**, 202, Oxford University Press

[42] J. Lipkowski, M. Pawlowska, D. Sybilska, *J. Chromatogr.*, **1979**, 176, 43

[43] C. Karunakaran, K.R.K. Thomas, A. Shunmugasundaram and R. Murugesan, *J. Mol. Struct.*, **2000**, 523

[44] W.D. Schaeffer, W.S. Dorsey, D.A. Skinner and C.G. Christian, *J. Am. Chem. Soc*., **1957**, 79

[45] J. Lipkowski, in *Inclusion Compounds formed by Werner MX_2A_4 coordination complexes. Inclusion Compounds*, **1984**, 1

[46] J. Lipkowsky, in *Werner Clathrates. Comprehensive Supramolecular Chemistry*, Polish Academy of Sciences, **1996**

[47] J. Lipkowski, in *Inclusion Compounds*, Vol 1**,** Chapter 3, Academic Press, New York, **1984**.

[48] I.S. Kerr and D.J. Williams, *Acta Crystallogr.*, **1977**, B33

[49] D.R. Bond, D.E. Jackson and L.R. Nassimbeni, *S. Afr. J. Chem.*, **1982**, 36

[50] D. V. Soldatov, G. D. Enright and J. A. Ripmeester, *Cryst. Growth Des.*, **2004**, 4, 1185.

[51] R. M. Barrer, in *Molecular Sieves, Adv. Chem. Ser.*; **1973,** Vol. 121, 1, W.M. Meier and J.B. Uytterhoeven, Eds.; American Chemical Society: Washington

[52] J. Lipkowski, in *XIth International Symposium on Supramolecular Chemistry*, Proceedings, 2000, Fukuoka (Japan), 64

[53] C. J. Adams, M. F. Haddow, D. J.Harding, T. J. Podesta and R. E. Waddington, *CrystEngComm*, **2011**, 13, 4909.

[54] S. Wohlert, I. Jess, U, Englert and C. Nather, *CrystEngComm*, **2013**, 5326.

[55] M. Lusi and L. J. Barbour, *CrystEngComm*, **2014**, 16, 36.

[56] M. Lusi and L. J. Barbour, *Angew. Chem. Int. Ed.*, **2012**, 51, 3928.

[57] E. Batisai, M. Lusi, T. Jacobs and L.J. Barbour, *Chem. Commun.*, **2012**, 12171.

[58] S. M. Soliman, Z. B. Elzawy, M. A. M. Abu-Youssef, J. Albering, K. Gatterer, L. Öhrström and S. F. A. Kettle, *Acta Cryst.*, **2014**, B70, 115.

[59] M.E. Brown, *Introduction to Thermal Analysis, Techniques and Applications*, Chapman and Hall, **1988**

[60] M.H. Moore, L.R. Nassimbeni, M.L.Niven and M.W. Taylor, *Inorg. Chim. Acta*, **1986**, 115, 211

[61] J. Lipkowski, *J. Mol. Struct.*, **1981**, 75, 13

[62] L.R. Nassimbeni, M.L. Niven and M.W. Taylor, *J. Chem. Soc. Dalton Trans.*, **1989,** 119

[63] A.W. Coats, J.P. Redfern, *Analyst,* **1963**, 88, 906

[64] Kirk-Othmer, *Separation Technology*, **2008**;Vol. 2, 2nd ed., Wiley, Hoboken

[65] J. Fabri, U. Graeser, T. A. Simo in *Ullmann's Encyclopedia of Industrial Chemistry*, **2000**, Wiley-VCH, Weinheim

[66] K.A.O. Santos, A.A. Dantas Neto, M.C.P.A. Moura and T.N. Castro Dantas, Separation of xylene isomers through adsorption on microporous materials: A review, *Brazilian Journal of Petroleum and Gas*, **2011**, 5, 255-268

[67] P. Trens, H. Belarbi, C. Shepherd, P. Gonzalez, N.A. Ramsahye, U-H. Lee, Y-K. Seo and J-S. Chang, *Micro. Mesopor. Mat.*, **2014**, 183, 17

[68] B. Wang, T-P. Huynh, W. Wu, N. Hayek, T.T. Do, J.C. Cancilla, J.S. Torecilla, M.M. Nahid, J.M. Colwell, O.Z. Gazit, S.R. Puniredd, C.R. McNeill, P. Sonar and H. Haick, *Adv. Mater.*, **2016**, 28, 4012

[69] A.M. Pivovar, K.T. Holman and M.D. Ward, *Chem. Mater*. **2001**, 13, 3018-3031

[70] J. Lewinski, T. Kaczorowski, I. Justyniak and D. Prochowicz, *Chem. Commun.*, **2010**, 47, 950-952

[71] A.M. Pivovar, K.T. Holman and M.D. Ward, *Chem. Mater.*, **2001**, 13, 3018

[72] M. Du, C-P. Li, C-S. Liu and S-M. Fang, *Coord. Chem. Rev.*, **2013**, 257, 1282 - 1305

[73] N.A. Mazlan, T.B.S.A. Ravoof, E.R.T. Tiekink, M.I.M. Tahir, A. Veerakumarasivam, and K.A. Crouse, *Transition Met. Chem*., **2014**, 39, 633 - 639

[74] J-T. Shi, K-F. Yue, B. Liu, Y-L Zhou, Z-G. Fang, and Y-Y. Wang, *CrystEngComm*., **2014**, 16, 3097 - 3102

[75] H.A. Habib, J. Sanchiz, and C. Janiak, *Dalton Trans*., **200**8, 13, 1734 - 1744

[76] C.A. Hunter and J.K.M. Sanders, *J. Am. Chem. Soc*., **1990**, 112, 5525

[77] C.B. Aakeröy, A.M. Beatty and D.S. Leinen, *Angew. Chem. Int. Ed.*, **1999,** 38, No. 12, 1815

[78] A. Werner, *Justus Liegig Ann. Chem.*, **1902**, 322, 261

[79] W.M. Latimer and W.H. Rodebush, *J. Am. Chem. Soc*., **1920**, 42, 1419

[80] L. Pauling, *J. Am. Chem. Soc.*, **1931**, 53, 1367

[81] P Gilli and G. Gilli, in *Supramolecular Chemistry; From Molecules to Nanomaterials*, **2012**, 6, 2829

[82] D.J. Sutor, *Nature*, **1962**, 68, 195

[83] D.J. Sutor, *J. Chem. Soc.*, **1963**, 1105

[84] R. Taylor and O. Kennard, *J. Am. Chem. Soc*., **1982**, 104, 5063

[85] J. Donohue, J. in Structural Chemistry and Molecular Biology; **1968**, 459, A. Rich, N. Davidson, Eds.; W. H. Freeman: San Francisco

[86] G.R. Desiraju, *Acc. Chem. Res.*, **1991**, 24, 290

[87] R. Taylor, *CrystEngComm*, **2014**, 16, 6852

[88] P. Dauber and A.T. Hagler, *Acc. Chem. Res.*, **1980**, 13, 105

[89] E.J. Corey, *Pure Appl. Chem.*, **1967**, 14, 19

[90] G.R. Desiraju and T. Steiner, in *The Weak Hydrogen Bond In Structural Chemistry and Biology*, **1999**, Oxford University Press, 293

[91] P. Brunet, M. Simard and J.D. Wuest, *J. Am. Chem. Soc.*, **1997**, 119, 2737

[92] G.R. Desiraju, *Angew. Chem., Int. Ed. Engl.*, **1995**, 34, 2311

[93] G.R. Desiraju, J.J. Vittal and A Ramanan, in *Crystal Engineering*, **2011**, IISc Press, World Scientific, 55

[94] M.C. Etter, *Acc. Chem. Res*, **1990**, 23, 120

[95] M.C. Etter, J.C. MacDonald and J. Bernstein, *Acta Cryst., Sect B*, **1990**, 46, 256

[96] C.B. Aakeröy and K.R. Sneddon, *Chem. Soc. Rev.*, **1993**, 22, 397

[97] C.B. Aakeröy, *Acta Cryst.*, **1997**, B53, 569

[98] C.B. Aakeröy, A.M. Beatty, and D.S. Leinen, *Angew. Chem. Int. Ed.* **1999**, 38, 12, 1815

[99] T. Friščič and W. Jones, *Cryst. Growth Des.*, **2009**, Vol. 9, No. 3, 1621

[100] T. Friščič, *Chem. Soc. Rev.*, **2012**, 41, 3493

[101] D. Hasa, E. Miniussi and W. Jones, *Cryst. Growth Des.*, **2016**, DOI:10.1021/acs.cgd.6b00682

[102] M.J. Fischer and A.M. Beatty, *CrystEngComm*, **2014**, 16, 7313

[103] J. Malakova, P. Pavek, L. Svecova, I. Jokesova, P. Zivny and V. Palicka, *J.Chromatogr. B*, **2009**, 877, 3226

Chapter 2

Experimental and Computational Methods

In this chapter, the general synthetic procedures for the host compounds and the clathrates are described. Techniques used for structural elucidation and full characterisation of the synthesised materials are presented.

Host Compounds

The following host compounds were prepared using a procedure initially recorded by Schaeffer *et al.*[1] and then pursued by Nassimbeni[2] who was instrumental in publishing a series of Werner clathrate studies between 1983 and 1993 with his co-workers.

$Ni(NCS)_2$ was prepared by adding NH_4NCS (2 mol,76.14 g) to $NiCl_2.6H_2O$ (1 mol, 237.72 g) and dissolving in ethanol. The solution, green in colour, was filtered to remove NH_4Cl precipitate. The Werner complex was synthesised with the slow addition of 4 mol of the ligand (plus 10% in excess) in an ethanolic solution with constant stirring according to the method of Bond.[3] In the case of **H1,** bis isothiocyanato tetrakis isoquinoline nickel(II), $Ni(NCS)_2(C_9H_7N)_4$; **H3,** bis isothiocyanato tetrakis 4-vinylpyridine nickel(II), $Ni(NCS)_2(C_7H_7N)_4$,; and **H5**, bis isothiocyanato tetrakis nicotinamide nickel(II), $Ni(NCS)_2(C_5H_6N_2O)_4$; precipitation occurred immediately. **H2**, bis isothiocyanato tetrakis 4-phenylpyridine nickel(II), $Ni(NCS)_2(C_{11}H_9N)_4$; **H4**, bis isothiocyanato bis isoquinoline bis 4-phenylpyridine nickel(II), $Ni(NCS)_2(C_9H_7N)_2(C_{11}H_9N)_2$; **H6,** bis isothiocyanato tetrakis isonicotinamide nickel(II), $Ni(NCS)_2(C_5H_6N_2O)_4$ and **H7**, bis isothiocyanato bis nicotinamide bis 4-isonicotinamide nickel(II) required overnight stirring at room temperature to allow the complex to precipitate. The compound was filtered and allowed to air dry for 24 hours. The purity of each host compound was confirmed by thermogravimetric analysis (TGA). All host compounds were of sufficient purity when synthesised and therefore were not recrystallised. Percentage yields obtained for the host complexes are **H1** (68.8%), **H2** (96.5%), **H3** (72.3%), **H4** (64.3%)**, H5** (97.4%), **H6** (70.5%) and **H7** (74.6%).

Details of the nickel Werner hosts synthesised and used for the following experimental chapters are given below. These include the molecular structures (Fig. 2.1); TG curves (Fig. 2.2) showing theoretical values under the curve and experimental values on the right of each curve, indicating the percentage mass loss found for the evaporation of each set of ligands; and PXRD profiles (Fig. 2.3)

obtained with Cu K_α (radiation λ = 1.5418 Å) of the solid starting materials used for each synthesis and final product produced.

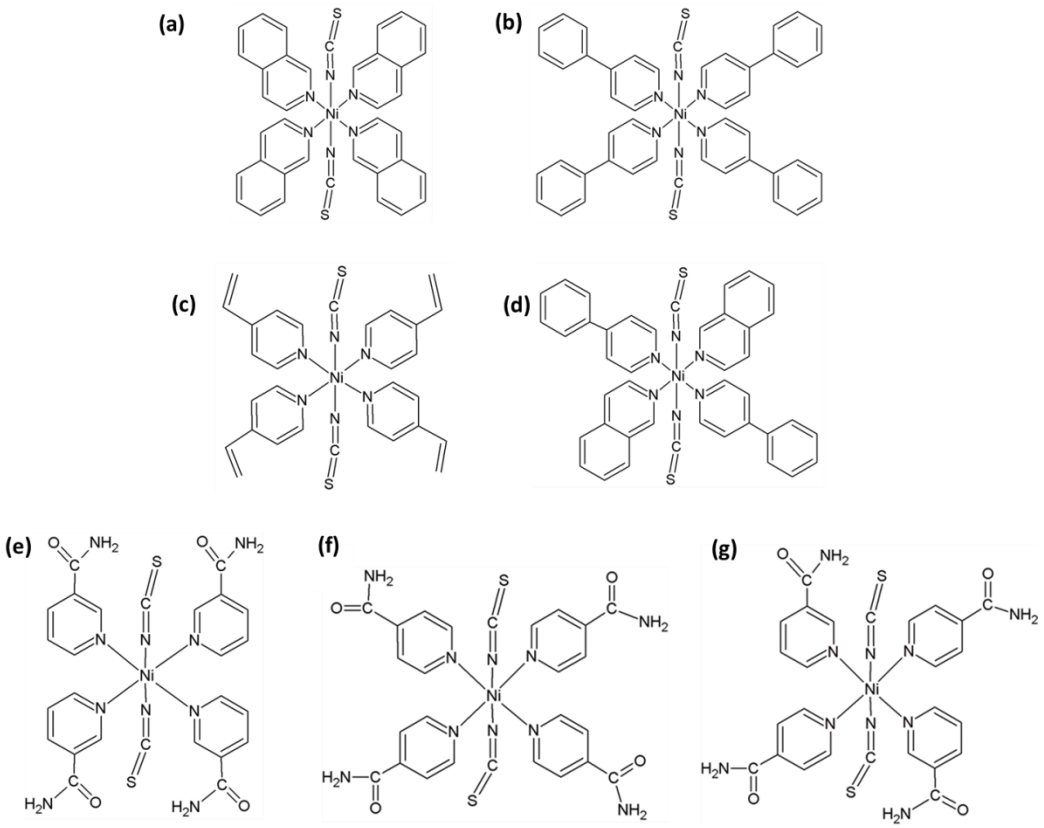

Figure 2.1 Structure of the hosts (a) **H1**; (b) **H2;** (c) **H3**; (d) **H4**; (e) **H5** ; (f) **H6** and (g) **H7**

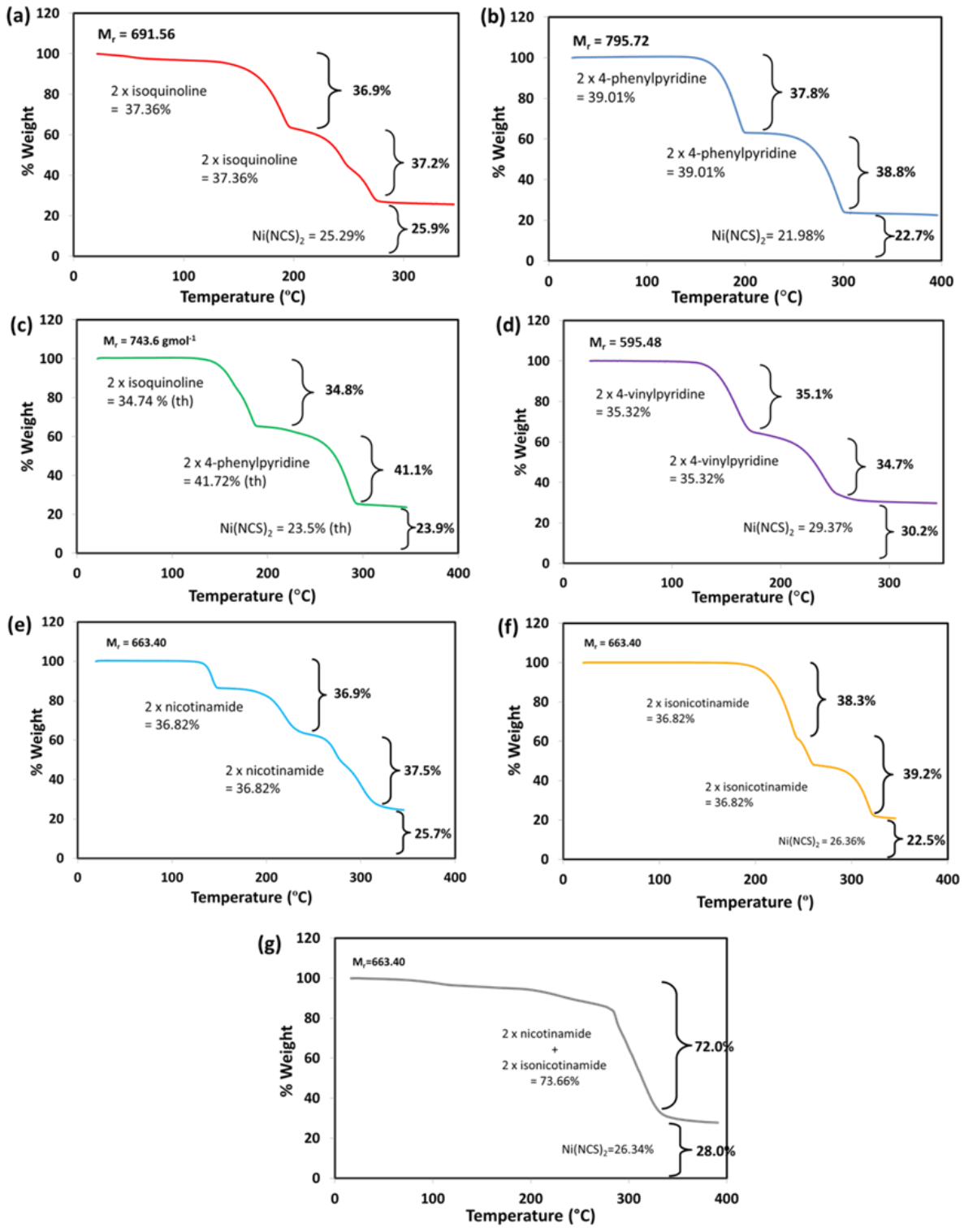

Figure 2.2 TGA curves for hosts **H1-H6**, showing the percentage loss of first 2 ligands, followed by percentage loss of second 2 ligands, with the final percentage $Ni(NCS)_2$ left at the end. In the case of **H7**, all four ligands were lost at the same time. Hosts as follows: (a) **H1**, (b) **H2**, (c) **H3**, (d) **H4**, (e) **H5**, (f) **H6** and (g) **H7**

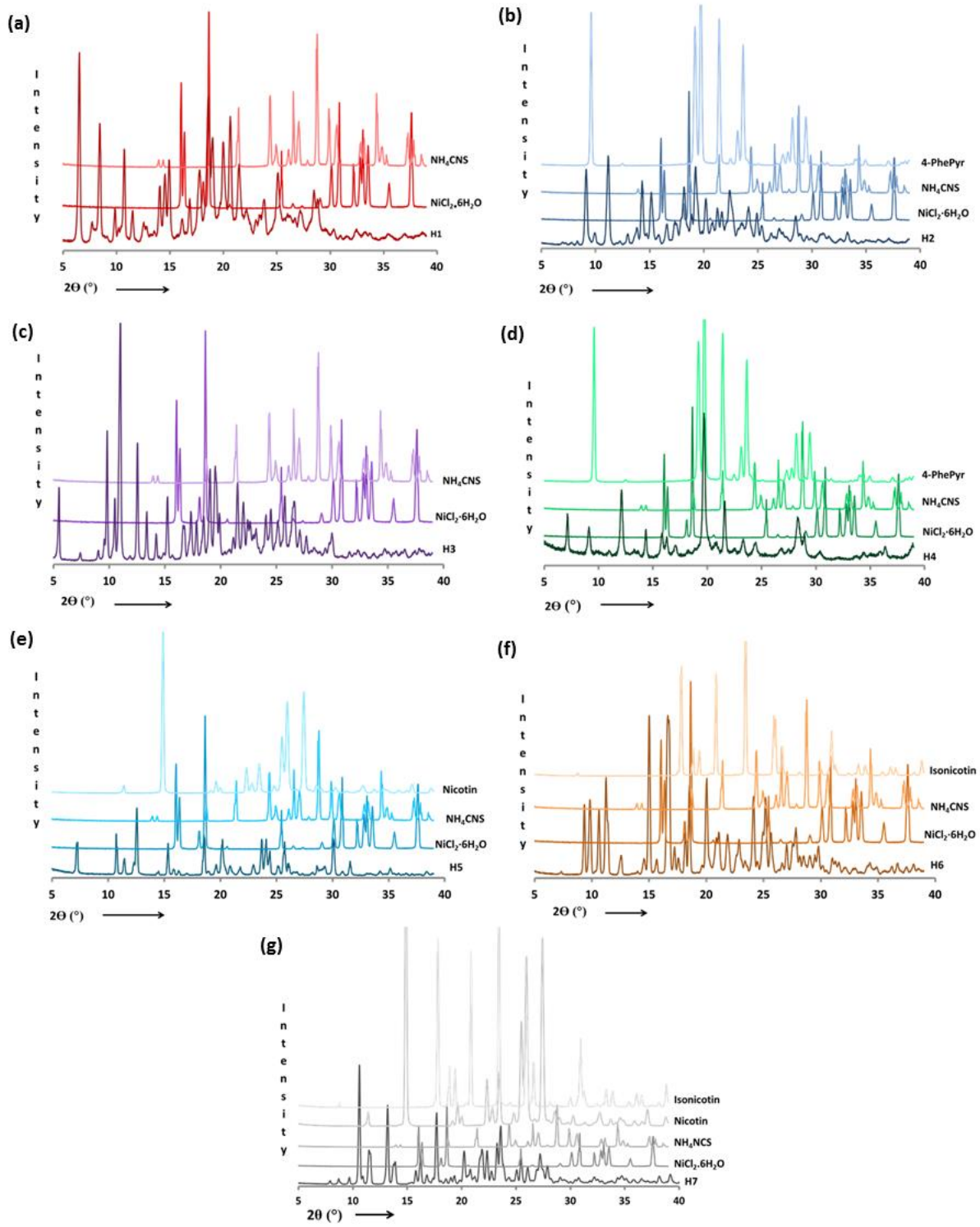

Figure 2.3 PXRD profiles showing the solid starting materials for host H1-H7 with the host profile. Note that label nicotin = nicotinamide and isonicotin = isonicotinamide in (e), (f) and (g)

Guest Compounds

Three xylene isomers (*para*-xylene (**px**), *meta*-xylene (**mx)** and *ortho*-xylene (**ox**) and ethylbenzene (**eb**)) and the polyaromatic hydrocarbons (PAHs), naphthalene, anthracene, phenanthrene, pyrene, fluorene, indene and azulene were purchased from Sigma-Aldrich chemical company. Alcohols (methanol, ethanol, 1-butanol, 1-pentanol, 2-methyl-1-propanol and 4-methylbenzoylalcohol) and ketones (dimethylformamide, 2-pentanone, 3-hexanone, pinacolone and 4-methylcyclohexanone) were guests in the 'sticky' ligand inclusion compounds. All guest compounds were used as supplied and no distillation, recrystallization, or other preparative work was necessary.

Crystal Growth

Three different methods of crystal growth were used, namely slow evaporation, crystal growth at low temperatures and slow cooling. In most cases, fixed molar ratios of host to guest were used although in some cases the guest was added in excess. Full details of the preparation of individual host-guest compounds are given in the relevant chapters.

- **Slow evaporation:** Crystals of the inclusion compounds were formed by dissolving the host compound in excess of guest(s) in the presence of a solvent (if needed). The solution was heated to 40 – 50 °C with stirring for 30 minutes and allowed to cool before filtering through 0.45 μm nylon syringe membranes. The solvent was allowed to evaporate slowly at room temperature with the vials left open, covered with pierced parafilm or sealed to respectively give decreasing rates of evaporation.
- **Crystal growth at low temperatures:** The crystal solutions were prepared as described in the previous section, sealed and placed in a refrigerator at a temperature of 4 °C.
- **Slow cooling:** Once the solution was prepared, the vials were sealed and placed in a thermoflask containing hot water and left to cool slowly overnight.

Mechanochemical Synthesis

Due to the demands on the chemical industry to manage the global problems of pollution and the growing energy crisis, the coupling of mechanical and chemical phenomena on a molecular scale to synthesize chemical products using only mechanical action has led to developments in areas of molecular cocrystals and metal-organic materials.[4] The process of kneading the host and guest together in a pestle and mortar, a ball mill or a vibratory mill, provided a solvent-free and environmentally friendly technique leading to different products. The host to guest ratio used was that of the inclusion compound grown from solution. The procedure was time controlled and the temperature monitored by using a brass mortar heated to the desired temperature. The product was analysed by powder X-ray diffraction (PXRD) and the profile compared with that derived from the single crystal structure. Extraordinary success in the creation of non-covalent interactions as well as metal-ligand coordination bonds and the development of liquid-assisted grinding (LAG, also known as kneading or solvent-drop grinding) has provided a means of systematic study in a solvent-free environment. [5] The kneading methodology, although introduced to increase the rate of multicomponent crystal formation, provided further benefits such as higher yield, higher crystallinity and control of polymorph formation.[6]

Solid-Vapour Experiments

Approximately 50 mg of host compound was spread in a watch glass and placed in a desiccator with a binary mixture of the volatile guests in a beaker below the perforated plate. The desiccator was closed or evacuated before keeping it at room temperature for a period of 18 to 60 hours to allow sorption to take place. The solid was removed from the desiccator, sorption determined by change in mass and the sample prepared for selectivity analysis by GC headspace or ^{1}HNMR spectroscopy.

Thermal analysis

The physical properties of the compounds were evaluated using thermogravimetric analysis (TGA). The changes in the physical properties of the sample as a function of the temperature were determined using this technique.

Thermogravimetric Analysis (TGA)

Thermogravimetric experiments were performed using a TA-Q50 instrument with 60 ml min^{-1} dry nitrogen gas flow rate and the results were analysed with the Universal Analysis 2000 software. The crystals of the inclusion compounds were lightly crushed and blotted dry on filter paper to remove surface solvent. The powdered sample mass of between 2 and 5 mg was placed in a tared crucible for the experiment. The programmed temperature runs started at 30 °C and ended at a temperature between 350 and 400 °C. Runs were recorded at 10 °C min^{-1} except in the case of the non-isothermal TGA curves analysed for the kinetic deterioration of the compounds.

The technique of TGA measures the change in the mass of a sample over a range of temperatures.[7] The sample pan which hangs off a hook is connected by a microgram balance arm to a tare pan. As the sample is heated, the composition or its thermal stability is determined by its mass changes. These are due to decomposition, reduction, evaporation or solvent loss. The change in weight of the sample is measured by the microgram balance and the temperature is monitored via a thermocouple. The weight loss of a sample as a function of temperature can be used to determine the stoichiometry of the inclusion compounds as the weight loss is usually due to guest release prior to ligand release. Accurate host to guest ratios are yielded with a precision of ~1%. These ratios are in turn used to assign the site occupancies of guest molecules when refining crystal structures.

Non-isothermal TGA experiments were performed at different heating rates viz. 2, 4, 8, 16 and 32 °C min^{-1} to measure the rate of weight loss against temperature using the method developed by Flynn and

Wall[8] for analysing the thermogravimetric rate. Activation energy calculations were completed over α ranges for each inclusion compound. The extent of reaction, is defined as

$$\alpha = (m_t - m_0)/(m_\infty - m_0)$$

with m_0 = initial mass, m_t = mass at time t and m_∞ = final mass. Plots of log β/β_0 *vs* 1000K/T for the compound where β is the heating rate provided the activation energies (E_a). β_0 is the standard heating rate, used in the y axis to prevent the log value from having units. These energies were calculated from the slopes

$$slope = -0.457\frac{E_a}{R}$$

and indicated the energy barrier associated with the thermal decomposition of the clathrates under consideration.

The author is aware that Werner clathrates can be non-stoichiometric with respect to Host : Guest ratios. However, in this thesis the guest mass loss as measured by Thermal Gravimetry was invariably within 1% of the theoretical value, and therefore stoichiometric formulae were employed, and site occupancy factors were not refined.

Competition Experiments

The selectivity of the host compound for a particular guest or isomer was evaluated using two different procedures, crystals obtained from mother liquor and solid-sorption technique. The experiments were performed between two or three guests or isomers at a time. In the case of binary competition experiments a series of six vials were prepared with mixtures of two guests such that the mole fraction of a given guest varied from 0 to 1 in steps of 0.2.

Crystals obtained from their mother liquor

Crystal formation of the host and guest mixture was performed using the crystal growth procedure as above. The host to guest ratio was kept constant with the guest present in excess relative to the host.

In general the ratio of total guest to host was at least 20:1. Crystals were harvested; blotted dry on filter paper and the relative amounts of the guests enclathrated in the crystals were determined by headspace gas chromatography.

Solid-sorption technique

The crushed host (approximately 50 mg) was exposed to a binary mixture of guests in an evacuated chamber at room temperature for 18 hours. The compound was removed from the chamber, weighed to determine the extent of sorption and analysed by headspace gas chromatography for the relative amounts of the guests absorbed. In some cases the 2-component competition experiments were extended to analyse simultaneous competition between three guests.

X-Ray Diffraction

Single crystal X-ray diffraction

This analysis was performed on good quality single crystals selected from the mother liquor. The crystals were immediately covered in Paratone oil® to prevent loss of included solvent or decomposition. A suitable single crystal was selected under a microscope and attached on a nylon loop connected to a rigid mounting on the goniometer head under a cold stream of nitrogen gas. Single crystal data collections were performed on one of two diffractometers. These were a Nonius Kappa CCD (charge-coupled device) Single Crystal X-ray Diffractometer using graphite-monochromated MoK_α radiation (λ = 0.71069 Å) generated by a Nonius FR590 generator operated at 50 kV and 30 mA or a Bruker DUO APEX II diffractometer[9] using MoK_α (λ = 0.71069 Å). X-rays were generated by a Bruker K780 generator powered at 50 kV and 30 mA. Data collections were carried out at low temperature (173(2) K) using a Cryostream cooler (Oxford Cryostems, UK) at a flow rate of 20 ml min^{-1}. Unit cell refinement and data reduction were carried out using the program SAINT.[10] The programme SADABS[11] was used to correct for Lorentz-polarisation and absorption effects on all intensity data.

For each structure, the space group was determined from systematic absences in the X-ray intensity data. The XPREP[12] program was used to confirm the space group. This programme prepares input files which are then used for structure solution by direct methods using the SHELXS[13] programme. All non-hydrogen atoms were located in the electron density map and refined by full matrix least squares minimisation of the sum of the squares of the differences between observed and calculated intensities ($\Sigma w(F_o^2 - kF_c^2)^2$).

During subsequent refinement the non-hydrogen atoms were allocated using anisotropic thermal parameters in the SHELXL[13] programme within the X-SEED[14] interface. The indirect measure of the accuracy of the structure, the residual index, *R*, is used to monitor the accuracy of the model. The agreement between measured and calculated structure factor amplitudes for the refinement against *F* is given by the residual index R_1 (expression 1), while the agreement between intensities for the refinement against F^2 is given by the residual index R_2 (expression 2).

$$R_1 = \frac{\sum||F_o|-|F_c||}{\sum|F_o|} \qquad (1)$$

$$wR_2 = \sqrt{\frac{\sum w(F_o^2 - F_c^2)^2}{\sum w(F_o^2)^2}} \qquad (2)$$

where F_0 values are the observed structure factors obtained from the measured reflection intensities, F_c values are the calculated structure factors derived from the model that is being refined and *w* is the weighting scheme. The residual index R_2 is based on F^2 resulting in it being two to three times larger than R_1. Comparison of the new structure solutions with the old ones based on *F* was done using the R_1 residual index.

During structure solution, a default weighting scheme, *w*, was used which is represented by the SHELX command WGHT 0.1. The weighting scheme (including the parameters *a* and *b*) is given by expression 3 and was refined for each structure at the end of the structure refinement where *P* is given by expression 4.

$$w = \frac{1}{\sigma^2 F_o^2 + (aP)^2 + bP} \qquad (3)$$

$$P = \frac{\max(0, F_o^2) + F_c^2}{3} \qquad (4)$$

For each structure the Goodness of Fit (*S*) was quoted and is based on F^2 (expression 5)

$$S = \left(\frac{\sum w(F_o^2 - F_c^2)^2}{n - p} \right)^{\frac{1}{2}} \qquad (5)$$

where *n* is the number of reflections and *p* is the total number of parameters refined.

In cases of severe disorder some non-hydrogen atoms were refined with isotropic temperature factors and specific details will be given in the data chapters. Hydrogen atoms were placed with geometric constraints and were refined with isotropic temperature factors. Ideal bond lengths (± 0.005 Å) and angles were achieved by applying the DFIX restraints in situations of disorder. Structure solution and refinement details for all individual structures are described in the relevant chapters.

The author is aware of the problems of locating the hydrogen atoms with X-ray diffraction data. If the intensity data collection is carried out at room temperature (≈ 298 K), their positions may not be revealed in the final difference electron density map. At lower temperatures (≈ 170 K) they are generally easier to locate and often appear with electron densities of ≈ 0.5 $eÅ^{-3}$. However, their positions do not correspond to the true nuclear positions, because the electron density is shifted towards the atom to which the hydrogen is covalently bonded. Therefore, if the hydrogen atom is allowed to refine freely, the typical bond length C-H is ≈ 0.95 Å and ≈ 0.9 Å for N-H and O-H.

When bonded to C, the hydrogen atoms can be placed geometrically and refined as a 'riding model'. This is not generally the case when we consider hydrogen bonding, typically of the type N-H···O and O-H···N. The author is aware of the article by Lusi and Barbour[15] which allows the calculation of the hydrogen atoms obtained from the distances between the donor and acceptor atoms D-H···A, based on data derived from neutron diffraction. However, this method was not employed, because it

generally gave rise to higher R factors and we relied on the D···A distances to infer the existence of the hydrogen bonds.

Powder X-ray diffraction (PXRD)

Powder diffraction experiments were performed on a Bruker D8 Advance diffractometer equipped with a Lynxeye detector using CuK_α radiation (λ = 1.5406 Å) at 298 K (25 °C). Samples crushed to a fine powder were placed on a zero background sample holder which rotated 10 r.p.m. and scanned over the 2θ range of 4 ° to 40 ° with a step size of 0.02 ° giving a total of 1758 steps. X-rays were generated by a current flow of 40 mA and an accelerating voltage of 30 kV. A receiving slit of 0.6 mm and primary and secondary slits of 2.5 mm were used. The total time of exposure of the sample to radiation was 20 minutes. The generated powder data were saved as text files and the PXRD traces plotted using Excel.

Calculated powder X-ray diffraction patterns were generated by LAZY PULVERIX[16] from single crystal X-ray data. The programme calculated PXRD patterns using the same X-ray source (λ = 1.5406 Å) as that used experimentally. These patterns are used to determine the phase purity of the bulk material by comparing them to the experimental PXRD patterns. Experimental PXRD patterns were also use to check that the desired product was made.

Gas chromatography

Gas chromatography was used to analyse host-guest inclusion compounds and to interpret the results of 2- and 3-component competition experiments. The relative amounts of the guests present in the starting solution and in crystals were analysed. Qualitative identification of the components was verified using high purity standards. GC analysis was performed on an Agilent 7890A instrument with Varian CP Wax capillary column (30 m x 250 μm x 0.25μm), nitrogen carrier gas and FID detector with inlet and detector temperatures of 280 °C.

The samples resulting from the competition experiments were prepared for GC analysis as follows:

In the case of liquid or volatile guests, crystals of the inclusion complexes were removed from the mother liquor and blotted dry on filter paper. The crystals were placed in air-tight glass headspace vials with silicone seals incorporated into screw-on lids. The vials were incubated at 60 °C for 10 minutes before injection onto the GC column.

The temperature gradient of the GC set to the following conditions:

The oven temperature was set at 30 °C for 3 minutes, followed by a gradient at 10 °C min^{-1} to 120 °C for 2 minutes.

The computer package ChemStation [17] was used to monitor and analyse the results. The gas chromatograph was calibrated using mixtures of known standard concentrations.

Computer Packages

The following computer packages were used for the analysis of crystal structures:

All molecular packing diagrams were created using **POV-RAY**.[18]

LAZY PULVERIX[16] was used for generation of calculated XRD traces from the crystal structure solution. Input to this programme included atomic fractional coordinates, thermal parameters and space group data.

X-SEED [19] was used as a graphical interface for SHELXS-97, SHELXL-97, POV-RAY, LAZY PULVERIX and SECTION[20]

The Cambridge Structural Database (CSD)[21,22] was used for investigation of the published crystal data for the comparison with the inclusion compounds presented in this thesis.

References

[1] W.D. Schaeffer, W.S. Dorsey, D.A. Skinner and C.G. Christian, *J. Am. Chem. Soc.*, **1957**, 79, 5870

[2] (a) D.R. Bond, G.E. Jackson, L.R. Nassimbeni, *S.Afr. J. Chem.*, **1983**, 36, 19 – 26;

(b) L.R. Nassimbeni, S. Papanicolaou and M.M. Moore, *J. Incl.Phen.*, **1986**, 4, 31 – 42;

(c) M.M. Moore, L.R. Nassimbeni, M.L. Niven and M.W. Taylor, *Inorg. Chim. Acta*, **1986**, 115, 211 – 217;

(d) M.M Moore, L.R. Nassimbeni and M.L. Niven, *J, Chem. Soc., Dalton Trans.*, **1987**, 2125 – 2140; (e) M.M. Moore, L.R. Nassimbeni and M.L. Niven, *Inorg. Chim. Acta*, **1987**, 131, 45 – 52;

(f) M.M. Moore, L.R. Nassimbeni and M.L. Niven, *Inorg. Chim. Acta*, **1987**, 132, 61 - 66;

(g) L.R. Nassimbeni, M.L. Niven and M.W. Taylor, *Inorg. Chim. Acta*, **1987**, 132, 67 - 73;

(h) L.R. Nassimbeni, M.L. Niven and A.P. Suckling, *Inorg. Chim. Acta*, **1989**, 159, 209 – 217; (i) L.R. Nassimbeni, M.L. Niven and M.W. Taylor, *J. Chem. Soc. Dalton. Trans.*, **1989**, 119;

(j) L.R. Nassimbeni, M.L. Niven and M.W. Taylor, *Acta. Cryst.*, **1990**, B46, 354 – 361;

(k) L. Lavelle and L.R. Nassimbeni, *J. Incl. Phen. Mol. Rec.Chem.*, **1993**, 16, 25 – 54

[3] D.R. Bond, in *Structures of Werner Clathrates*, MSc thesis, University of Cape Town, **1982**, 15

[4] T. Friščič, I. Halasz, V. Štrukil, M. Eckert-Maksić and R.E., Dinnebierd, *Croat. Chem. Acta.*, **2012**, 85, 367–378

[5] T. Friščič, *Chem. Soc. Rev*., **2012**, 41, 3493

[6] T. Friščič and W. Jones, *Cryst. Growth Des.*, **2009**, Vol.9, 3, 1621

[7] A.W. Coats, J.P. Redfern, *Analyst*, **1963**, 88, 906

[8] J.H. Flynn and L.A. Wall, *Polymer Letters*, **1966**, 4, 323

[9] Bruker **2005**. APEX2. Version 1.0-27. Bruker AXS Inc., Madison, Wisconsin, USA

[10] Bruker **2004**. SAINT-Plus (including XPREP). Version 7.12. Bruker AXS Inc., Madison, Wisconsin, USA

[11] G.M. Sheldrick, *SADABS, version 2.05*, **2007**

[12] XPREP, Data Preparation and Reciprocal Space Exploration, Version 5.1 © Bruker Analytical X-ray Systems, **1997**

[13] (a) G.M. Sheldrick, SHELXS-97, Program for Crystal Structure Solution, University of Göttingen, Germany, **1997**, (b) G.M. Sheldrick, SHELXL-97, Program for Crystal Structure Solution, University of Göttingen, Germany, **1997**

[14] L.J. Barbour, *J. Supramol. Chem.*, **2001**, 1, 189

[15] M. Lusi and L.J. Barbour, *Cryst. Growth Des.*, **2011**, 11, 5515

[16] K. Yvon, W. Jeitschko and E. Parthé, *J. Appl Cryst.*,**1977**, 46, 371

[17] ChemStation, Rev., A.10.02 [1757], Copyright©Agilent Technologies **1990 – 2003**

[18] Pov-Ray for Windows, Version 3.1e.watcom.win32, The persistence of vision development team, © **1991-1999**

[19] L.J. Barbour, X-SEED, A graphic interface to SHELX, University of Missouri, Columbia, USA, **1999**

[20] L.J. Barbour, *J. Appl. Cryst.*, **1999**, 32, 353

[21] C. R. Groom, I. J. Bruno, M. P. Lightfoot and S. C. Ward, *Acta Cryst.*, **2016**, B72, 171-179

[22] F. H. Allen, *Acta Cryst*., **2002**, B58, 380-388

Chapter 3

Isoquinoline-based Werner clathrates with xylene isomers: Aromatic interactions vs. molecular flexibility

The crystal structures of the Werner clathrates $Ni(NCS)_2(isoquinoline)_4$ (**H1**) with *para*-xylene (**px**), *meta*-xylene (**mx**) and *ortho*-xylene (**ox**) have been elucidated. The kinetics of thermal decomposition of the three inclusion compounds were performed using the isothermal technique. Selectivity of **H1** for the xylene isomers was determined for both the liquid and vapour phase binary mixtures of the guests. The chosen ligand has a larger aromatic system to improve the possible π interactions between **H1** and the selected xylenes. The planarity of the isoquinoline ligand causes **H1** rigidity and its selectivity was compared to a related Werner complex containing the more pliable 4-phenylpyridine using Hirshfeld surfaces and fingerprint plots of close interactions. The flexibility of torsion angles in a range of pyridine derivative ligands was investigated to substantiate the findings for lack of selectivity with this host.

Publication of Chapter 3:

Isoquinoline-based Werner clathrates with xylene isomers: Aromatic interactions vs. molecular flexibility

Merrill M. Wicht, Nikoletta B. Báthori and Luigi R. Nassimbeni

Dalton Trans., **2015**, 44, 6863 – 6870

DOI: 10.1039/c5dt00084j

This chapter has been published in Dalton Transactions and has been structured according to the journal's format

Introduction

In this chapter we present the structures, thermal decomposition kinetics and the selectivity of the Werner host [$Ni(NCS)_2$(iso-quinoline)$_4$, **H1**] with *para*-, *meta*- and *ortho*-xylene (**px**, **mx** and **ox**, respectively). The ligand isoquinoline has a fused ring structure which according to the Cambridge Structural Database[1], has previously only been encountered once as a ligand in Werner clathrates[2] but its selectivity was not investigated. This ligand was chosen because its two fused rings give it a large aromatic surface area which is important for C-H···π and π···π host:guest interactions. The structural line diagrams and atomic numbering scheme for the **H1** and the xylene guests are shown in Scheme 3.1.[3]

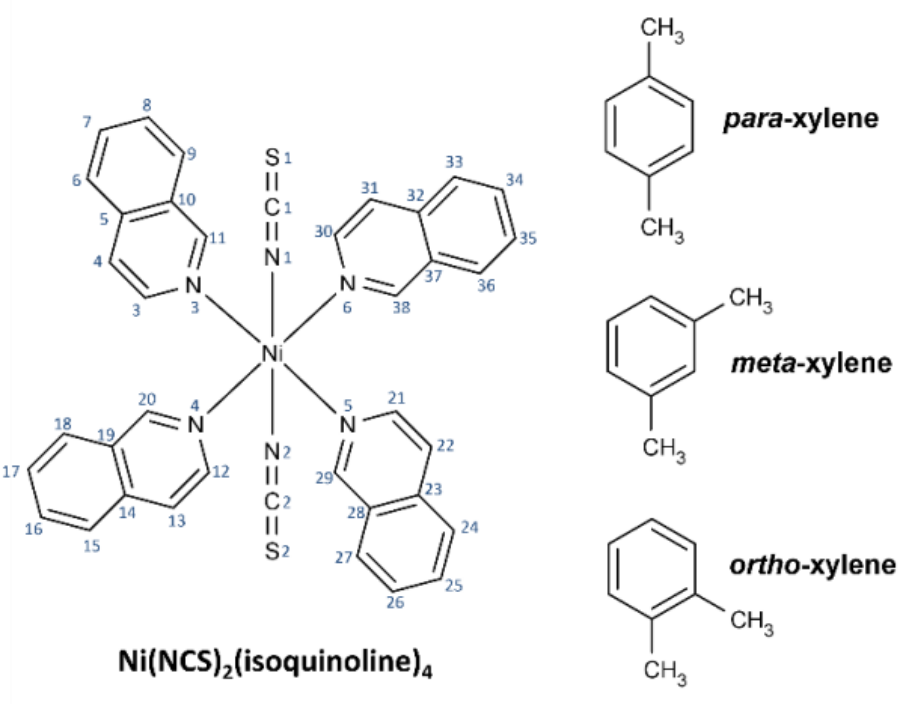

Scheme 3.1 Structural line diagrams and atomic numbering scheme of the host, $Ni(NCS)_2$(isoquinoline)$_4$, and the xylene isomers

Results and discussion

Crystal structures of H1•px, H1•mx and H1•ox

The structure of **H1•px** was solved in the hexagonal space group $P6_1$ (No. 169) and the details of the data collection and refinement are summarised in Table 3.1. The asymmetric unit consists of one host and one guest molecule (Fig.3.1(a)). The host is positioned in *Wyckoff* position *a* and severely disordered. Two of the isoquinoline ligands lying *trans* across the Ni centre are disordered and eventually were modelled with 50% site occupancy. The final model of the ligand had refined the C and N atoms anisotropic and the Hs with the usual riding model. The other two isoquinoline ligands and the thiocyanate groups were ordered and refined uneventfully. The atomic positions of the **px** guest were located unequivocally from the difference electron density map. However, convergence of the refinement could only be achieved with the guest treated isotropically with appropriate bond length constrains. The ordered **px** molecules are situated in cavities (Fig. 3.1(b), **px** is presented with spacefill model, red) and form a helical arrangement along the *c* axis (Fig 3.1(c)).

Table 3.1 Crystallographic data for **H1•px, H1•mx** and **H1•ox**

	H1•px	**H1•mx**	**H1•ox**
Chemical Formula	$Ni(NCS)_2(C_9H_7N)_4$• C_8H_{10}	$Ni(NCS)_2(C_9H_7N)_4$• C_8H_{10}	$Ni(NCS)_2(C_9H_7N)_4$• C_8H_{10}
Host:guest ratio	1:1	1:1	1:1
Formula Weight	797.65	797.65	797.65
Temperature/K	133(2)	133(2)	133(2)
Crystal System	hexagonal	hexagonal	monoclinic
Space Group (no.)	$P6_1$ (no.169)	$P6_5$ (no.170)	$C2/c$ (no. 15)
a/Å	10.7810(15)	10.8390(15)	10.671(2)
b/Å	10.7810(15)	10.8390(15)	19.132(4)
c/Å	59.780(12)	59.167(12)	59.609(12)
α/°	90	90	90
β/°	90	90	91.49(3)
γ/°	120	120	90
V/A^3	6017.3(17)	6019.9(17)	12166(4)
Z'/Z	1/6	1/6	1.5/12
D_{calc}/$Mg.m^{-3}$	1.321	1.320	1.302
Radiation type	MoKα	MoKα	MoKα
F(000)	2496	2466	4956
Crystal size/mm	0.41 x 0.45 x 0.51	0.24 x 0.26 x 0.53	0.08 x 0.19 x 0.34
Colour, crystal form	Blue, octahedral	Blue, octahedral	Blue, octahedral
No. of total reflections	8794	5150	9660
No. of unique reflections	7094	4048	7315
$\Theta_{min-max}$/°	2.04/ 27.12	12.00/ 26.89	2.13/ 27.26
$R[F^2>2\sigma(F^2)]$	0.0692	0.0461	0.0686
$wR2(F^2)$	0.1963	0.1055	0.1595
S	1.017	1.028	1.057
No. of parameters/data	680/8794	667/5150	893/9660
Res.peak(max/min)/e A^{-3}	0.336/-0.723	0.229/ -0.166	0.796/ -0.622

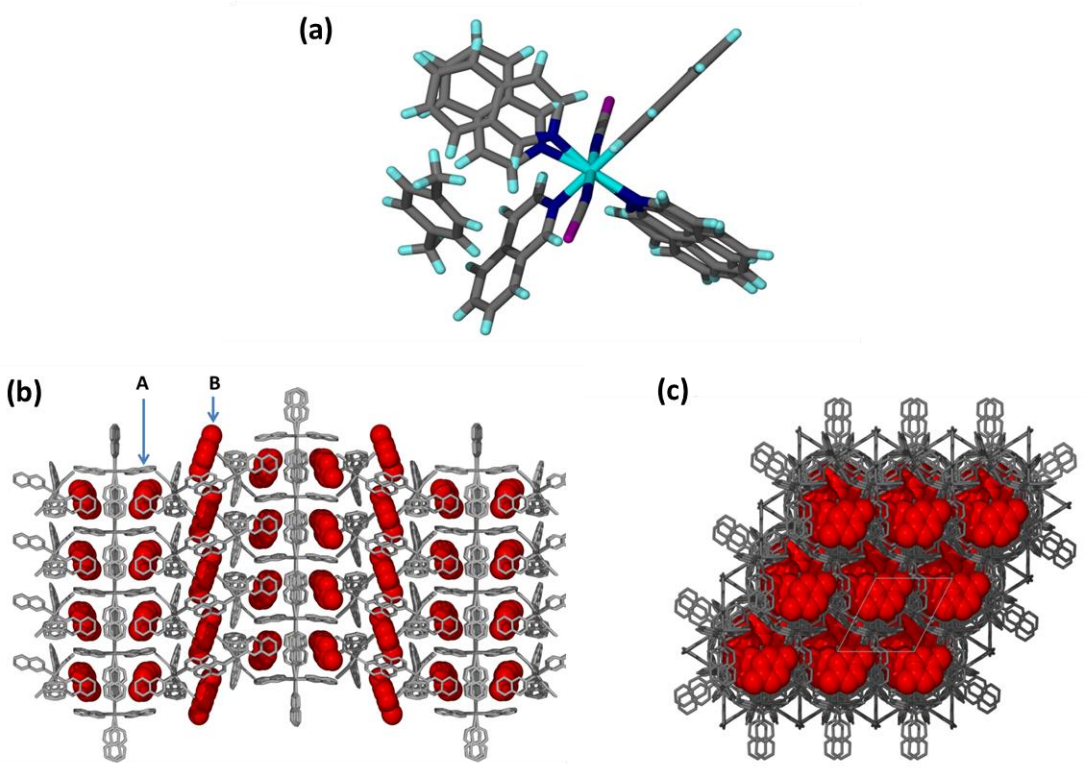

Figure 3.1. Structure of **H1•px** ((a) molecular structure, (b) packing viewed down *a*, **px** is presented with spacefill model, red and (c) helical arrangement viewed down *c*

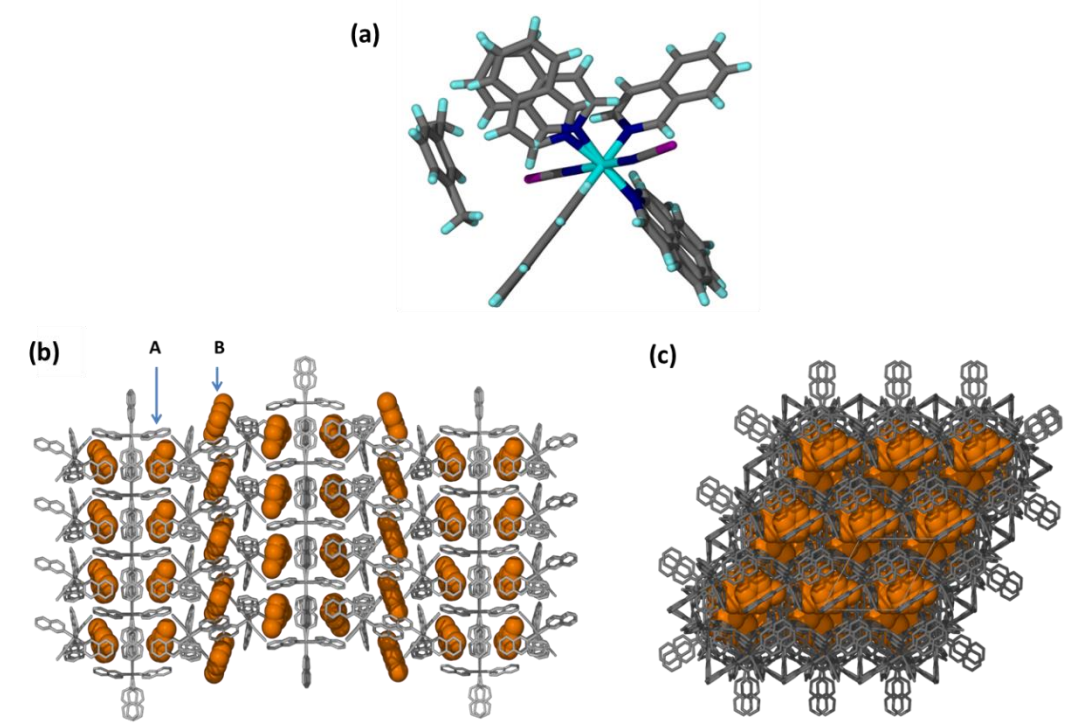

Figure 3.2 Structure of **H1•mx** ((a) molecular structure, (b) packing viewed down *a*, **mx** is presented with spacefill model, orange) and (c) the honeycomb structure when viewing down *c*.

The **H1•mx** structure displays similar features to that of the **H1•px** and crystallised in the $P6_5$ (No. 170) space group. The asymmetric unit contains one host and one guest and the host positoned in *Wyckoff* position *a*. In a similar manner to **H1•px,** the host has two ordered and two disordered isoquinoline ligands which were refined with 50% S.O.Fs (Fig 3.2(a)). The **mx** guest is ordered and positioned in cavities (Fig. 2(b)) and the packing is enantiomeric with **H1•px** and when viewing along [001] a framework resembling a honeycomb structure is observed (Fig. 2(c)).

The structure of **H1•ox** was solved in the monoclinic *C*2/*c* (No. 15) space group. One host molecule is in a general position (*Wyckoff f*) and one is located in a diad (*Wyckoff e*). Similarly, one guest is in a general position and the second guest is on a centre of inversion (*Wyckoff b*), thus the asymmetric unit is composed of 1.5 host and 1.5 guest molecules (Fig. 3.3(a)). The host molecule in the general position has one of its four isoquinoline ligands which is disordered and refined to S.O.Fs 77% and 23%, while the host molecule in a special position has two of the ligands located on the diad, which are disordered. Both the ordered (Fig. 3.3(b), molecule A, yellow) and the disordered guest (Fig. 3.3(b), molecule B, green) are located in cavities. The structure shows remarkable similarity with **H1•px** and **H1•mx** from [100] direction. The lack of honeycomb packing is shown in Fig 3.3(c) and is due to the disordered guest overlapping with the host ligands.

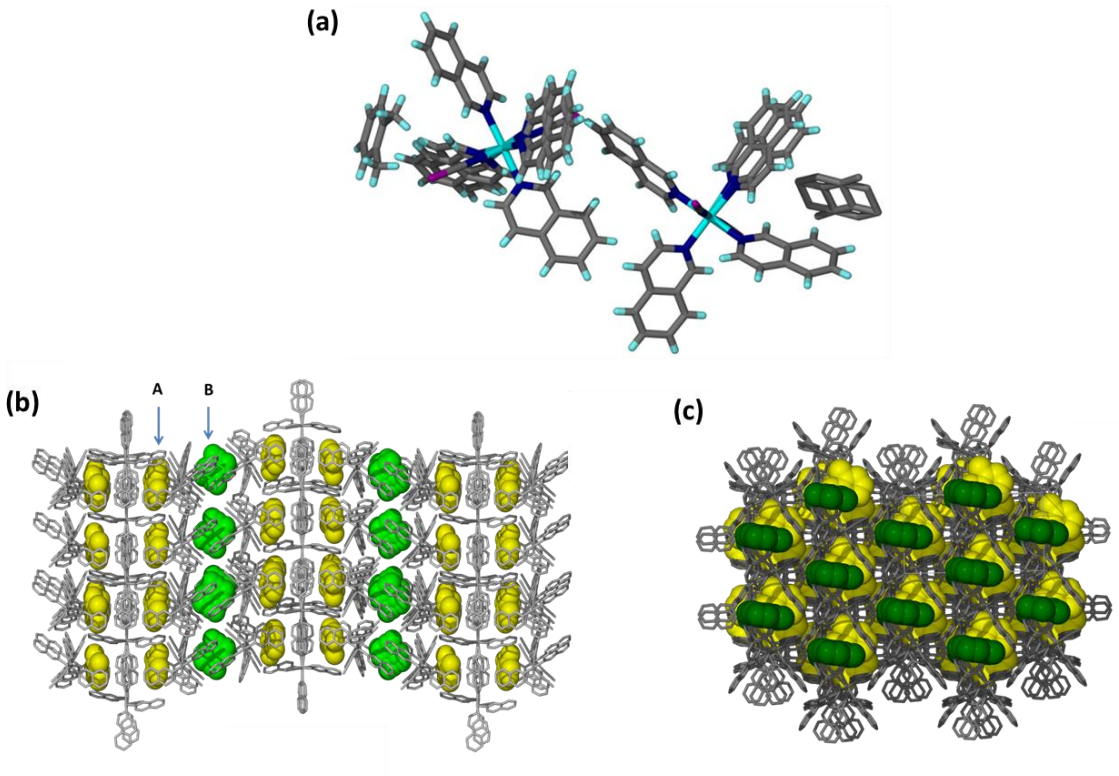

Figure 3.3 Structure of **H1•ox** ((a) molecular structure, (b) packing viewed down *a*, **ox** is presented with spacefill model, yellow and green) and viewed along [001], there is a lack of honeycomb packing due to the disordered guest in green overlapping with the host ligands

The intermolecular interactions between the xylene guests and the host framework were analysed using the program Crystal Explorer[4] which calculates the Hirshfeld surface[5] of a target molecule in a crystal structure and depicts all its interactions with the neighbouring molecules. Fig. 3.4 shows the **px** guest surrounded by its Hirshfeld surface when enclosed by host molecules and the generated fingerprint plot[6], the 2D representation of the 3D surface. The red areas on the surface indicate C-H···π close contacts between the **px** and the hosts. The fingerprint plot was generated using one pair of the two disordered isoquinoline moieties. The resulting plot, generated by using the alternative pair of ligands, is very similar. The C···H contacts are highlighted in blue, and comprise ca. 48% of the interactions. The upper lobe, labelled ①, represents close contacts between the **px** hydrogens to the aromatic system of the host, while the lower lobe ② shows the contacts between the hydrogens of the ligands and the aromatic region of the **px**. The structure also displays a number of C-H···π interactions between the host molecules. Fig.3.5 displays the **mx** guest in its Hirshfeld surface and the

corresponding fingerprint plot shows a similar environment for the guest to the **H1·px** structure with ca. 47% C···H contacts. In case of **H1•ox**, the disordered guest was not analysed. The Hirshfeld surface of the ordered guest shows less intensive interactions with the nearby hosts (smaller area on Fig. 3.6). This corresponds to the amount of observed C···H contacts (ca. 44%) and their generally longer nature. Interestingly there are significant (**ox**)C-H···S(host) contacts with (d_i+d_e)= 2.7Å. This type of hydrogen bonding has previously been identified by Đaković et al. in Ni(II) complexes.[7]

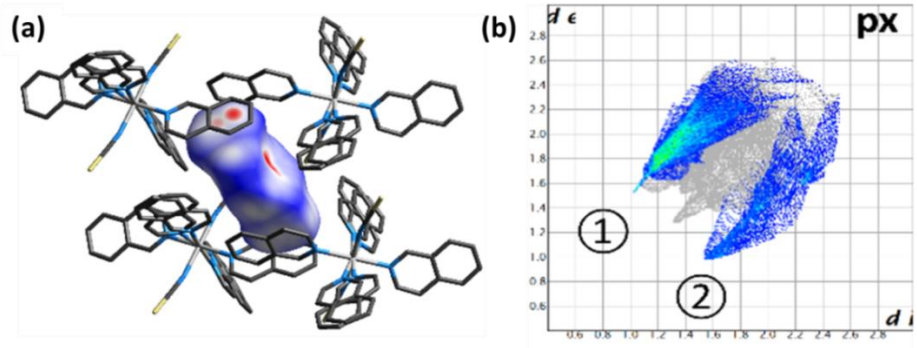

Figure 3.4 (a) Hirshfeld surfaces and their (b) fingerprint plots of **px**; ① indicates close contacts between the guest hydrogens to the aromatic system of the host, while ② shows the contacts between the ligand hydrogens and the aromatic region of the guest.

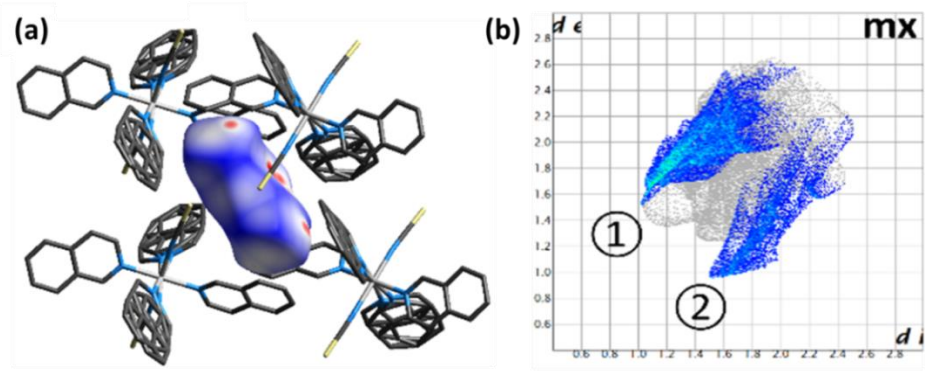

Figure 3.5 (a) Hirshfeld surfaces and their (b) fingerprint plots of **mx,** ① indicates close contacts between the guest hydrogens to the aromatic system of the host, while ② shows the contacts between the ligand hydrogens and the aromatic region of the guest.

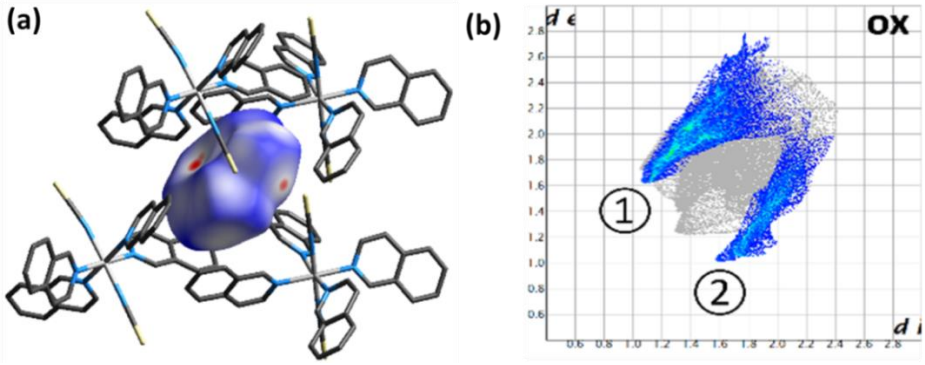

Figure 3.6 (a) Hirshfeld surfaces and their (b) fingerprint plots of **ox** (ordered guest only); ① indicates close contacts between the guest hydrogens to the aromatic system of the host, while ② shows the contacts between the ligand hydrogens and the aromatic region of the guest.

Kinetics of thermal decomposition

The kinetics of thermal decomposition of all three inclusion compounds were carried out by the non-isothermal technique of Flynn and Wall.[8] Desorption curves were recorded at fixed heating rates β = 2, 4, 8, 16 and 32 K min^{-1} for all three clathrates. A set of curves for **H1•px** is shown in Fig. 3.7. The decomposition takes place in three distinct steps. **Step 1** represents the disintegration of the inclusion compound via loss of the guest. This step is calculated as a 13.3% loss in mass. **Step 2** and **Step 3** correspond to the decomposition of the host, in each step the mass loss of two isoquinoline ligands at a percentage loss of 32.4% each. The observed and calculated mass losses are summarised in Table 3.2.

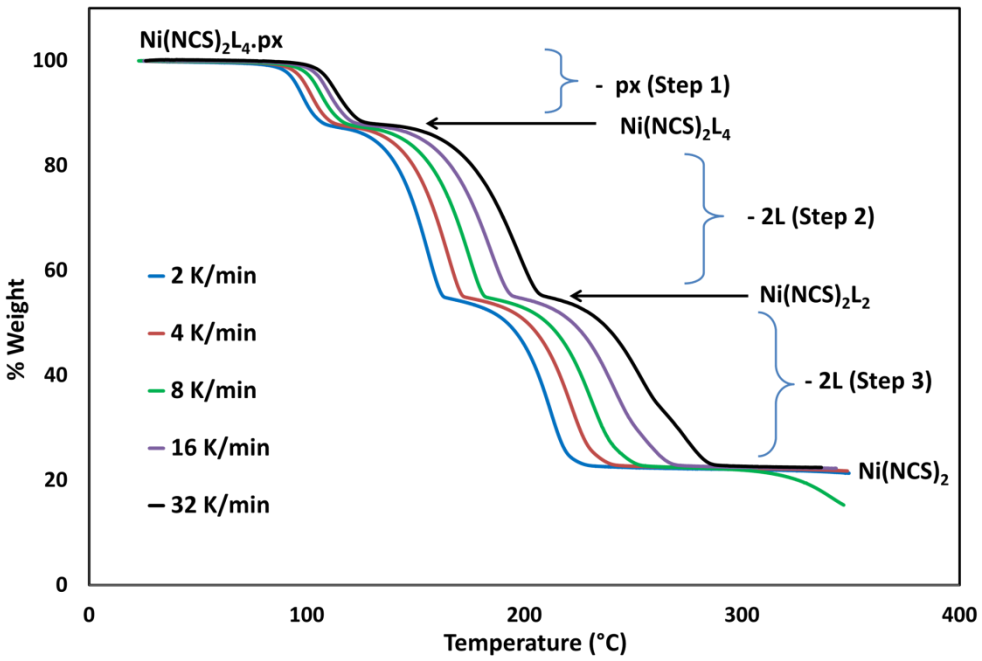

Figure 3.7 Non-isothermal TG curves for **H1•px**

The decomposition curves of **H1•mx** and **H1•ox** are similar and are shown in Fig. 3.8 and Fig. 3.9, respectively. The calculated and experimental TG results for **H1•px**, **H1•mx** and **H1•ox** are summarised in Table 3.2.

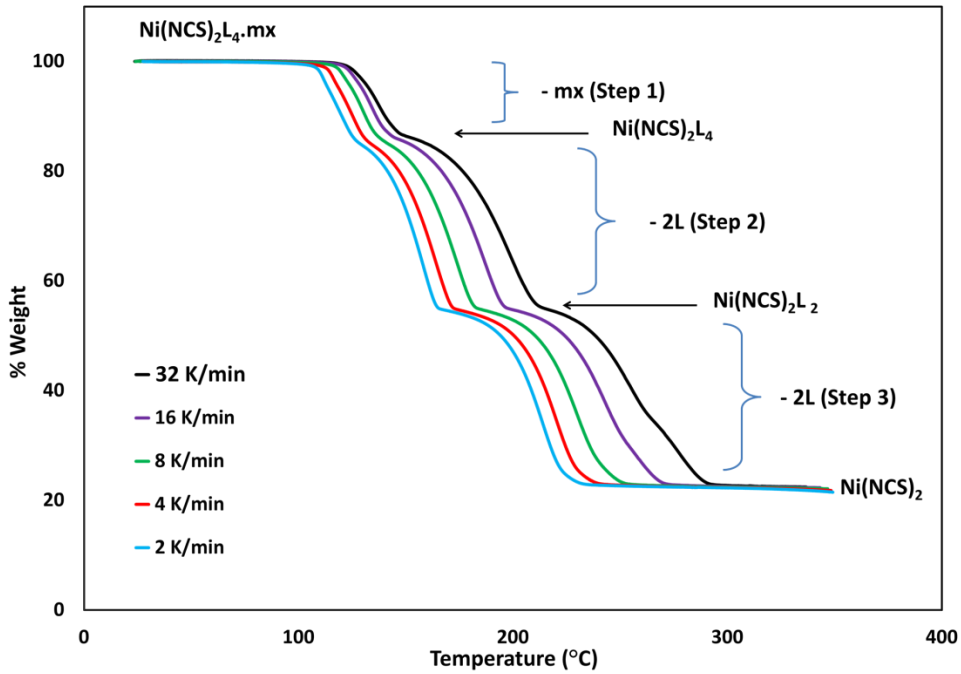

Figure 3.8 Non-isothermal curves for **H1•mx**

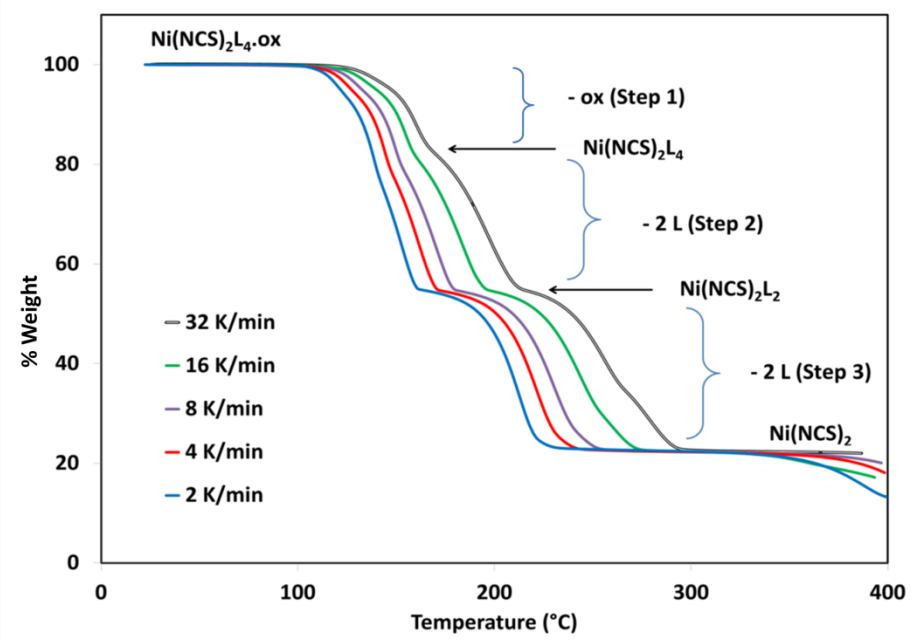

Figure 3.9 Non-isothermal curves for **H1•ox**

Table 3.2 Thermal analysis results for **H1•px**, **H1•mx** and **H1•ox**

Compound / Mass Loss	**H1•px** Exp (Calc) %	**H1•mx** Exp (Calc) %	**H1•ox** Exp (Calc) %
Step 1	13.1 (13.3)	13.1 (13.3)	13.2 (13.3)
Step 2	32.3 (32.4)	32.1 (32.4)	31.8 (32.4)
Step 3	32.1 (32.4)	31.8 (32.4)	32.1 (32.4)

The observed mass losses are all within 1% of their calculated values. In addition the various decomposition curves all begin and end at the same values in figures 3.7, 3.8 and 3.9. This may be regarded as an excellent experimental result of thermal decomposition under variable temperature conditions.

For **Step 1** the mass loss corresponding to the loss of 1 mole of guest and activation energy were calculated over α ranges for each of the three inclusion compounds and are indicated in Table 3.3. The extent of reaction is defined in Chapter 2. Plots of log β *vs* 1/T for the **H1•px** where β is the heating rate are given in Fig. 3.10. The activation energies for α positions 0.2, 0.5 and 0.75 of **Step 1** are

illustrated in Fig. 3.10(a). Similarly, **Step 2** at α positions 0.2, 0.5 and 0.8 and **Step 3** at α positions 0.3, 0.45 and 0.6 are demonstrated in Fig. 3.10(b) and 3.10(c), respectively.

The activation energies for the three thermal decomposition steps for each compound are shown in Table 3.3. Graphical information for **H1•mx** and **H1•ox** are given in Fig. 3.11 and Fig. 3.12 respectively. **Step 1** decomposition reaction required the largest activation energy. The activation energy for **Step 2** is the lowest for the three steps and is 105-108 for **H1•px,** 103-116 for **H1•mx** and 93-100 kJ.mol^{-1} for **H1•ox**. The higher values of the activation energies associated with the loss of the volatile xylene guests can be justified in terms of the topologies of the structures of the clathrates. In each case the xylene guest is trapped in a cavity, thus requiring a severe disruption of the host framework in order to release the guest. The effect of topology on the thermal stability and kinetics of decomposition of inclusion compounds has been reviewed[9] and, in general, structures that may be described as intercalates are less stable than tubulates which, in turn are less stable than cryptates. The latter often have higher activation energies of desorption. This is because in intercalates, guest molecules have two-dimensional freedom of movement upon desorption, while in tubulates they have one and in cryptates they are completely entrapped.

Table 3.3 Activation energy ranges for thermal decomposition (kJ.mol^{-1})

Reaction Step	H1•px	H1•mx	H1•ox
Step 1	178 – 192	170 – 177	138 – 142
Step 2	105 – 108	103 – 116	93 – 100
Step 3	115 – 120	118 – 120	112

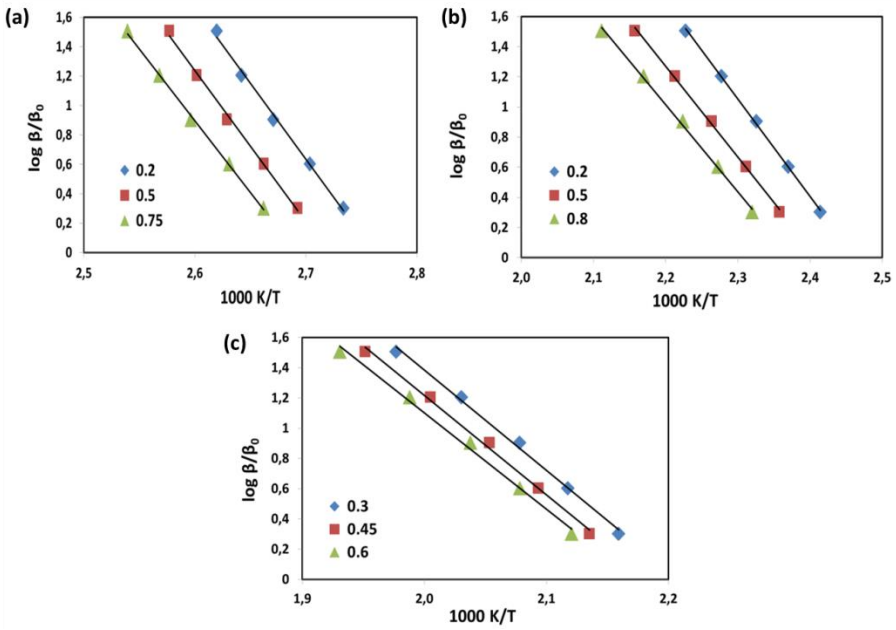

Figure 3.10 Activation energies for (a) **Step 1**, (b) **Step 2** and (c) **Step 3** for **H1•px**

β_0 is defined as the standard heating rate of 1 K min^{-1}. The reason for plotting log β/β_0 vs $1/T$ rather than log β is because the logarithm of a parameter with units is not allowed, because a dimensionless argument is necessary for the log function.

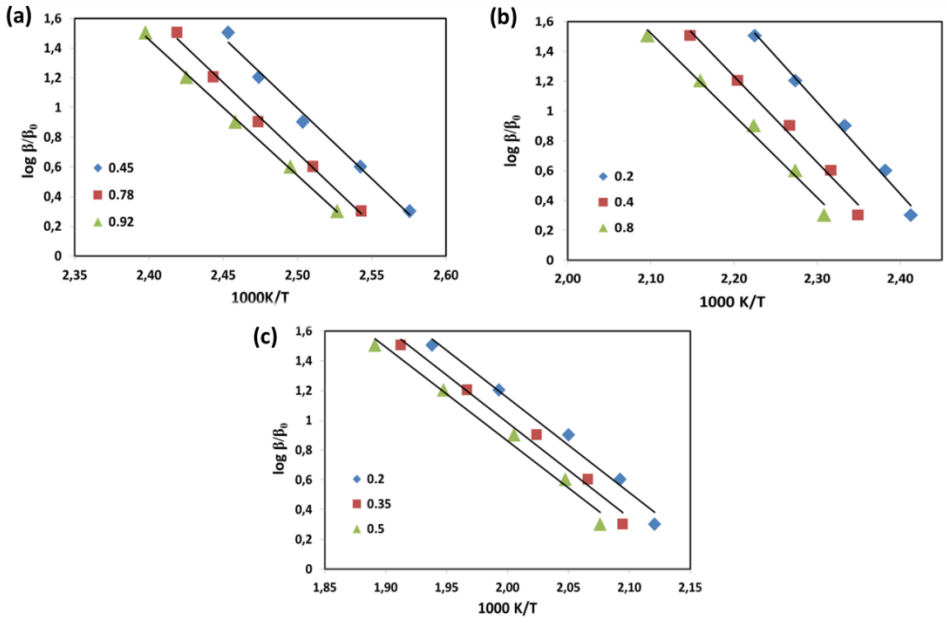

Figure 3.11 Activation energies for (a) **Step 1**, (b) **Step 2** and (c) **Step 3** for **H1•mx**

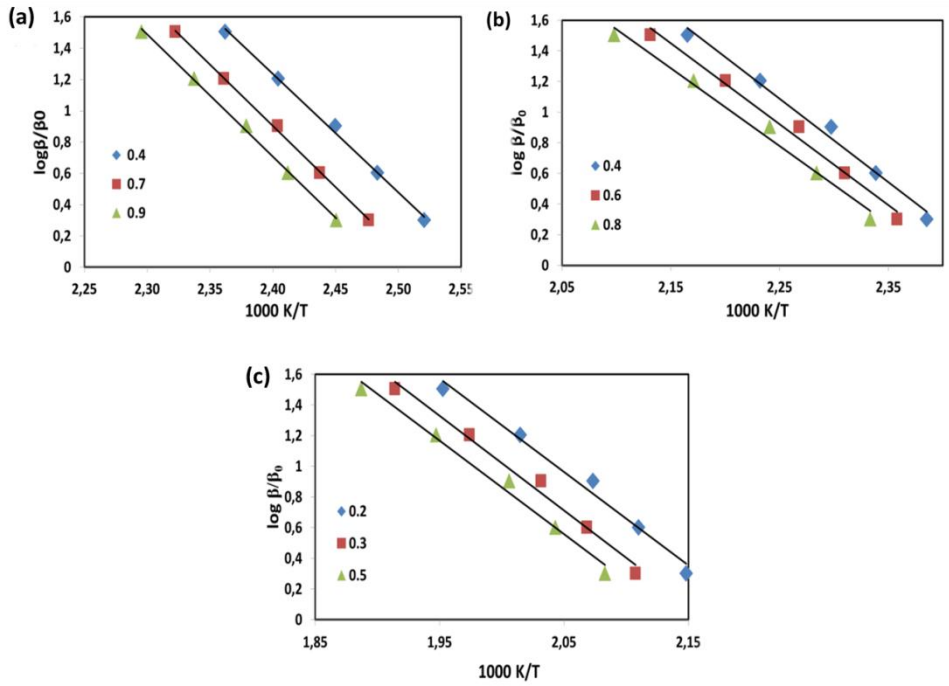

Figure 3.12 Activation energies for (a) **Step 1**, (b) **Step 2** and (c) **Step 3** for **H1•ox**

Selectivity experiments

Experiments to determine the selectivity profile of this host were carried out by two methods. Firstly by dissolving the host in liquid mixtures of the guests with known proportions and harvesting the crystals of the ensuing inclusion compounds for analysis; secondly by exposing the powdered apohost to mixtures of the guest vapours (solid vapour sorption) and subsequent analysis by headspace gas chromatography. These competition experiments between pairs of xylene isomers (**ox/px**, **ox/mx** and **mx/px**) were performed at different molar ratios (0:1; 0.2:0.8; 0.4:0.6; 0.6:0.4; 0.8:0.2 and 1:0). The crystals were harvested, dried and lightly crushed for analysis.

The results of the competition experiments are shown in Fig. 3.13 in which the mole fraction of a given guest in solution (X_{guest}) is plotted against its mole fraction in the solid state (Z_{guest}). In Fig. 3.13(a) a small amount of preference is shown for **ox** over **px** for the composition mixture of **ox/px.** Fig. 3.13(b) indicates the selectivity of **ox** compared with **mx** in the crystal structure with the host shows no preference for one over the other. Similarly in Fig. 3.13(c) there is no preference for the host to enclathrate one of **mx** or **ox** over the other. Selectivity for both procedures (crystallisation and

solid-vapour sorption) is shown graphically and no preference for either of the two xylenes is observed. That is, in all three cases no selectivity is found for one of the isomers over the other two.

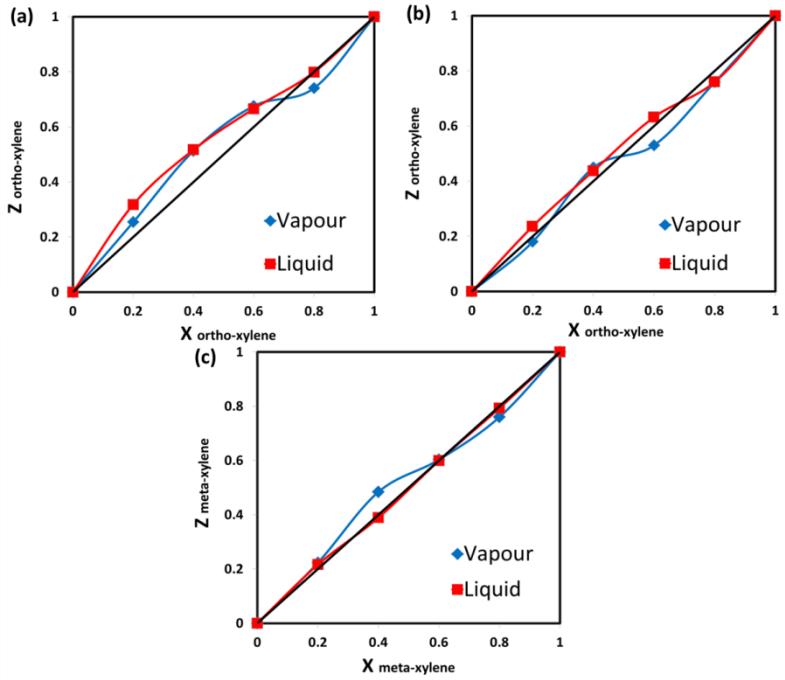

Figure 3.13 Selectivity curves for (a) **ox/px**; (b) **ox/mx** and (c) **mx/px**

Discussion

The question to be addressed is why the isoquinoline host under discussion, **H1**, is not selective towards any of the xylene isomers either from liquid or vapour mixtures, while the host bis(isothiocyanato) tetrakis(4-phenylpyridine) nickel (II), **H2**, has been shown to discriminate efficiently between *ortho*-, *meta*- and *para*-xylenes.[10] Competition experiments with the latter host between equimolar pairs of two isomers and an equimolar mixture of all three xylenes in the vapour state, show the preference for enclathration to be in the order **ox** > **mx** > **px**. We have therefore analysed the non-bonded interactions which occur between a given guest and this host. We have chosen to compare the structures containing the *ortho*- and *meta*-xylene guests, because they are similar in that they both have a host:guest ratio of 1:1, while the structure of *para*-xylene has a host:guest ratio of 1:3. The Hirshfeld surfaces of the **ox** and **mx** molecules were calculated and their fingerprint plots were generated (Fig. 3.14)

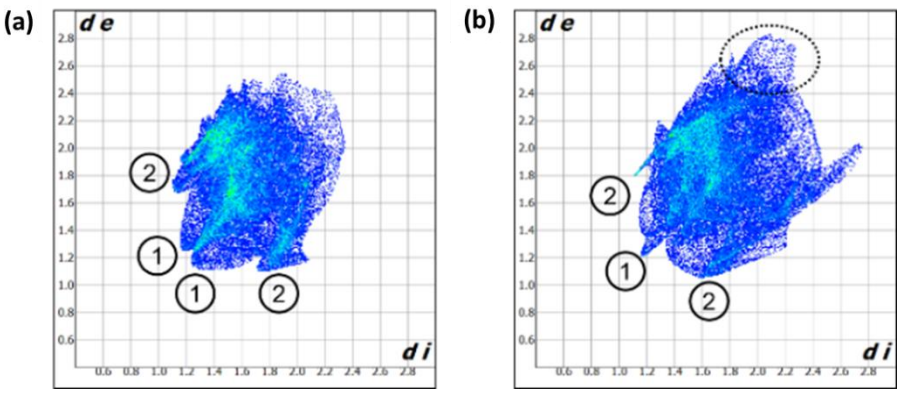

Figure 3.14 Fingerprint plots for (a) **ox** guest and (b) **mx** guest in their inclusion compounds with $Ni(NCS)_2$(4-phenylpyridine)$_4$, **H2**

Figure 3.14(a) shows the fingerprint plot of the **ox** guest. The two peaks labelled ① are associated with H···H interactions at $(d_i+d_e) \approx 2.48$ Å (57% of the close contacts) while those labelled ② are due to C···H contacts with $(d_i+d_e) \approx 2.87$ Å (37%). In contrast, the **mx** structure, shown in Fig. 3.14(b), has H···H contacts labelled ① at 2.43 Å (68%) and C···H contacts, labelled ② at 2.85 Å (28%). The Hirshfeld surface analysis supports the experimental results and explains why the host favours the **ox** guest. Also it demonstrates that the H···H and C···H interactions occur at similar distances, slightly over the sum of the van der Waals radii of 2.40 and 2.90 Å[11] respectively, but there is a greater percentage of C···H attractions in the **ox** structure and the circled area in Fig. 3.14(b) shows that there are many long H···H contacts, resulting in a less efficient packing of the **mx** structure.

In addition to the host-guest non-bonded interactions, however, the host with 4-phenylpyridine ligands possesses considerable torsional flexibility in its pyridine and phenyl rings. This fact has been discussed in detail previously.[12] The labelling of the four torsion angles (τ_1, τ_3, τ_5 and τ_7) between the pyridine ring and the thiocyanato ligand (N-Ni-N-C) was carried out cyclically in a manner to yield the minimum in the sum of the square of their differences. The eight torsion angles of each of the three structures have been tabulated and labelled as before[11] (Fig. 3.15) and their values are summarized in Table 3.5. It was noted that the differences in the torsion angles τ_3 and τ_4 as well as τ_7

and τ_8 observed in the **mx** structure indicated large rotations of the phenyl ring (Table 3.5 for **mx**, Δ values in bold) compared with τ_1/τ_2 and τ_5/τ_6 differences. The selectivity for **mx** is less than **ox** but greater than **px**. In the case of **ox**, alternating positive and negative torsion rotations are observed (τ_1/τ_2 and τ_5/τ_6 negative; τ_3/τ_4 and τ_7/τ_8 positive). This attests to the fact that this is a highly flexible ligand, which easily adapts to the requirement of a given guest, rendering it selective.

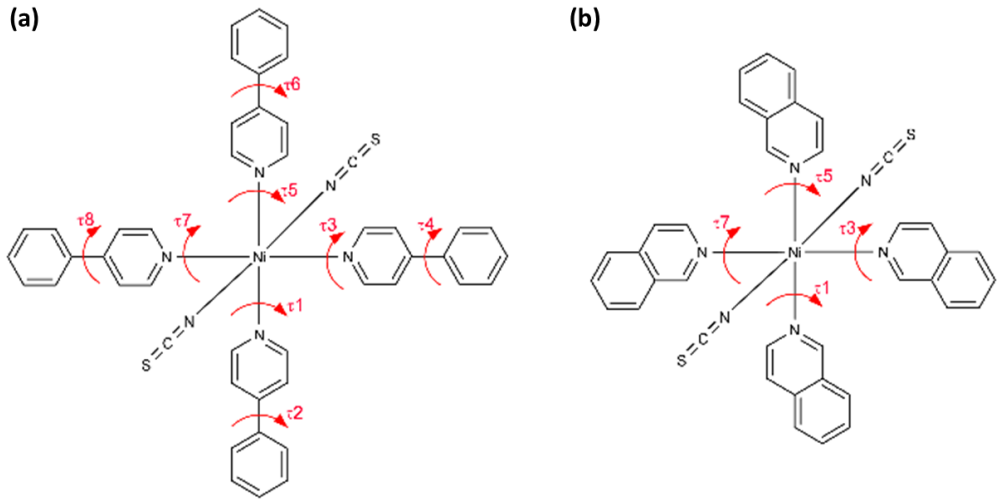

Figure 3.15 Torsion angles in (a) $Ni(NCS)_2(4\text{-phenylpyridine})_4$, **H2** and (b) $Ni(NCS)_2(4\text{-isoquinoline})_4$, **H1**

Table 3.5 Torsion angles of $Ni(NCS)_2(4\text{-phenylpyridine})_4$, **H2**, in its crystals of xylene isomers.

Guest	τ_1 / τ_2	τ_3 / τ_4	τ_5 / τ_6	τ_7 / τ_8
px	23.0	34.6	40.2	39.7
	34.7	19.2	40.0	27.1
Δ	-11.7	15.4	0.2	12.6
mx	20.3	20.8	46.6	34.4
	21.8	-29.7	15.5	-30.1
Δ	-1.5	**50.5**	31.1	**64.5**
ox	32.4	39.7	34.1	43.9
	45.1	25.7	44.4	31.3
Δ	-12.7	14.0	-10.3	12.8

The torsion angles describing the pyridine moieties in the currently investigated host **H1** (τ_1, τ_3, τ_5 and τ_7) are remarkably similar to previously analysed compounds. They correspond to the 'four-blade

propeller' configuration found in the structures of analogous compounds containing pyridine (**W1**), 4-methyl- (**W2**), 4-vinyl- (**W3**), and 4-phenylpyridines (**W4**). This corresponds to the ++++ configuration described by Lipkowski.[13,14] Table 3.6 and Fig. 3.16 show the range of torsion angles for these apohosts, as well as the torsion angles for the currently discussed three structures **H1•px**, **H1•mx** and **H1•ox.** Despite presenting four positively rotated ligands in the isoquinoline host **H1**, the torsion angles also indicate two large and two smaller angles. This shows compensation for the interaction of the host with the guest, whereas, in the apohost structures, no guest is present.

Table 3.6 Torsion angles τ_1, τ_3, τ_5 and τ_7 for **H1** and some typical nickel Werner clathrates where the ligands are pyridine (**W1**), 4-methyl- (**W2**), 4-vinyl- (**W3**), and 4-phenyl- (**W4**) pyridine.

Compound	τ_1 (°)	τ_3 (°)	τ_5 (°)	τ_7(°)
H1•px	16.5	49.9	17.9	50.3
H1•mx	24.5	25.1	48.3	50.3
H1•ox	24.2	50.8	26.4	59.3
W1	15.7	21.6	51.6	34.5
W2	30.4	39.8	35.7	40.6
W3	33.3	36.8	44.5	38.5
W4	29.2	36.0	43.9	48.0

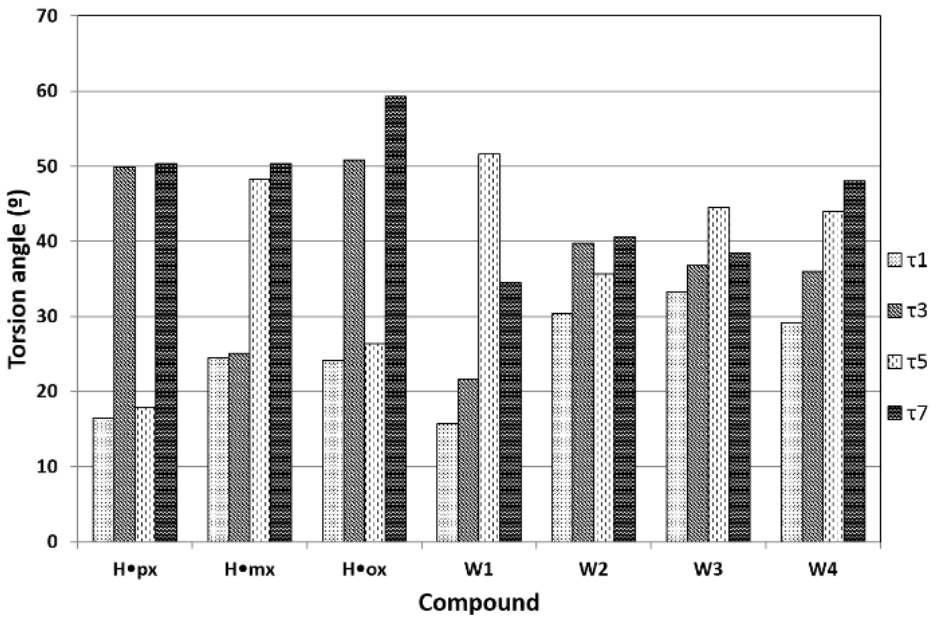

Figure 3.16 Bar chart showing Werner complex torsion angles based on values presented in Table 3.6

Conclusion

A Werner clathrate $Ni(NCS)_2(isoquinoline)_4$, **H1**, has been synthesised and its properties elucidated. Due to the importance of the xylene isomers in the petroleum industry, *para*-, *meta*- and *ortho*-xylenes were considered as the guests in this study. Single crystal structures of the host-guest compounds were analysed and the packing established. The analysis of the fingerprint plots revealed the importance of the C-H···π interactions and unique C-H···S interactions were observed in the **H1•ox** structure.

The non-isothermal technique of Flynn and Wall was used to record the kinetics of thermal decomposition of the three inclusion compounds. Similar plots for the three compounds show initial loss of the guest, followed by two steps, each denoting the mass loss of two isoquinoline ligands.

The selectivity of **H1** towards the xylene isomers was determined using two methods, viz. solid vapour sorption and crystallisation from a liquid solution of host and a binary mixture of two of the guests. The results were analysed using headspace gas chromatography. No significant preference for one of the xylene isomers over the other two was found, showing poor selectivity of this host.

The poor selectivity of this host **H1** was compared to that of the related host $[Ni(NCS)_2(4\text{-phenylpyridine})_4$, **H2**. The success of the latter host was attributed to the torsional flexibility of the phenyl moieties in the ligands. In contrast, the isoquinoline ligands, although containing larger aromatic systems, have no such flexibility and their relative conformation is largely controlled by their *ortho*-hydrogens.

Experimental Section

Preparation of Werner clathrate

The host compound, **H1**, bis (isothiocyanato) tetrakis (isoquinoline) nickel(II), was prepared by adding stoichiometric quantities of an ethanolic solution of isoquinoline (20 ml, 0.01 M) to an

ethanolic solution of nickel-isothiocyanate (5 ml, 0.01 M). Blue crystals of $Ni(NCS)_2(C_9H_7N)_4$ formed immediately and were filtered and allowed to air dry overnight.

Enclathration of any given xylene guest was carried out by dissolving the host in benzene, adding the xylene isomer (**px**, **mx** and **ox**) dropwise and stirring at 60 °C for 30 minutes, cooling and filtering. Crystallisation occurred within 24 hours. Deep blue crystals of **H1•px**, **H1•mx** and **H1•ox** were formed.

Single crystal X-ray analysis

Intensity data of a selected single crystal for compounds **H1•px**, **H1•mx** and **H1•ox** were collected on a Bruker DUO APEX II diffractometer[15] with graphite monochromated Mo $K_{\alpha 1}$ radiation (λ = 0.71073 Å) at 173 K using an Oxford Cryostream 700. Data reduction and cell refinement were performed using *SAINT-Plus*.[16] The space group was determined from systematic absences by *XPREP*.[17] The structure was solved using *SHELXS-97*[18] and refined using full matrix least squares methods in *SHELXL-97*[28] with the aid of the program *X-Seed*.[19] The hydrogen atoms bound to carbon atoms were placed at idealized positions and refined as riding atoms. Diagrams and publication material were generated using *PLATON*,[20] *X-Seed* and *Mercury (3.1)*.[21] Crystal data and structure refinement parameters are given in Table 1. CCDC 1041252-1041254 contain the supplementary crystallographic data for structures **H1•px**, **H1•mx** and **H1•ox**; all files are included in the Supplementary Data.

Powder X-ray diffraction

Powder X-ray diffraction experiments were carried out on a Bruker D8 diffractometer using Cu K_α (1.5406 Å) radiation. The sample was ground to a fine powder and loaded onto a zero background silicon sample holder in the instrument. The spectrum was run from 2θ values of 4º to 40º.

Thermogravimetric analysis

Thermal analyses were performed on a TA Q500 instrument from 25 to 400 °C at a heating rate of 10 ºC min^{-1} for comparison of the percentage mass loss with the expected compound. For kinetic studies, the non-isothermal runs were performed at 2, 4, 8, 16 and 32 °C min^{-1} with a purge gas of dry nitrogen

flowing at 60 ml min^{-1}. All samples were dried on filter paper and placed in an open crucible for thermogravimetric analysis. Sample masses varied from 2 to 5 mg.

Competition experiments

The selectivity of the host for a particular isomer was evaluated using two different procedures and analysing both by headspace gas chromatography. The first was a solid-vapour experiment in which crushed host was exposed to a mixture of two xylene guests in an evacuated chamber at room temperature for 18 hours. The compound was removed from the chamber, dried and placed in a headspace vial for GC analysis. The second method involved crystal formation of the host with guest mixture using the same procedure mentioned above. Crystals were harvested, dried and placed in headspace vials for GC analysis.

Gas chromatography

GC analysis was performed on an Agilent 7890A instrument with Varian CP Wax capillary column (30 m x 250 μm x 0.25μm), nitrogen carrier gas and FID detector with inlet and detector temperatures of 280 °C. Vials were incubated at 60 °C for 10 minutes before injection; oven temperature at 30 °C for 3 minutes, followed by a gradient at 10 ° C min^{-1} to 120 ° C for 2 minutes.

References

[1] F. Allen, *Acta Crystallogr.*, Sect. B, **2002**, 58, 380.

[2] P. Baran, M. Boča, R. Boča, A. Krutošíková, J Miklovič, J. Pelikán and J. Tituš, *Polyhedron*, **2005**, 24, 1510.

[3] MarvinSketch 14.8.11.0, **2014**, ChemAxon (http://www.chemaxon.com)

[4] CrystalExplorer (Version 3.1), S. K. Wolff, D. J. Grimwood, J. J. McKinnon, M. J. Turner, D. Jayatilaka and M. A. Spackman, University of Western Australia, **2012**.

[5] M. A. Spackman and D. Jayatilaka, *CrystEngComm*, **2009**, 11, 19.

[6] (a) M.A.Spackman and J.J. McKinnon, *CrystEngComm*, **2002**, 4, 378; (b) McKinnon, J.J.; Jayatilaka, D.; Spackman, M.A. *Chem.Commun*., **2007**, 3814.

[7] M. Đaković, D. Vila-Viçosa, M.J. Calhorda and Z. Popović, *CrystEngComm*, **2011**, 13, 5863

[8] J. H. Flynn and L. A. Wall, *Polymer Lett.*, **1966**, 4, 323.

[9] L. R. Nassimbeni, *Acc. Chem. Res*., **2003**, 36, 631.

[10] M. Lusi and L. J. Barbour, *Angew. Chem. Int. Ed*. **2012**, 51, 3928.

[11] A. Bondi, *J.Phys.Chem*., **1964**, 68, 441.

[12] L. R. Nassimbeni, M. L. Niven and M. W. Taylor, *Inorg. Chim. Acta*, **1987**, 132, 67.

[13] J. Lipkowski, in *Inclusion Compounds*, Vol.1, Chapter 3, Academic Press, New York, **1984**

[14] J. Lipkowski, *J. Mol. Struct*.,**1981**, 75, 13.

[15] Bruker **2005**. APEX2. Version 1.0-27. Bruker AXS Inc., Madison, Wisconsin, USA.

[16] Bruker **2004**. SAINT-Plus (including XPREP). Version 7.12. Bruker AXS Inc., Madison, Wisconsin, USA.

[17] Bruker **2003**, XPREP2. Version 6.14. Bruker AXS Inc., Madison, Wisconsin, USA.

[18] G. M. Sheldrick, SHELXS-97 and SHELXL-97 Programs for crystal structure determination and refinement. University of Göttingen, **1997**.

[19] L. J. Barbour, *J. Supramol. Chem*., **2001**, 1, 189.

[20] A. L. Spek, PLATON, A Multipurpose Crystallographic Tool, Utrecht University, Utrecht, The Netherlands, **2008**.

[21] C. F. Macrae, I. J. Bruno, J. A. Chisholm, P. R. Edgington, P. McCabe, E. Pidcock, L. Rodriguez-Monge, R. Taylor, J. van de Streek, P. A. Wood, *J. Appl. Cryst*., **2008**, 41, 466.

Chapter 4

Werner clathrate formation with polyaromatic hydrocarbons: comparison of different crystallisation methods

The single crystal structures of the Werner host, bis-isothiocyanato tetrakis-vinylpyridine nickel (II), **H3**, with seven polyaromatic hydrocarbons (PAHs), indene (**IND**), naphthalene (**NAP**), azulene (**AZU**), fluorene (**FLU**), anthracene (**ANT**), phenanthrene (**PHE**) and pyrene (**PYR**) have been elucidated. These structures were scrutinised for isomorphism and isostructurality. The inclusion compounds can be formed using a variety of crystallisation methods such as solution crystallisation, grinding, slurrying and co-melting methods. Grinding allowed for the determination of rate constants of formation for the host with **NAP** at room temperature and with **AZU** at 35 °C. The kinetics of thermal decomposition of the inclusion compounds using non-isothermal methods permitted the establishment of the activation energies of the decomposition reactions with **NAP** and **IND**. Product formation in an ambient water slurry was successful with guests **NAP** and **IND** showing low solubility at room temperature; for **PHE**, **PYR** and **FLU** this occurred only after longer stirring at a higher temperature (50 °C) at which the guests had low levels of solubility and for **ANT** no successful slurrying results were reached. Co-melting procedures were unsuccessful due to the host's melting point being higher than 400 °C.

Publication of Chapter 4:

Werner clathrate formation with polyaromatic hydrocarbons: comparison of different crystallisation methods

Merrill M. Wicht, Hong Su, Nikoletta B. Báthori and Luigi R. Nassimbeni

CrystEngComm, **2016**, 18, 2509 – 2519

DOI: 10.1039/c5ce02185e

This chapter has been published in CrystEngComm and has been structured according to the journal's format

Introduction

'Green' or 'sustainable' chemistry, based on product design without the generation of hazardous substances, is an effective manner of inclusion complex preparation.[1] Generally, crystallisation of an inclusion compound is conducted by dissolution of the host and guest compounds in a suitable inert solvent, followed by the formation of crystals using slow solvent evaporation. Simplification of experimental procedures and minimisation of labour costs for industrial applications, make solid-solid reactions attractive. Inclusion complexation can occur by mixing and grinding powdered compounds in a solid-state reaction.[2] The progress of these solid-state reactions can be monitored using suitable measurements such as infra-red or ultra-violet spectroscopy or powder X-ray diffraction (PXRD).

Mechanochemical synthesis (manual grinding or ball milling) has been applied to the construction of metal-ligand coordination bonds as well as non-covalent interactions in supramolecular chemistry such as hydrogen bonds, halogen bonds and π···π interactions.[3] Various methods of cocrystallisation such as neat grinding, crystallisation from the melt, solution growth and slurrying have been compared with single crystal analysis. Neat grinding is independent of solubility effects resulting in the avoidance of solubility and solvent competition encountered in solution crystallisation.[4] Two other processes are slurrying with a suitable solvent and melt cooling. The melt process allows the guest compound to be heated and then melted into the host compound. If the solid does not decompose on heating and melting, melt cooling is an acceptable method of crystallization.[5] In slurrying, the process is favoured when the mechanism is via solvent diffusion into the host via molecular recognition.

Successful solvent-free reactions have been promoted despite the limitations of solid-solid reactions. Often products of solid-state reactions differ from those obtained in the solution phase due to spatial orientation or packing of the crystalline material. However, an ordered structure can be obtained by simply mixing components thoroughly to form host-guest systems.[2] Solid-vapour inclusion formations with Werner clathrates have received little attention although they have been considered in

the separation of isomers[6] where the sorption properties of three Werner clathrates were investigated and the mechanochemical processing produced homogeneous solid solutions.[7]

Polycyclic aromatic hydrocarbons (PAHs), consisting of two or more unsubstituted aromatic fused rings are the result of incomplete burning of coal, oil and gas and other organic substances. They are a class of environmental pollutants with carcinogenic properties.[8] Apart from the zeolitic channel sorption of anthracene,[9] the structures of aromatic hydrocarbons as guests in inclusion compounds have not been considerably scrutinised. The development of simple and low cost methods for quantitative recovery of PAHs from solution is a challenging task[10] due to their variety of sizes, shapes and properties.[11] The host 3,5-dinitrobenzonitrile forms clathrates with various hydrocarbons and aza donor molecules, with their host network yielding 3D channels filled by guest molecules.[12] The structures of a series of PAHs as guests in clathrates formed by head-to-tail hydrogen bonding links in a xanthenol host have been elucidated[13] and the solid-solid reaction kinetics were monitored by PXRD. More recently, host compounds derived from dipyridyl linkers and arylboronate esters have been shown to capture a variety of PAHs, and were employed to sequester specific hydrocarbons from a mixture. PAH inclusion selectivity is related to size-fitting adaptations to the octahedral-shaped cavity formed through CH•••π interactions of the host.[14] The structures of PAHs as guests in Werner hosts are represented in the Cambridge Structural Database[15] in only seven cases. These include naphthalene as well as bromonaphthalene and azulene in layered clathrate structures with $Ni(NCS)_2(4\text{-methylpyridine})_4$ by Lipkowski and co-workers.[16]

Having previously considered selectivity of xylene isomers with an isoquinoline-based Werner host,[17] we now present the results of inclusion compounds formed between the Werner host bis-(isothiocyanato) tetrakis-vinylpyridine nickel(II), **H3**, shown in Scheme 4.1, with the PAHs in Scheme 4.2. This compound is an example of a Werner host, that have the ability to enclathrate a variety of guests and can display distinct selectivity.[18,19,20] The structures of the host $Ni(NCS)_2(4\text{-phenylpyridine})_4$, **H2**, as the apohost, as well as those of its inclusion compounds with the isomers of

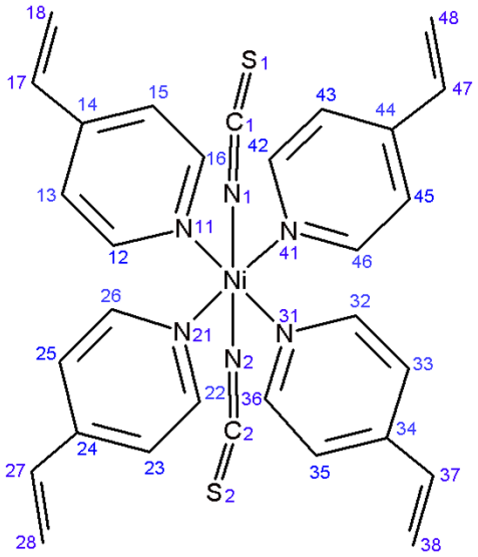

Scheme 4.1: Structural line diagram and atomic numbering of the host, **H3,** bis (isothiocyanato) tetrakis (4-vinylpyridine) nickel(II)

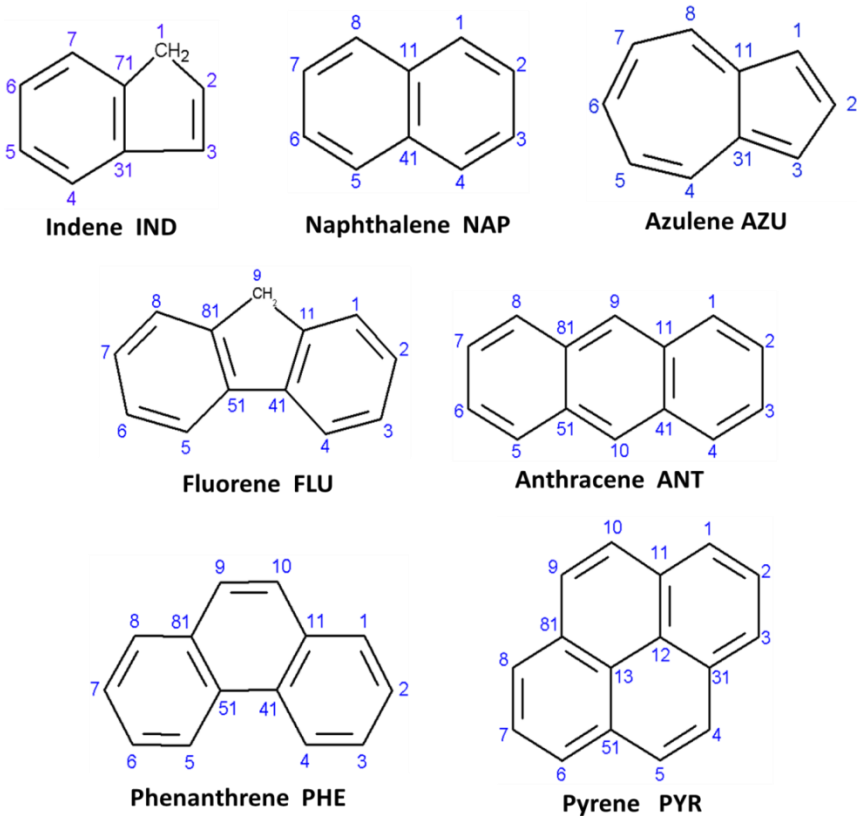

Scheme 4.2: Structural line diagrams and atomic numbering of the seven polycyclic aromatic hydrocarbon guests

xylene, have been interpreted.[21,22] In addition, thermal and structural studies of this host **H3** with halogenated methanes[23,24] and cyclic hydrocarbons[25] have been carried out. Recently the structures of three Werner complexes have been analysed in terms of their packing, and the results confirmed that

nickel(II) thiocyanato complexes relate their crystal design to relatively weak forces such as hydrogen bonding or π•••π interactions especially with pyridine derivatives or other similar ligands.[26]

Compared with our previous work,[17] in which the rigidity of the isoquinoline ligand was found to play an important role in selectivity, the properties of this more flexible ligand, 4-vinylpyridine, are investigated. Here the crystal structures of the host, **H3**, $Ni(NCS)_2(4\text{-vinylpyridine})_4$ with each of the seven polyaromatic hydrocarbon guests: indene (**IND**), naphthalene (**NAP**), azulene (**AZU**), fluorene (**FLU**), anthracene (**ANT**), phenanthrene (**PHE**) and pyrene (**PYR**) were obtained from solvent crystallisation. These Werner clathrates were also synthesised via other methods (neat grinding, slurrying and melting) and their formation and decomposition kinetics are discussed.

Results and discussion

Crystal Structures

Between the nine crystal structures, summarised in Table 4.1 and Table 4.2, a number of similarities were found. The structures of **H3•IND**, **H3•NAP** and **H3•AZU** are isomorphous and crystallise in the space group $Pna2_1$ with Z=4. The asymmetric unit of **H3•IND**, comprising one host and two guests is shown in Fig. 4.1(a) and the packing shown along [001] in Fig 4.1(b) has the guest molecules lying in crossed channels which run along [010] and [001]. The void spacing in Fig 4.1(c) shows these crossed channels depicted by the blue arrows. The structure of **H3•NAP** is analogous with that of **H3•IND**. However, although **H3•AZU** is isomorphous, the azulene guests are disordered and are located about pseudo centres of symmetry, with partial site occupancies of 0.808(7) / 0.192(7) and 0.783(8) / 0.217(8). The asymmetric unit of **H3•AZU** is shown in Fig 4.2.

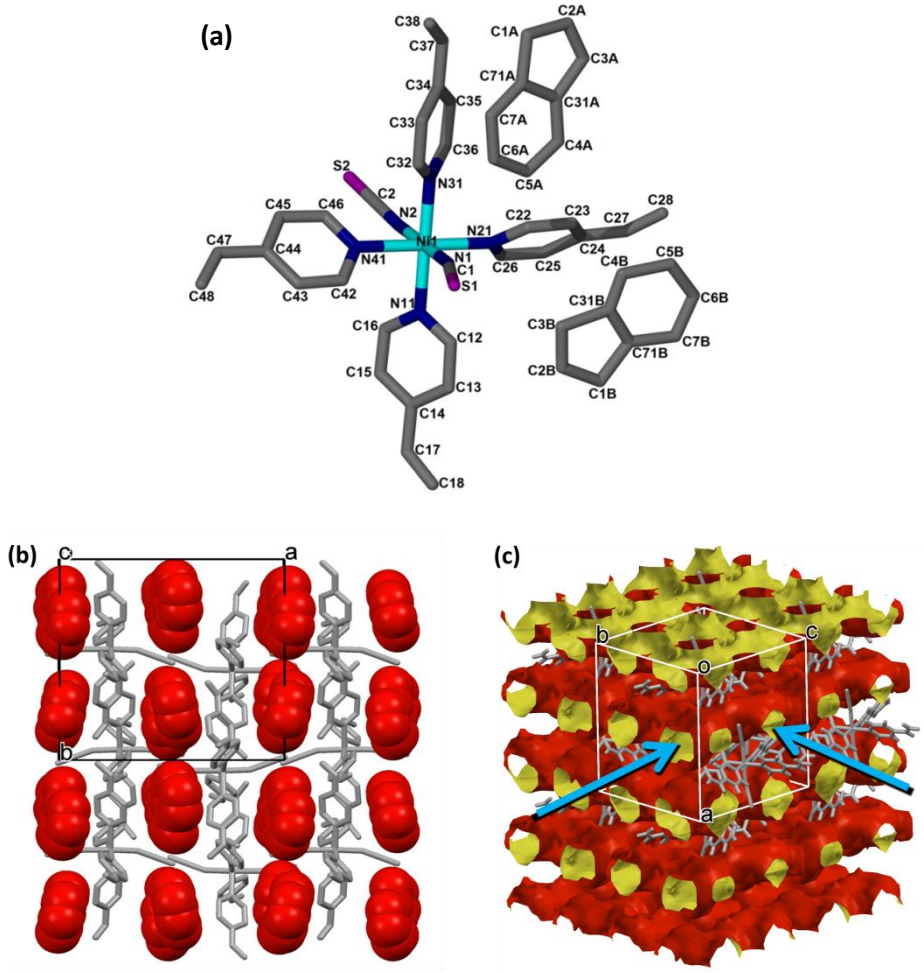

Figure 4.1(a) Asymmetric unit of **H3•IND** (Hydrogen atoms are omitted for clarity); **(b)** Packing down [001] showing the indene molecules occupying the channels in red spacefill model; and **(c)** Void spacing of **H3•IND** viewed down the apex to show the crossing channels down [100] and [010] with blue arrows

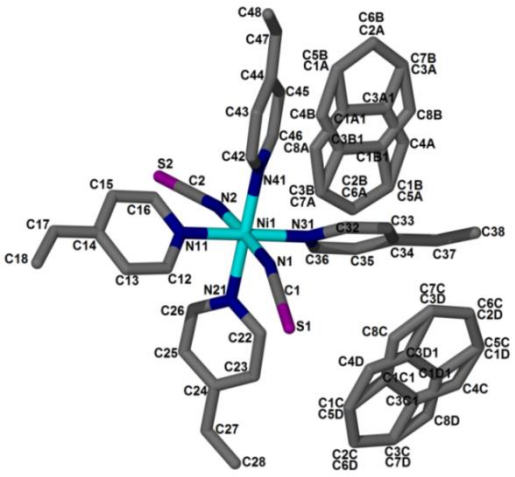

Figure 4.2 The asymmetric unit of **H3•AZU** with disordered guest molecules

The structures obtained with fluorene as guest, gave rise to crystals of distinctly different habits, namely plates (**H3•FLU(I)**) and blocks, (**H3•FLU(II)**). Phenanthrene also forms two different crystal structures, labelled **H3•PHE** and **H3•PHE•BEN**; the latter containing benzene as second guest. **H3•FLU(I)** and **H3•PHE** form an isomorphous pair each with two hosts and 1.5 guests in the asymmetric unit. The packing diagram of **H3•FLU(I)** is shown in Fig. 4.3, viewed down [100]. One guest molecule, labelled **A**, is ordered and located in a general position. The second guest molecule, **B**, is disordered by translation along the b axis, and occupies positions which straddle both centres of inversion at Wyckoff position *a* and *d*. **H3•FLU(I)** forms 3-way channels down the central diagonal axis.

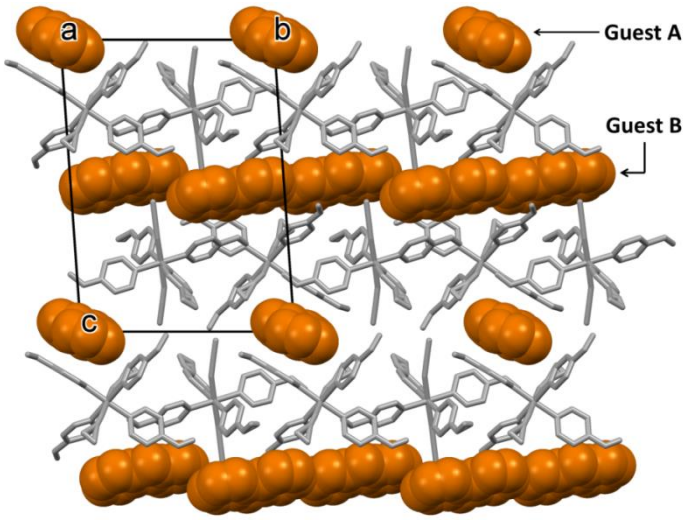

Figure 4.3 Packing diagram of **H3•FLU(I)** down [100] with the guests in orange spacefill model. (Guest A – ordered, Guest B – disordered)

H3•PHE•BEN crystallises with two host, one phenanthrene and one benzene molecules in the asymmetric unit with all moieties ordered. The phenanthrene and benzene molecules are in channels along both [100] and [010] shown in Fig 4.4 with the phenanthrenes depicted in green and the benzenes in blue spacefill models.

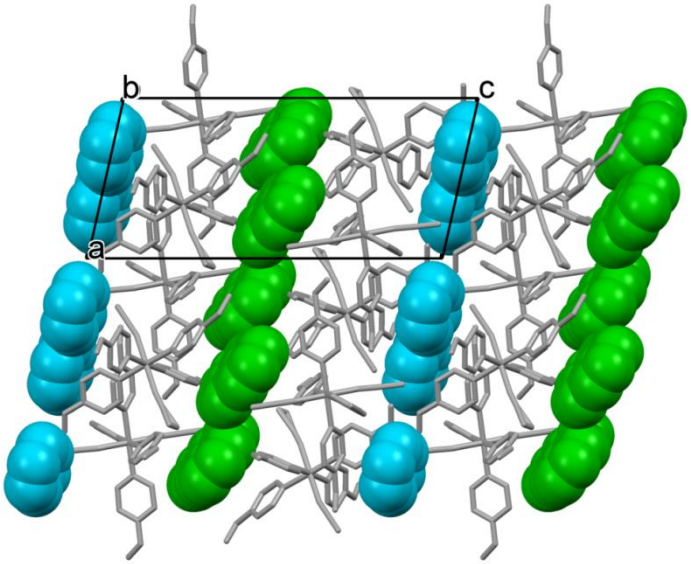

Figure 4.4 Packing of **H3•PHE•BEN** (**PHE** in green, **BEN** in blue spacefill)

H3•ANT crystallises with two hosts and half an anthracene in the asymmetric unit. The anthracene is translationally disordered along the *a* axis, covering *Wyckoff* positions *c* and *e*, shown in Fig 4.5 viewed down [100]. The position of the phenanthrene guest in **H3•PHE•BEN** enforces a 2Å longer *c* axis than in **H3•ANT**, hence they are not isostructural.

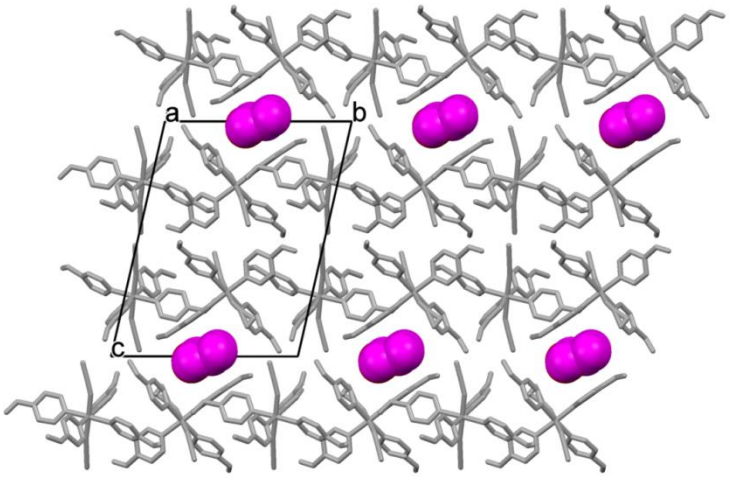

Figure 4.5 **H3•ANT** down [100] (disordered **ANT** in magenta spacefill)

The asymmetric unit of **H3•FLU(II)** comprises four hosts in general positions and two guests, both translationally disordered along the a axis. The host molecules display disorder of the NCS and some vinyl moieties. The guests are crystallographically independent, positioned on *Wyckoff* positions *a* and

d (illustrated in dark blue in Fig. 4.6(a)); and the other on *Wyckoff* positions *g* and *h* (illustrated in light blue in Fig. 4.6(b)). The translational disorder of the guests is shown down [010] in Fig. 4.6(b).

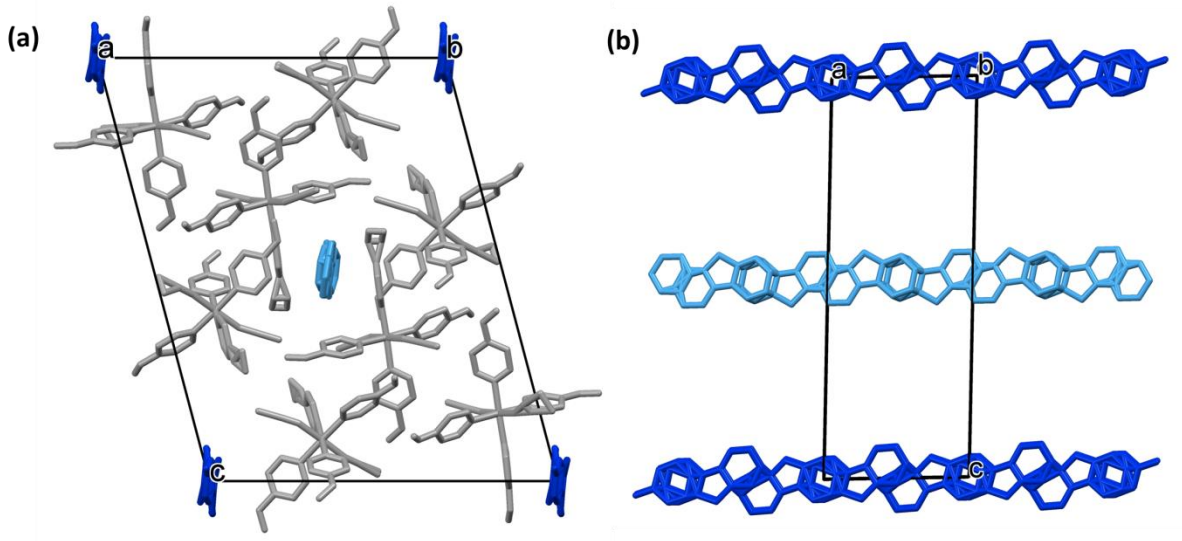

Figure 4.6(a) Packing diagram of **H3•FLU(II)** with disordered **FLU** viewed edge-on down [100];**(b)** The disorder of **FLU** in **H3•FLU(II)** shown down [010] (the two independent guests are in different shades of blue

H3•PYR•MeOH crystallises with one host, two pyrene and 0.5 methanol in the asymmetric unit. The host and pyrene molecules are ordered except for one vinyl group showing disorder. The methanol is disordered and lies near a centre of inversion at Wyckoff position *c*. The packing is shown in Fig. 4.7, viewed down [010]. The pyrenes are illustrated in purple and the methanols in yellow spacefill.

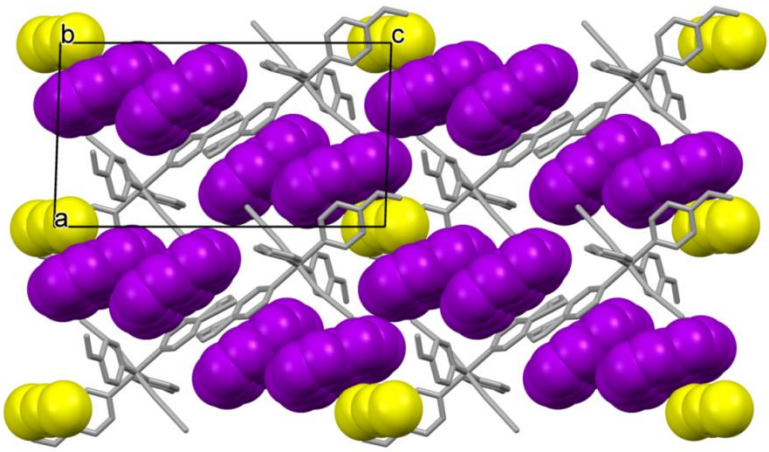

Figure 4.7 H3•PYR•MeOH down [010] (**PYR** in purple and **MeOH** in yellow spacefill models)

Table 4.1: Crystallographic data of **H3•IND**, **H3•NAP** and **H3•AZU**

	H3•IND	**H3•NAP**	**H3•AZU**
Chemical Formula	$Ni(NCS)_2(C_7H_7N)_4•2(C_9H_8)$	$Ni(NCS)_2(C_7H_7N)_4•2(C_{10}H_8)$	$Ni(NCS)_2(C_7H_7N)_4•2(C_{10}H_8)$
Formula weight	827.72	851.74	851.84
Temperature/K	173(2)	173(2)	173(2)
Crystal System	Orthorhombic	Orthorhombic	Orthorhombic
Space group (no.)	$Pna2_1$ (no. 33)	$Pna2_1$ (no. 33)	$Pna2_1$ (no. 33)
a/Å	16.9052(11)	16.8137(18)	16.7378(12)
b/Å	15.7416(10)	16.1198(19)	16.1297(12)
c/Å	16.3948(11)	16.3865(19)	16.4588(12)
α/°	90	90	90
β/°	90	90	90
γ/°	90	90	90
V/Å^3	4362.9(5)	4441.3(9)	4443.5(6)
Z'/Z	1 / 4	1 / 4	1 / 4
$D_{calc.}$/Mg m^{-3}	1.260	1.274	1.273
Radiation type	MoKα	MoKα	MoKα
F(000)	1736	1784	1784
Crystal size/mm	0.44x0.38x0.37	0.25x0.20x0.07	0.38x0.31x0.20
Colour, Crystal form	Violet, Block	Violet, Block	Dark Blue, Block
Total reflections	87546	32257	74997
Unique reflections	10914	10039	10650
$\Theta_{min-max}$/°	1.77 /28.42	1.75 / 28.37	1.75/ 27.95
$R[F^2>2\sigma(F^2)]$	0.0354	0.0424	0.0276
$wR2(F^2)$	0.0939	0.074	0.0611
S	1.040	1.003	1.014
Parameters/ data	515/10914	533/10039	607/10650
Res. Peak (max/min)/eÅ^{-3}	0.700/-0.651	0.213/-0.254	0.219/-0.246

Table 4.2: Crystallographic data of **H3•FLU(I), H3•PHE, H3•FLU(II), H3•ANT, H3•PHE•BEN** and **H3•PYR•MeOH**

	H3•FLU(I)	**H3•PHE**	**H3•FLU(II)**	**H3•ANT**	**H3•PHE•BEN**	**H3•PYR•MeOH**
Chemical Formula	$4Ni(NCS)_2(C_7H_7N)_4$•3 ($C_{13}H_{10}$)	$Ni(NCS)_2(C_7H_7N)_4$ •⅝($C_{14}H_{10}$)	$4Ni(NCS)_2(C_7H_7N)_4$•($C_{13}H_{10}$)	$2Ni(NCS)_2(C_7H_7N)_4$• ⅞(C_8)	$2Ni(NCS)_2(C_7H_7N)_4$•($C_{14}H_{10}$)•(C_6H_6)	$2Ni(NCS)_2(C_7H_7N)_4$ •4($C_{16}H_{10}$)•(CH_3OH)
Formula weight	2880.61	706.80	2537.71	1275.03	1447.12	2032.05
Temperature/K	173(2)	173(2)	173(2)	173(2)	173(2)	173(2)
Crystal System	Triclinic	Triclinic	Triclinic	Triclinic	Triclinic	Triclinic
Space group (no.)	$P\bar{1}$ (no. 2)	$P\bar{1}$ (no. 2)	$P\bar{1}$ (no. 2)	$P\bar{1}$ (no. 2)	$P\bar{1}$ (no. 2)	$P\bar{1}$ (no. 2)
a/Å	10.3322(10)	10.3117(8)	10.1821	10.1289(4)	10.4819(9)	10.9587(7)
b/Å	16.8462(10)	16.8992(14)	23.1916	16.4770(9)	16.8458(14)	12.1349(8)
c/Å	22.134(2)	22.3884(17)	28.6186	20.6537(10)	22.5690(5)	19.7621(12)
α/°	84.603(2)	81.874(2)	74.602	100.430(2)	100.059(2)	93.9070(10)
β/°	84.385(3)	83.128(2)	85.683	97.129(3)	100.131(2)	91.4260(10)
γ/°	74.788(3)	76.007(10)	81.596	105.351(3)	102.908(2)	97.8780(10)
V/Å^3	3690.3(5)	3732.8(5)	6440.7	3214.8(3)	3727.6(5)	2595.6(3)
Z'/Z	½ / 1	2 / 4	1 / 2	1 / 2	1 / 2	½ / 1
$D_{calc.}$/Mg m^{-3}	1.296	1.258	1.314	1.322	1.289	1.300
Radiation type	MoKα	MoKα	MoKα	MoKα	MoKα	MoKα
F(000)	1504	1475	2656	1334	1512	1062
Crystal size/mm	0.23x0.15x0.04	0.22x0.18x0.03	0.26x0.19x0.18	0.20x0.18x0.09	0.48x0.34x0.32	0.50x0.40x0.20
Colour, Crystal form	Violet, Plate	Violet, Block	Violet, Block	Violet, Block	Violet, Block	Violet, Block
Total reflections	94121	39815	156695	24868	89108	98932
Unique reflections	14995	16209	32284	13088	17210	13093
$\Theta_{min-max}$/°	2.87 / 26.39	2.04/27.09	1.48 / 28.43	2.12 / 26.37	2.23 / 26.41	1.92 / 28.54
$R[F^2>2\sigma(F^2)]$;	0.0496;	0.0561;	0.1101;	0.0635;	0.0445;	0.0365;
$wR2(F^2)$;	0.0911;	0.1454;	0.2973;	0.1919;	0.1254;	0.1056;
S	1.001	1.015	.033	1.003	1.022	1.027
Parameters/ data	986/14995	968/16209	1583/32284	764/13088	894/17210	679/13093
Res. Peak (max/min)/eÅ^{-3}	0.538/-0.259	0.688/-0.447	1.283/-1.736	0.816/-0.515	0.868/-0.387	0.787/-0.339

Unit cell volume versus number of non-hydrogen atoms

When the volume of the unit cell (ordinate) is plotted against the total number of non-H-atoms of the guest, the points fall on a straight line. In this series of fused ring guests the straight line has a slope, measured in $Å^3$ per guest non-hydrogen atom, of 17.1 (Fig. 4.8). This corresponds to the volume measurement per carbon atom in the guest molecule. According to Dunitz and Gavezzotti[27], attractive and repulsive forces as well as stabilizing and destabilizing energies play a part in the tightness of packing in the crystal structures of the condensed ring aromatic hydrocarbons and can be calculated as the packing coefficient. An interesting observation is the positioning of the isomorphic structures on the graph: isomorphic structure of **H3•IND**, **H3•NAP** and **H3•AZU** as well as the isomorphic pair **H3•FLU(I)** and **H3•PHE** form clusters on the graph.

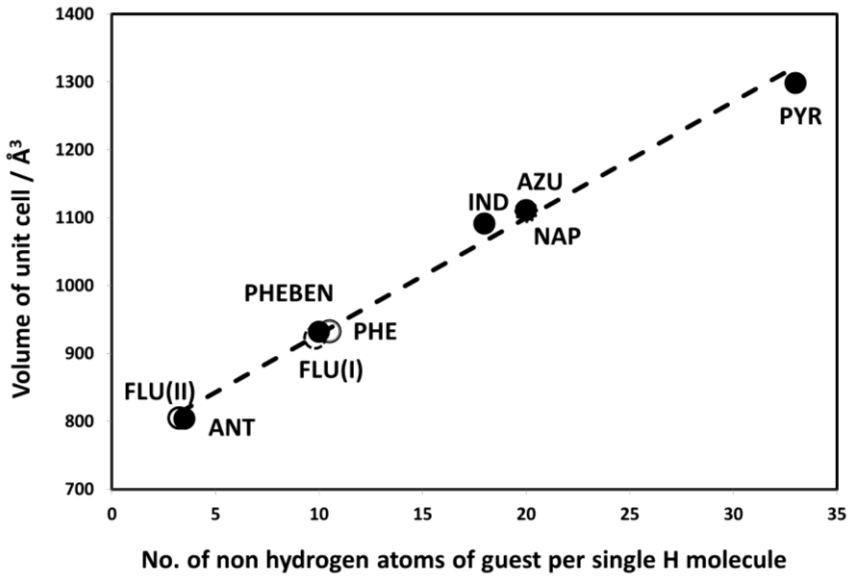

Figure 4.8 Relationship between number of carbons and the volume of the unit cell in $Å^3$

Mechanochemical synthesis

Environmentally attractive solid-solid reactions are a well-known format for generating multicomponent crystals or cocrystals. Rastogi[28,29] discussed the kinetics of solid-solid reactions between selected hydrocarbons and picric acid. Principal mechanisms for the formation of cocrystals have been established as surface migration and diffusion through the vapour phase of the aromatic

hydrocarbon.[4] Braga *et al*.[30] relates the interactions between the components to be diffusion controlled, or in the case of co-grinding, an intermediate eutectic phase is formed. In our case this would involve π stacking of the aromatic rings of the guest and the Werner host.

Solid-solid reactions were carried out between the **H3** and all solid guests by grinding stoichiometric quantities of the solids in a mortar at 298 K or at a higher temperature in a brass mortar. The reactions were monitored by interrupting grinding at given periods and adding a fixed quantity of diamond powder to the sample before PXRD analysis. Certain reflections associated with the starting materials decrease in intensity while those of the new compound increase in intensity based on the time of grinding.

In Figure 4.9 the **NAP** diffraction patterns are presented: the computed pattern derived from the single crystal structure of **H3•NAP** (A), the host, **H3** (B), **NAP**, the guest (C), the sample after 15 minutes of grinding (D), and the pattern after a slurry experiment was performed (E).

The vapour pressure of the guest is critical in the effectiveness of a grinding experiment. Of the guests, with the exclusion of **IND** (liq.), **NAP** has the lowest melting point of 80 – 82 ºC and its higher vapour pressure influences the amount of diffusion occurring on grinding. The shaded sections in the PXRD pattern in Fig 4.9 indicate a number of peaks of interest. When Peak 1 (9.3 º at 2θ) and Peak 2 (21.1 º) were monitored, a gradual increase during grinding was observed. However, the decrease in intensity of Peak 3 at 12.6 º during the grinding process (relative to (111) peak of diamond at 44.1 º 2θ) is shown in Figure 4.10, as a plot of *ln(peak intensity) vs time*. This yielded a straight line (**A**) indicating a first order reaction with a rate constant of 0.137 min^{-1} and a half-life of 5.06 mins.

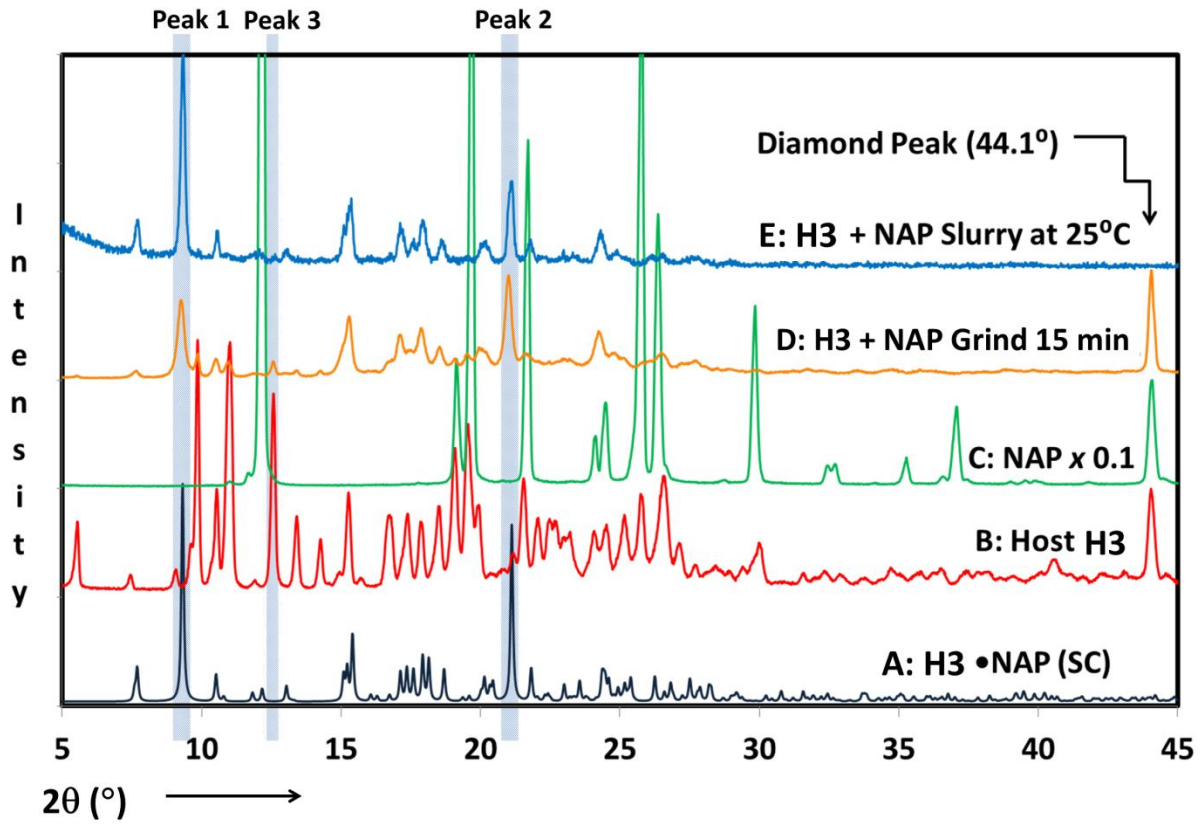

Figure 4.9 PXRD profiles: A: **H3•NAP** generated pattern; B: pure host; C: pure **NAP**; D: **H3** + **NAP** after 15 minutes grinding at RT; and E: slurry experiment at 25 ^{0}C. The grey highlights show the peaks of interest and the peak at 44.1 ^{0} 2 Θ is the diamond internal standard peak

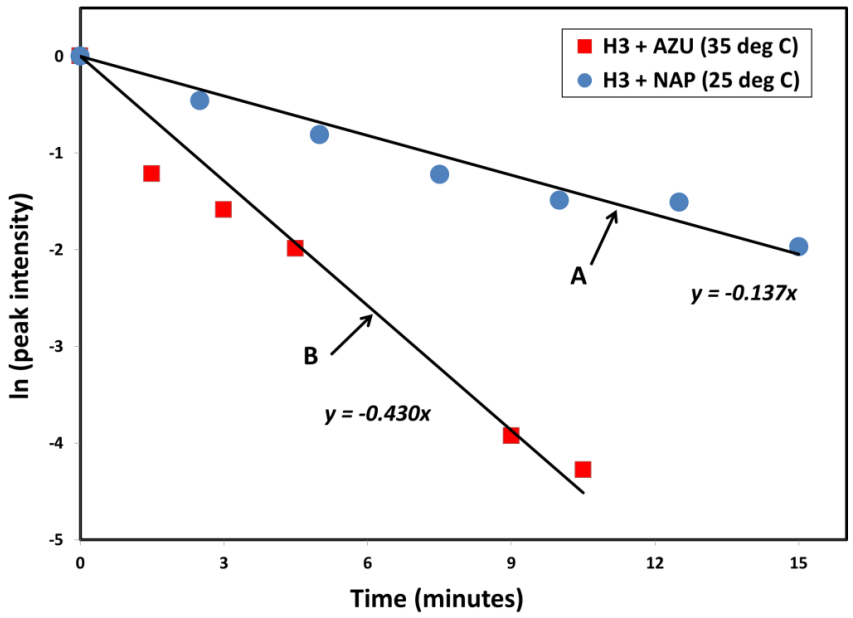

Figure 4.10 Kinetics of the grinding reactions between host **H3** and **NAP** at 25 ºC (**A**), and **H3** and **AZU** at 35 ºC (**B**).

The vapour pressures of the solid guests were considered at temperatures of 25 and 50 ºC in an attempt to predict the outcome of the grinding experiments.[31,32] Grinding **H3** with **NAP**, (vapour pressure of 11.5 Pa at 25 °C) was successful at room temperature. At 50 ºC (75.8 Pa), co-grinding of **H3** and **NAP** produced the final product after just 2.5 minutes. As **AZU** was deemed to require a slightly higher temperature to reach an acceptable vapour pressure (11.1 Pa at 35 °C), favourable grinding in a brass mortar at 35 ºC was achieved. The **AZU** peak at 11.6 º decreased in intensity as shown in Figure 4.10, plot **B**, giving a rate constant of 0.430 min^{-1} with a half-life of 1.61 minutes. This is a good example to highlight the importance of vapour pressure and the significance of gas phase diffusion in these grinding experiments.

Sets of PXRD profiles for each solid guest, manually ground with the host **H3** over a period of time are given in figures 4.11 to 4.16. The effectiveness of each of these grinding experiments is discussed with each relevant figure.

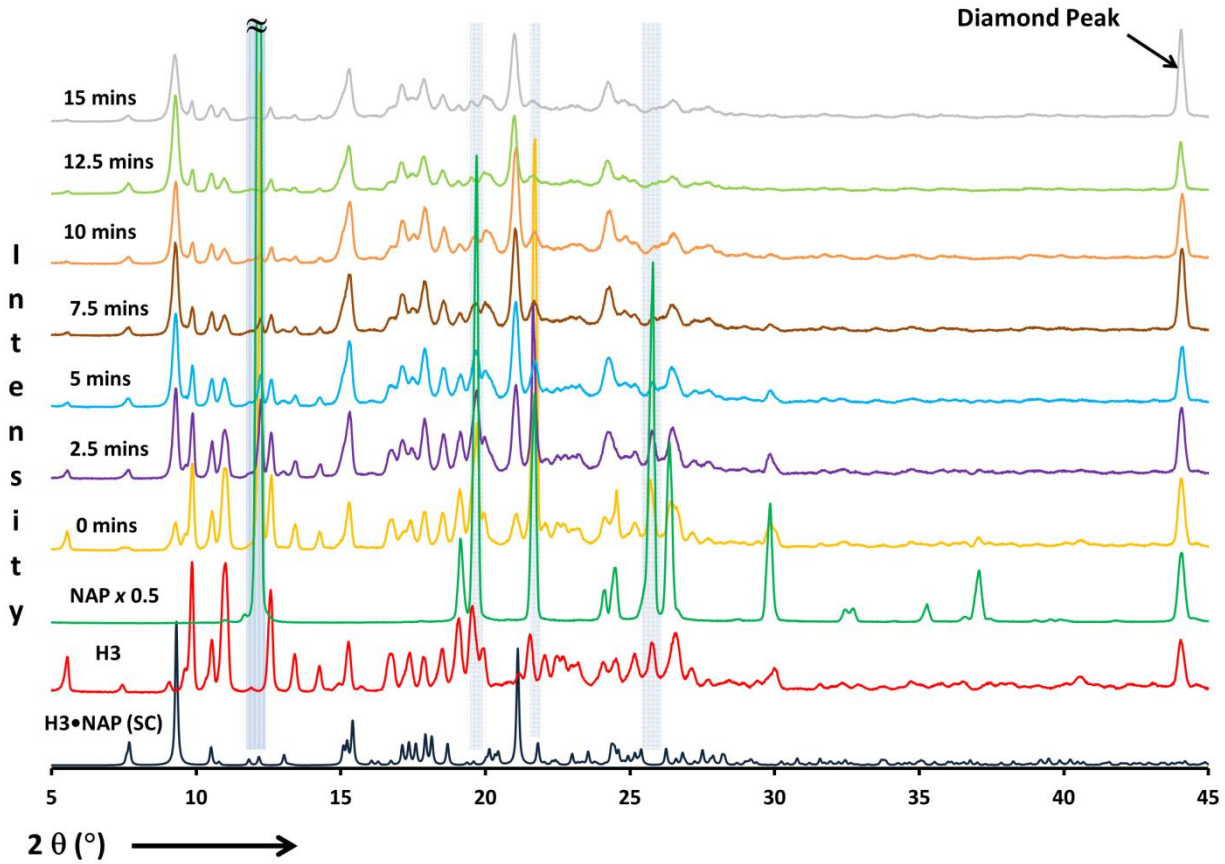

Figure 4.11 PXRD profiles of the product with grinding of **H3** and **NAP** for the indicated time at 25 °C

The successful grinding of **H3** and **NAP** at 25 °C was shown by the increase in size of the peaks at 2θ of 9.3 and 21.1 ° 2θ in Fig. 4.11. The 2θ peaks at 12.6, 19.6, 21.8 and 26.0 ° decreased in size with grinding. These are naphthalene peaks and verify the transformation from a mix of host and guest to a compound matching the crystal structure of **H3•NAP.** The diamond peak appears at 44.1 ° and is used as a reference in each profile.

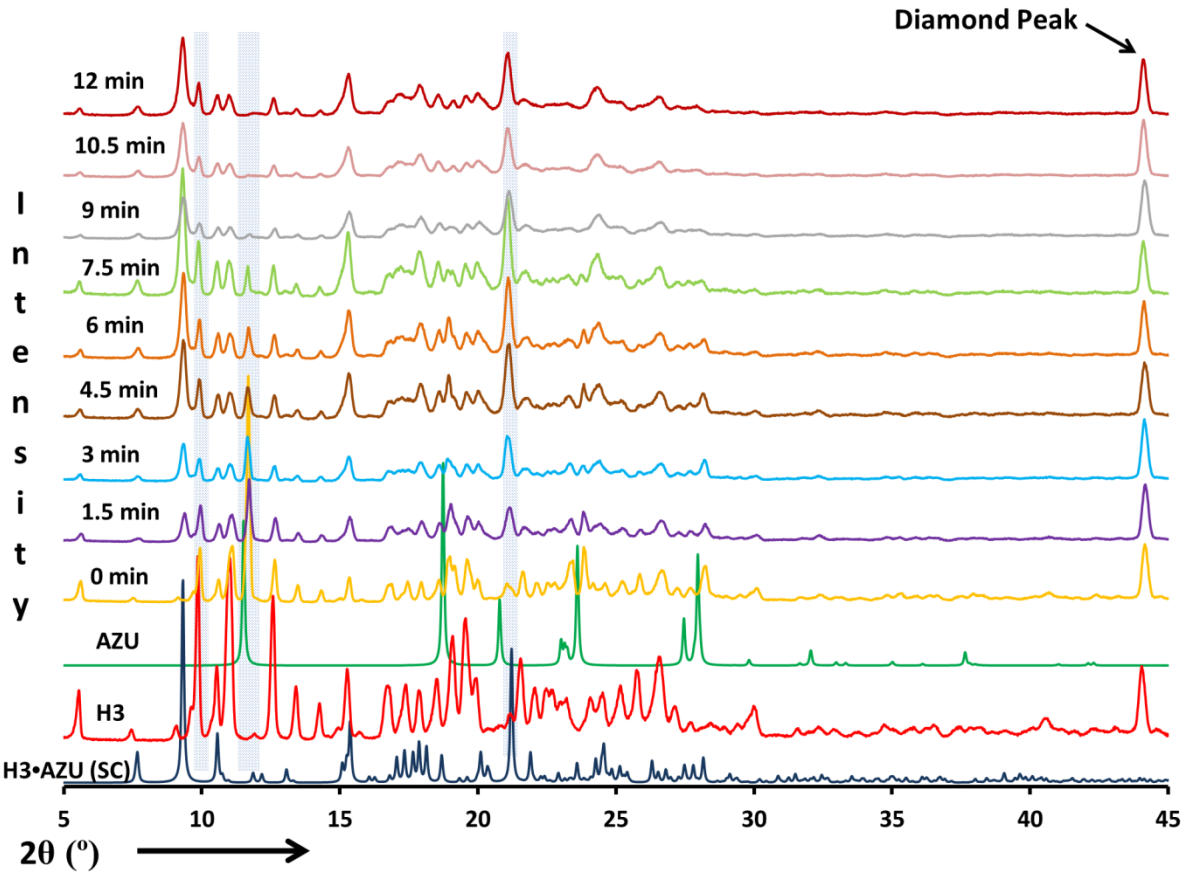

Figure 4.12 PXRD profiles of the product with grinding of **H3** and **AZU** for the indicated time at 35 °C

The effective grinding of **H3** and **AZU** at 35 °C is shown in Fig. 4.12 with the peaks of interest shown in grey highlights. The **AZU** peak at 11.6 ° decreases in size with grinding, as does the host peak at 10.0 º, while the peak at 21.6 ° increases in size. In 12 minutes of grinding success is achieved and a similar product is observed in the PXRD profile to the one calculated assuming **H3•AZU** crystal structure.

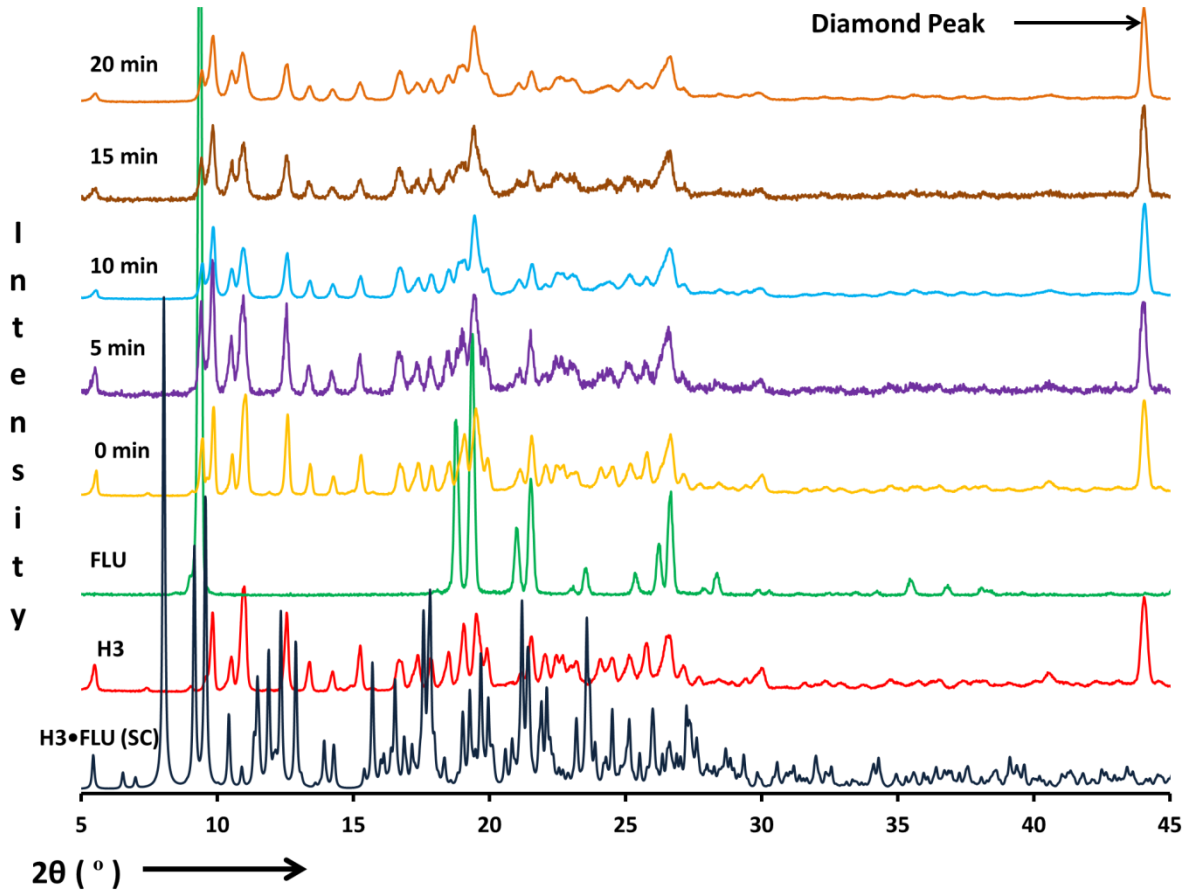

Figure 4.13 PXRD profiles of the product with grinding of **H3** and **FLU** for the indicated time at 25 °C

In the case of the grinding experiment with **H3** and **FLU** changes in the size of certain peaks was observed. However, the achievement of a product with a similar PXRD profile to that of the **H3•FLU** crystal was ineffective after 20 minutes of grinding at 25 °C. The vapour pressure of **FLU** (0.183 Pa at 25 ºC; 1.682 Pa at 50 ºC), considerably lower than that of **NAP,** suggests that, even at a temperature of 50 ºC, production of a compound with a similar PXRD profile to that of the crystal is difficult to achieve.

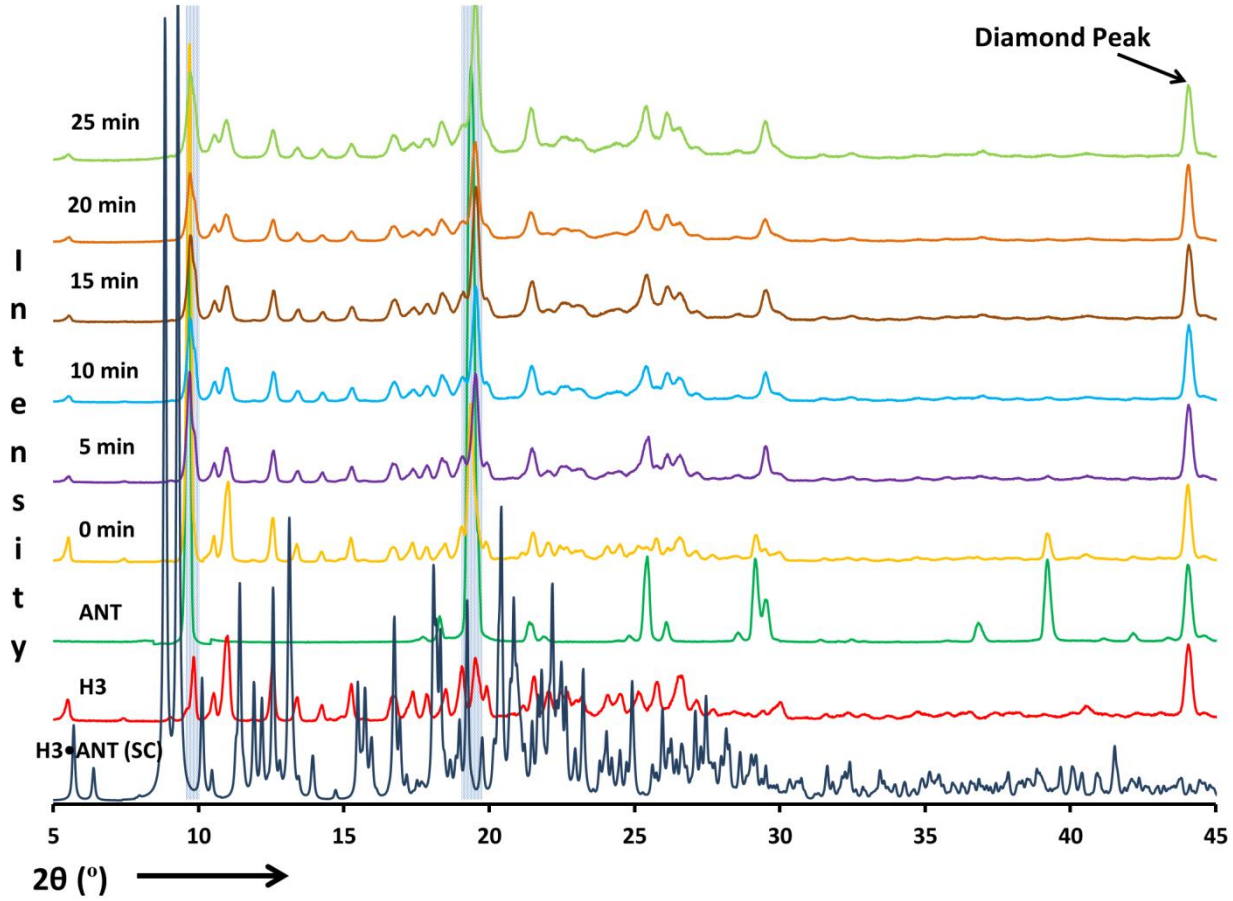

Figure 4.14 PXRD profiles of the product with grinding of **H3** and **ANT** for the indicated time at 25 °C

The PXRD profiles on mixing **H3** with **ANT** initially showed a mixture of the two compounds. On grinding, small decreases occurred in the sizes of two peaks at 9.5 and 19.3 ° 2θ as shown by the grey highlights in Fig. 4.14. However, this did not progress to a compound with a PXRD profile which matched that of the **H3•ANT** crystal after 25 minutes of grinding at 25 °C. The vapour pressure of **ANT** is the lowest of the PAHs studied in this project, *viz.* 2.9 x 10^{-3} Pa at 25 ºC and 4.4 x 10^{-3} Pa at 50 ºC, indicating that the guest does not encourage product formation on grinding at 25 ºC. A much higher temperature would be required which is not suitable for this experiment.

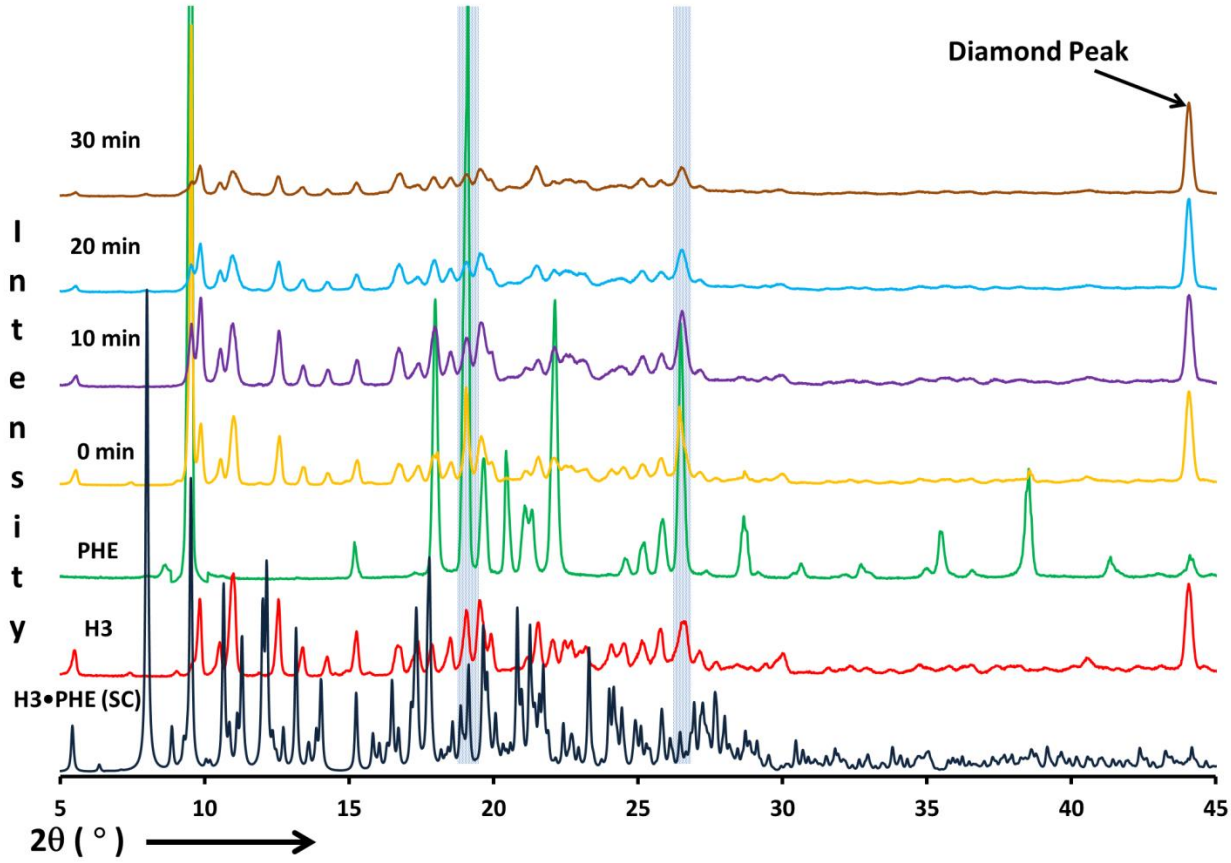

Figure 4.15 PXRD profiles of the product with grinding of **H3** and **PHE** for the indicated time at 25 °C

On grinding **H3** and **PHE** together, the outcome is similar to the previous experiment in that the product does not match the crystal structure **H3•PHE** despite the reduction in size of the peaks highlighted in grey in Fig. 4.15. The vapour pressure for **PHE** (0.1 Pa at 25 ºC; 0.958 Pa at 50 ºC), although higher than **ANT**'s vapour pressure, is about a hundredth of the **NAP** vapour pressure.

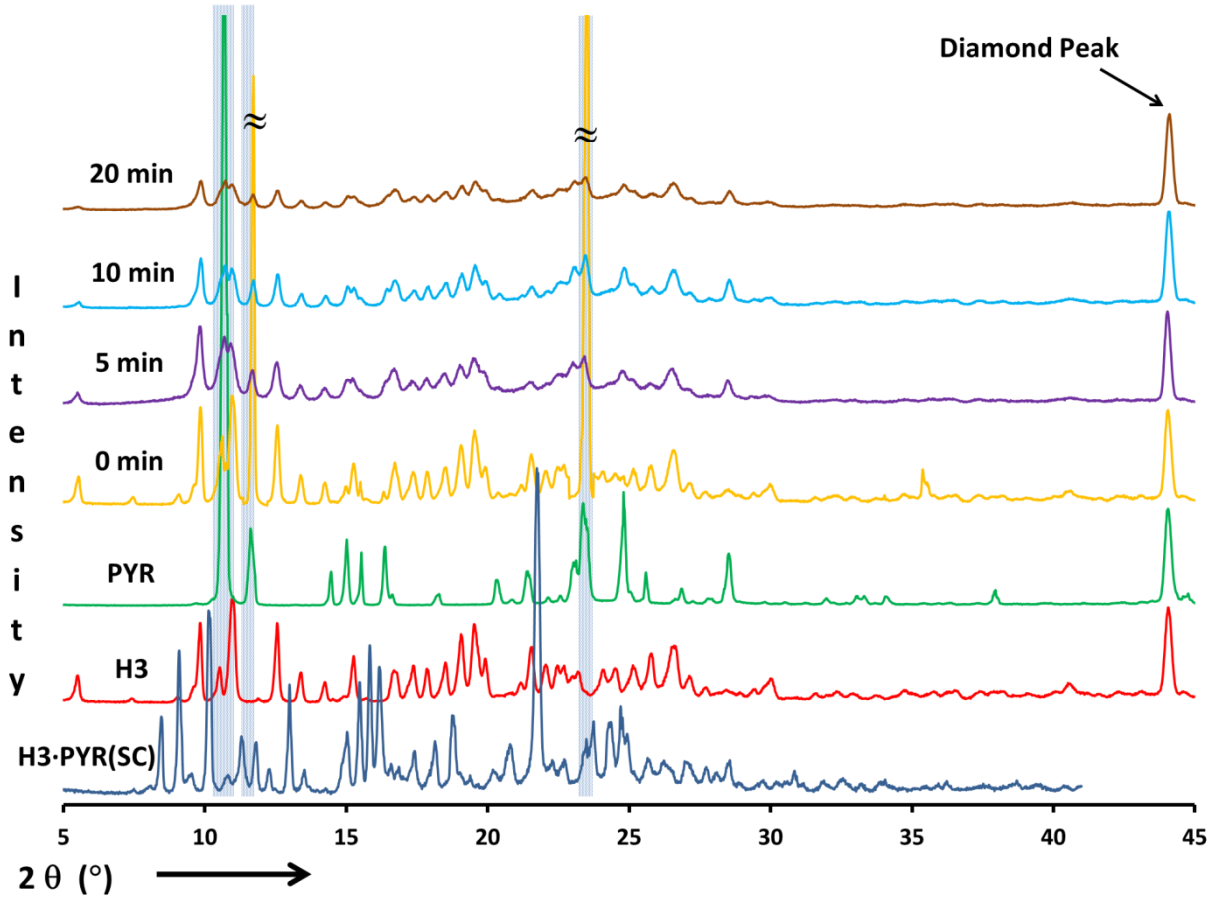

Figure 4.16 PXRD profiles of the product with grinding of **H3** and **PYR** for the indicated time at 25 °C

In Fig 4.16, the peaks at 10.7, 11.8 and 23.3 ° 2θ in the grinding of **H3** and **PYR** decreased in size. Specific peaks in the PXRD of the **H3•PYR** crystal have not appeared after 20 minutes grinding at 25 °C. This was not a successful result for this experiment, and the low **PYR** vapour pressure (0.0094 Pa at 25 ºC; 0.0091 at 50 ºC) is accountable for the product not forming on grinding at 25 ºC. At a temperature of 60 ºC, the success would still be limited as the vapour pressure (0.207 Pa) is lower than that of **NAP** at 25 ºC by a factor of five.

Successful agreement between the single crystal structure and ground products were reached with the guest **NAP** at room temperature and **AZU** at 35 ºC. The other guests did not show acceptable correspondence between the two methods at 25 °C and their vapour pressure values suggested that temperatures would be too high to perform manual grinding; hence the experiment would become too difficult to perform in an industrial application.

Slurry Experiments

Stoichiometric amounts of the host and guest were placed in a vial and 1 mL of distilled water added to the mixture. This was stirred (550 rpm, 54 hours at 25 ºC) and the slurry was filtered and dried prior to analysis by PXRD. The **H3•NAP** pattern obtained from the slurry experiment is labelled E (Fig 4.9). Peak1 and Peak2 appeared while Peak 3 (12.5 º 2θ) has completely disappeared. Pattern E agrees well with that of the **H3•NAP** crystal. The solubility of both the **H3** and the guest (0.003 %m/m at 25 ºC)[31,32] in water (S_w) is low thus water is a suitable solvent for the slurry experiment.

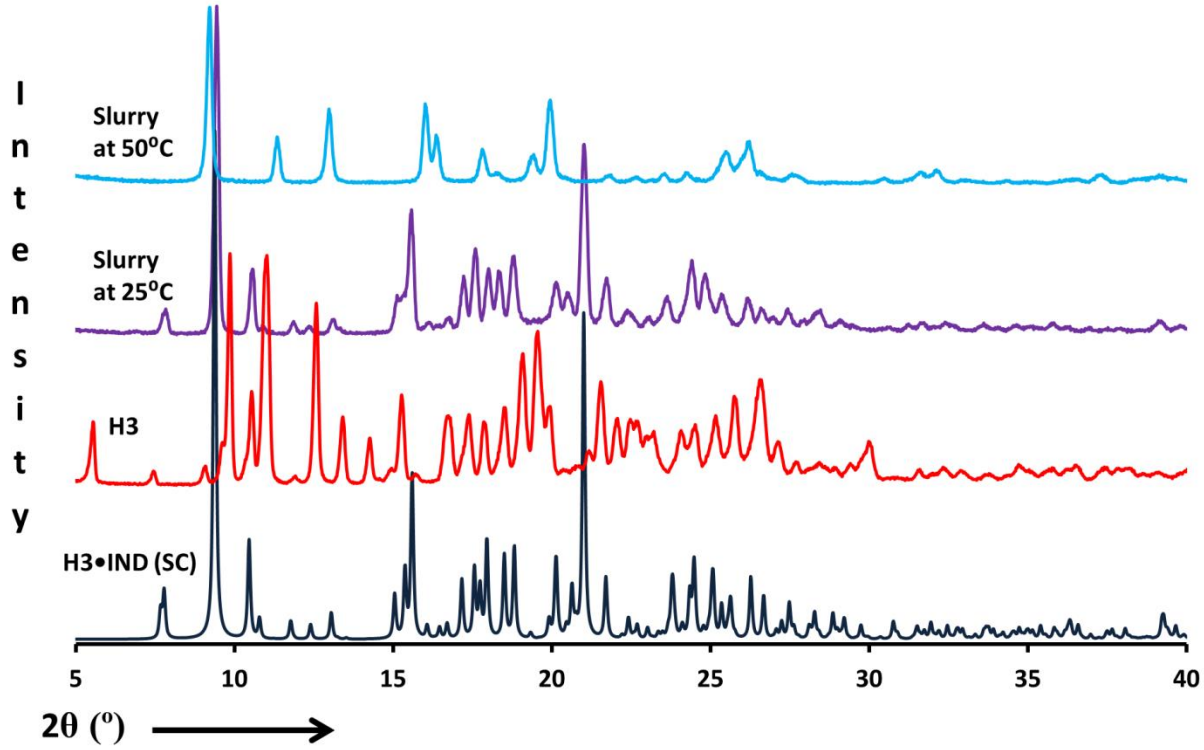

Figure **4.17** PXRD profiles of **H3** and **IND** in a slurry at 25 and 50 °C

The product formation with **H3** and **IND** was successful and a set of PXRD profiles are found in Fig. 4.17. The peaks in the PXRD profile after slurrying at 25 ºC match those in the **H3•IND** crystal as seen in the figure. These larger peaks occur at 2θ values of 7.8, 9.4, 10.4, 15.7 and 21.0 º. Despite indene's aqueous insolubility, the slurry of the liquid guest was more successful than certain other guests in reaching a profile similar to that of the desired crystal. At the higher temperature of 50 ºC, the match between the single crystal pattern and the slurry has decreased, showing that the temperature of 25 ºC is a more suitable temperature for the slurry experiment.

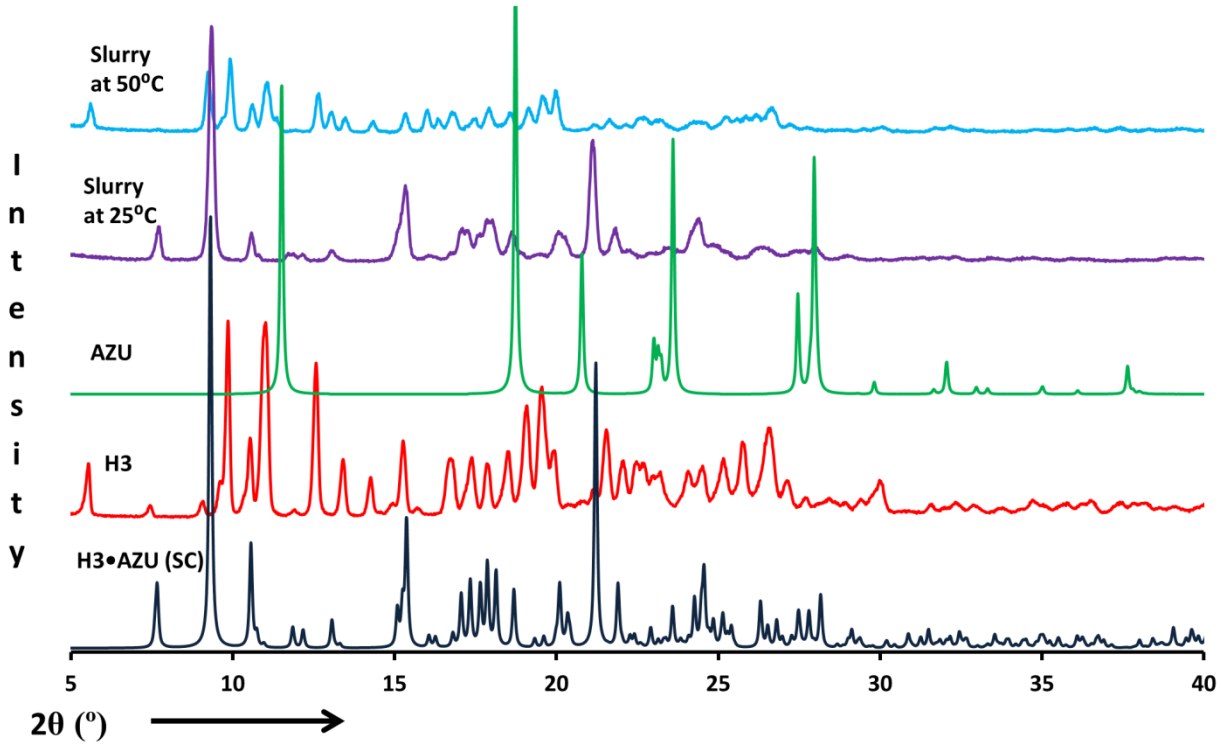

Figure 4.18: PXRD profiles of **H3** and **AZU** in a slurry at 25 and 50 °C

In the case of **H3** and **AZU**, (S_w=0.002 %m/m at 25 ºC), a number of corresponding peaks between the slurry product and the generated pattern were found and can be seen in Fig 4.18. Azulene's aqueous solubility is similar to that of naphthalene at 25 ºC (0.003 %m/m) and on comparison of the two profiles shown in the figure, a distinct similarity between the PXRD profile of the **H3•AZU** crystal and that of the slurry after grinding for 54 hours at 25 ºC is reached. At a temperature of 50 ºC, the pattern's correlation with that of the generated single crystal pattern has decreased, thus slurrying at 25 ºC is a more suitable temperature for this experiment. This procedure of slurrying at 25 ºC is an acceptable method for preparation of the same compound as the crystal formed by solution crystallisation, thus a solvent-free or green method.

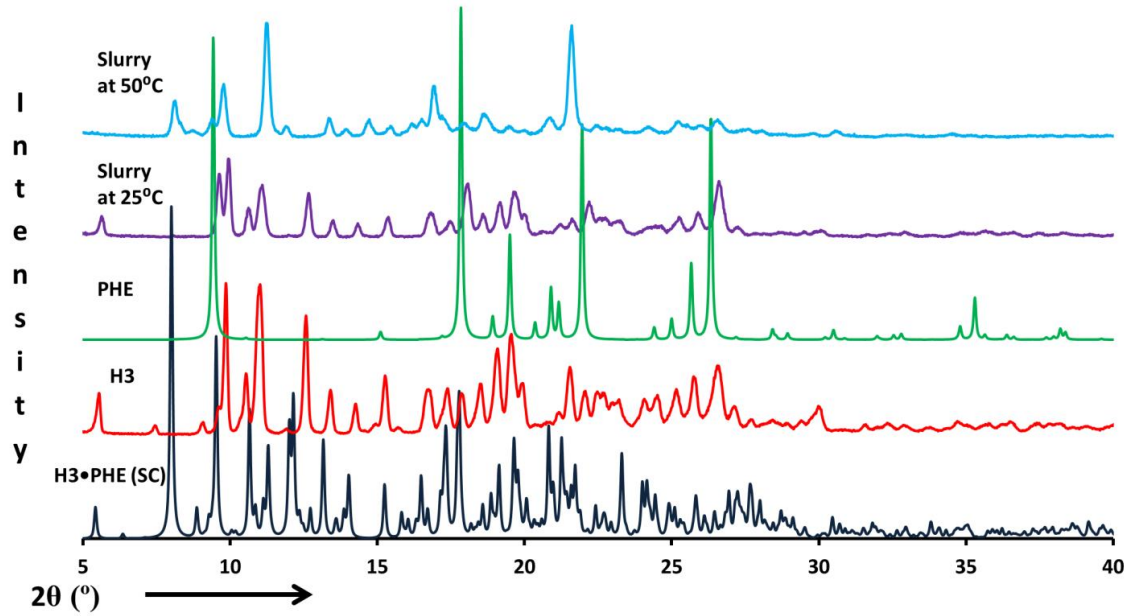

Figure 4.19: PXRD profiles of **H3** and **PHE** in a slurry at 25 and 50 °C

Slurry experiments with the other guests were carried out for 72 hours at 50 ºC. In the case of using **PHE** (S_w=4.0x10^{-4} %m/m, 50 ºC) as a guest, partial agreement with the crystal was noted (peak at 8 º 2θ as shown in Fig 4.19).

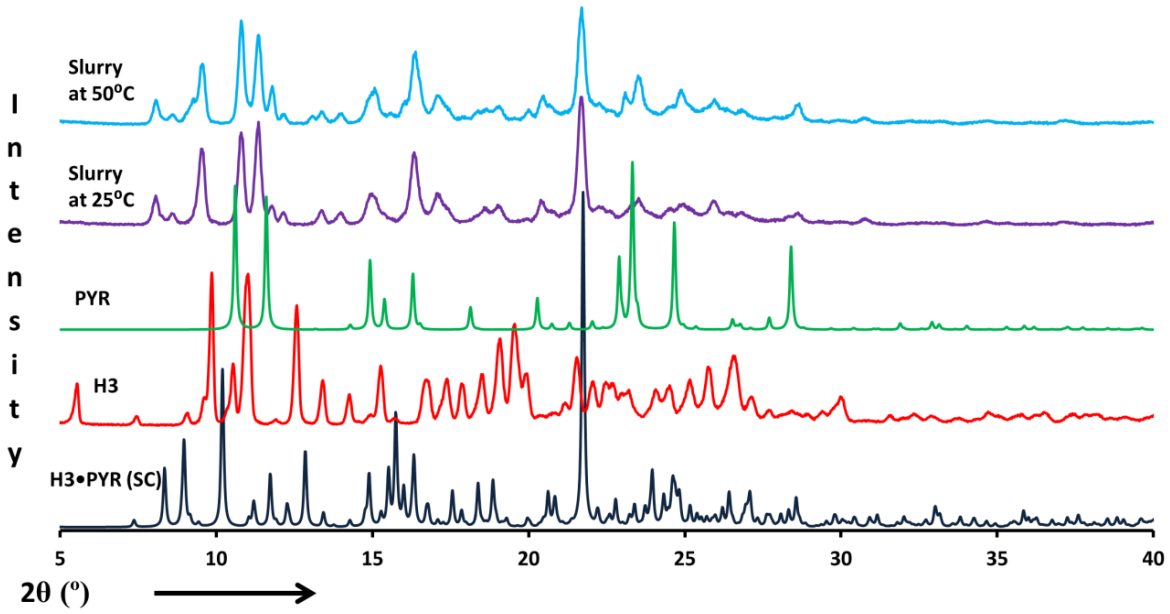

Figure 4.20: PXRD profiles of **H3** and **PYR** in a slurry at 25 and 50 °C

In the same way, a peak for **PYR** (S_w=9.0x10^{-5} %m/m, 50 ºC) at 21.8 º 2θ (Fig 4.20) and for **FLU** (S_w=6.0x10^{-4} %m/m, 50 ºC) at 8 º 2θ (Fig.4.21), indicated that the experiment was partially successful.

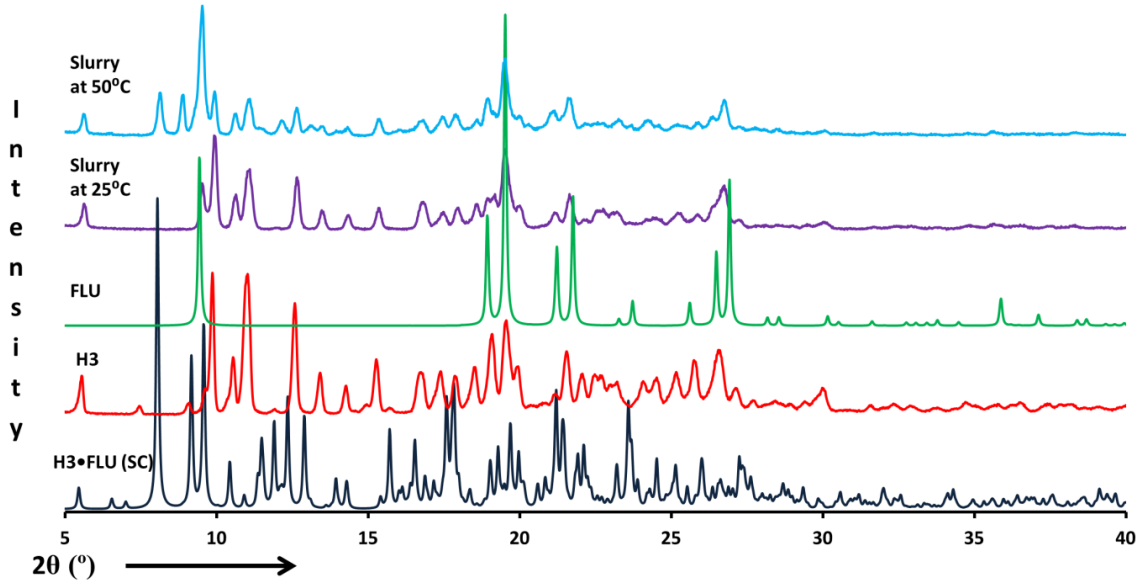

Figure 4.21 PXRD profiles of **H3** and **FLU** in a slurry at 25 and 50 °C

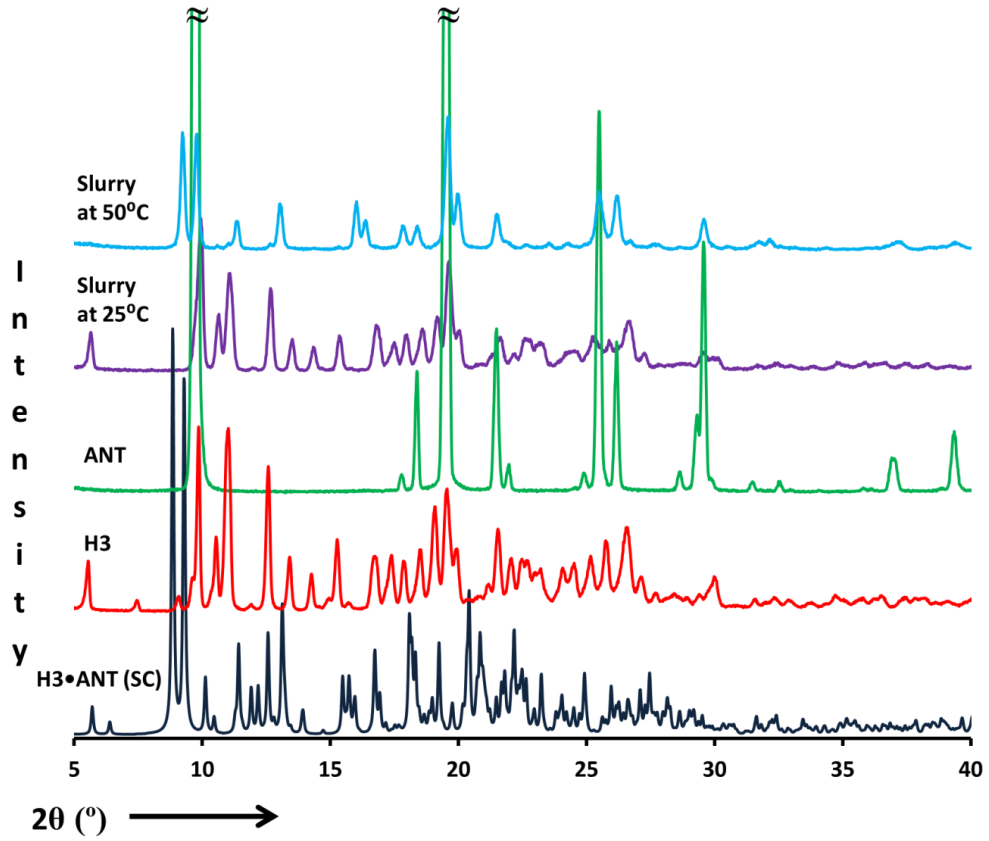

Figure 4.22 PXRD profiles of **H3** and **ANT** in a slurry at 25 and 50 °C

Guest **ANT** (S_w=4.5 x 10^{-6} %m/m, 25 ºC) was not fully successful in this experiment although stirring at a higher temperature (50 ºC) for 96 hours produced similarities with the generated crystal pattern in the 2θ range of 5 º to 20 º.

Co-melting

Co-melting was performed on a hot-stage microscope with **NAP** allowed to melt into the host compound. The melt mixture was left at a temperature 92 ºC (10 º C > mp NAP) for 10 mins. The PXRD analysis revealed that the product is a physical mixture of the starting materials. Due to the melting point of the host being so much higher (> 400 ºC), this experiment was unsuccessful and was not attempted for the other guests due to their higher melting points.

Kinetics of thermal decomposition

The kinetics of thermal decomposition were measured for **H3•NAP** and **H3•IND** using the method of Flynn and Wall[33] , in which the mass losses of the compound were recorded at various heating rates varying from 2 to 32 $Kmin^{-1}$. These non-isothermal thermogravimetric curves for **H3•NAP** are shown in Fig. 4.23 and for **H3•IND** in Fig. 4.24.

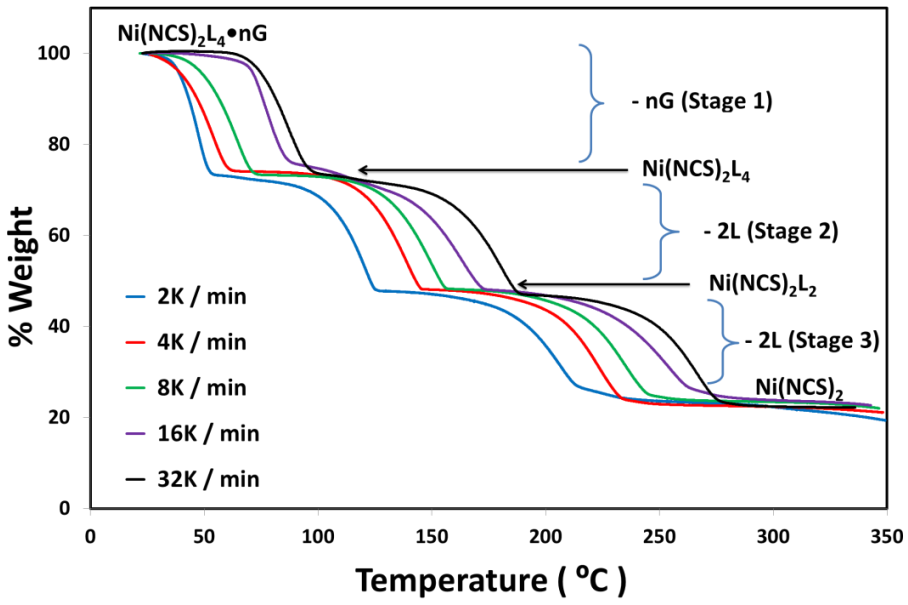

Fig 4.23 Non-isothermal TG curves for **H3•NAP** (L = NAP)

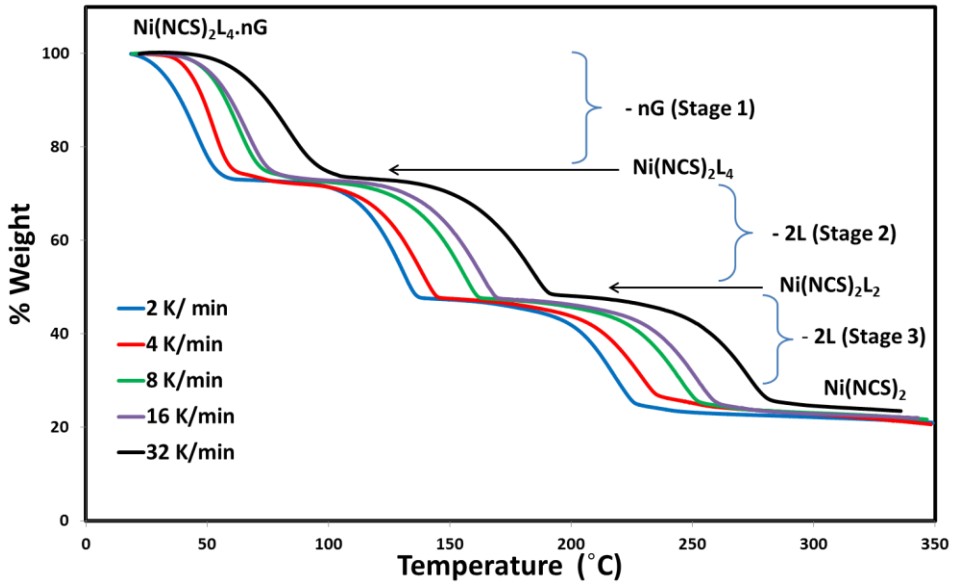

Fig 4.24 Non-isothermal TG curves for **H3•IND** (L = IND)

The decomposition occurred in three stages: Stage 1 was due to the loss of the two guests, while stage 2 and 3 could each be attributed to the loss of pairs of vinyl pyridine ligands. In **H3•NAP** the guest is found in channels along [010] and [100] and forms an intercalate structure with a high guest to host ratio; thus the thermal stability and kinetics of decomposition are expected to be lower than that associated with the loss of the ligands from the host compound (Table 4.3).

For Stage 1 the corresponding mass losses and activation energies were calculated over α ranges for the inclusion compounds and are indicated in Table 4.3.

Plots of log β/β_o vs. 1/T for the **H3•NAP** where β is the heating rate are shown in Fig. 4.25. Stage 2 and 3 are similar, showing increasing activation energies. These energies are typical for a crystal structure with guests in channels. The same tendency was observed in **H3•IND** (Fig. 4.26 and Table 4.3) which is isostructural with **H3•NAP**.

Table 4.3: Thermal analysis results and activation energy ranges for the three stages of decomposition of **H3•NAP** and **H3•IND**

Reaction Stage	H3•NAP		H3•IND	
	Mass loss % Exp (calc.)	Activation energy range (kJ mol^{-1})	Mass loss % Exp (calc.)	Activation energy range (kJ mol^{-1})
Stage 1	30.1 (30.1)	54.5 – 56.7	27.6 (28.1)	64.0 – 69.3
Stage 2	24.7 (24.8)	66.1 – 67.8	25.3 (25.4)	66.7 – 76.7
Stage 3	24.7 (24.8)	95.3 – 105.1	25.1 (25.4)	105.9 – 109.0

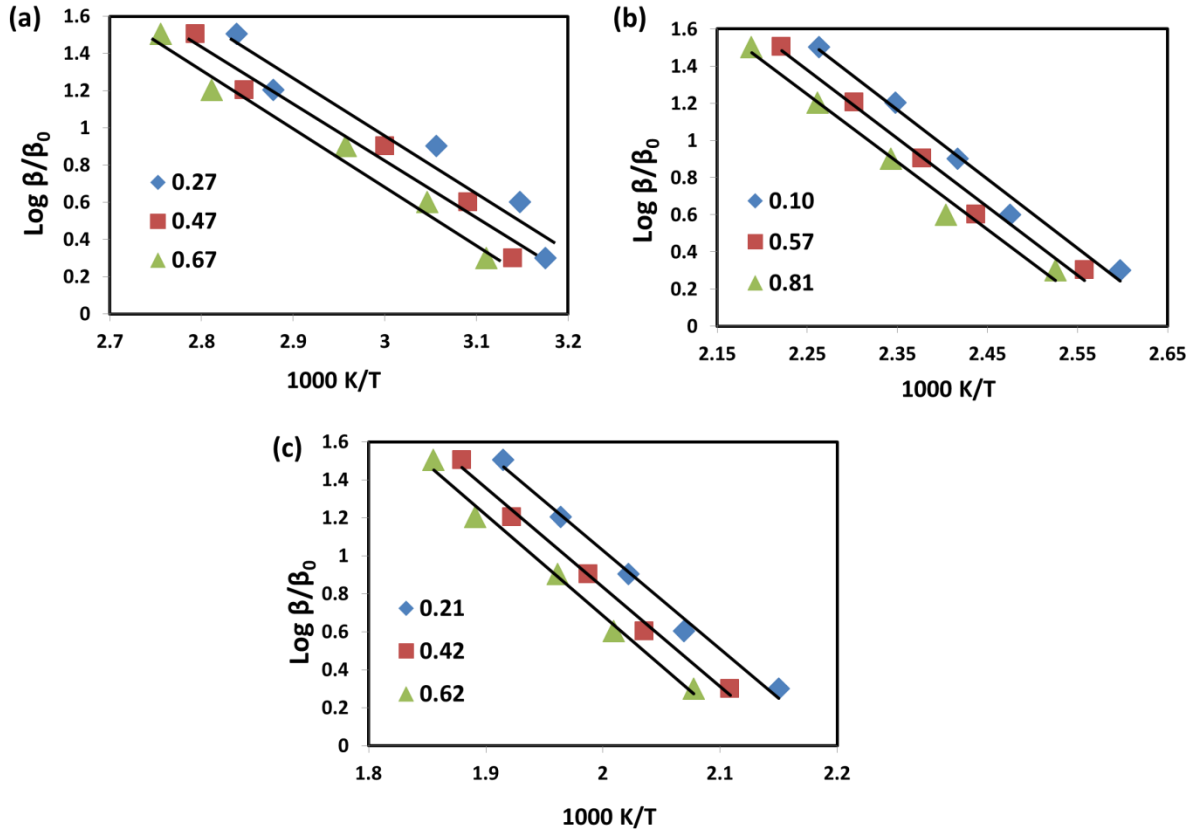

Fig 4.25 Activation energies of Stage 1 (a), Stage 2 (b) and Stage 3 (c) for **H3•NAP**. The values shown in each graph legend refer to the percentage of each stage in the non-isothermal TG curve at which the measurements were taken.

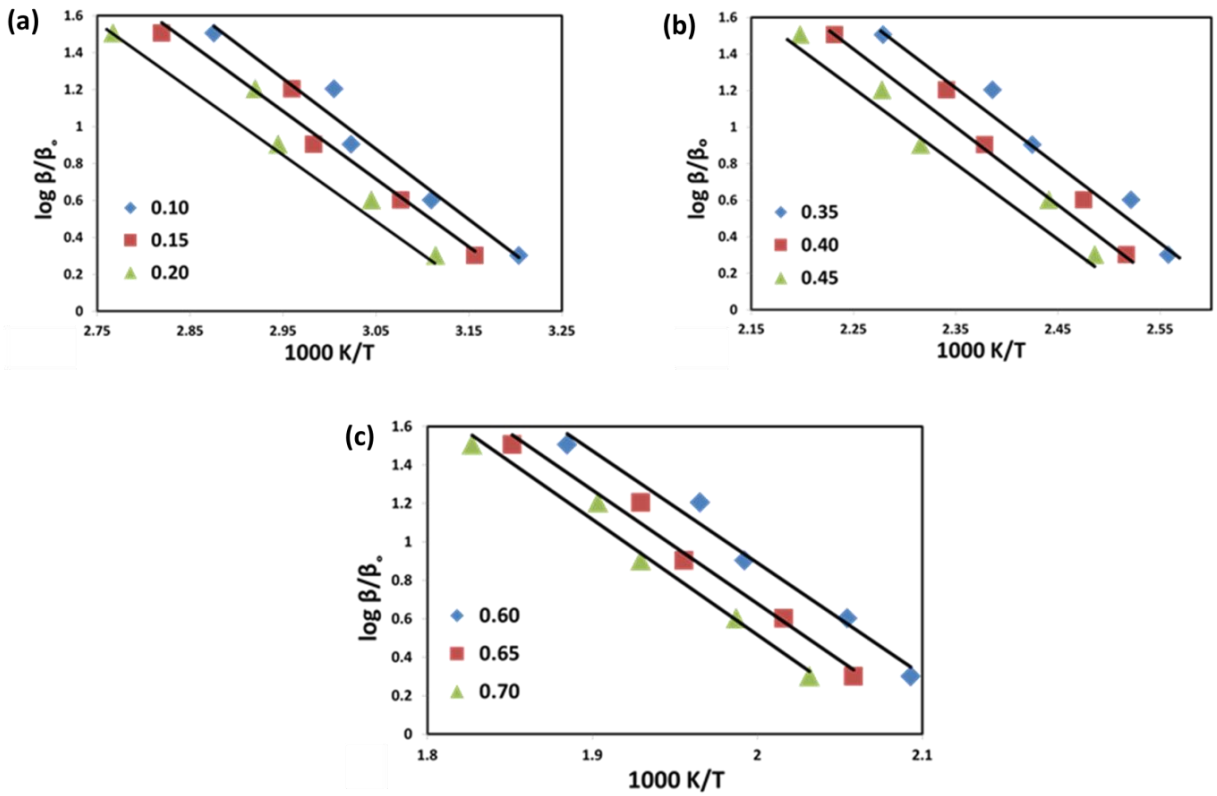

Fig 4.26 Activation energies of Stage 1 (a), Stage 2 (b) and Stage 3 (c) for **H3•IND**

Conclusion

The Werner clathrate $Ni(NCS)_2(4\text{-vinylpyridine})_4$ has been synthesised and used as a host in the synthesis of nine inclusion compounds with a selection of seven polycyclic aromatic hydrocarbons (PAHs). Green chemistry methods were used to enclathrate these environmental contaminants with the Werner host.

Single crystal structural analysis revealed two types of crystal arrangements. Indene, naphthalene and azulene yield isomorphous structures ($Pna2_1$) with the guests in crossed channels down [100] and [010]. The azulene guest was disordered in the same way as described by Robertson and co-workers.[34] The remaining inclusion compounds all crystallised in space group $P\bar{1}$ with the guests located in channels along [010]. Disorder was observed in certain thiocyanato and vinyl groups as well as in anthracene, phenanthrene and fluorene guests.

The enhancement of green chemistry was pursued in the formation methods of corresponding compounds with grinding, slurrying or melt procedures. Interesting results were obtained in the grinding experiments, many of which proved to be successful. The success of compound formation by grinding was dependent on diffusion as shown by the guests' naphthalene and azulene. Naphthalene, with low vapour pressures 11.5 Pa (25 ºC) and 75.8 Pa (50 ºC), favoured grinding to produce the final product, reaching this in just 2.5 minutes at 50 ºC. At a temperature of 35 ºC, azulene also provided a result similar to the generated **H3•AZU** crystal pattern. The rate constant and half-life were determined for the reaction between the host with these two guests. The addition of diamond powder after the grinding process provided and internal standard, against which the peak heights were measured for accurate determination.

Product formation with slurry methods with naphthalene, indene and azulene were successful at 25 ºC while with phenanthrene, fluorene and pyrene partial success was reached at 50 ºC. These guests all possessed minimal solubility in water at the corresponding temperatures to which the success of these experiments were related.

Non-isothermal thermogravimetric analysis was used to determine the kinetics of thermal decomposition for the clathrate crystals of indene and naphthalene. The intercalate form of the compound was displayed by lower activation energy for the release of the guest, which is not covalently bound to the nickel ion, than that of the loss of the host ligands.

Previously it was shown that the enclathration properties of Werner compounds may be altered by different crystallisation procedures but interestingly, this selected Werner host gives equivalent products when different ways of crystal formations are employed. The introduction of grinding and slurrying produced similar results to the single crystal generated patterns at temperatures which were directly related to the vapour pressures or solubilities respectively, of their guests.

Experimental section

Preparation of Werner clathrate

The host compound, **H3**, bis(isothiocyanato)tetrakis(4-vinylpyridine)nickel(II), was prepared by adding stoichiometric quantities of ethanolic solution of 4-vinylpyridine (20 ml, 0.01 M) to an ethanolic solution of nickel isothiocyanate (5 ml, 0.01 M). Blue crystals of $Ni(NCS)_2(C_7H_7N)_4$ were formed immediately and were filtered and allowed to air dry overnight.

Enclathration of any of the given guests via solution crystallisation was carried out by dissolving the host and the guest separately in warm alcohol, followed by addition of the guest solution to the host dropwise and stirring at a temperature of 50 ºC for 30 minutes. The solution was cooled, filtered and allowed to crystallise by slow solvent evaporation. Deep blue or violet crystals of each inclusion compound were formed.

Single crystal X-ray analysis

Intensity data of a selected single crystal for compounds **H3•IND**, **H3•NAP**, **H3•AZU**, **H3•FLU(I)**, **H3•FLU(II)**, **H3•ANT**, **H3•PHE**, **H3•PHE•BEN** and **H3•PYR•MeOH** were collected on a Bruker DUO APEX II diffractometer[35] with graphite monochromated Mo $K_{\alpha 1}$ radiation (λ = 0.71073 Å) at 173 K using an Oxford Cryostream 700. Data reduction and cell refinement were performed using SAINT-Plus.[36] The space group was determined from systematic absences by XPREP. The structure was solved using SHELXS-97[37] and refined using full matrix least squares methods in SHELXL-97[36] with the aid of the program X-Seed.[38] The hydrogen atoms bound to carbon atoms were placed at idealized positions and refined as riding atoms. In **H3•FLU(II)** and **H3•ANT** the guests were treated isotropically and the hydrogens were not added due to the high level of disorder. Diagrams and publication material were generated using PLATON,[39] X-Seed and Mercury (3.1).[40] Crystal data and structure refinement parameters are given in Table 4.1 and Table 4.2. Supplementary crystallographic data for structures are in: CDC1431480 (**H3•IND**); CCDC1431481 (**H3•NAP**); CCDC1431482 (**H3•AZU**); CCDC143143 (**H3•FLU(I)**); CCDC1431484 (**H3•FLU(II)**); CCDC1431485 (**H3•PHE•BEN**); CCDC1431486 (**H3•PHE**), CCDC1431487 (**H3•ANT**) and CCDC1431488 (**H3•PYR•MeOH**).

Solid-solid grinding experiments

Stoichiometric amounts of the host and guest were placed in a mortar and were ground at room or higher temperature as required for different time periods. The grinding was interrupted for a fixed amount of diamond powder to be added as internal standard before the product was analysed by a Bruker D8 X-ray powder diffractometer. The traces were compared with those of the starting materials and those generated from the single crystal structure. The rate constant and half-life of the reaction were determined from the graphic representation of the findings. The crystallinity of **NAP** did not change between 0 and 15 minutes grinding.

Co-crystallisation by slurry methodology

The slurry experiments were run at room temperature for 48 to 96 hours in water. The product was filtered, dried and analysed by PXRD. From the X-ray profiles, the reaction between the host and guest was determined by comparison with the pattern of the inclusion compound.

Melt experimentation

A mixture of stoichiometric amounts of the host and the guest were placed on the hot-stage microscope and the temperature was slowly raised 10 degrees above the guest's melting point and kept there for ten minutes and the product was analysed by powder X-ray diffraction.

References

[1] K. Tanaka and F. Toda, *Chem. Rev.*, **2000**, 100, 1025

[2] G. Nagendrappa, *Resonance*, **2002**, 7, 59

[3] T. Friščič, *Chem. Soc. Rev.*, **2012**, 41, 3493

[4] T. Friščič and W. Jones, *Cryst. Growth. Des.*, **2009**, 9, 1621

[5] G.R. Desiraju, J.J. Vittal and A. Ramanan, *Crystal Engineering*, **2011**, 79

[6] M. Lusi and L.J. Barbour, *Angew. Chem. Int. Ed.*, **2012**, 51, 1

[7] E. Batisai, M. Lusi, T. Jacobs and L.J. Barbour, *Chem. Commun.*, **2012**, 48, 12171

[8] J. Jacob, *Pure & Appl. Chem.*, **1996**, 68, 301

[9] A. Moissette, S. Marquis, I. Generb and C. Brémarda, *Phys. Chem. Chem. Phys.*, **2002**, 4, 5690

[10] M. Raters, and R. Matissek, *J. Agric. Food Chem.*, **2014**, 62, 10666

[11] J.-M. Lehn, *Supramolecular Chemistry Concepts and Perspectives*, **2009**, Wiley-VCH: Weinham, Germany

[12] K.K. Arora and V.R. Pedireddi, *Tetrahedron*, **2004**, 60, 919-925

[13] E. Curtis, L.R. Nassimbeni, H.Su and J.H. Taljaard, *Cryst.Growth.Des.*, **2006**, 6, 2716-2719

[14] A.D. Herrera-España, G. Campillo-Alvarado, P. Román-Bravo, D. Herrera-Ruiz, H. Höpfl and H. Morales-Rojas, *Cryst.Growth.Des*, **2015**, 15, 1572

[15] F. H. Allen, *Acta Cryst.*, **2002**, B58, 380-388

[16] J. Lipkowski, L. Gluzinski, K. Suwinska and G. D. Andreetti, *J. Incl. Phen.*, **1984**, 2, 327

[17] M.M. Wicht, N.B. Báthori and L.R. Nassimbeni, *Dalton. Trans.*, **2015**, 44, 6863

[18] W.D. Schaeffer, W.S. Dorsey, A. Skinner and C.G. Christian, *J.Am.Chem.Soc.*, **1957**, 79, 5870

[19] J. Lipkowski, in *Inclusion Compounds*, Academic Press, New York, **1984**, vol.1, ch.3

[20] J.Lipkowski, in *Comprehensive Supramolecular Chemistry*, ed. D.D. MacNicol, F. Toda and R. Bishop, Elsevier Science, Oxford, **1996**, vol.6, ch.20

[21] J. Lipkowski, K. Suwinska, J. Halt, A. Zielenkiewicz and W. Zielenkiewicz, *J. Inclusion Phenom., Mol. Rec. Chem.*, **1984**, 2, 317

[22] M.H. Moore, L.R. Nassimbeni, M.L. Niven and M.W. Taylor, *Inorg. Chim. Acta*, **1986**, 115, 211

[23] M.H. Moore, L.R. Nassimbeni and M.L. Niven, *Inorg. Chem. Acta*, **1987**, 131, 45

[24] L.R. Nassimbeni, M.L. Niven and A.P. Suckling, *Inorg. Chim. Acta*, **1989**, 159, 209

[25] L. Lavelle and L.R. Nassimbeni, *J. Incl. Phenom. Mol. Rec. Chem.*, **1993**, 16, 25

[26] S. M. Soliman, Z. B. Elzawy, M. A. M. Abu-Youssef, J. Albering, K. Gatterer, L. Öhrström and S. F. A. Kettle, *Acta Cryst.*, **2014**, B70, 115.

[27] J.D. Dunitz and A. Gavezzotti, *Acc.Chem.Res.*, **1999**, 32, 677

[28] R.P. Rastogi, P.S. Bassi, S.L. Chadha, *J.Phys. Chem.*, **1963**, 67, 2569

[29] R.P. Rastogi and N.B. Singh, *J.Phys. Chem.*, **1968**, 72, 4446

[30] D. Braga, S.L. Giaffreda, F. Grepioni, A. Pettersen, L. Maini, M. Curzi and M. Polito, *Dalton Trans.*, **2006**, 1249

[31] *CRC Handbook of Chemistry and Physics*, 87th Edition, **2006 – 2007**, CRC Press

[32] *Lange's Handbook of Chemistry*, 12th Edition, **1979**, McGraw-Hill Book Company

[33] J.H. Flynn and L.A. Wall, *Polymer Lett*., **1966**, 4, 323

[34] J. M. Robertson, H. M. M. Shearer, G. A. Sim and D. G. Watson, *Acta Cryst*., **1962**, 15, 1

[35] Bruker **2005**. APEX2. Version 1.0-27. Bruker AXS Inc., Madison, Wisconsin, USA.

[36] Bruker **2004**. SAINT-Plus (including XPREP). Version 7.12. Bruker AXS Inc., Madison, Wisconsin, USA.

[37] Bruker **2003**, XPREP2. Version 6.14. Bruker AXS Inc., Madison, Wisconsin, USA.

[38] L. J. Barbour, *J. Supramol. Chem*., **2001**, 1, 189.

[39] A. L. Spek, PLATON, A Multipurpose Crystallographic Tool, Utrecht University, Utrecht, The Netherlands, **2008**.

[40]C. F. Macrae, I. J. Bruno, J. A. Chisholm, P. R. Edgington, P. McCabe, E. Pidcock, L. Rodriguez-Monge, R. Taylor, J. van de Streek, P. A. Wood, *J. Appl. Cryst*., **2008**, 41, 466

Chapter 5

Enhanced selectivity towards xylene isomers of mixed ligand Werner complex

A new Werner complex, bis (isothiocyanato) bis (isoquinoline) bis (4-phenylpyridine) nickel(II), **H4**, was synthesised using the mixed-ligand approach to form structural intricacy. Elucidation of the crystal structures with xylene isomers produced different packing arrangements between **mx** compared with **ox** and **px**. Competition experiments were derived from the crystals obtained from solutions of mixed guests and analysing the resulting product using headspace GC and 1H NMR by sweating the crystal and dissolving the condensate in $CDCl_3$. This led to differentiation with **mx** the favoured isomer over the other two isomers as well as ethylbenzene, a similar C8 aromatic compound. Kinetics of thermal decomposition and Hirshfeld surface analysis were used to verify the stability and the close interactions found in the preferred clathrate, respectively.

Publication of Chapter 5:

Enhanced selectivity towards xylene isomers of mixed ligand Ni(II) thiocyanato complex

Merrill M. Wicht, Nikoletta B. Báthori and Luigi R. Nassimbeni

Polyhedron, **2016**, 119, 127-133

DOI:10.1016/j.poly.2016.08.022

Introduction

The separation of a mixture of structural isomers into their individual components using traditional methods is not feasible should their physical properties be similar. An important commodity of the petrochemical industry, para-xylene, is one of the most valuable products obtained from crude oil and used as raw material for the production of polyethylene terephthalate (PET), fibres, and polyester films.[1] In the case of the three xylene isomers, ortho (**ox**), meta (**mx**) and para (**px**), and ethylbenzene (**eb**), with respective boiling points of 144.4 °C, 139.1 °C, 138.4 °C and 136.5 °C, distillation is an ineffective undertaking for differentiation, especially in terms of the latter three aromatics. Other creative, but less conventional approaches, such as selective sorption or inclusion within a host material have been broadly studied and significant success has been achieved.[2] Contemporary inclusion resources such as metal-organic hosts[3,4] demonstrate the ability for selective inclusion and prediction of crystal structures and their properties. If one of the guest isomers is preferentially selected, the crystalline material can be filtered and retrieved from the solution and extracted, allowing the host substance to be recycled. Werner complexes, of general formula MX_2L_4, where M is a divalent metal cation (Ni^{2+}, Co^{2+}, Fe^{2+}, Cu^{2+} or Mn^{2+}), X is an anionic ligand (NCS^-, NCO^-, CN^-, NO^{3-} or halide) and L is a substituted pyridine or α-arylalkylamine, can accommodate changes in the anion (X^-) or ligand (L). Alterations in the 'tunability' of these Werner hosts arise on transformation of the nature and size of the inclusion cavities formed by the packing in square-planar or octahedral geometries.[5] These Werner compounds, although similar in structure, lack 'sticky' or attractive (such as hydrogen bonding) functionality, and rely on different architectures of the host suitable for the set of guest isomers.[2] In Chapter 3, the lack of preference of a Werner compound for one of the aromatic guest isomers was shown to be due to the rigidity of the isoquinoline ligand[6] leading to uniformity in the architecture of the structures. In Chapter 4, the enclathration properties of the Werner host $Ni(NCS)_2(4\text{-vinylpyridine})_4$ gave equivalent products on altering the methods of crystal formation with polyaromatic hydrocarbons.[7] However, the sorption properties of the Werner clathrate

$Ni(NCS)_2(4\text{-phenylpyridine})_4$ were investigated recently[8] giving discriminatory results with respect to the xylene isomers.

The concept of using a mixed-ligand host has previously been used in a variety of examples, and has reached better performances in a range of tasks which have included selectivity and sorption. The creation of new crystalline solids has considered the class of hybrid materials, existing as lattices of metal ions with organic ligand scaffolds. Structural complexity is reached by combining two different ligands to advocate a mixed-ligand approach.[9] In many of these cases, the current advances consider coordination polymer systems which bridge via mixed ligands. The combination of both acidic and basic ligands in the same structural assembly was more effective than acid – acid or base – base systems. Biological activity against human cancer cell lines were enhanced by the Cu(II) salicaldehyde-4-methyl-3-thiosemicarbazone mixed-ligand complex with imidazole and benzimidazole.[10] Two new three-dimensional porous structures of cadmium and cobalt demonstrated selective gas adsorption of CO_2 rather than N_2 and H_2. In both cases the mixed ligands were flexible and rigid organic ligands with different linear trinuclear metal carboxylate cores.[11] In a third example, an increase in fluorescence emission was observed following zinc coordination not seen in the free ligand.[12]

We based this study on the formation of a host with mixed ligands, one rigid and one flexible, to enhance discrimination of the xylene isomers by selective crystallization. Our speculation was that modification to the nature and size of the voids would be achieved for guest inclusion by the new host formed. Werner complexes usually contain four identical ligands, in fact, following a Cambridge Structural Database search,[13,14] in only four previous occasions has a Werner clathrate been synthesised with two different ligands, notably 4-methylpyridine and 4-phenylpyridine, positioned

trans to each other in host, $Ni(NCS)_2(4\text{-methylpyridine})_2(4\text{-phenylpyridine})_2$[15,16] and 4-methylpyridine and 4-carboxypyridine in a rhodium host (CSD Refcode GAGMOS).

A mixture of two previously used ligands, viz. isoquinoline the ligand in **H1**, and 4-phenylpyridine from **H2**, were considered. A new host, composed of two of each of the ligands, with the formula $Ni(NCS)_2(isoquinoline)_2(4\text{-phenylpyridine})_2$, **H4**, was synthesised. As the availability of the nitrogen lone pairs on these ligands is not reduced by steric hindrance, the basicity of each is similar (pKa values of the protonated bases are 5.08 (4-phenylpyridine) and 5.46 (isoquinoline))[17,18] and given equimolar amounts of isoquinoline and 4-phenylpyridine in the solution, they combine in an equivalent way to give Werner compound **H4**. Thermal gravimetric analysis was used to confirm the stoichiometry of this mixed ligand host.

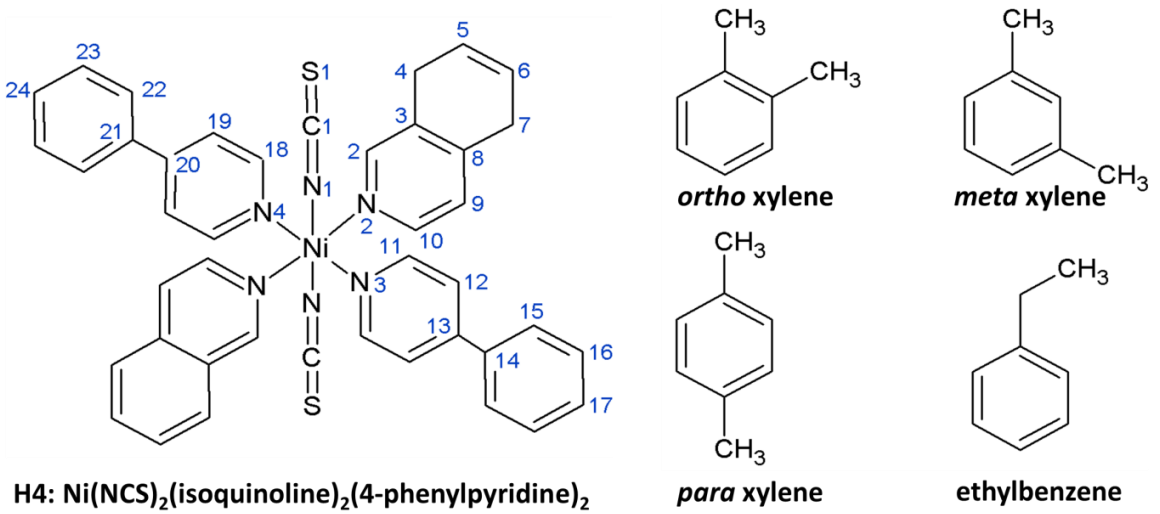

Scheme 5.1. Structural line diagrams and atomic numbering scheme of the host **H4**, Ni(NCS)2(isoquinoline)$_2$(4-phenylpyridine)$_2$, and guests, the three xylene isomers and ethylbenzene

Scheme 5.1 illustrates the host **H4** and the four guests, *ortho-*, *meta-* and *para* xylene isomers and ethylbenzene, a group of C8 compounds, difficult to separate and encountered in the petrochemical industry. The enhanced selectivity of this host for the xylene isomers is reported in this study.

Results and discussion

Crystal Structures

The structure of **H4•4px** was solved in the orthorhombic space group *Pbcn* (No. 60) and the details of the data collection and refinement are summarized in Table 5.1. The host molecule is located on a diad at Wyckoff position *c*. Therefore the asymmetric unit consists of half a host and two guests, one ordered (red) and one disordered (shown in two shades of purple) (Fig. 5.1(a)). **H4•2mx** crystallises in the space group *C2/c* (No. 15) with Z=4 (Fig. 5.1(b)), the Ni atom is located at Wyckoff position *e* and the host:guest ratio is 1:2. The isoquinoline ligands of the host are disordered and the ASU contains half a host and one guest. The structure of **H4•4ox** (Fig. 5.1(c)) is isomorphous with **H4•4px**, but shows no disorder. The crystal synthesised from a 50:50 mixture of **ox** and **px** selected both isomers to the same degree, giving the ratio **H4•2px•2ox**. The **ox** molecule presented disorder, and are shown in two shades of blue while the **px** guest is shown in red. The compound crystallised in the monoclinic space group *C2/c* with the Ni atom located in a centre of inversion at Wyckoff position *c*.

Table 5.1. Crystallographic data for **H4•4px**, **H4•2mx**, **H4•4ox and H4•2ox•2px**

·	**H4•4px**	**H4•2mx**	**H4•4ox**	**H4•2ox•2px**
Chemical Formula	$Ni(NCS)_2(C_{11}H_9N)_2$ $(C_9H_7N)_2$•$4(C_8H_{10})$	$Ni(NCS)_2(C_{11}H_9N)_2$ $(C_9H_7N)_2$•$2(C_8H_{10})$	$Ni(NCS)_2(C_{11}H_9N)_2$ $(C_9H_7N)_2$•$4(C_8H_{10})$	$Ni(NCS)_2(C_{11}H_9N)_2$ $(C_9H_7N)_2$•$2(C_8H_{10})$ •$2(C_8H_{10})$
Host:guest ratio	1:4	1:2	1:4	1:4
Formula Weight	1168.19	955.89	1168.21	1168.21
Temperature/K	173	173	173	173
Crystal System	orthorhombic	monoclinic	orthorhombic	monoclinic
Space Group (no.)	*Pbcn* (no.60)	*C*2/*c* (no. 15)	*Pbcn* (no.60)	*C2/c* (no.15)
a/Å	10.501(2)	10.912(2)	10.218(2)	10.031(2)
b/Å	22.981(5)	20.120(4)	22.863(5)	22.968(5)
c/Å	26.611(5)	23.100(5)	27.154(5)	28.095(6)
α/º	90	90	90	90
β/º	90	99.94(3)	90	91.92(3)
γ/º	90	90	90	90
V/A^3	6422(2)	4995.4(17)	6343(2)	6469(2)
Z´/Z	½ / 4	½ / 4	½ / 4	½ / 4
D_{calc}/$Mg.m^{-3}$	1.208	1.271	1.223	1.199
Radiation type	MoKα	MoKα	MoKα	MoKα
*F(*000)	2472	2008	2472	2472
Crystal size/mm	0.16 x 0.14 x 0.12	0.16 x 0.14 x 0.12	0.23 x 0.10 x 0.03	0.30 x 0.17 x 0.14
Colour, crystal form	Blue block	Blue block	Blue block	Blue block
No. of total reflections	36413	9949	26182	48086
No. of unique reflections	7168	4367	5820	7389
$\Theta_{min\text{-}max}$/º	2.3 / 27.2	1.8 / 25.04	1.5 / 25.4	1.45 / 27.50
$R[F^2>2\sigma(F^2)]$	0.0385	0.0695	0.0670	0.0511
$wR2(F^2)$	0.1017	0.1890	0.1783	0.1074
S	1.015	1.030	1.045	1.135
No. of parameters/data	458/7168	293/4367	383/5820	458/7389
Res.peak(max/min)/e A^{-3}	0.952 / 0.937	0.922 / 0.0941	0.910 / 0.988	0.887 / 0.945

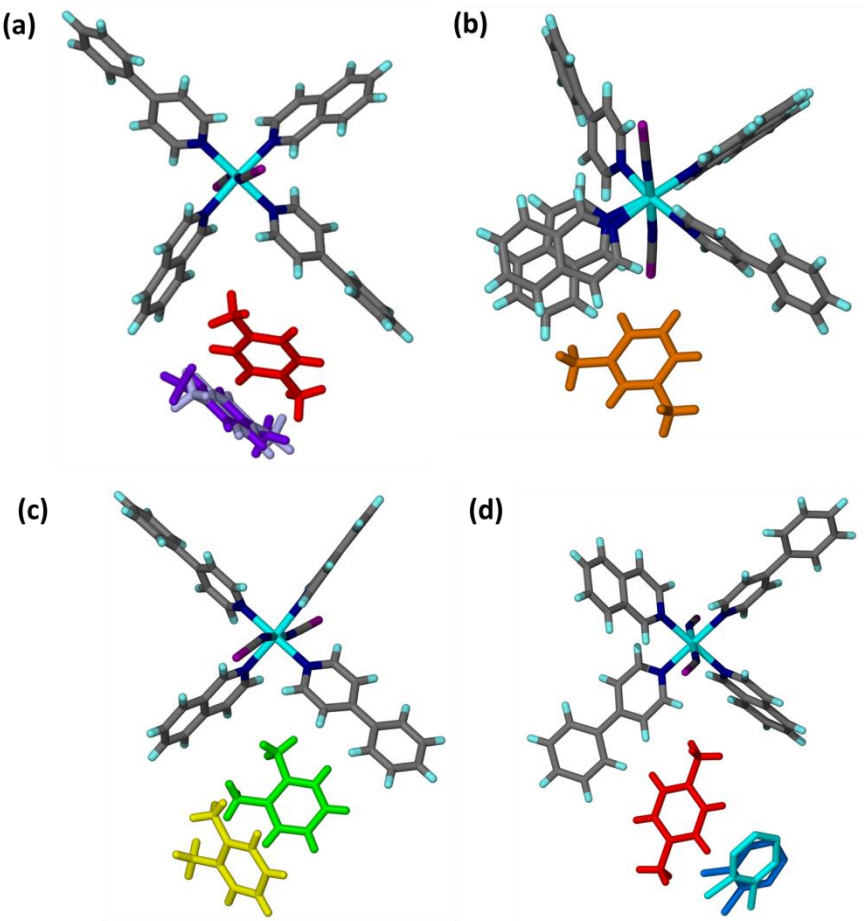

Figure 5.1 Molecular structure of (a) **H4•4px**, showing the two guests, one ordered in red capped stick model, and the second disordered shown in two shades of purple; (b) **H4•2mx** with the isoquinoline ligands disordered; with the ordered guest in orange capped stick model; (c) **H4•4ox** with two ox guests in edge to face arrangement in green and yellow capped stick model; and (d) **H4•2px•2ox** with the ordered px in red capped stick model and the disordered ox guests (without hydrogen atoms) in two shades of blue capped stick model

The aromatic rings of the two guests are in an edge to face arrangement and are found in channels running along [100] in both **H4•4px** and **H4•4ox** (see Fig 5.2(a) and Fig 5.2(c)). The high guest to host ratio is typical of the topology of a tubulate structure. In both cases the host is positioned in Wyckoff position *c*. In **H4•2mx**, the ordered **mx** guests are aligned in a head to head arrangement in cavities (Fig 5.2(b)).

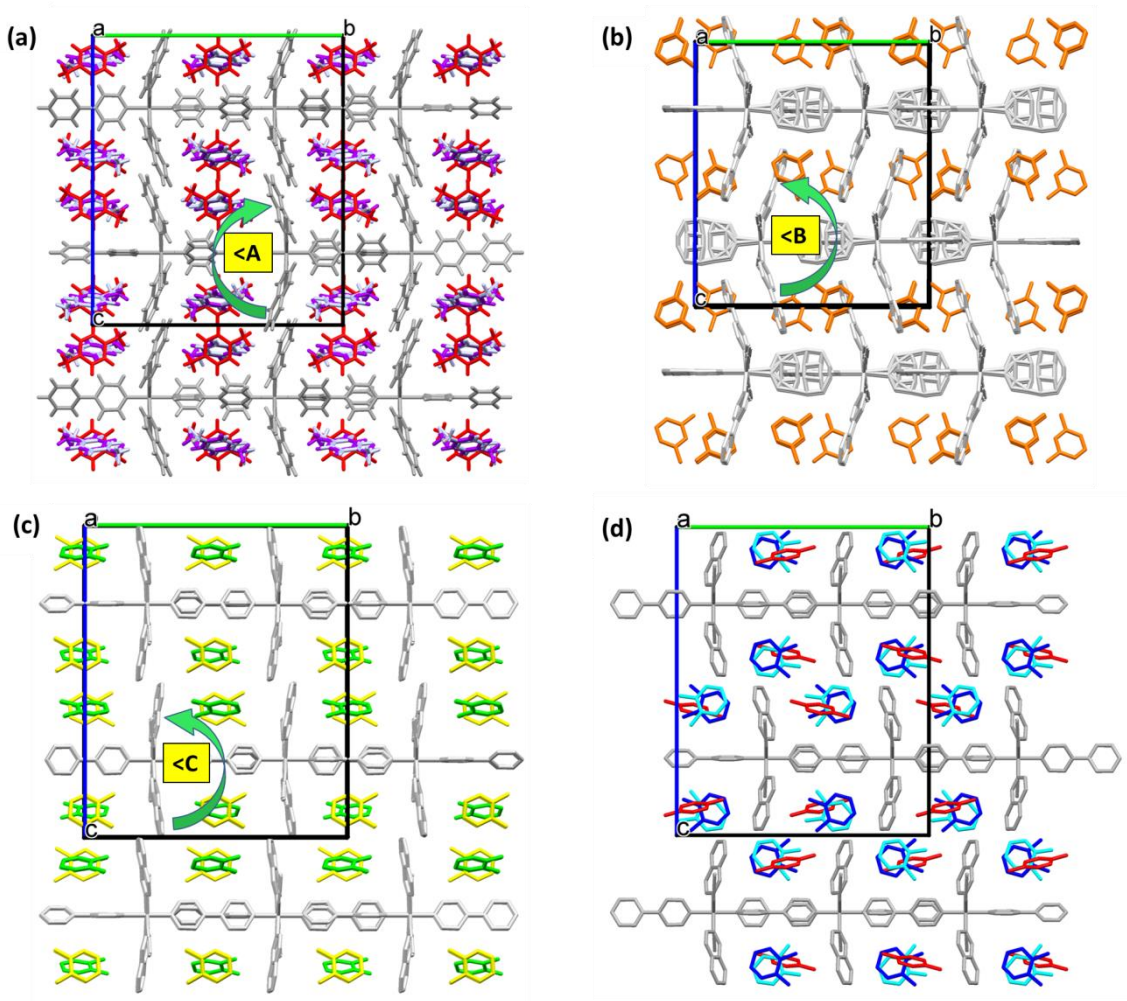

Figure 5.2 Packing of (a) **H4•4px** viewed down *a*, with the ordered **px** presented with capped stick model, red and disordered **px** in light and dark purple; plane angle shown as a green arrow with yellow annotation (**<A**); (b) **H4•2mx** viewed down *a*, with the guest **px** presented in orange capped stick model in a face to face arrangement in cavities between the host. Note the disorder in the isoquinoline ligands of the host; plane angle **<B**; (c) **H4•2ox** viewed down *a*, with the **ox** guests shown in green and yellow capped stick model in edge to face arrangement in channels down a; plane angle (**<C)** and (d) **H4•2px•2ox** viewed down *a*, with the **px** guests shown in red capped stick model and the disordered **ox** guests in two shades of blue. All molecules are shown without hydrogens

In all three cases, distortion of the ligands gives a wave shape of the packing that is different from previously studied Werner clathrates. The angle between the planes of the isoquinoline ligands, as illustrated in Fig. 5.3, ranges from values between 128.2 º and 152.3 º in the crystal structures, smaller

than the 180 º expected. This is shown in the packing diagrams Fig. 5.2(a), (b) and (c) where the angle C_aNiC_b is 128.2 ° in **H4•4px (**< A in Fig 5.2(a)) and 152.3 ° in **H4·4ox** (<**C** in Fig 5.2(c)) showing the bending of the ligands away from linearity typically found in Werner clathrates. In the case of **H4•2mx** the 4-phenylpyridine ligands bend giving an angle of 130.5 ° between the two planes (<**B** in Fig.5.2(b)) with small torsion angles of 11.2 ° and 12.3 ° at the linking bond between the two aromatic rings in the ligand. In the case of **H4•2px•2ox** trans ligands 4-phenylpyridine form a linear arrangement as shown in Fig 5.2(d) and the isoquinoline ligands tilt in opposite directions along the Ni···N bonds giving some flexibility in the host.

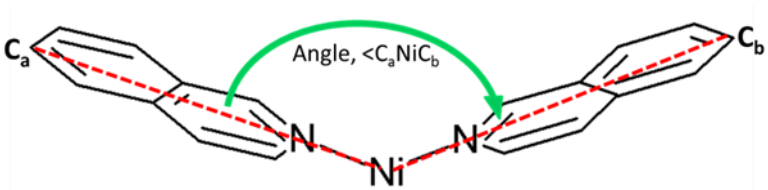

Figure 5.3 Illustration of the angle between the isoquinoline ligands and Ni which bends to form the wave packing design in these clathrates

Kinetics of thermal decomposition

The kinetics of thermal decomposition were measured for **H4•4px** and **H4•4ox** using the method of Flynn and Wall,[19] in which the mass losses of the compound were recorded at various heating rates varying from 2 to 32 $Kmin^{-1}$. The non-isothermal thermogravimetric curves for **H4•4px** are shown in Fig 5.4.

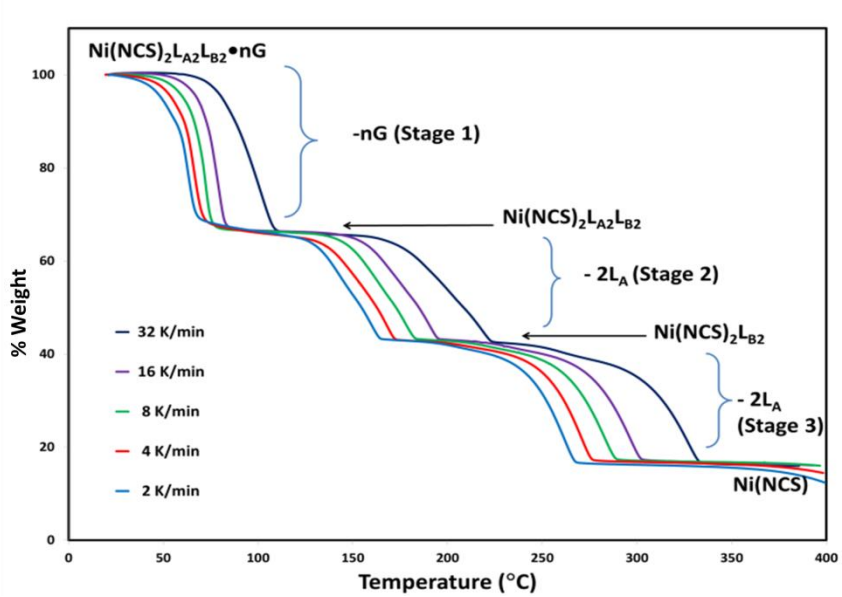

Figure 5.4 Non-isothermal curves for **H4•4px**

The decomposition occurred in three stages:

Stage 1 was due to the loss of the four guests in the case of **H4•4px** at a theoretical percentage of 36.35% with the experimental value matching this at 35.15%. Stage 2 could be attributed to the loss of the pair of isoquinoline ligands and Stage 3 the loss of the two 4-phenylpyridine ligands. Corresponding mass losses and activation energies calculated over α ranges for the inclusion compounds are indicated in Table 5.2. Activation energies were calculated from the slopes of the log β/β_0 vs 1/T graphs shown in Fig. 5.5.

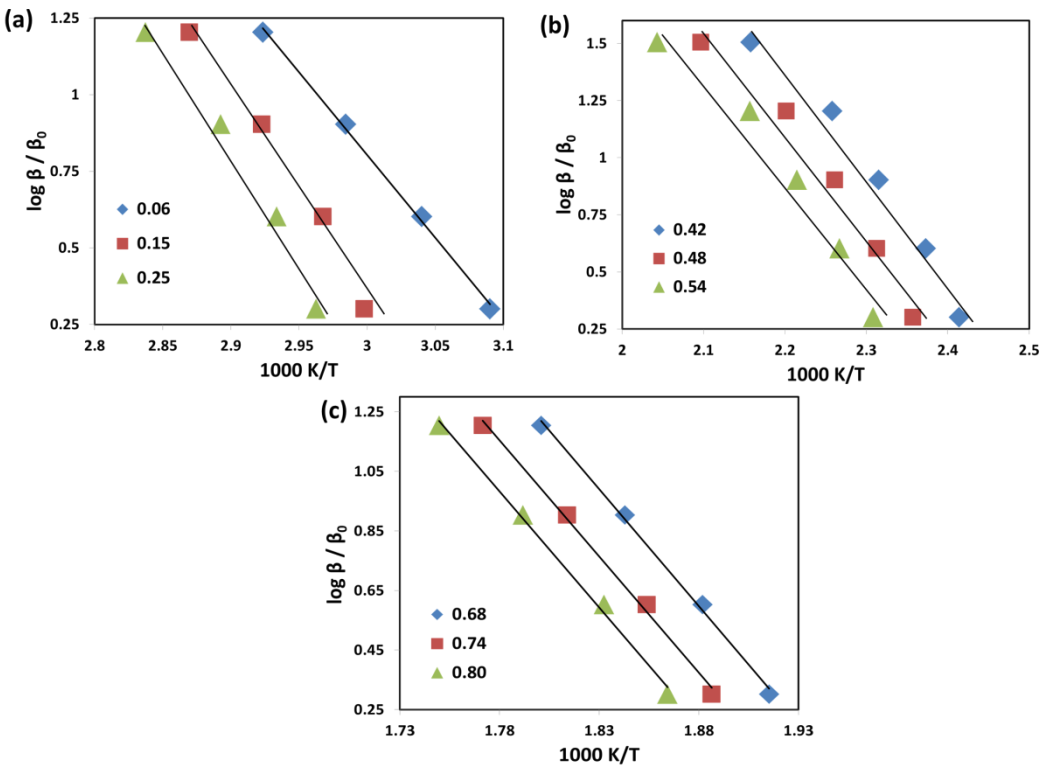

Figure 5.5 Activation energies for (a) Stage 1, (b) Stage 2 and (c) Stage 3 of **H4•4px**. The values in the legend are the percentage decomposition over the entire decomposition seen in Fig 5.4

The values shown in the legend of each graph are an indication of the extent to which the reaction has progressed from 0 to 1. β_0 is the standard heating rate, used in the y axis to prevent the log value from having units.

In the case of **H4•4px**, the Stage 3 decomposition required the largest activation energy of 141.8 – 142.9 kJ mol^{-1}, with Stage 2 the lowest activation energy of 81.7 – 84.8 $kJmol^{-1}$ (Table 5.2). The effect of the geometric property of the crystal on the thermal stability and kinetics of decomposition of inclusion compounds has been reviewed.[20] In **H4•4px** the guest is found in channels along the axis [100] and the tubulate structure confirms that the thermal stability and kinetics of decomposition of the first pair of ligands is expected to be lower than the loss of the guests from the host compound.

Even though the host:guest ratio in **H4•4ox** is 1:4, the guests are not always strongly enclathrated especially in the case of a volatile guest such as *ortho*-xylene. It is seen that the resultant overall molar mass of 913.53 $gmol^{-1}$ with the percentage guest is theoretically 18.60% but experimentally 17.94%. The full set of experimental and theoretical values are given in Table 5.2 and the non-isothermal thermogravimetric curves for **H4•4ox** are shown in Fig 5.6.

Table 5.2 Thermal analysis results and activation energy ranges for the three stages of decomposition of **H4•4px** and **H4•4ox**

	H4•4px		**H4•4ox**	
Reaction stage	**Mass loss % Exp. (Calc.)**	**Activation Energy range ($kJmol^{-1}$)**	**Mass loss % Exp. (Calc.)**	**Activation Energy range ($kJmol^{-1}$)**
Stage 1	35.15 (36.35)	98.3 – 128.8	17.94 (18.60)	104.5
Stage 2	22.57 (22.11)	81.7 – 84.8	28.40 (28.29)	61.4 – 67.8
Stage 3	26.22 (26.58)	141.8 – 142.9	32.44 (33.99)	86.9 – 92.0

In a similar way to **H4•4px**, Stage 3 of the **H4•4ox** decomposition has the highest activation energy of 86.9 – 92.0 kJ mol^{-1} and Stage 2 the lowest activation energy of 61.4 – 67.8 kJ mol^{-1}. The resemblance between the two structures, that is, the guest in channels giving a tubulate format, that generally leads to Stage 2 having the lowest activation energy. In both cases the loss of the guests constituted the highest activation energy of 98.3 – 128.8 kJ mol^{-1} (**H4•4px**) and 104.5 kJ mol^{-1} (**H4•4ox**) and these are shown in Table 5.2 with the activation energies of **H4•4ox** shown in Fig. 5.7.

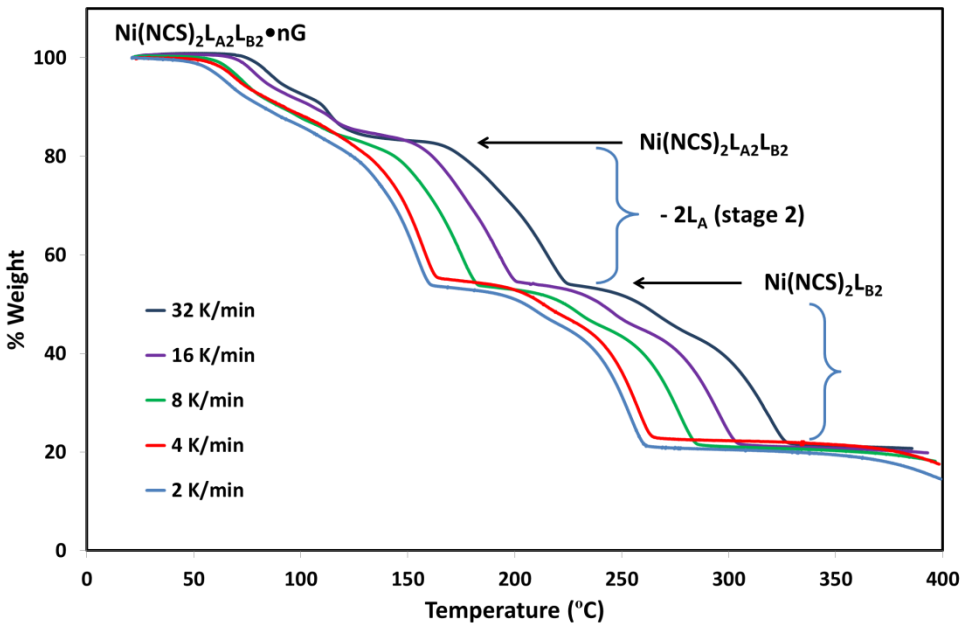

Figure 5.6 Non-isothermal curves for **H4•4ox**

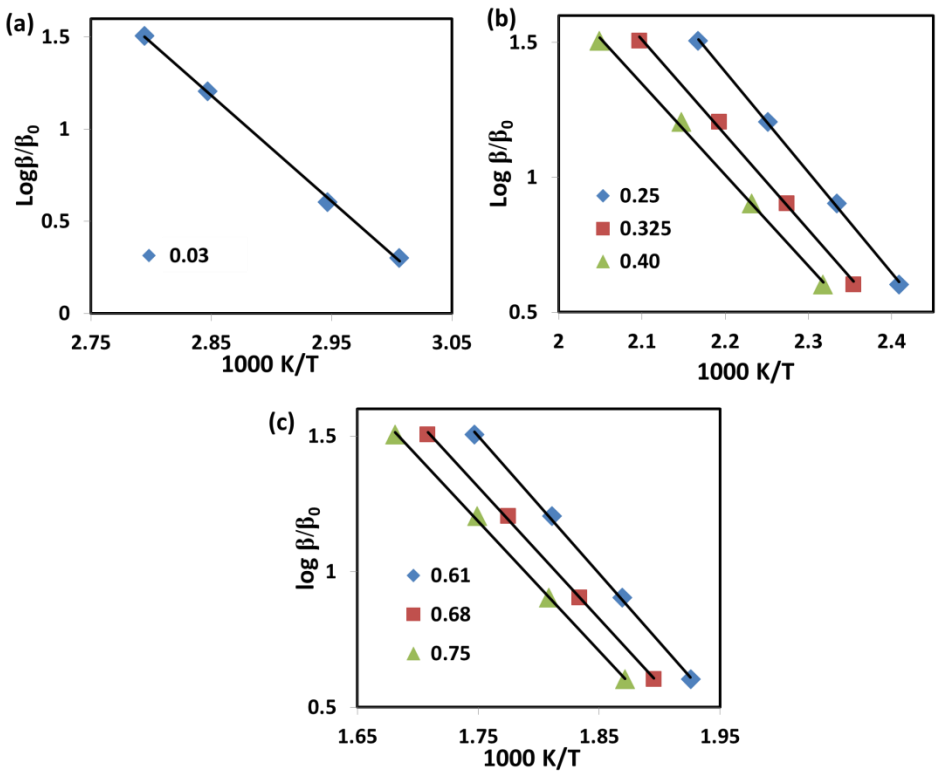

Figure 5.7 Activation energies for (a) Stage 1, (b) Stage 2 and (c) Stage 3 of **H4•4ox**

Selectivity Experiments

Previous work[8] has shown that discrimination between the three xylene isomers was found in the solid-vapour experiment with host $Ni(NCS)_2(4\text{-phenylpyridine})_4$. Using a combination of this ligand, which is flexible between the two aromatic rings, and isoquinoline with a large rigid aromatic surface area which is important for C-H···π and π···π host:guest interactions, the arrival at a discriminatory host for xylene isomer discretion was investigated.

The selectivity profile of this host **H4** was carried out by the method of dissolving the host in liquid mixtures of the guests with known proportions and harvesting the crystals of the ensuing inclusion compounds for analysis. Two methods of determination employed were headspace gas chromatography and NMR analysis. Due to the paramagnetic properties of nickel, NMR measurements were performed on metal-free samples. The guest was allowed to sweat from the crystal, condensed on the sides of the vial and washed into deuterated chloroform for NMR analysis. The competition experiments between pairs of xylene isomers (**ox/px**, **ox/mx** and **mx/px**) were performed at different ratios (0:1; 0.2:0.8; 0.4:0.6; 0.5:0.5; 0.6:0.4; 0.8:0.2 and 1:0). The crystals were harvested, dried and lightly crushed for analysis.

Solubility

During the preparation of crystallization solutions in binary and ternary xylene solutions, the solubility of the hosts in each xylene isomer were determined as shown in Table 5.3

Table 5.3. Solubility of hosts in xylene solutions

	ox	mx	px	o/m/p x
H1	*δ*	*i*	*i*	*δ*
H2	*i*	*i*	*δ*	*i*
H4	*s*	*δ*	*s*	*s*

i = insoluble; *δ* = slight; *s* = soluble

The solubility of **H4** in the xylenes was confirmed by the measurement of the intensity of the blue colour of the solution seen in Fig. 5.8 for the **mx/px** solutions. The measurement of the solutions in the visible spectrum resulted in λ_{max} at a wavelength of 584 nm. The spectra have been plotted in Fig. 5.9 for **mx/px**. The host is soluble in **px** but only slightly soluble in **mx.** In Fig 5.8 an increase in the blue intensity can be related to the increase in absorbance at 584 nm as the ratio of **mx** in the solution is decreased and **px** increased.

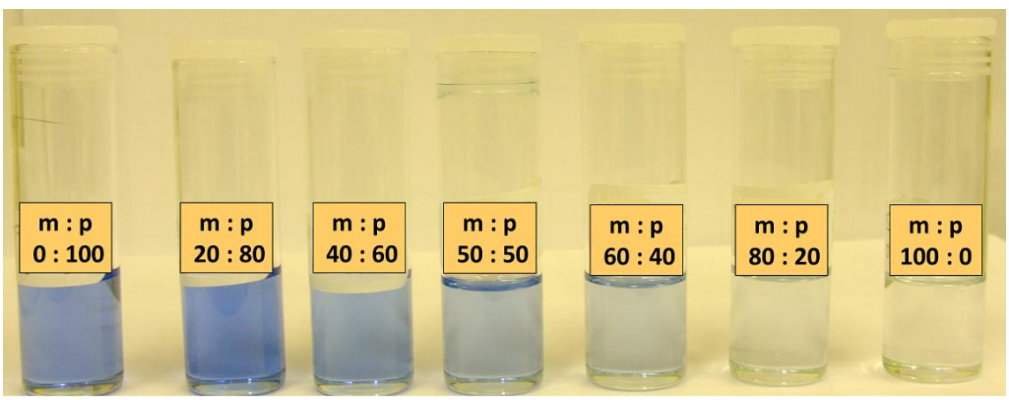

Figure 5.8 Set of solutions of **H4** in a combination of **mx/px** solutions showing the range of blue intensity related to the ratio of the two xylenes

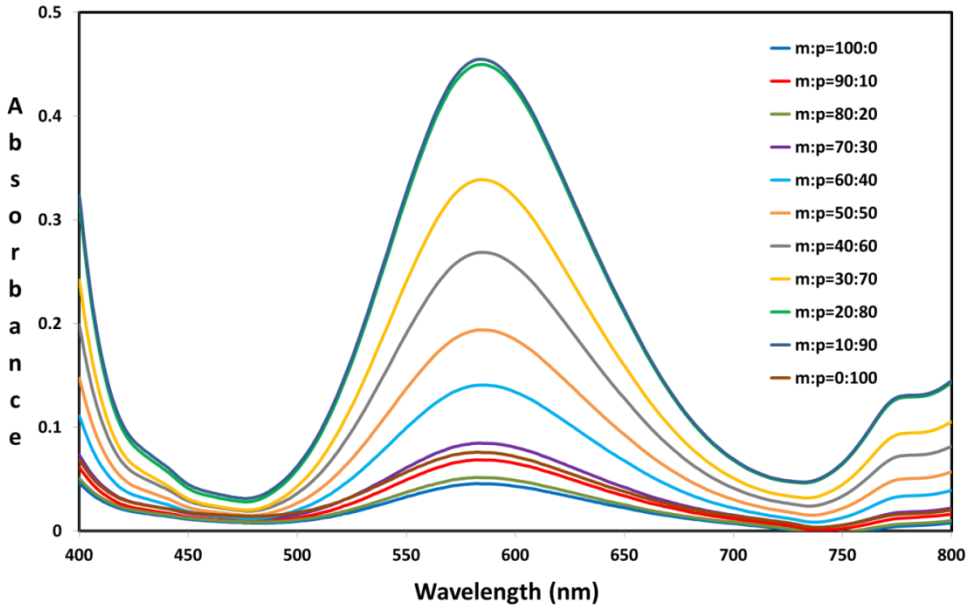

Figure 5.9 Spectra of the host **H4** solutions with a range of **mx:px** solutions

The **mx:px** solutions of 20:80 and 10:90 showed the maximum absorbance at 584 nm and the solution 20:80 has the most intense blue colour (see Fig. 5.8).

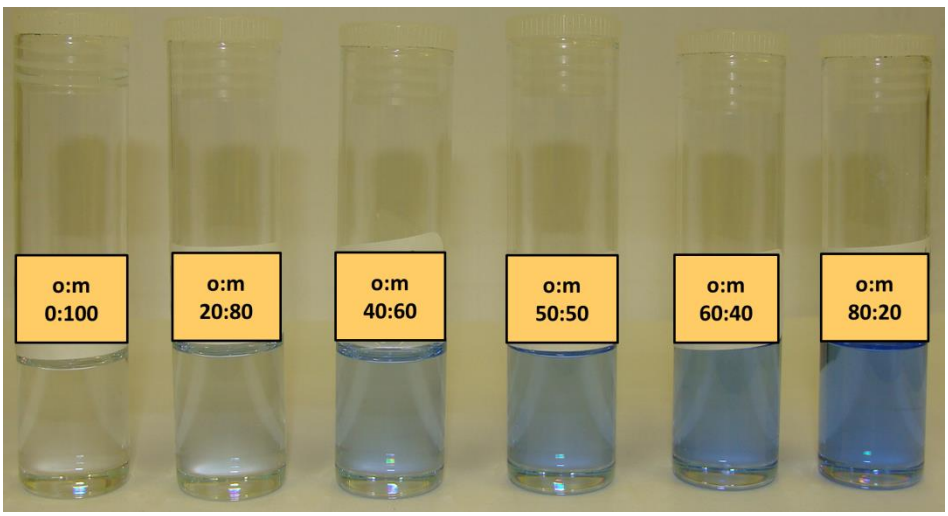

Figure 5.10 Set of solutions of **H4** in a combination of **ox/mx** solutions showing the range of blue intensity related to the ratio of the two xylenes

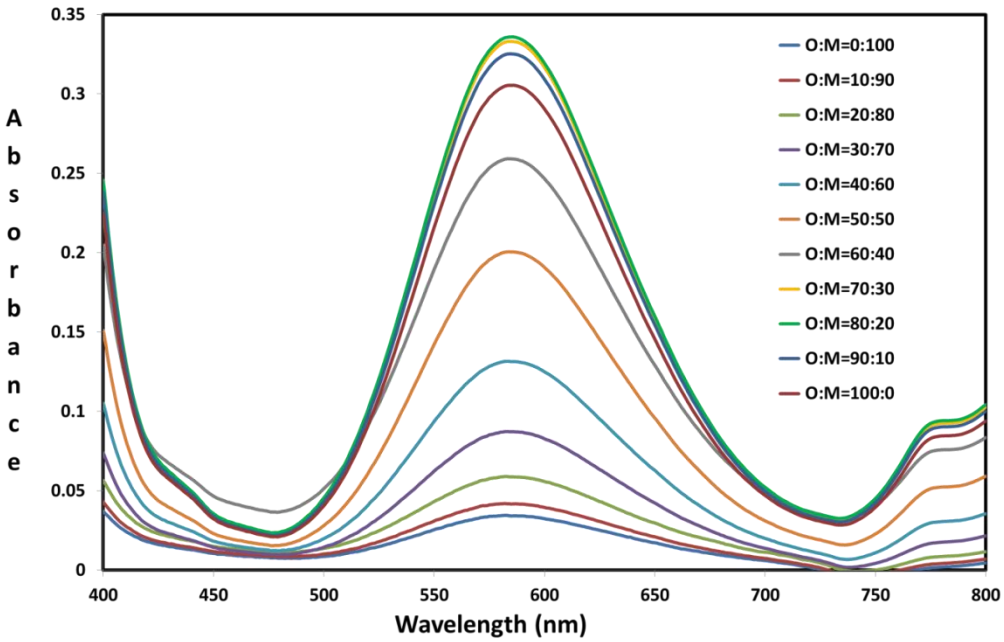

Figure 5.11 Spectra of the host **H4** solutions with a range of **ox:mx** solutions

Similarly to the **px:ox** solution, it was shown that the **ox:mx** solutions demonstrate a lack of solubility for **mx** together with good solubility of **ox**, resulting in the highest blue intensity in the solution with 80:20 ratio of **ox:mx** (Fig.5.10). This was observed in the spectra (Fig.5.11) with the highest absorbance at 584 nm occurring in **ox:mx** solution of 80:20.

Competition Experiments

The results of the competition experiments are shown in Fig. 5.12 in which the mole fraction of a given guest in solution (X_{guest}) is plotted against its mole fraction in the solid state (Z_{guest}). Blue points represent the headspace GC analysis and the red points are the NMR analysis results. NMR analyses were performed for a selection of the points. Acceptable agreement was reached between the two

methods; reproducibility of the GC results gave a mean standard deviation of 0.018; a coefficient of variation of 3.5%. The GC and NMR results are given in Table 5.4.

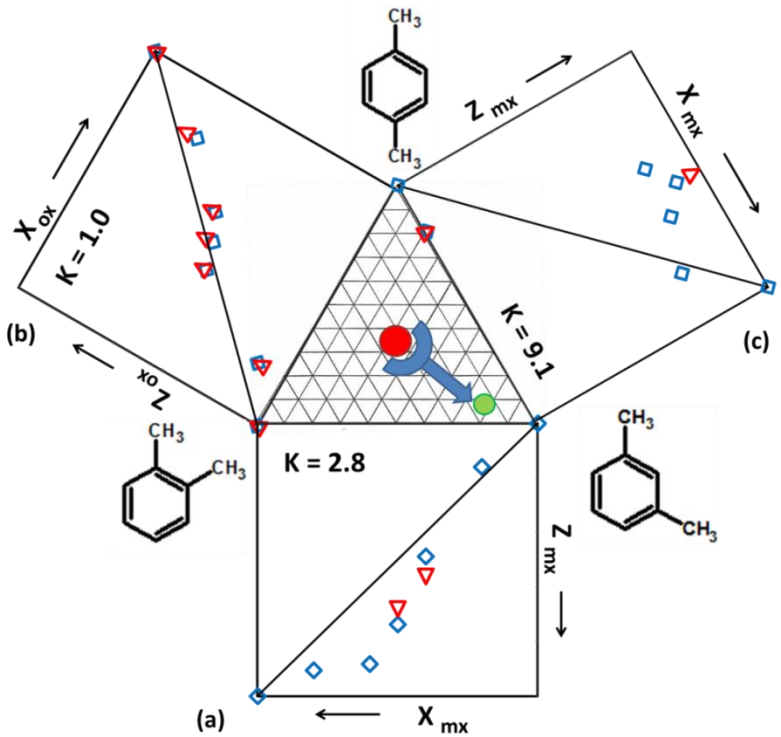

Figure 5.12. Selectivity of the host in binary guest mixtures of (a) **mx / ox**; (b) **ox / px** and (c) **mx / px** and **px / mx / ox** in the middle triangle. On the binary graphs, blue diamonds show the GC results and red triangles the NMR results.

Preference is shown for **mx** over **ox** for the composition mixture of **ox / mx** when $X_{meta} > 0.4$ and is shown in Fig 5.12(a). The selectivity of **ox** compared with **px** in the crystal structure is shown in Fig 5.12(b) with the host showing no preference for one over the other. This matches the similar solubility of the **H4** in **ox** and **px**. The selectivity profile of **mx / px** is contrasted with the **ox / px** competition as a distinct preference for **mx** with the greatest preference occurring between $0.4 < X_{meta} < 0.6$ (Fig 5.12(c)). The selectivity constants for the three pairs of guests, derived from their equimolar mixtures,

are estimated as follows: **mx / ox** : 2.8; **ox / px** : 1.0; and **mx / px** : 9.1. The host preference **mx** > **ox** > **px** is derived from these constants. In order to verify these preferences, the three isomers in a solution ratio of p:m:o : ⅓:⅓:⅓ gave the solid state result by GC of 7.2 : 77.0 : 15.8 and confirmed by NMR of 4.8 : 79.3 : 15.9. This is shown in the middle triangle of Fig 5.12 as the green circle which has moved from the equimolar point (red circle).

Table 5.4 GC and NMR results for selectivity analyses for the competition experiments

Guests	**Mole ratio** $X_A : X_B$	**GC result (%) (± std dev.)**	**NMR**	**Guests**	**Mole ratio** $X_A : X_B$	**GC result (± std dev.)**	**NMR**
mx:ox	0:100	0	0	**ox:px**	0:100	0	0
	20:80	15.9 ± 1.7	na		20:80	11.2 ± 0.7	9.9
	40:60	48.7 ± 2.1	55.9		40:60	44.2	45.7
	50:50	73.6 ± 8.5	67.6		50:50	49.0 ± 3.8	51.2
	60:40	88.1 ± 3.0	na		60:40	51.8	53.6
	80:20	90.5 ± 1.5	na		80:20	71.0	75.8
	100:0	100	100		100:0	100	100
mx:px	0:100	0	0	**px:mx:ox**	33:33:33	7.2 (px)	4.8
	20:80	0.9 ± 0	1.0			77.0 (mx)	79.3
	40:60	82.6 ± 6.0	na			15.8 (ox)	15.9
	50:50	90.1 ± 2.2	97.1				
	60:40	82.0 ± 7.2	na	**eb**:**px**:**mx**:**ox**	25:25:25:25	25.2 (eb)	
	80:20	74.9	na			10.2 (px)	
	100:0	100	na			46.6 (mx)	
						18.0 (ox)	

na = not available

A foursome selectivity experiment with the three xylene isomers and ethylbenzene in an equimolar (25% each) solution gave the outcome 25 : 10 : 47 : 18 for **eb** : **px** : **mx** : **ox**. The isomer of choice is **mx**, followed by **eb**, **ox** and **px**.

Hirshfeld surface analysis

The intermolecular interactions between the xylene guests and the host framework were analysed using the program Crystal Explorer[21] which calculates the Hirshfeld surface[22] of a target molecule in a crystal structure and depicts all its interactions with the neighbouring molecules. In Fig. 5.13(a) the form of **mx** covered by its Hirshfeld surface when surrounded by host and associate guest molecules are presented and the generated fingerprint plot[23], the 2D representation of the 3D surface, is given in Fig. 5.13(b). The red area on the surface indicates C-H···π close contacts between the guest and the host with an estimated distance of 2.7 Å as shown by ② in Fig 5.13(b). This contact is closer than expected in a C···H interaction (2.9 Å)[24]. Overall, the fingerprint plot indicates relatively close packing.

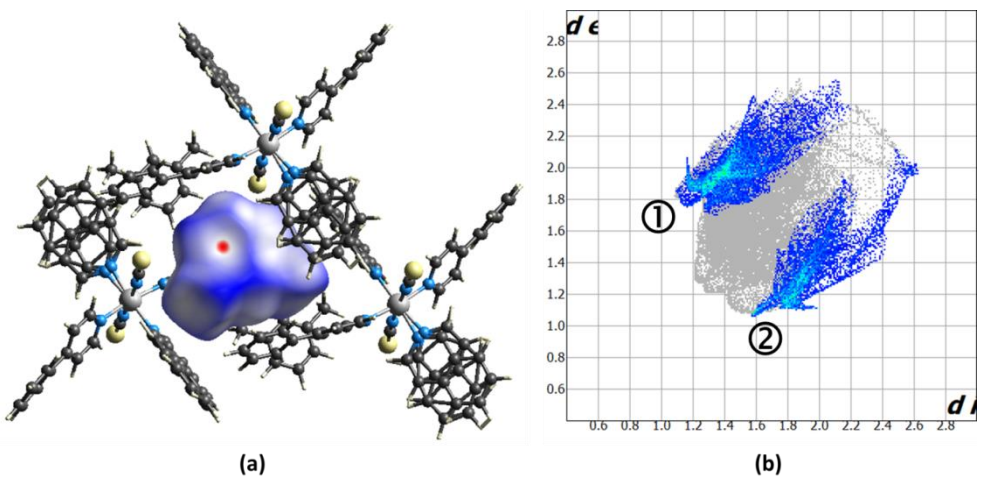

Figure 5.13. (a) Hirshfeld surface of the inclusion compound **H4•2mx** and (b) fingerprint plot of the **H4•2mx** C···H interactions, with ① showing C-H···π of host to guest and ② the C-H···π of guest to host interactions

Hirshfeld surfaces and fingerprint plots are shown for the **px** guests in **H4•4px**, with the ordered guest 1 in Fig 5.14 (a), (b) and (c) and each of the disordered guests in Fig.5.14 (d), (e) and (f) (guest 2a) and Fig.5.14 (g), (h) and (i) (guest 2b). The C···H contacts in blue in the fingerprint plot comprise an approximate percentage of the interactions. These are summarised in Fig 5.16 in which the orange bar shows the percentages for all C···H interactions for the selected molecule and allocated between the molecule and its surrounding. The H···H interactions are shown as percentages in the green bars and the other interactions, which include S···H interactions are shown in the blue band. In **H4•2mx** 3% of the interactions involve sulphur.

For the **px** guest 1, the C···H interactions are 2.85 Å and 2.63 Å and for H···H the shortest distance is 2.4 Å, which is very similar to the sum of the van der Waal's radii. For **px** guest 2a (disordered), the distances for the C···H interactions in Fig.5.14(e) are 2.75 Å and 2.85 Å. However, in Fig.5.14(f) the shortest H···H interaction is 2.3 Å which may refer to repulsion between the hydrogens. The interactions of 4.9 Å and 5.05 Å, show that the packing in this structure is not as intimate as those with shorter interactions, such as **H4•4px** guest 1 and **H4•2mx**. Of note in the **H4•4px** Hirshfeld surface with the second disordered guest 2b are the H···H interactions which vary from 2.5 Å to 4.9 Å, again showing loose packing, similar to disordered guest 2a and shown in Fig 5.14(i).

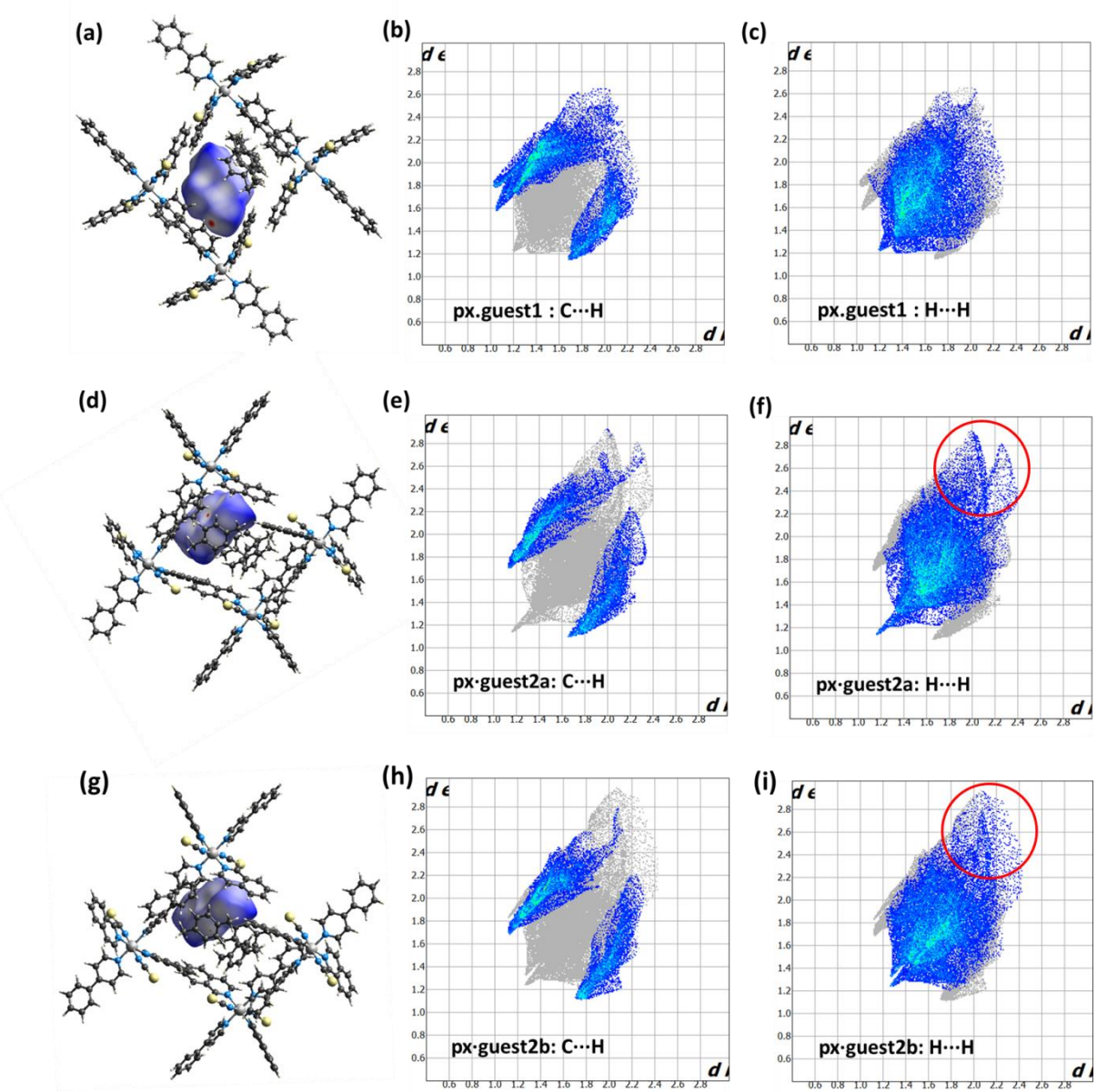

Figure 5.14 (a) Hirshfeld surface of ordered guest 1 in **H4•4px** with the fingerprint plots of (b) C···H and (c) H···H interactions; (d) Hirshfeld surface of guest 2a (first disorder) in **H4•4px** with the fingerprint plots of (e) C···H and (f) H···H interactions; and (g) Hirshfeld surface of guest 2b (second disorder) in **H4•4px** with the fingerprint plots of (h) C···H and (i) H···H interactions. Possible repulsion at a distance of 2.2 Å and loose packing is shown by the red circle in (f) and (i)

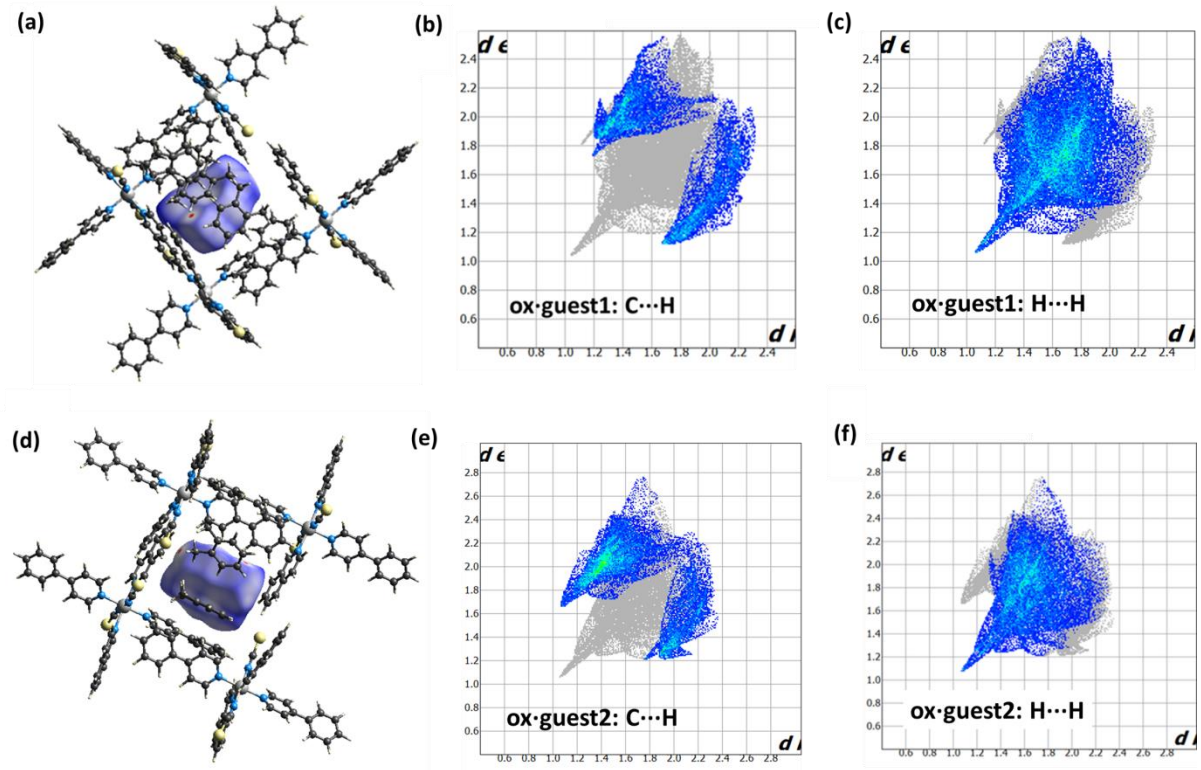

Figure 5.15 (a) Hirshfeld surface of guest 1 in **H4•4ox** with the fingerprint plots of (b) C···H and (c) H···H interactions and (d) Hirshfeld surface of guest 2 in **H4•4ox** with the fingerprint plots of (e) C···H and (f) H···H interactions

Hirshfeld surfaces for **H4•4ox** are shown in Fig 5.15. The C···H interactions for the guest 1 structure are found with interaction distances of 2.75 Å and 2.85 Å and are shown in Fig. 5.15(b). Despite these relatively short distances, H···H interactions between the two guests are indicated by the peak in Fig 5.15(c) with an interaction distance of 2.2 Å, shorter than the standard interaction length of 2.4 Å. Repulsion between the hydrogen atoms is feasible at these smaller distances. Intimate C···H interactions in **H4•4ox** guest 2 are found (2.95 Å and 2.75 Å) and these are shown by the red dots in the Hirshfeld surface diagram Fig 5.15(d). Similar results to guest 1 were found for this guest 2, showing a close relationship and perhaps repulsive mode between the host and guest hydrogens with interactions of (2.15 Å).

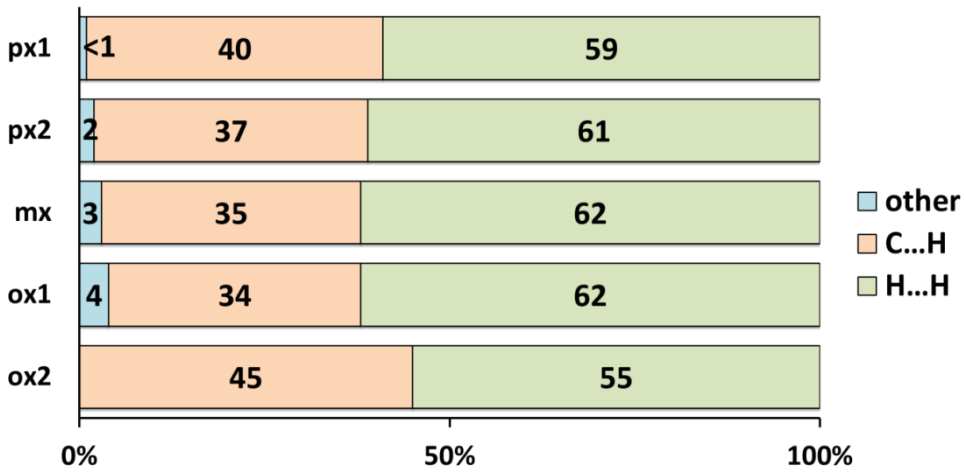

Figure 5.16. Summary of the intermolecular interactions for **px Guest 1**; **px disordered Guest 2**; **mx**; and **ox Guest 1** and **ox Guest 2**

Fig. 5.16 summarises the intermolecular interactions calculated for the selected guests, showing the percentage of the C···H, H···H and other interactions. In cases where repulsive interactions were plausible, and possible loose packing observed, as is the case with **H4•4px** and **H4•4ox**, no discrimination was found. However, in the case of **H4•2mx,** repulsive interactions were not perceived and positive discrimination was found.

Comparison of voids

The final analysis of the voids present in each crystal discussed in this chapter were carried out using Mercury (3.8)[25] with the criteria set to a probe radius of 1.2 Å and approximate grid spacing of 0.8 Å. The diagrams obtained are shown in Fig. 5.17. It was noted that the packing of **H4•4px**, **H4•4ox** and **H4•2px•2ox** were similar with all showing a tubular structure with a similar percentage void spacing in the unit cell. In Table 5.5 the percentage void and the volume in $Å^3$ are listed.

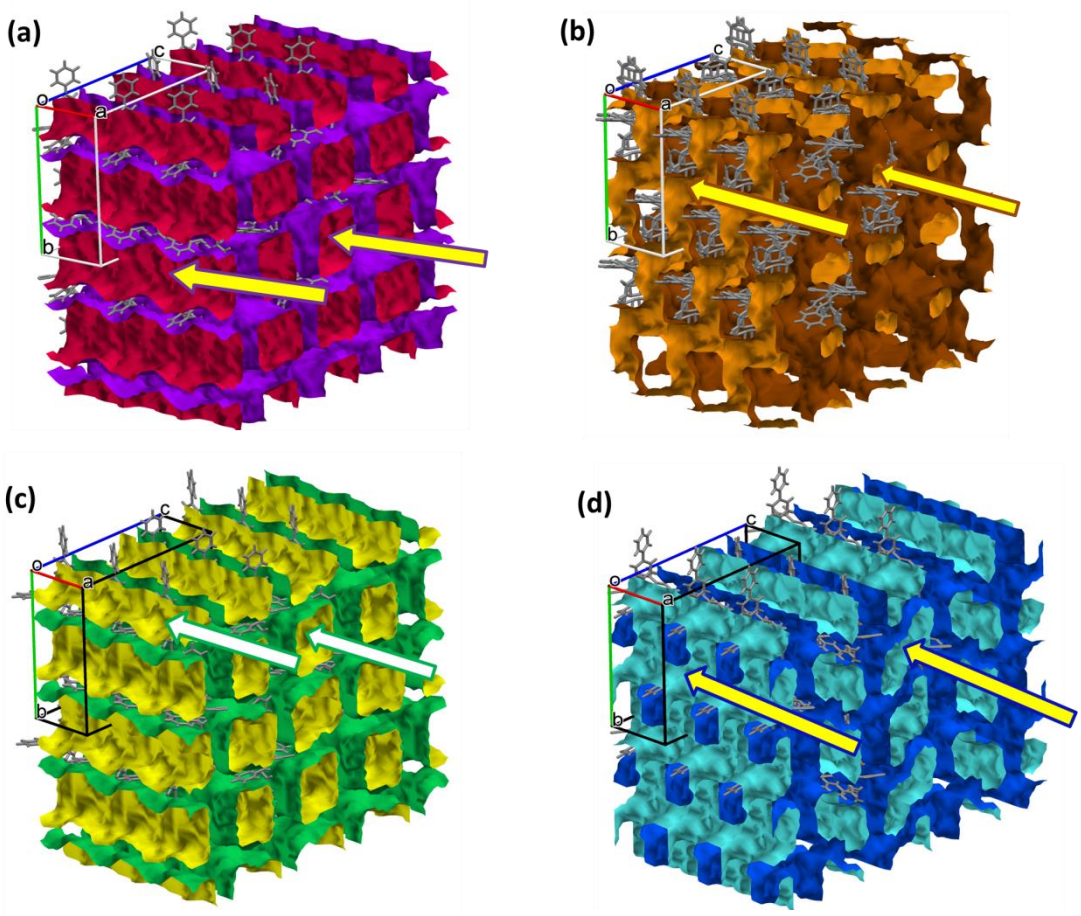

Figure 5.17 Void spacing shown for (a) of **H4•4px**, (b) **H4•2mx,** (c) **H4•4ox** and (d) **H4•2px•2ox** with the arrows pointing to the tubes formed along [100]

Table 5.5 Void spacing in the unit cells

	H4•4px	**H4•2mx**	**H4•4ox**	**H4•2px•2ox**
Percentage Void (%)	49.7	27.8	49.5	48.6
Volume ($Å^3$)	3191.4	1386.6	3142.5	3145.1
Density (Mg/m^{-3})	1.208	1.271	1.223	1.199

In **H4•2mx**, the smaller percentage and volume of the voids is further evidence of more efficient packing and the arrows in Fig.5.17(b), although denoting a channel, signify a smaller and irregular

periphery resulting in minimal vacant space. The density values for these clathrates, given in Table 5.5, endorse the observation of the Hirshfeld surfaces and the void spacing determination.

Conclusion

A new Werner complex has been formed by mixing ligands from two different hosts in equimolar proportions. The ligands *trans* coordinated to the $Ni(NCS)_2$ compound, forming the host $Ni(NCS)_2(isoquinoline)_2(4\text{-phenylpyridine})_2$ which contained both the rigid isoquinoline and the flexible 4-phenylpyridine ligands.

The crystal structures of this host with the three xylene isomers, *ortho*-, *meta*- and *para*-xylene, and a 50:50 mixture of *ortho:para* were elucidated and the packing scrutinised. The arrangement of the ligands gave the new host flexibility to pack *meta* xylene more intimately than the other two isomers, giving it the advantage of the favoured isomer in terms of selectivity hence the **mx** > **ox** > **px** outcome of this study. This finding was confirmed by Hirshfeld surface analysis as well as void spacing determination.

The mixed ligand Werner complex, probed in this work, has the ability to differentiate between the four C8 aromatic compounds, in the order **mx** > **eb** > **ox** > **px**, a beneficial discovery in the selectivity of Werner inclusion compounds.

Experimental Section

Preparation of Werner clathrate

The host compound, **H4**, bis (isothiocyanato) bis (isoquinoline) bis (4-phenylpyridine) nickel(II), was prepared by adding an equimolar ethanolic mixture of isoquinoline and 4-phenylpyridine to $Ni(NCS)_2$ aqueous solution in the ratio 2:1. The solution was stirred at room temperature until precipitation occurred. Filtration and air drying for 24 hours followed, giving a violet crystalline compound of **$Ni(NCS)_2(C_9H_7N)_2(C_{11}H_9N)_2$**.

Enclathration of the given xylene guests or mixtures of guests were carried out by stirring **H4** in the guest solution at 48ºC for 30 minutes, filtering and allowing for crystallisation to occur within one to seven days. Small deep blue crystals of **H4•4px**, **H4•2mx, H4•4ox** and **H4•2px•2ox** were formed.

Single crystal X-ray analysis

Intensity data of a selected single crystal for compounds **H4•4px**, **H4•2mx, H4•4ox** and **H4•2px•2ox** were collected on a Bruker DUO APEX II diffractometer[26] with graphite monochromated Mo $K_{\alpha 1}$ radiation (λ = 0.71073 Å) at 173 K using an Oxford Cryostream 700. Data reduction and cell refinement were performed using SAINT-Plus.[27] The space group was determined from systematic absences by XPREP.[28] The structure was solved using SHELXS-97[29] and refined using full matrix least squares methods in SHELXL-97[28] with the aid of the program X-Seed.[30] The hydrogen atoms bound to carbon atoms were placed at idealized positions and refined as riding atoms. Diagrams and publication material were generated using PLATON,[31] X-Seed and Mercury (3.8).[30] Crystal data and structure refinement parameters are given in Table 1, CCDC 1484847 – 1484849 which contain the supplementary crystallographic data for structures **H4•4px**, **H4•2mx** and **H4•4ox**. All files can also be found in the Supplementary Data.

Thermogravimetric analysis

Thermal analyses were performed on a TA Q500 instrument from 25 to 400 °C at heating rates of 2, 4, 8, 16 and 32 °C min^{-1} with a purge gas of dry nitrogen flowing at 60 ml min^{-1}. All samples were dried on filter paper and placed in an open crucible for thermogravimetric analysis. Sample masses varied from 2 to 5 mg.

Competition experiments

The selectivity of the host for a particular isomer was evaluated using solution crystallisation and analysing both by headspace gas chromatography and NMR spectroscopy. The method involved crystal formation of the host with guest mixture using the same procedure mentioned above. Crystals were harvested, dried and placed in headspace vials for GC analysis. In the case of NMR analysis, the crystals were dried, crushed and allowed to sweat to allow the guest to evaporate and condense on the inside of the vial. This was washed into deuterated chloroform for NMR analysis.

Gas chromatography

GC analysis was performed on an Agilent 7890A instrument with Varian CP Wax capillary column (30 m x 250 µm x 0.25µm), nitrogen carrier gas and FID detector with inlet and detector temperatures of 280 °C. Vials were incubated at 60 °C for 10 minutes before injection; oven temperature at 30 °C for 3 minutes, followed by a gradient at 10 °C min^{-1} to 120 °C for 2 minutes.

NMR Spectroscopy

^{1}HNMR spectroscopy was performed on a Bruker ultrashield 400+ spectrometer with the ^{1}H spectra calibrated with deuterated chloroform, $CDCl_3$.

References

[1] M.S.P Silvaa, J.P.B. Mota, and A.E Rodrigues, *Separation and Purification Technology*, **2012**, 90, 246 - 256

[2] A.M Pivovar, K.T. Holman, and M.D. Ward, *Chem. Mater*., **2001**, 13, 3018 - 3031

[3] M.J. Zaworotko, *Chem. Commun*., **2001**, 1 – 9

[4] D. Braga, J. Chem. Soc., *Dalton Trans*., **2000**, 3705 - 3713

[5] C.B. Aakeröy, A.M. Beatty and D.S. Leinen, *Angew. Chem. Int. Ed*., **1999**, 38, 12, 1815 - 1819

[6] M.M. Wicht, N.B. Báthori and L.R. Nassimbeni, *Dalton Trans*., **2015**, 44, 6863

[7] M.M. Wicht, H. Su, N.B.Báthori and L.R. Nassimbeni, *CrystEngComm*, **2016**, 18, 2509 - 2516

[8] M. Lusi, and L. Barbour, *Angew. Chem., Int. Ed*., **2012**, 51, 3928 – 3931.

[9] M. Du, C-P. Li, C-S. Liu and S-M. Fang, *Coord. Chem. Rev.*, **2013,** 257, 1282.

[10] N.A. Mazlan, T.B.S.A. Ravoof, E.R.T. Tiekink, M.I.M. Tahir, A. Veerakumarasivam, and K.A. Crouse, *Transition Met Chem*., **2014**, 39, 633 - 639

[11] J-T. Shi, K-F. Yue, B. Liu, Y-L Zhou, Z-G. Fang, and Y-Y. Wang, *CrystEngComm*., **2014**, 16, 3097 - 3102

[12] H.A. Habib, J. Sanchiz, and C. Janiak, *Dalton Trans*., **200**8, 13, 1734 - 1744

[13] C. R. Groom, I. J. Bruno, M. P. Lightfoot and S. C. Ward, *Acta Cryst*., **2016**, B72, 171-179

[14] F. H. Allen, *Acta Cryst*., **2002**, B58, 380-388

[15] D.R. Bond, G.E. Jackson and L.R. Nassimbeni, *S.Afr.J.Chem*., **1983**, 36, 19

[16] L.R. Nassimbeni, M.L. Niven, and M.W. Taylor, *J.Coord.Chem*., **1989**, 19, 339

[17] Marvin 16.1.18, **2016**, ChemAxon (http://www.chemaxon.com)

[18] R.S. Hosmane, J.F. Liebman, *Struct. Chem.*, **2009**, 20, 693 - 697

[19] J.H. Flynn and L.A. Wall, *Polymer Lett*., 1966, 4, 323

[20] L.R. Nassimbeni, *Acc. Chem. Res*., 2003,36, 631

[21] CrystalExplorer (Version 3.1), S. K. Wolff, D. J. Grimwood, J. J. McKinnon, M. J. Turner, D. Jayatilaka and M. A. Spackman, University of Western Australia, 2012.

[22] M. A. Spackman and D. Jayatilaka, *CrystEngComm*, **2009**, *11*, 19

[23](a) M.A. Spackman and J.J. McKinnon, *CrystEngComm*, **2002**, *4*, 378; (b) J.J. McKinnon, D. Jayatilaka, M.A. Spackman, *Chem Commun*., **2007**, 3814

[24] A. Bondi, *J.Phys.Chem.*, **1964**, *68*, 441

[25] C.F. Macrae, I.J. Bruno, J.A. Chisholm, P.R. Edgington, P. McCabe, E. Pidcock, L. Rodriguez-Monge, R. Taylor, J. van de Streek and P.A. Wood, *J. Appl. Cryst*., **2008**, *41*, 466

[26] Bruker **2005**. APEX2. Version 1.0-27. Bruker AXS Inc., Madison, Wisconsin, USA.

[27] Bruker **2004**. SAINT-Plus (including XPREP). Version 7.12. Bruker AXS Inc., Madison, Wisconsin, USA.

[28] Bruker **2003**, XPREP2. Version 6.14. Bruker AXS Inc., Madison, Wisconsin, USA.

[29] G. M. Sheldrick, SHELXS-97 and SHELXL-97 Programs for crystal structure determination and refinement. University of Göttingen, **1997**

[30] L. Barbour, *J. Supramol. Chem.*, **2001**, *1*, 189

[31] A.L. Spek, PLATON, A Multipurpose Crystallographic Tool, Utrecht University, Utrecht, The Netherlands, **2008**

Chapter 6

Werner complexes with hydrogen bonding functionalities

The single crystal structures of the Werner host, bis-isothiocyanato tetrakis-nicotinamide nickel (II), **H5,** with alcohols ethanol (**EtOH**), 1-butanol (**BuOH**), 1-pentanol (**PeOH**), 2-methyl-1-propanol (**MePrOH**) and 4-methylbenzoylalcohol (**MeBeOH**) have been evaluated and scrutinised for packing efficiency and behaviour. The single crystal structures of five other guests with carbonyl functionalities, dimethyl formamide (**DMF)**, 2-pentanone (**PEN**), 3-hexanone (**HEX**), pinacolone (**PIN**) and 4-methylcyclohexanone (**MCH**) were also analysed. Packing factors were estimated and compared using molecular and unit cell sizes and void analyses were conducted. Similarly, the structures of three inclusion compounds with host bis-isothiocyanato tetrakis-isonicotinamide nickel (II), **H6,** have been elucidated. The guests in these compounds are water (**H_2O**), ethanol / water (**EtOH•H_2O**) and isonicotinamide / ethanol (**INic•EtOH**). A mixed-ligand Werner complex bis-isothiocyanato bis-nicotinamide bis-isonicotinamide nickel (II), **H7**, was synthesised and the effectiveness of packing with guests methanol and water (**MeOH•H_2O**) interpreted.

The main objective of this chapter, to investigate the enclathration behaviour of Werner hosts, designed with 'sticky' ligands capable of forming hydrogen bonds with encapsulated guests, was achieved. The utilisation of these hydrogen bonds in the formation of the crystals was analysed and is presented. The selectivity experiment of the **H5** host with two pairs of compounds, one 50:50 alcohol mixture and one 50:50 ketone mixture were successful.

The physical properties of the **H5** inclusion compounds were compared. The interactions between the host and guest and the packing arrangements were considered to predict the efficiency of formation of these clathrates.

Introduction

Separation of a mixture of molecular isomers with similar physical properties is not feasible by distillation[1] or liquid-liquid extractions[2] due to their similarity in volatility or solubility respectively. Less conventional tactics, such as selective sorption[3] or inclusion within a host material,[4] may be considered. Apart from inorganic zeolites, with a high level of success in selectivity, metal-organic hosts such as Werner complexes allow chemical modification to produce designer molecules.[5] However, a change in the size and/or shape of the inclusion cavities is usually unpredictable. Schaefer *et al.* used the Werner complex, $Ni(NCS)_2(4\text{-methylpyridine})_4$, to separate various aromatic hydrocarbons from petroleum fractions by clathration.[6] The behaviour of aromatic host-guest complexes are often constrained by the structure of the host, and $\pi\cdots\pi$ interactions are affected by the orientations of the host and guest.[7] The formation of Werner complexes with pyridine derivative ligands, such as 4-phenylpyridine or 4-vinylpyridine, has been discussed extensively by Lipkowski[8] and Nassimbeni[9] and co-workers. In some cases selectivity has been achieved due to torsional flexibility in the ligands. This was recently proved in the selectivity of the xylene isomers[10] in the vapour phase by the host $Ni(NCS)_2(4\text{-phenylpyridine})_4$.

The use of 'sticky ligands', i.e. ligands with hydrogen bonding functionalities, has not been extensively considered in Werner clathrates but studies have included metal organic frameworks in which hydrogen bonding is promoted by the use of organic ligands such as coumarilic acid or nicotinamide. Mixed ligand studies of coumarilic acid with metal ions are rare, hence Köse *et al.*[11] investigated the structure of Co(II) and Zn(II) complexes with two nicotinamide, two 2-benzofurancarboxylate and two aqua ligands. Hydrogen bonding between the carbonyl oxygen of coumarilic acid and amide hydrogens of nicotinamide forms a framework.

Although molecular host-guest complexes are not as sturdy as naturally existing zeolites, they do have the advantage of 'tunability' in terms of the nature and size of pore concerned.[4] The use of metal centres provides geometries not easily accessible in organic molecules. Together with the flexibility

of hydrogen bonds, compounds can be formed which offer improved opportunities for inclusion or separation.[12]

Previous chapters of this thesis have dealt with Werner complexes which have ligands forming C-H···π and π···π interactions. These ligands had either aromatic properties with rigidity or provided flexibility between two aromatic rings. Selectivity of xylene isomers were investigated in chapters 3 and 5; and in chapter 4, different crystallisation methods were considered. Hydrogen bonding is one of the most important interactions which occur in crystals either between the host molecules and / or between the host and guest molecules. With a view to broadening our knowledge of Werner clathrates, this chapter deals with complexes which lend themselves to hydrogen bonding. Two host complexes with general formula $Ni(NCS)_2L_4$ were synthesised, namely, Ni(II)thiocyanate with four nicotinamide (**H5**) or with four isonicotinamide ligands (**H6**). Their properties of enclathration and packing as hosts for a selection of alcohols and ketones were studied. With the success of selectivity with mixed ligands found in chapter 5, $Ni(NCS)_2$(nicotinamide)$_2$(isonicotinamide)$_2$, a mixed ligand complex (**H7**) was synthesised and its properties are discussed. The structural line diagrams are shown for these hosts in Scheme 6.1, with the guests shown in Scheme 6.2 and 6.3.

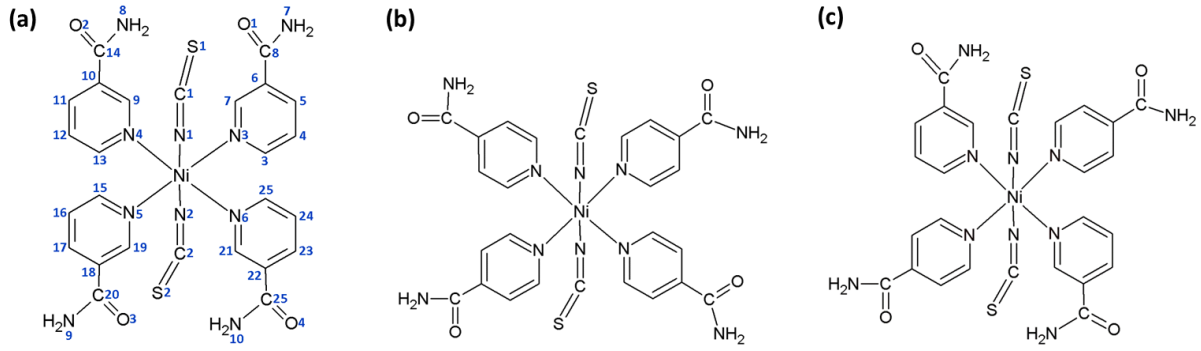

Scheme 6.1 Structural line diagrams of the hosts (a) **H5**, $Ni(NCS)_2$(nicotinamide)$_4$; (b) **H6**, $Ni(NCS)_2$(isonicotinamide)$_4$; and (c) **H7**, $Ni(NCS)_2$(nicotinamide)$_2$(isonicotinamide)$_2$

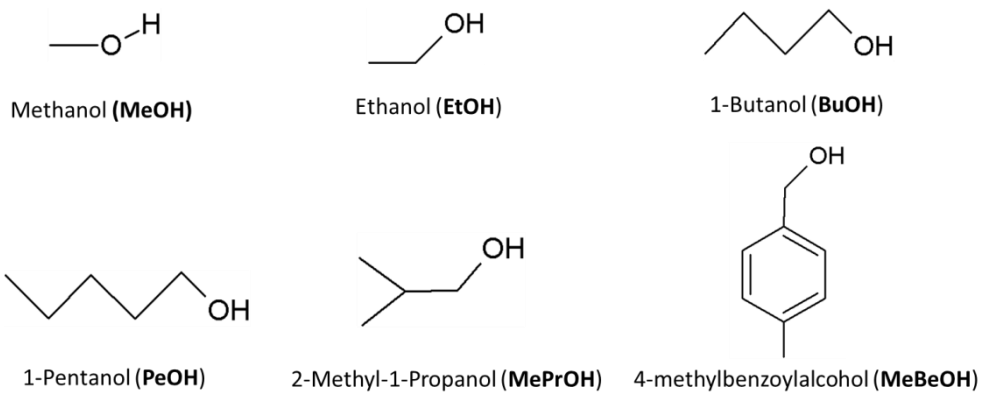

Scheme 6.2 Structural line diagrams of the alcohol guests with symbols used to describe each structure

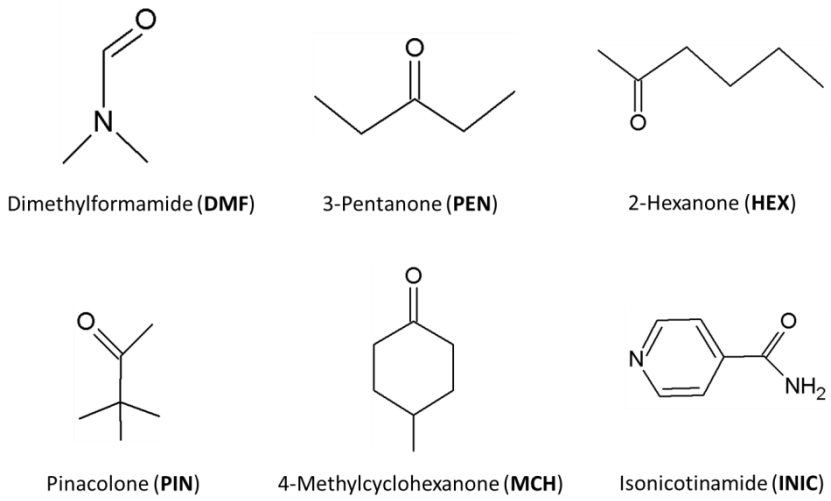

Scheme 6.3 Structural line diagrams of the carbonyl guests with symbols used to describe each structure

Results and discussion

Crystal Structures of alcohol inclusions with H5 host

In the first group of **H5** structures, with alcohol guests, and summarised in Table 6.1, a number of similarities were found. The structures of **H5•2EtOH**, **H5•2BuOH**, **H5•2MePrOH, H5•PeOH** and **H5•2MeBeOH** crystallise in the space group $P\bar{1}$ with Z=1. The asymmetric unit of each structure comprises half a host and one guest molecule with **H5•2BuOH** in a general position and **H5•2EtOH** in Wyckoff position *e*. In **H5•PeOH**, in Wyckoff position *e*, one possible position of the disordered **PeOH** is used. **H5•2MePrOH** and **H5•2MeBeOH** are both in Wyckoff position *c* with ordered **MePrOH** and disordered **MeBeOH**.

Table 6.1: Crystallographic data of **H5** host with alcohol guests

	H5•2EtOH	**H5•2BuOH**	**H5•2MePrOH**	**H5•PeOH**	**H5•2MeBeOH**
Chemical Formula	$Ni(NCS)_2$ $(C_6H_6N_2O)_4$ $•2(C_2H_6O)$	$Ni(NCS)_2$ $(C_6H_6N_2O)_4$ $•2(C_4H_{10}O)$	$Ni(NCS)_2$ $(C_6H_6N_2O)_4$ $•2(C_3H_{10}O)$	$Ni(NCS)_2$ $(C_6H_6N_2O)_4$ $•C_5H_{10}O$	$Ni(NCS)_2$ $(C_6H_6N_2O)_4$ $•2(C_8H_{10}O)$
Formula weight	755.52	811.62	811.62	751.53	785.52
Temperature/K	173(2)	173(2)	173(2)	173(2)	173(2)
Crystal System	triclinic	triclinic	triclinic	triclinic	triclinic
Space group (no.)	$P\bar{1}$(No.2)	$P\bar{1}$(No.2)	$P\bar{1}$(No.2)	$P\bar{1}$(No.2)	$P\bar{1}$(No.2)
a/Å	8.6905(1)	8.9362(2)	9.1546(2)	8.9021(1)	8.8908(2)
b/Å	9.3945(1)	9.4398(2)	9.4839(2)	9.3966(1)	9.5819(2)
c/Å	13.2805(1)	13.391(3)	13.269(3)	12.7522(17)	13.135(3)
α/º	70.21(1)	94.16(3)	93.02(3)	71.241(3)	96.15(3)
β/º	73.48(1)	107.08(3)	104.01(3)	76.201(3)	105.43(3)
γ/º	63.13(1)	117.90(3)	118.07(3)	64.274(3)	117.42(3)
V/Å^3	898.9(1)	924.3(3)	947.0(3)	903.8(4)	922.3(3)
Z'/Z	0.5/1	0.5/1	0.5/1	0.5/1	0.5/1
$D_{calc.}$/Mg m^{-3}	1.396	1.458	1.423	1.381	1.414
Radiation type	MoKα	MoKα	MoKα	MoKα	MoKα
F(000)	394	426	426	392	408
Crystal size/mm	0.20 x 0.38 x 0.37	0.21 x 0.14 x 0.13	0.29 x 0.28 x 0.23	0.04 x 0.07 x 0.12	0.45 x 0.44 x 0.32
Colour, Crystal form	Blue, block	Blue, block	Blue, block	Blue, block	Blue, block
Total reflections	49836	25564	37226	20010	21100
Unique reflections	4445	4442	4763	4318	4113
$\Theta_{min-max}$/º	3.32/28.29	1.64/27.96	1.65/28.41	1.70/ 27.98	2.49/27.26
$R[F^2>2\sigma(F^2)]$	0.0334	0.0361	0.0262	0.0652	0.0480
$wR2(F^2)$	0.0792	0.0949	0.0667	0.1758	0.1499
S	1.052	1.064	1.044	1.042	1.051
Parameters/ data	225/4445	242/4442	244/4763	247/ 4318	286/4113
Res. Peak (max/min)/eÅ^{-3}	0.544/-0.427	0.698/ -0.555	0.361/-0.284	1.857/ -0.887	1.65/-0.419

Hydrogen Bonding

The hydrogen bond is a three-centre-four-electron shared-proton interaction with the general form R-D-H···:A-R' with D the proton donor and A the proton acceptor. The classification of H-bonds has been addressed by Gilli and Gilli in Supramolecular Chemistry.[13] In **H5**, the hydrogen bonds fit into Group 1, a conventional group of H-bonds. This group involves the most electronegative atoms (nitrogen and oxygen) and the bonding denotes intermolecular topology. The H-bond is a nucleophilic substitution reaction along the bimolecular proton-transfer route leading from D:···H-A via D···H···A transition state to D-H···:A. When the H-bond energy is moderate it is electrostatic-covalent in nature with the distance D-H < H···A and with bond distance of H···A lying between 1.5 and 2.2 Å and 2.5 to 3.2 Å for D···A. The D-H-A angle lies between 130 and 180 °. The hydrogen bond information for the clathrates synthesised from **H5** and alcohols is seen in Table 6.2 and Fig.6.1 and Fig.6.2 show the format for each crystal. Refer to page 48 for the explanation of how the hydrogen atoms were positioned.

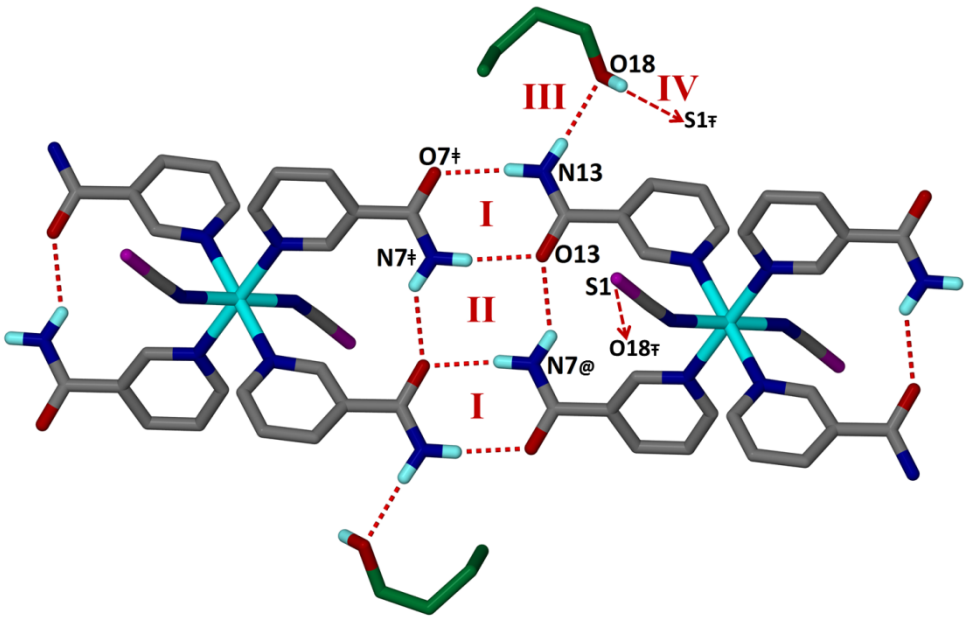

Figure 6.1 **H5•2BuOH** structure with BuOH shown in green capped stick model and I, II, III and IV indicating the synthons (@ -x, -y, 1-z; ǂ 1+x, y, 1+z; Ŧ 1-x, -y, 1-z)

Regular repeating sets of hosts interact via hydrogen bonds in each crystal and Fig.6.1 shows the arrangement of **H5•2BuOH** which is typical of the **H5•alcohol** structures. The primary amides may

control the structure of crystal nucleation sites, as the same hydrogen bond pattern is characteristic of this series of compounds.[14] The hydrogen bond motif is described by a graph set which includes its pattern designator (*G*), its degree (*r*), number of donors (*d*) and acceptors (*a*) in the format $G_d^a(r)$. A higher-order network may consist of a combination of motifs from different kinds of hydrogen bonds such as chains and rings.

In **H5•2BuOH**, two amide groups form amide dimers *via* N-H···O interactions. The two carbonyl oxygens (O13 and O7‡) hydrogen bond to the two nitrogens (N7‡ and N13, respectively) resulting in the $R_2^2(8)$ motif, labelled I in Fig. 6.1 and this motif is continued through the crystal *via* symmetry. The second ring (labelled II in Fig 6.1) has the graph set $R_4^2(8)$ and contains two intermolecular and two intramolecular hydrogen bonds. N7$^{@}$ is the donor atom which bonds *via* its two hydrogen atoms to O13 and O13$^{\mathbf{\mp}}$.

Two hydrogen bonds occur between guest and host. The first non-cyclic dimer, between N13 and O18, labelled III in Fig 6.1, is a discrete bond with motif $D_1^1(3)$ and the second (labelled IV) is a unique bond between O18-H18···S1$^{\mathbf{\mp}}$ with graph set $D_1^1(3)$. The similar bond between O18$^{\mathbf{\mp}}$-H18$^{\mathbf{\mp}}$ ··· S1 is also shown in Fig 6.1.

The other four **H5•alcohol** structures have a similar set of hydrogen bonds which are shown in Fig. 6.2, with the list of interactions shown in Table 6.2. As in the discussion on **H5•2BuOH**, the four hydrogen bonding motifs are shown by the same key as Fig. 6.1. The three amide dimer groups, represented by I ($R_2^2(8)$) and II ($R_4^2(8)$) connect the hosts *via* intermolecular H-bonds and form host-host interactions throughout all the structures. Hydrogen bonding between the guest and host are shown by symbols III which is a discrete bond with motif $D_1^1(3)$ and the second (labelled IV) is a unique bond between O-H···S with graph set $D_1^1(3)$.

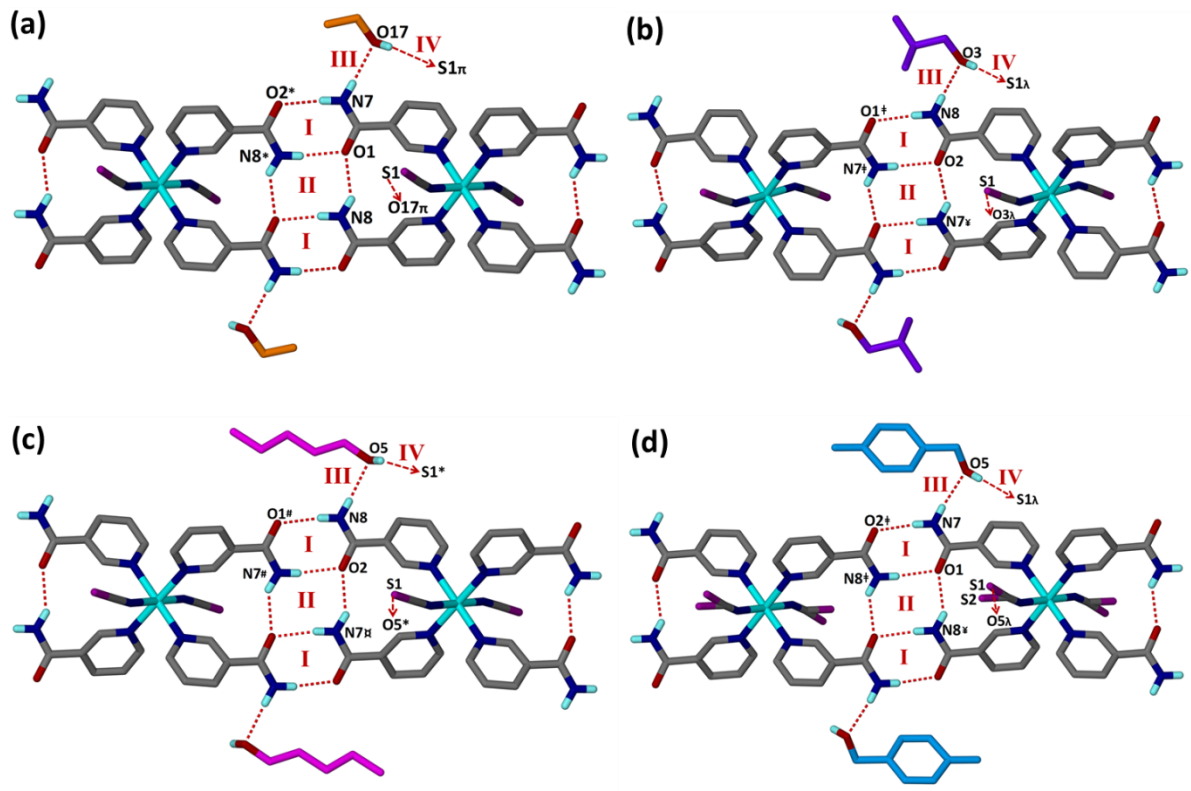

Figure 6.2 Hydrogen bond systems in (a) **H5•2EtOH** (Orange EtOH), (b) **H5•2MePrOH** (Purple MePrOH), (c) **H5•PeOH** (Pink PeOH) and (d) **H5•2MeBeOH** (Blue MeBeOH), with synthons labelled I, II, III and IV (* -x,1-y, 1-z; # x-1, y, 1+z; ʁ 1-x, 1-y, 1-z; ɤ -x, 1-y, 2-z; ǂ 1+x, y, 1+z; @ -x, -y, 1-z; ₸ 1-x, -y, 1-z; π -x, 1-y, -z; λ 1-x, 1-y, 2-z)

Table 6.2 Hydrogen bond parameters for alcohol complexes with **H5**

	D-H / Å	H···A / Å	D···A / Å	< D-H···A / °
H5•2BuOH				
N13-H13A···O7‡	0.88	2.04	2.193(2)	172.7
N13-H13B···O18	0.88	2.15	3.005(3)	165.3
N7‡-H7A‡···O13	0.88	2.06	2.932(2)	172.4
N7$^{@}$-H7B···O13	0.88	2.24	2.970(1)	140.4
O18-H18··· S1$^{₮}$	0.84	2.49	3.286(3)	174.3
H5•2EtOH				
N7-H7AN···O2*	0.88	2.06	2.923(2)	168.5
N7-H7BN···O17	0.88	2.11	2.951(2)	161.0
N8*-H8AN*···O1	0.88	2.03	2.904(2)	172.8
N8-H8BN···O1	0.88	2.19	2.931(2)	141.5
O17-H17···S1^{π}	0.84	2.47	3.303(2)	172.8
H5•2MePrOH				
N8-H8AN···O1‡	0.88	2.05	2.926(2)	173.2
N8-H8BN···O3	0.88	2.12	2.956(2)	158.8
N7‡-H7A‡···O2	0.88	2.05	2.928(2)	173.9
N7$^{¥}$-H7B$^{¥}$···O2	0.88	2.24	2.971(1)	140.4
O3-H3··· S1^{λ}	0.84	2.41	3.245(2)	172.9
H5•PeOH				
N8-H8AN···O1$^{#}$	0.88	2.03	2.906(4)	172.5
N8-H8BN···O5	0.88	2.11	2.964(6)	162.8
N7$^{#}$-H7A$^{#}$···O2	0.88	2.05	2.924(4)	170.2
N7$^{¤}$-H7B$^{¤}$···O2	0.88	2.20	2.953(4)	143.9
O5-H5O··· S1*	0.84	2.70	3.446(7)	148.5
H5•2MeBeOH				
N7-H7A···O2‡	0.88	2.06	2.932(3)	171.9
N7-H7B···O5	0.88	2.18	2.991(4)	153.8
N8‡-H8A‡···O1	0.88	2.06	2.929(3)	169.1
N8$^{¥}$-N8B$^{¥}$···O1	0.88	2.18	2.941(3)	144.4
O5-H5···S1^{λ}	0.84	2.39	3.216(4)	169.9

Symmetry codes: * –x, -y+1, -z+1; ‡ x+1, y, z+1; $^{¥}$ –x, 1-y, 2-z; $^{#}$ x-1, y, z+1; $^{@}$ -x, -y, 1-z; $^{₮}$ 1-x, -y, 2-z; $^{¤}$ 1-x, 1-y, 1-z;^{π}-x, 1-y, -z; ^{λ} 1-x, 1-y, 2-z

Although a weaker acceptor than oxygen, sulphur is considered a conventional hydrogen bond acceptor. Mean hydrogen bond distances (S···H) for >C=S acceptors are about 0.5 Å longer than for C=O acceptors.[15] The longer bond distance is due to the larger van der Waals radii (1.80 Å (S) compared with 1.52 Å (O)) as well as the reduced electronegativity of sulphur (2.58) compared with oxygen (3.44).[16]

These hydrogen bonds were investigated using the Cambridge Structural Database[17, 18] using typical criteria for a hydrogen bond. The parameters for the bond distance was set to the van der Waals cut-off definition of $\boldsymbol{d} \leq 2.9$ Å for S···H and for the angle O-H···S between 140° and 180°, the typical angle for hydrogen bonds. The mean values found were $\boldsymbol{d_1}$: O-H (0.86 Å), $\boldsymbol{d_2}$: H···S (2.48 Å) and $\boldsymbol{d_3}$: O···S (3.30 Å). The distributions for these distances are shown in Fig. 6.3 with $\boldsymbol{d_1}$ in (a), $\boldsymbol{d_2}$ in (b) and $\boldsymbol{d_3}$ in (c) for the analysis of 178 hits in the CSD. In our five structures, the mean values were $\boldsymbol{d_1}$ = 0.84 Å, $\boldsymbol{d_2}$ = 2.49 Å and $\boldsymbol{d_3}$ = 3.30 Å with the individual values shown in Table 6.2. The mean O-H···S angle for our structures of 167.7 ° was consistent with the CSD mean of 163.1 °. In all these cases our hydrogen bond distances and angles are within the ranges found in the reported structures of a hydrogen bond from an organic alcohol to the sulphur of a thiocyanato transition metal complex.

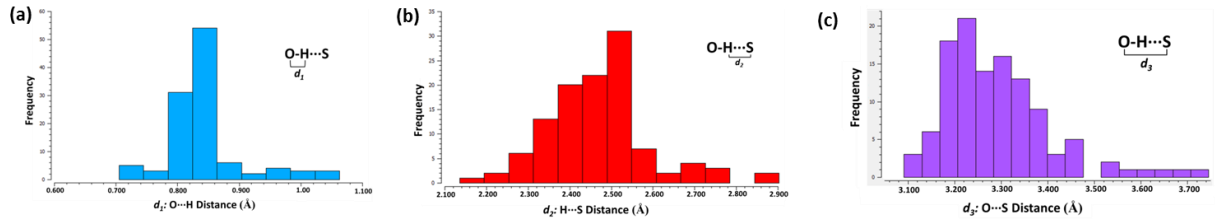

Figure 6.3 Distributions of distances in intermolecular O−H···S=C hydrogen bonds analysed from the Cambridge Structural Database with (a) $\boldsymbol{d_1}$ (O−H); (b) $\boldsymbol{d_2}$ (H···S) and (c) $\boldsymbol{d_3}$ (O···S) distances in Å

Packing

Similar packing is found in the five **H5** crystals with the host forming columns between which the guests are placed. Intermolecular hydrogen bonding between the amide groups of the hosts enable a layer structure to be formed and the guests form hydrogen bonds between the oxygen and H-N as well

as between O-H and sulphur. In Fig 6.4, **H5•2BuOH** is shown along [001] with the host layers in (a), the host with guest in (b) and the representation of the voids in (c).

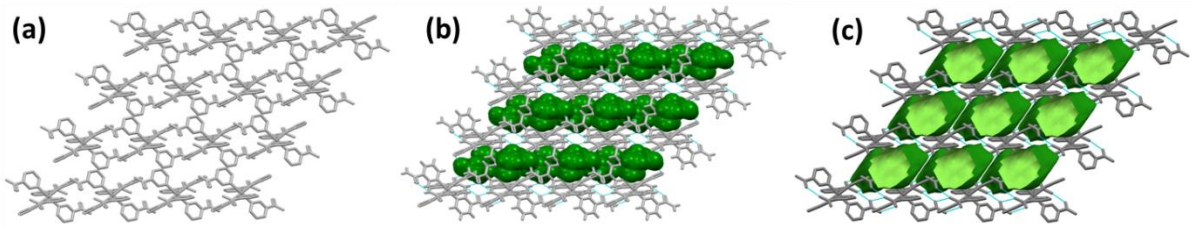

Figure 6.4 The layers of the host in **H5•2BuOH** are shown in (a), with the guests in position in (b) and the voids shown in green in (c).

In Fig. 6.5, the packing is shown along [100] with the layer effect evident on observing down the *c* axis. Hydrogen bonding is shown in red between the host molecules as discussed in Fig. 6.2. The guests are shown in the same colours as Fig. 6.2, but are in spacefill model. In Fig 6.5(e) the guest, 4-methylbenzoyl alcohol, in **H5•2MeBeOH**, appears to be considerably larger than the other guests. However, as this is a disordered guest, both are shown in this diagram. In the case of **H5•PeOH**, it is also noted that the host:guest ratio is 1:1 whereas in the other structures the ratio is 1:2.

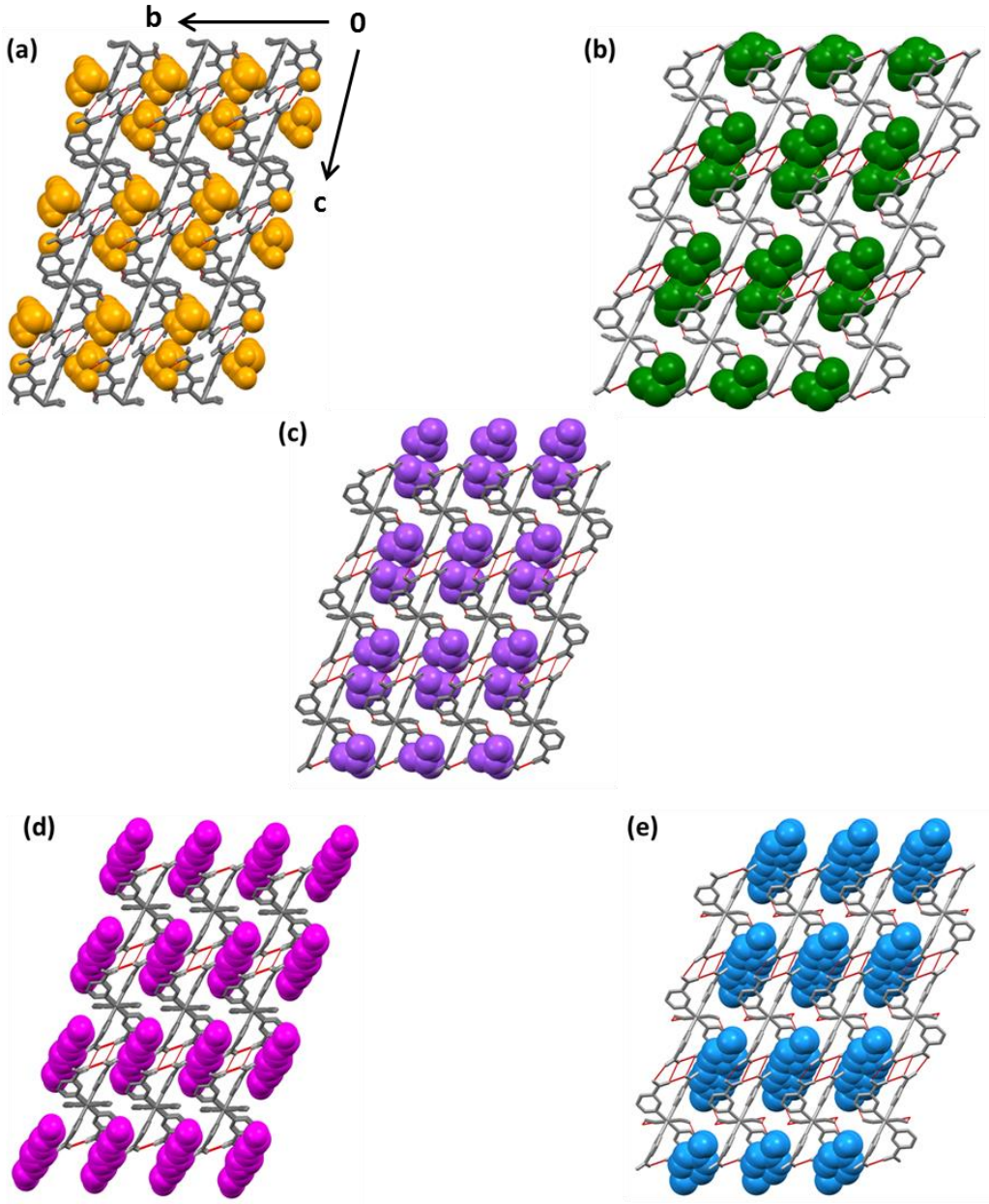

Figure 6.5 Packing of (a) **H5•2EtOH**, (b) **H5•2BuOH**, (c) **H5•2MePrOH**, (d) **H5•PeOH** and (e) **H5•2MeBeOH** showing the similar format of the host (in grey capped stick model) with the intermolecular hydrogen bonds shown in red, and the guest in coloured spacefill model.

Packing density of a crystal is specified by

$$k = Z \bullet {}^{V_0}/_{V}$$

and is also known as the "coefficient of molecular packing". In this equation V_0 is the molecular volume, calculated from the atomic and molecular radii and valence angles using *X-Seed*[19], Z the number of molecules in the cell and V the cell volume.[20] In Table 6.3, parameters affecting the

packing factor (PF*) or packing coefficient of each crystal are listed. The values for the packing factor (reported as a percentage) vary from 66.9 % (**H5•PeOH**) to 81.0 % (**H5•2MeBeOH**). The guest 4-methylbenzoylalcohol is a flat molecule, characteristic of an aromatic ring. The space consumed by this guest is larger than that of the other alcohols because its molecular volume is the biggest of the alcohols considered in this discussion. However, $\pi \cdots \pi$ interactions between the aromatic ring of **MeBeOH** with that of the nicotinamide is significant and leads to attraction between the two aromatic rings. The average distance between the planes of the two rings is 3.75 Å which lies between the suggested distance of 3.3 – 3.8 Å.[21]

Table 6.3 Description of the values of interest in the closeness of packing in the **H5** alcohol clathrates

	H5•2EtOH	**H5•2BuOH**	**H5•2MePrOH**	**H5•PeOH**	**H5•2MeBeOH**
Space Group	$P\bar{1}$	$P\bar{1}$	$P\bar{1}$	$P\bar{1}$	$P\bar{1}$
Z	1	1	1	1	1
Cell Volume (Å^3)	898.91	924.33	947.00	903.79	922.31
Guest Mol.Vol (Å^3)	49.3	81.1	81.9	97.4	119.7
Host Mol. Vol (Å^3)	507.3	507.3	507.3	507.3	507.3
Total Mol. Vol (Å^3)	605.9	669.5	671.1	604.7	746.7
PF* (%)	67.4	72.4	70.9	66.9	81.0
Percentage Void	20.1	18.9	21.0	21.1	18.1
Void Volume (Å^3)	181.1	174.45	198.8	190.6	167.3

The void analysis was done in Mercury (3.8)[15] using a probe radius of 1.2 Å and grid spacing of 0.8 Å. The choice of 1.2 Å for the radius of the probe sphere is a compromise between a very fine probe (1.0 Å) and a gross value of 1.5 Å. This allows us to make fair comparisons of the void volumes with fair accuracy and comparable precision. For **H5•2BuOH** the void is 18.9 % of the cell with a volume of 174.45 Å^3. The values for the other crystals are as follows **H5•2EtOH** (20.1 %; 181.1 Å^3); **H5•2MePrOH** (21.0 %; 198.8 Å^3); **H5•PeOH** (21.1 %; 190.6 Å3) and **H5•2MeBeOH** (18.1 %; 167.3 Å^3).

Crystal Structures of H5 inclusion compounds of guests with carbonyl functionality

The second group of structures for **H5**, which included guests with carbonyl functionality, are summarised in Table 6.4. Similarities were found with **H5•2HEX**, **H5•2PIN**, and **H5•2MCH**, all crystallising in the space group $P2_1/c$ with Z=2. The asymmetric unit of each structure comprises half a host and one guest molecule with **H5•2HEX** and **H5•2MCH** in Wyckoff position *b* and **H5•2PIN** in Wyckoff position *d*. **H5•2DMF** is in a general position in space group $P\bar{1}$, and **H5•2PEN**, also in a general position, in space group *Pbca.*

Disorder was observed in the guests in the **H5•2DMF, H5•2PEN** and **H5•2HEX** structures and these are shown in Fig. 6.6. From these diagrams in which the molecule is shown in a capped stick format inside a transparent spacefill model, it can be seen how the disorder impacts on the size required for inclusion of the guest.

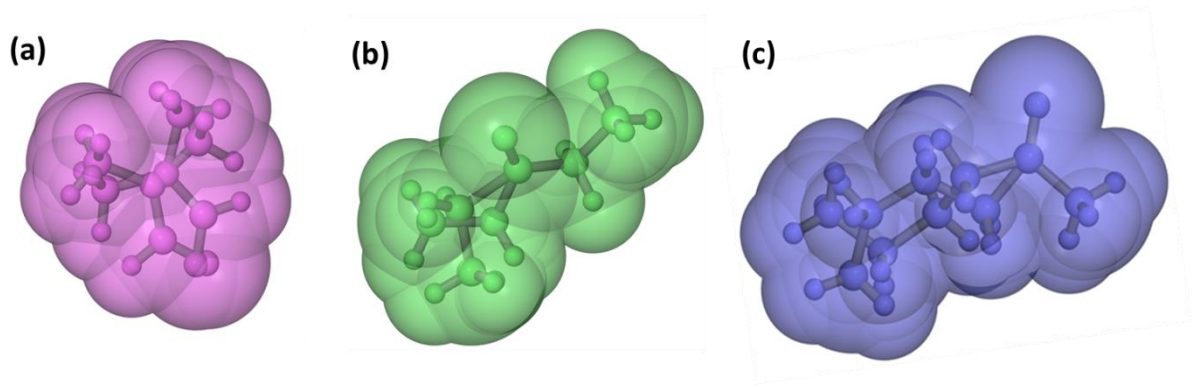

Figure 6.6 The disordered structures of (a) **DMF,** (b) **PEN** and (c) **HEX** showing the space required in the structure for the guest.

Table 6.4: Crystallographic data of H5 host with carbonyl guests

	H5•2DMF	**H5•2PEN**	**H5•2HEX**	**H5•2PIN**	**H5•2MCH**
Chemical Formula	$Ni(NCS)_2$ $(C_6H_6N_2O)_4$ $•2(C_3H_7NO)$	$Ni(NCS)_2$ $(C_6H_6N_2O)_4$ $•2(C_5H_{10}O)$	$Ni(NCS)_2$ $(C_6H_6N_2O)_4$ $•2(C_6H_{12}O)$	$Ni(NCS)_2$ $(C_6H_6N_2O)_4$ $•2(C_6H_{12}O)$	$Ni(NCS)_2$ $(C_6H_6N_2O)_4$ $•2(C_7H_{12}O)$
Formula weight (g/mol.)	809.57	835.64	863.69	863.69	887.71
Temperature/K	173(2)	173(2)	173(2)	173(2)	173(2)
Crystal System	$P\bar{1}$	*Pbca*	$P2_1/c$	$P2_1/c$	$P2_1/c$
Space group (no.)	No. 2	No. 61	No.14	No.14	No.14
a/Å	9.1698(18)	15.550(3)	9.926(2)	10.252(2)	10.485(2)
b/Å	9.6248(19)	13.544(3)	16.094(3)	15.896(3)	15.595(3)
c/Å	12.779(3)	19.268(4)	13.637(3)	13.574(3)	13.559(3)
α/º	96.47(3)	90	90	90	90
β/º	105.43(3)	90	92.59(3)	102.01(3)	90.35(3)
γ/º	116.32(3)	90	90	90	90
V/Å^3	939.1(3)	4058.0(14)	2176.6	2163.7(8)	2217.0(8)
Z'/Z	0.5 / 1	0.5 / 4	0.5 / 2	0.5 / 2	0.5 / 2
$D_{calc.}$/Mg m^{-3}	1.431	1.368	1.318	1.326	1.330
Radiation type	MoKα	MoKα	MoKα	MoKα	MoKα
F(000)	422	1752	908	908	932
Crystal size/mm	0.16 x 0.14 x 0.04	0.23 x 0.12 x 0.08	0.16 x 0.15 x 0.12	0.25 x 0.23 x 0.08	0.24 x 0.21 x 0.08
Colour, Crystal form	Blue, block	Blue, block	Blue, Rosette plates	Blue, block	Blue, block
Total reflections	24748	43856	28663	40931	32187
Unique reflections	4517	4868	5206	5154	5279
$\Theta_{min-max}$/º	1.72 / 28.03	2.11 / 27.94	1.96 / 27.99	2.00 / 27.89	1.94 / 27.86
$R[F^2>2\sigma(F^2)]$	0.0347	0.0552	0.0459	0.0373	0.0389
$wR2(F^2)$	0.0777	0.1294	0.1079	0.0864	0.0930
S	1.041	1.033	1.022	1.033	1.019
Parameters / data	291 / 4517	272 / 4868	299 / 5206	264 / 5154	269 / 5279
Res. Peak (max/min)/eÅ^{-3}	0.544 / -0.533	1.660 / -1.638	0.330 / -0.373	0.681 / -0.379	0.813 / -0.325

Hydrogen Bonding

In each crystal, the host molecules interact *via* hydrogen bonds. Fig.6.7 shows the arrangement of **H5•2PIN** with hydrogen bonding between each molecule resulting in layering of the hosts. Two amide groups form amide dimers *via* N-H···O interactions (labelled I in Fig 6.7), which are described by the motifs $R_2^2(8)$. The middle ring (labelled II in Fig 6.7) has two intermolecular bonds and intramolecular H-bonds (N7$^{\#}$-H7A$^{\#}$···O1 and N7*-H7B*···O1) to form motif $R_4^2(8)$. Between the host and guest, the H-bond from nitrogen donor atom (N8) to acceptor atom oxygen (O5) is a discrete bond with motif $D_1^1(3)$ and is labelled III in Fig. 6.7. The hydrogen bond data for **H5** with carbonyls is shown in Table 6.5 with Fig.6.7 and 6.8 showing the diagrammatical format for each crystal.

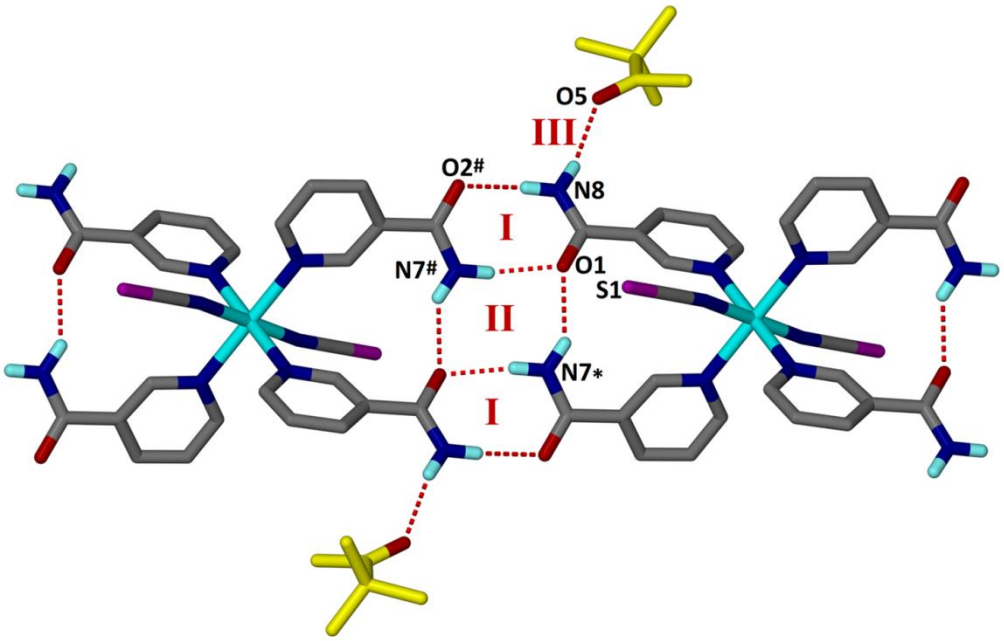

Figure 6.7 **H5•2PIN** structure, showing the hydrogen-bonded amide dimers (I and II) between the nicotinamide ligands and discrete H-bond between host and guest (III) with **PIN** in yellow.
(* 1-x, -y, 1-z; $^{\#}$ x, y, 1+z)

Fig 6.8 shows the other four carbonyl structures, **H5•2DMF** (pink DMF), **H5•2PEN** (green PEN); **H5•2HEX** (lavender HEX) and **H5•2MCH** (teal MCH). In each structure the intermolecular amide dimers between the hosts are shown and are defined by labels I (graph set $R_2^2(8)$); and the ring, including intramolecular hydrogen bonding is shown by label II (graph set $R_4^2(8)$). The discrete

interaction between donor atom N (host) and carbonyl acceptor atom O (guest), is labelled III (graph set $D_1^1(3)$). The list of interactions can be found in Table 6.5.

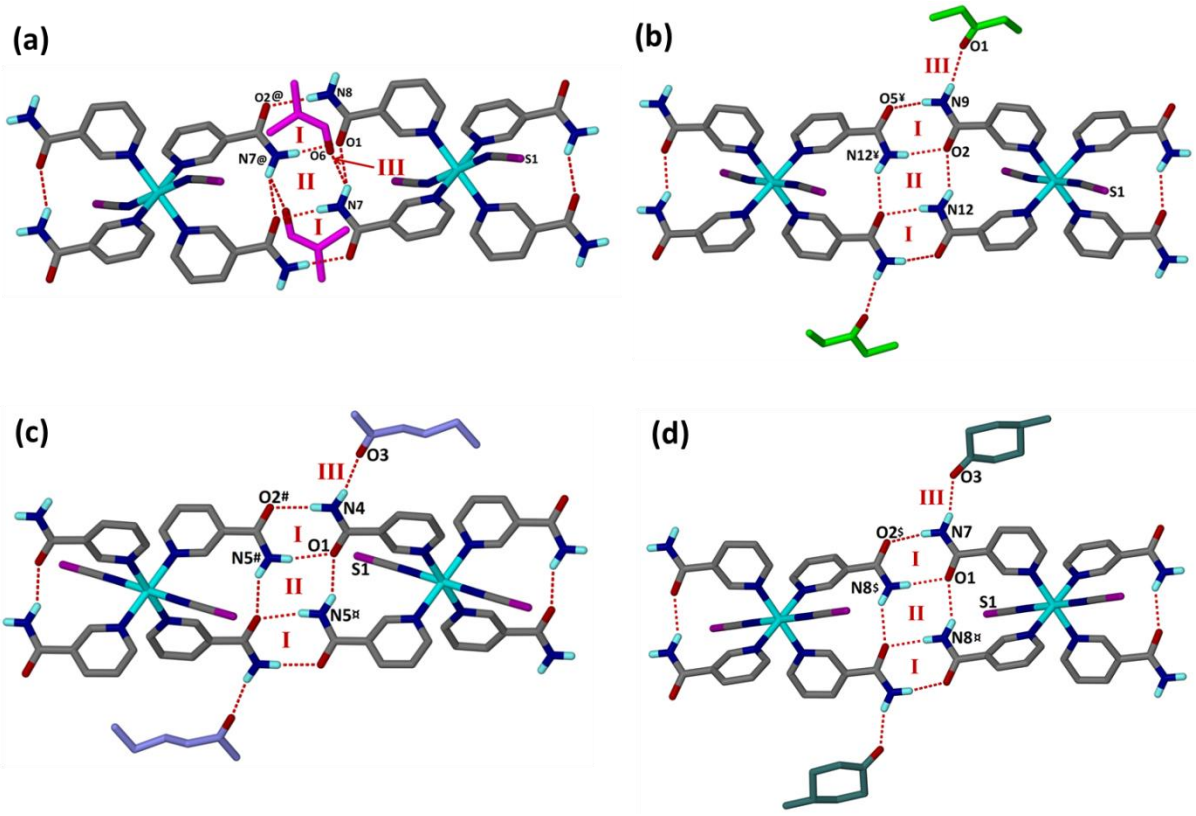

Figure 6.8 Structures of (a) **H5•2DMF** (pink DMF), (b) **H5•2PEN** (green PEN); (c) **H5•2HEX** (lavender HEX), and (d) **H5•2MCH** (teal MCH) showing hydrogen-bonded amide dimers (I and II) between the nicotinamide ligands and discrete H-bond between host and guest (III).

(@ 1-x, 2-y, -z; ¥ -x, -y-1, -z; ¤ 1-x, -y, -z; $ x, y, z-1; *1-x, -y, 1-z; # x, y, 1+z;)

Table 6.5 Hydrogen bond parameters for carbonyl complexes with **H5**

	D-H / Å	H···A / Å	D···A / Å	< D-H···A / °
H5•2PIN				
N8-H8A···O2[#]	0.88	2.12	2.968(2)	162.3
N8-H8B···O5	0.88	2.09	2.941(2)	163.5
N7[#]-H7A[#]···O1	0.88	2.02	2.884(2)	165.9
N7*-H7B*···O1	0.88	2.20	2.961(2)	144.6
H5•2DMF				
N8-H8AN···O2[@]	0.88	2.04	2.915(2)	173.5
N7-H7BN···O1	0.88	2.37	3.343(2)	170.3
N7[@]-H7AN[@]···O1	0.88	2.03	2.899(2)	155.4
N7-H7BN···O6	0.88	2.37	2.913(2)	120.2
H5•2PEN				
N9-H9A···O5[¥]	0.88	2.12	2.955(3)	158.8
N9-H9B···O1	0.88	2.17	3.043(4)	169.4
N12[¥]-H12A[¥]···O2	0.88	2.04	2.895(3)	163.3
N12-H12B···O2	0.88	2.19	2.942(4)	143.4
H5•2HEX				
N4-H4A···O2[#]	0.88	2.11	2.944(3)	159.2
N4-H4B···O3	0.88	2.10	2.964(3)	168.1
N5[#]-H5A[#]···O1	0.88	2.07	2.914(3)	161.2
N5[¤]-H5B[¤]···O1	0.88	2.23	2.977(3)	143.2
H5•2MCH				
N7-H7A···O2[$]	0.88	2.09	2.939(2)	160.7
N7-H7B···O3	0.88	2.06	2.903(3)	161.1
N8[$]-H8A[$]···O1	0.88	2.04	2.894(2)	163.7
N8[¤]-H8B[¤]···O1	0.88	2.20	2.956(2)	144.6

(Symmetry codes: [#] x, y, 1+z; *1-x, -y, 1-z; [@] 1-x, 2-y, -z; [¥] -x, -y-1, -z; [¤] 1-x, -y, -z; [$] 1-x, y-½, ³/₂-z)

Packing

A comparison of the packing present in the 5 inclusion compounds was considered in a similar way to the previous alcohol inclusions. The structure of **H5•2DMF,** which crystallises in the $P\bar{1}$ space group,

displays similar packing characteristics to those of the **H5** structures with alcohol inclusions. These are illustrated in Fig. 6.9, showing the host structure in (a), with the **DMF** in pink spacefill model in (b), and the void spacing, also shown in pink in (c). The guest fills the voids as is shown in (b) and (c). The packing factor is 69.4 % and the void percentage is 20.6 % with void volume of 193.2 $Å^3$.

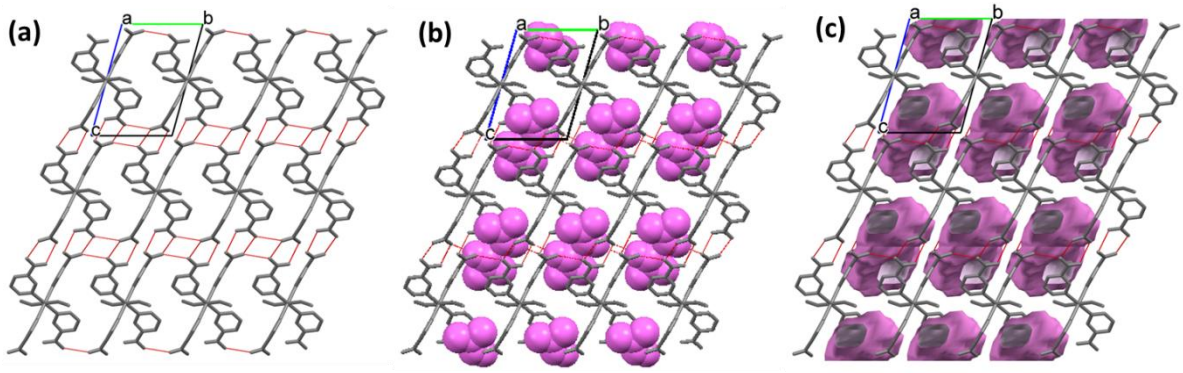

Figure 6.9 Packing patterns down [100] of (a) host structure of **H5•2DMF**; (b) host with **DMF** guest in pink spacefill model and (c) void analysis of the **H5•2DMF** structure. Hydrogen bond interactions are shown in red

In Table 6.4 it can be seen that **H5•2PEN** (space group *Pbca*) has a unit cell with a doubling of one of the axes, compared with **H5•2HEX**, **H5•2PIN** and **H5•2MCH** (space group $P2_1/c$). Using the **H5•2MCH** structure as an example in Fig. 6.10, the packing of these four structures is shown. Firstly, the arrangement of the host is elucidated and secondly, the inclusion of the guest in the host architecture is discussed. The host forms bands by interacting *via* hydrogen bonds by means of amide dimer groups. This is shown down [100] in Fig 6.10(a) with the hosts forming a sheet of these bands. Layers can be seen when viewing down [010] as is shown in Fig 6.10(b). Between these layers are the spaces for the guest to occupy and these can be seen in the void analysis shown by red arrows which point to crossing columns in Fig 6.10(c). This intercalate structure is emphasised in Fig. 6.10(d) and (e) as the guests in capped stick and spacefill model are shown in the guest layers

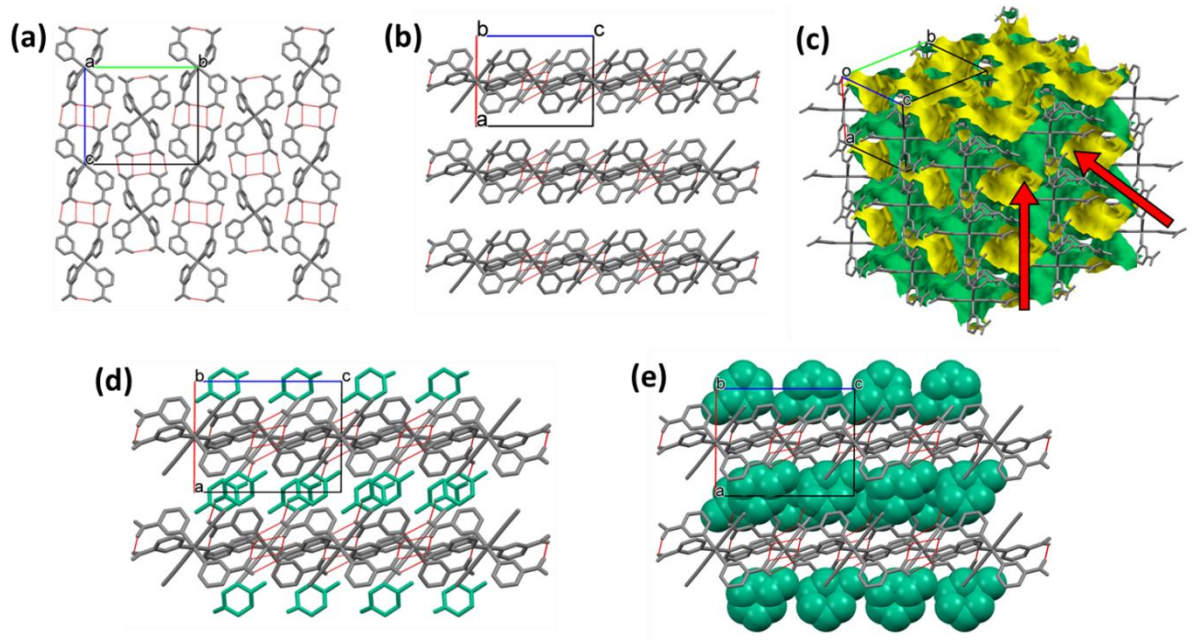

Figure 6.10 Structure of **H5•2MCH** with (a) the sheets of hosts seen down [100]; (b) layers of the host shown down [010]; (c) the void analysis with columns for the guest shown with red arrows; (d) **MCH** in green capped stick model and (e) **MCH** in spacefill model

The other three structures show a similar format, that is, the hosts appear in layers of sheets of bands which are made up of hydrogen bonded molecules. The guests fill these layers in an intercalate manner, giving structures of **H5•2PEN**, **H5•2HEX** and **H5•2PIN** which show the same architecture as that shown in Fig 6.10 for **H5•2MCH**.

The voids were analysed using a probe radius of 1.2 Å and grid spacing of 0.8 Å in Mercury (3.8) and are shown in Fig 6.10(c) for **H5•2MCH**. The void space was 39.5 % with a volume of 860.42 $Å^3$.

The packing data for all the compounds which included carbonyls is shown in Table 6.6. The packing factor (PF*), ranging from 66.3 (**H5•2MCH**) to 69.4 % (**H5•2DMF**), is in agreement with coefficients for the majority of crystals. The percentage void ranges from 20.6 % (**DMF**), the smallest guest, to 40.2 % (**MCH**), the largest guest. All the guests except **PIN** and **MCH** were disordered hence there was enough space in the structure for the guest to allocate different positions.

Table 6.6 Description of the values of interest in the closeness of packing in the **H5** carbonyl clathrates

	H5•2DMF	**H5•2PEN**	**H5•2HEX**	**H5•2PIN**	**H5•2MCH**
Space Group	$P\bar{1}$	*Pbca*	$P2_1/c$	$P2_1/c$	$P2_1/c$
Z	1	4	2	2	2
Cell Volume (Å^3)	939.1	4058.0	2176.6	2163.7	2217.0
Guest Mol.Vol (Å^3)	72.3	91.5	107.8	108.2	114.0
Host Mol Vol (Å^3)	507.3	507.3	507.3	507.3	507.3
Total Mol Vol (Å^3)	651.9	2761.2	1445.8	1447.4	1470.6
PF* (%)	69.4	68.0	66.4	66.9	66.3
Percentage Void	20.6	29.6	39.5	33.2	40.2
Void Volume (Å^3)	193.2	1201.1	860.0	717.6	892.0

Comparison of thermal stability and structural features of H5 inclusion compounds with alcohols and those with H5 carbonyl inclusion compounds

The crystal structures of the two sets of clathrates obtained, firstly with alcohol guests and secondly with guests with carbonyl functionalities, illustrated how the architecture of the host compound is flexible in the design of the inclusion compound. In the case of the alcohols the guests were present in voids as shown in Fig. 6.4 but the carbonyl guests were present in layers between the host channels. **DMF**, however, differed, as it presented itself in voids rather than layers. The crystal structure was more similar to the alcohol inclusions than the carbonyl inclusions.

Apart from the difference in packing, there was a significant difference in the hydrogen bonding between the host and guest. The alcohol guests formed two hydrogen bonds, a N−H···O bond as well as an O−H···S bond. Even though the hydrogen bond involving sulphur as the acceptor is weaker than one with an oxygen acceptor, the effect of two bonds may lead to a higher temperature of desolvation for the alcohol inclusion compared with its analogous carbonyl. The temperatures of desolvation were determined from TGA profiles in which the peak of the differential curve located the temperature at which the kinetics of desorption was at its maximum. TGA profiles of **H5•2BuOH** and **H5•2HEX** are shown in Fig 6.11(a) and (b), respectively.

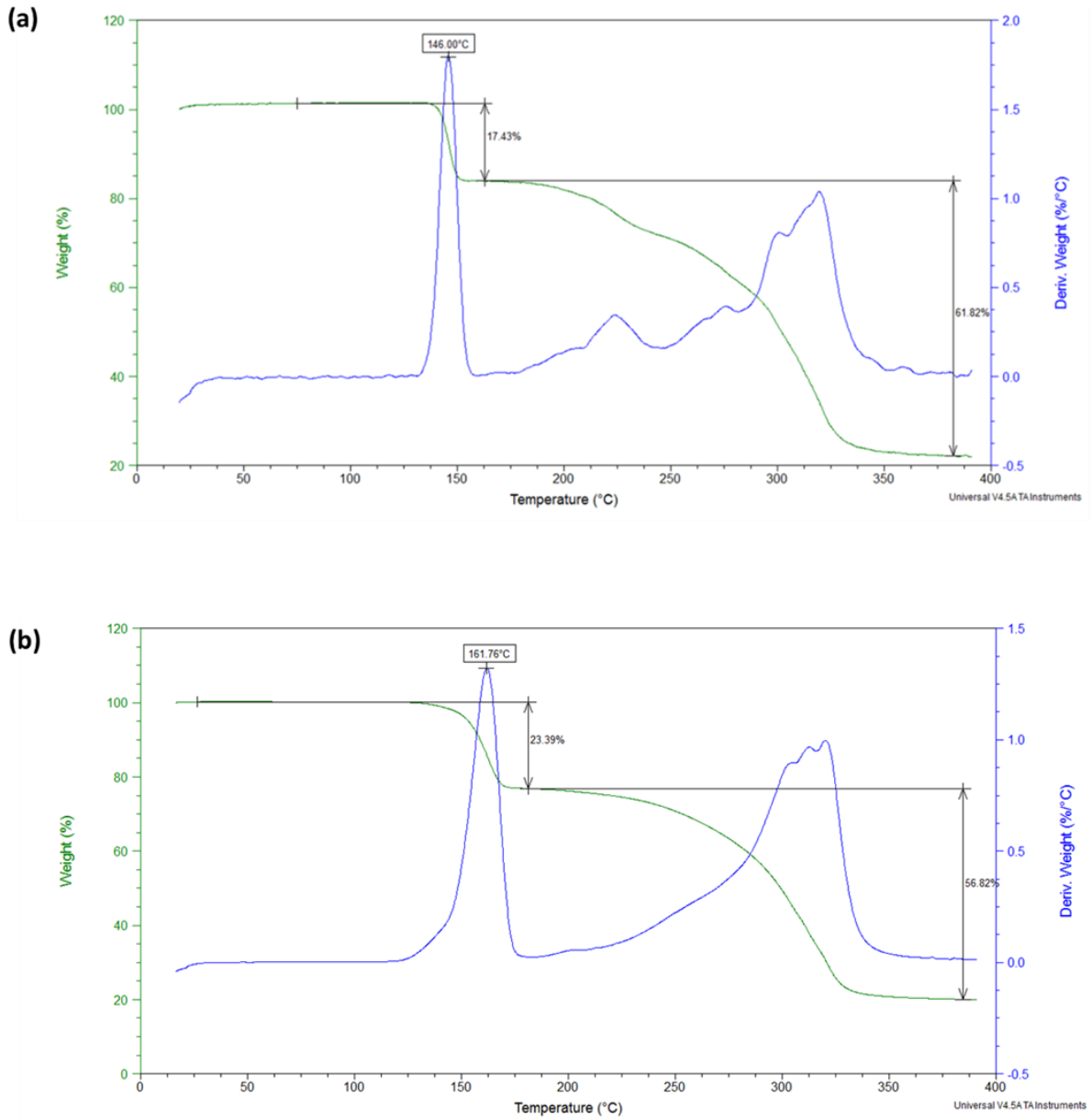

Figure 6.11 TGA profiles of (a) **H5•2BuOH** and (b) **H5•2HEX** are shown with the desolvation temperature indicated at the tip of the differential peak

The desolvation temperatures were compared with the boiling points of each guest. This is shown in Table 6.7 and the differences between these two temperatures are designated. A range of different temperatures were observed and comparisons are discussed here.

Table 6.7 Boiling points compared to desolvation temperatures for **H5** with alcohols and with carbonyl guests

	Boiling Point (°C) (T_{BP})	Desolvation Temperature (°C) (T_{DS})	ΔT (°C) ($T_{DS} - T_{BP}$)
Alcohol Guests			
EtOH	78.4	156.0	77.6
BuOH	117.7	146.0	28.3
PeOH	138.0	205.2	67.2
MePrOH	108.0	157.5	49.5
MeBeOH	217.0	196.0	- 21.0
Carbonyl Guests			
DMF	153.0	151.3	- 1.7
PEN	101.0	163.7	62.7
HEX	127.6	161.8	34.2
PIN	104.5	161.0	56.5
MCH	170.0	189.0	19.0

Two features of the crystal structures were considered in this discussion.

Firstly, the alcohols were more effectively captured in the host:guest inclusion compounds and were held by two hydrogen bonds. However, the hydrogen bonding in the carbonyl compounds was less significant as only a bond between the carbonyl group and the amide functional group was present.

Secondly, we argue that the packing difference between the alcohol inclusion compounds and the carbonyl structures produces more efficient entrapment as the alcohols fill voids in their structures. The carbonyls are present in channels between the host layers and their release would be easier because they are only bound by one hydrogen bond.

The higher temperatures required to release the guests from these structures, as shown in Table 6.7, substantiates the above reasoning in our discussion of two of the physical properties of the inclusion compounds we have considered.

Crystal Structures of H6 host

The second host, **H6**, with four isonicotinamide ligands, also has hydrogen bonding capabilities and three crystal structures were elucidated. In the three compounds, the host included the solvent/s used for solution crystallisation and / or the ligand was included. The synthesis of these compounds yielded some hydrated compounds. This was serendipitous because no special precautions were taken to dry the solvents.

The first clathrate, **H6•EtOH•0.4H_2O**, contains ethanol and water, and crystallised in the orthorhombic space group *Pbcn* with Z = 8. The host : guest ratio was confirmed by single crystal analysis and by thermal gravimetric means. Two different types of crystals were formed from the same crystallisation mixture. These were **H6•3H_2O**, purple crystals, with water included as guest; and blue crystals, **H6•2INic•EtOH**, with included ethanol and isonicotinamide ligands. This is an example of self-inclusion of the ligand in the structure. **H6•3H_2O** crystallised in the orthorhombic space group *Pbcn* with Z = 4 and **H6•2INic•EtOH** crystallised in the triclinic $P\bar{1}$ space group with Z = 2. The crystal data of these three **H6** inclusions are summarised in Table 6.8.

Table 6.8 Crystallographic Data of **H6** host in three clathrates

	H6•EtOH•0.4H_2O	**H6•3H_2O**	**H6•2INIC•EtOH**
Chemical Formula	$Ni(NCS)_2$ $(C_6H_6N_2O)_4$ •(C_2H_6O) •0.4(H_2O)	$Ni(NCS)_2$ $(C_6H_6N_2O)_4$ •3(H_2O)	$Ni(NCS)_2$ $(C_6H_6N_2O)_4$ •2$(C_6H_6N_2O)$ •(C_2H_6O)
Formula weight (g/mol.)	716.66	717.43	953.71
Temperature/K	173(2)	173(2)	173(2)
Crystal System	orthorhombic	orthorhombic	triclinic
Space group (no.)	*Pbcn* (No. 60)	*Pbcn* (No. 60)	$P\bar{1}$ (No. 2)
a/Å	23.7637(5)	18.2295(4)	9.1222(9)
b/Å	19.0013(4)	20.4332(4)	13.6473(3)
c/Å	15.0035(2)	8.4499(4)	20.188(4)
α/º	90	90	104.12(3)
β/º	90	90	97.20(3)
γ/º	90	90	109.48(3)
V/Å^3	6774.5(2)	3147.5(5)	2236.9(8)
Z'/Z	1 / 8	0.5 / 4	0.5 / 2
$D_{calc.}$/Mg m^{-3}	1.405	1.514	1.416
Radiation type	MoKα	MoKα	MoKα
F(000)	2976	1488	992
Crystal size/mm	0.23 × 0.10 × 0.06	0.48 × 0.16 × 0.15	0.18 × 0.17 × 0.06
Colour, Crystal form	Blue, block	Purple, block	Blue, block
Total reflections	149902	70020	10705
Unique reflections	6917	3776	7998
$\Theta_{min-max}$/º	2.75 / 26.41	1.99 / 27.94	1.66 / 28.00
$R[F^2>2\sigma(F^2)]$	0.0392	0.0255	0.0459
$wR2(F^2)$	0.0968	0.0672	0.1049
S	1.040	1.061	1.087
No of Parameters / data	429 / 6917	221 / 3776	609 / 7998
Res. Peak (max/min)/eÅ^{-3}	0.604 / -0.547	0.394 / -0.381	0.374 / -0.431

Hydrogen Bonding

The hydrogen bonded hosts do not form layers as in the structures of inclusions by **H5**, but the supramolecular unit can be described as a hydrogen bonded network. In Fig. 6.12, the ASU of **H6•EtOH•0.4H_2O** is shown with the hydrogen bonds illustrated in red. There are three amide dimers

each represented by graph set $R_2^2(8)$ and are labelled **I** in the figure. Hydrogen bonding between the guest and host are shown by symbol **II** which is a discrete bond between donor N8 and acceptor O5 of ethanol with graph set $D_1^1(3)$ and the second (labelled **III**) is a unique bond between O5-H5···S1¤ with graph set $D_1^1(3)$. Other discrete hydrogen bonds occur between nitrogen and oxygen atoms, all with graph sets $D_1^1(3)$, and interact with another four different host molecules. From the set of interactions in this structure, it was found that the supramolecular unit was made up of eight host molecules. Details of the hydrogen bond parameters are given in Table 6.9.

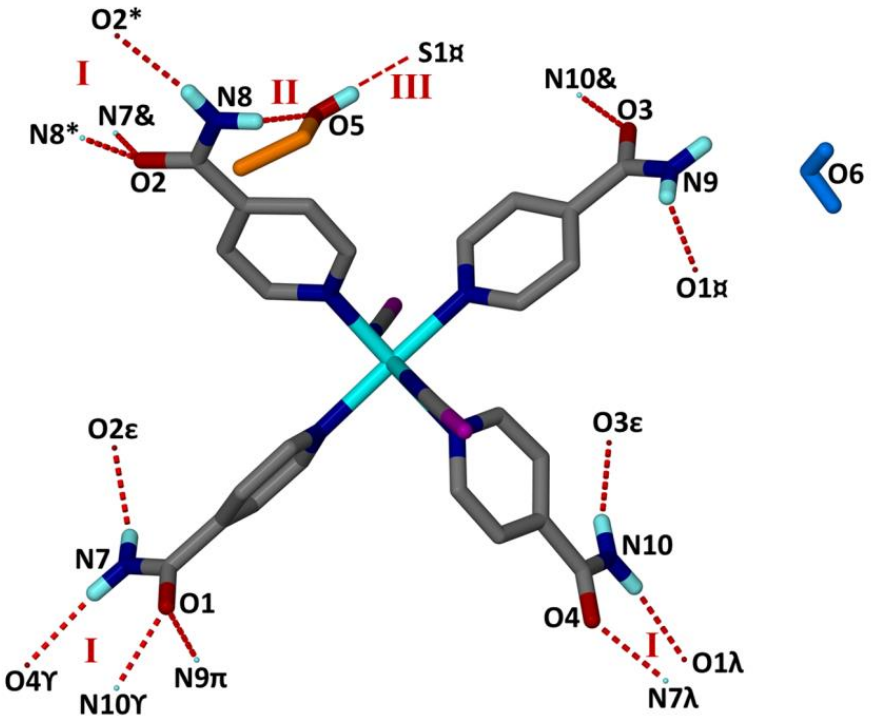

Figure 6.12 ASU of **H6•EtOH•0.4H_2O** showing the hydrogen bonds to symmetry generated molecules. The amide dimer groups are labelled **I** and the discrete hydrogen bonds are labelled **II** and **III.**

(***** 1-x, y, -z-½; **&** x, 1-y, z-½;**¤** ½-x, ½-y, z-½; **ε** x, 1-y, ½+z; **λ** x-½, ½-y, 1-z; **π** ½-x, ½-y, ½+z; **ϒ** ½+x, ½-y, 1-z)

Orthorhombic **H6•3H_2O**, is a structure in which the water molecules form a chain between two rows of host molecules. These hydrogen bonds are shown in Fig.6.13 with the host molecules in RSC-defined colours and the water molecules in blue capped stick model. Label **I** indicates the host - guest hydrogen bond O2#-H2O#···O1#, and is represented by graph set $D_1^1(3)$. These bonds form the intermediary means of forming bands of the host. Guest – guest hydrogen bonds are shown by label **II**

and are indicated O2$^{\#}$-H2O$^{\#}$···O3$^{\#}$. These H-bonds form a chain along *c* that is represented by the motif $C_1^1(3)$. Intermolecular H-bonds are shown by **III** in Fig 6.13 between N10 and O1¤ with motif $D_1^1(3)$ and the unique bond between N10 and S2¥ with graph set $D_1^1(3)$ and labelled **IV**. The host bands interact with neighbouring bands *via* bonds **III** and **IV**.

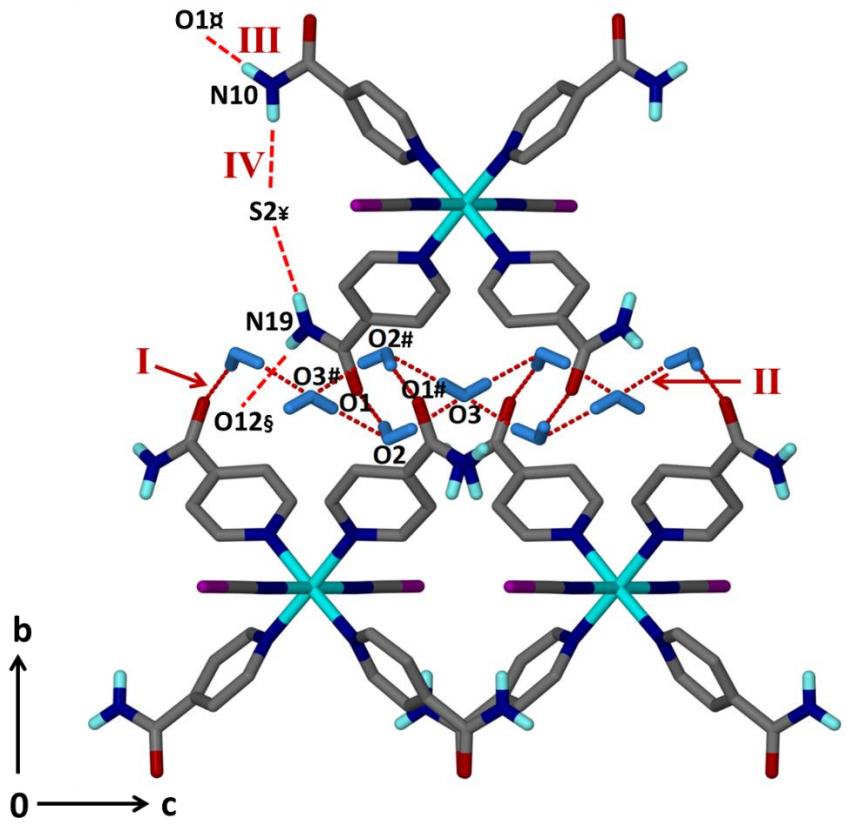

Figure 6.13 H6•3H$_2$O structure with the hydrogen bond chain shown along *c* and labelled **I** and **II**. The amide dimer group between N19 and O1¤ is labelled **III** and the unique bonds from N to S labelled **IV**.
(* 1-x, y, -z-½; $^{\#}$ x, -y, ½+z; $^{\&}$ x, 1-y, z-½; $^{\$}$ -x, -y, -z+1; ‡ 1-x, 1-y, -z; $^{¤}$ -x+½, -y+½, z-½; $^{¥}$ x, y, z-1; § -x+½, y-½, z)

Host **H6** self-included two isonicotinamide ligands as well as EtOH solvent into the clathrate **H6•2INic•EtOH**. Many intermolecular bonding conditions are met leading to a well-defined structure. The isonicotinamide guests bond to each other *via* an amide H-bond, shown in Fig 6.14, labelled **I**, between N13 and O6 and with the motif $D_1^1(3)$. The nitrogen donates *via* its second hydrogen to an oxygen of the host molecule, shown by label **II**, between N14-H14A···O4, and also with the graph set $D_1^1(3)$. A third hydrogen bond between the aromatic nitrogen of the isonicotinamide and the amide nitrogen of the host is labelled **III**, with two sites N8$^{\Delta}$-H8A$^{\Delta}$···N11 and

N9$^{@}$-H9A$^{@}$···N12 and the graph set $D_1^1(3)$. Host oxygen O2 accepts protons from two donor atoms, one the alcoholic functional group on the ethanol guest, labelled **IV** with the depiction O8-O8O···O2$^{\Delta}$; and the second from the amide group on the nearby host, labelled **V** and with atoms N9-H9B···O2$^{\Delta}$ engaged in the interaction. Each H-bond has the graph set $D_1^1(3)$. Data for all hydrogen bonds are listed in Table 6.9.

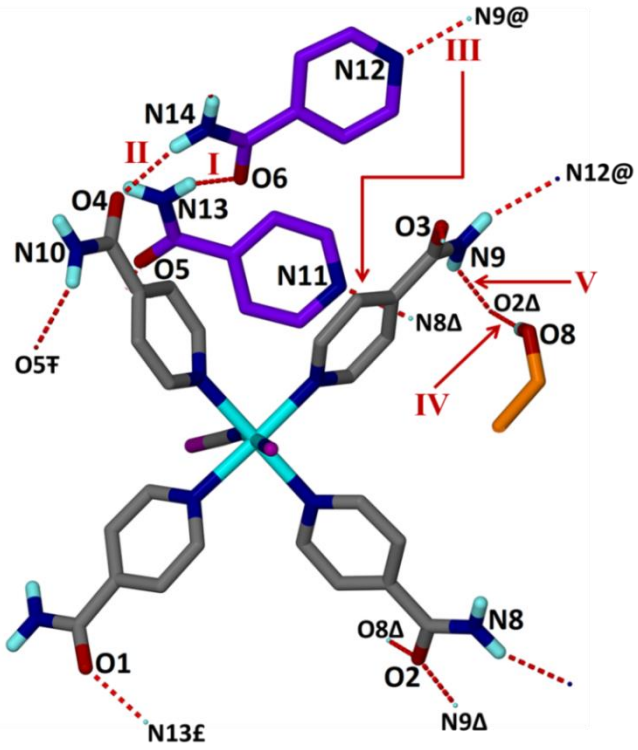

Figure 6.14 Hydrogen bonding sites in structure **H6•2INic•EtOH**, with I, II, III, IV and V labels showing the position of each bond explained in the text. Atoms outside the ASU are labelled with a symmetry code. ($^{@}$ -x, 2-y, 1-z; $^{\Delta}$ 1-x, 1-y,1-z; $^{£}$ x, y+1,z; ^{Ŧ} –x, 1-y,-z)

Table 6.9 Hydrogen bond parameters for complexes with host **H6**

	D-H / Å	H···A / Å	D···A / Å	< D-H···A / °
H6•EtOH•0.4H_2O				
N8-H8A···O2[*]	0.88	2.08	2.956(3)	173.1
N8-H8B···O5	0.88	2.08	2.856(3)	146.9
N7-H7B···O4[ϒ]	0.88	2.10	2.972(1)	171.7
N7-H7A···O2[ε]	0.88	2.10	2.912(3)	153.7
N9-H9A···O6	0.88	2.29	2.917(8)	128.6
N9-H9B···O1[¤]	0.88	2.11	2.935(3)	156.9
N10-H10A···O1[λ]	0.88	2.04	2.911 (3)	173.0
N10-H10B···O3[ε]	0.88	2.05	2.901(3)	163.8
O5-H5···S1[¤]	0.84	2.59	3.374(2)	155.6
H6•3H_2O				
O2-H1···O1	0.76	2.13	2.874(2)	166.8
O2-H2···O3	0.83	1.99	2.812(2)	170.9
O3-H12···O2[$]	0.78	2.07	2.850(2)	179.3
N10-H10A···O1[¤]	0.88	2.36	3.143(1)	147.6
N19-H19A···O12[§]	0.88	2.27	2.992(1)	138.6
N10-H10B···S2[¥]	0.88	2.63	3.501(1)	171.52
N19-H19B···S2[¥]	0.88	2.80	3.664(1)	169.8
H6•2INIC•EtOH				
N14-H14A···O4	0.88	2.07	2.905(3)	158.5
N13-H13B···O6	0.88	1.94	2.767(3)	156.5
N13[£]-H13A[£]···O1	0.88	2.02	2.838(3)	155.0
N10-H10B···O5[₸]	0.88	2.22	3.057(3)	159.3
N8[Δ]-H8A[Δ]···N11	0.88	2.11	2.944(3)	157.5
N9-H9A···N12[@]	0.88	2.08	2.924(3)	161.5
N9-H9B···O2[Δ]	0.88	2.12	2.871 (3)	143.3
O8[Δ]-H8O[Δ]···O2	0.84	2.13	2.958 (9)	169.7
N10-H10A···S1[₸]	0.88	2.66	3.508(1)	161.6
N7-H7B···S2[ǂ]	0.88	2.24	2.985(1)	160.1

Symmetry codes: ([#] x, -y, ½+z; [*] 1-x, y, -z-½; [&] x, 1-y, z-½; [ǂ]1-x, 1-y, -z; [$] -x, -y, -z+1; [¤] -x+½, -y+½, z-½; [¥] x, y, z-1; [§] -x+½, y-½, z; [@] -x, 2-y, 1-z; [Δ] 1-x, 1-y,1-z; [£] x, y+1,z; [₸] –x, 1-y,-z; [ǂ] -x, -y, -z; [ϒ] ½+x, ½-y, 1-z; [ε] x, 1-y, ½+z)

Packing

The packing of structure **H6•EtOH•0.4H_2O** is shown in Fig.6.15. The host architecture is shown viewed down [100] in (a) and down [001] in (b). The molecules in (a) are arranged in a zigzag or interrupted herringbone pattern with the thiocyanato arms overlapping on traversing along *c*. In (b), the pattern has a lacework design with the hydrogen bonds linking the host molecules to form a 3-dimensional network. The space group, *Pbcn*, shows a spiral of molecules occurring along a two-fold screw axis with two glide planes. Hydrogen bonding occurs between molecules above and below the plane. Two hydrogen bond centres are noted and are shown in Fig. 6.15(b), circled and labelled as A and B. Six host molecules share the H-bonding at site A. In circle B, eight molecules, each shown in a different colour, engage to form the network of interactions, and are shown as red H-bonds between the amide functional groups on each ligand.

Fig. 6.15(c) and (d) describe the guest packing into the voids between the host molecules, also shown down [100] and [001] respectively. EtOH is shown in orange and water in blue spacefill model, all molecules without hydrogens. In Fig 6.16 (a) and (b), the structure shows the positioning of the guests in the structural arrangement and the void analysis indicates these spaces. Void analysis (using probe radius of 1.2 Å and grid spacing of 0.8 Å), gave a percentage of 10% and a volume of 677.32 $Å^3$.

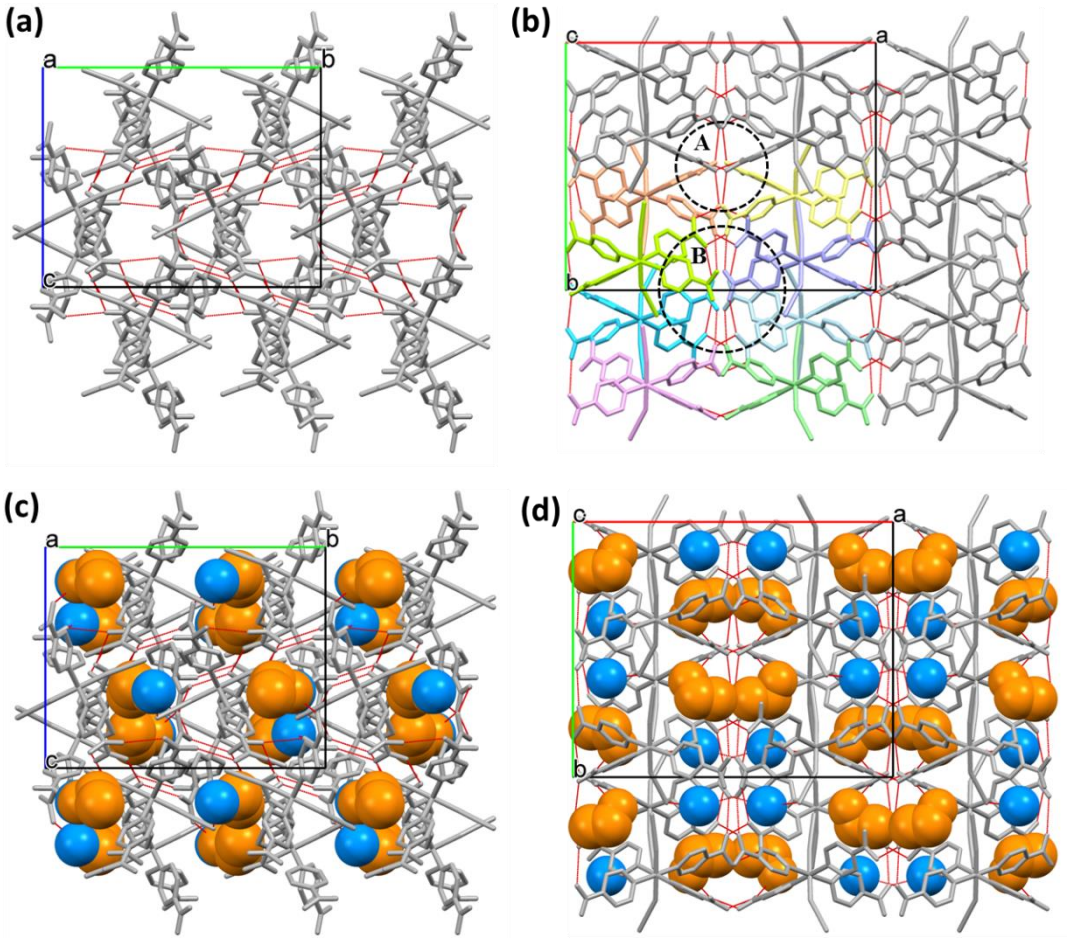

Figure 6.15 Host structure of **H6•EtOH•0.4H_2O** shown in (a) down *a* and (b) down *c*. The positioning of the two hydrogen bonding axes are shown by circle A and B, with the eight surrounding hosts coloured for emphasis on the 3D design in this space group; (c) and (d) illustrate the arrangement of the guests in the crystal structure, with EtOH in orange and H_2O in blue, without the presence of hydrogens

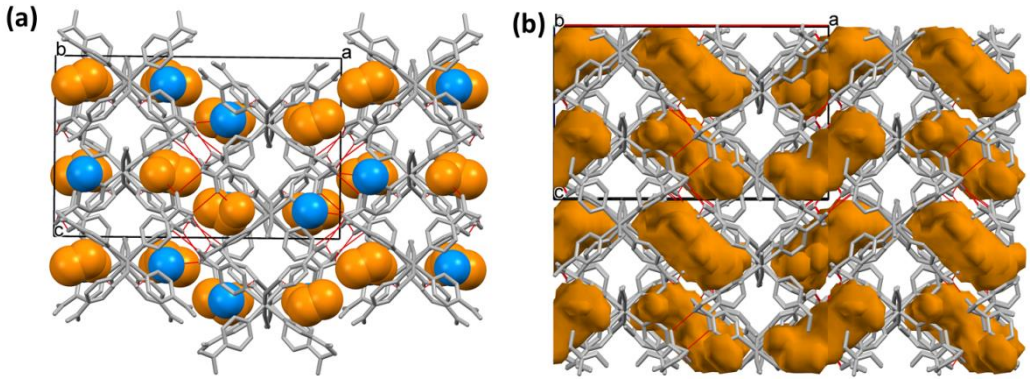

Figure 6.16 Views of **H6•EtOH•0.4H_2O** showing (a) the EtOH (orange spacefill) and H_2O (blue) in voids down *b* ; (b) Void spacing showing the channels down *b*, in which the guests are found

The tubulate structure **H6•3H$_2$O** is shown in Fig 6.17, with the view down [001]. Water molecules in blue capped stick model fill the channel between the hosts along *c* in Fig 6.17 (a) and the hydrogen bonds between **H$_2$O ··· H$_2$O** and **H$_2$O ··· host** are shown. In Fig 6.17 (b), the guests are absent and the channels are indicated by blue diamonds. The **H$_2$O** molecules hold the hosts together with H-bonds in the channel of size 12 Å x 10 Å. These measurements were made from atom to atom hence the van der Waals radii were not taken into account. In Fig 6.17(c) the void analysis of the structure, with a void percentage of 8.3 % and a void volume of 262.44 Å, is shown.

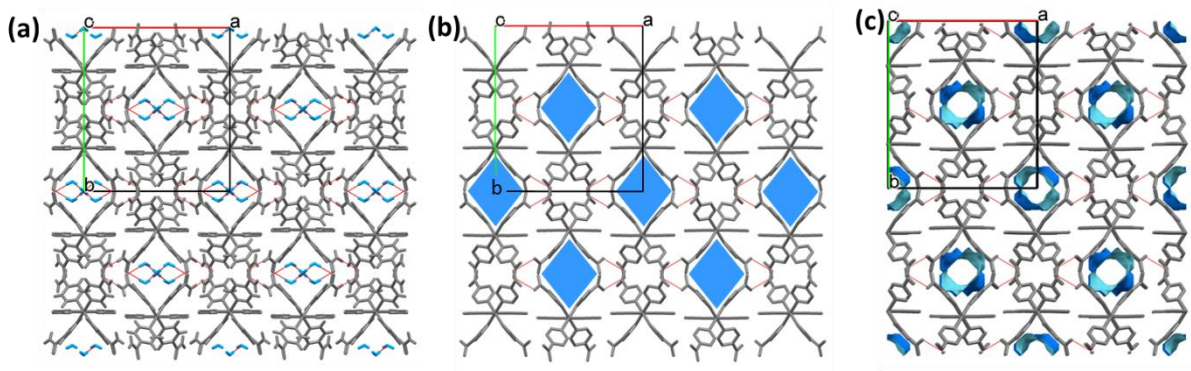

Figure 6.17 Structure of **H6•3H$_2$O** viewed down *c*, with (a) the water molecules shown in blue capped stick model showing the hydrogen bonds between **H$_2$O** and the host; (b) blue diamonds indicate the channels in the host arrangement; and (c) the void analysis shows a small percentage of void space in the compound.

The packing of structure **H6•2INic•EtOH** is shown in Fig 6.18, with the view down [100]. Isonicotinamides in purple and ethanols in orange end-capped models fill the channels between the hosts along *a* in Fig 6.18 (a). The hydrogen bonding is shown in red and is evident as host-host, host-guest and guest-guest interactions. The metal complexes link through four unique N-H···O amide-amide hydrogen bonds to form cationic sheets. Similar hydrogen bonds connect to the sheets above and below to generate a three-dimensional network. In Fig 6.18(b), the view is offset from *a* to show the hydrogen bonds between the layers encircled in red. Large channels shown by orange diamonds (A) and purple hourglass-shapes (B) are shown in Fig 6.18(c). The diamond shapes (size 11 Å x 11 Å) are occupied by ethanols; and the hour-glass shapes (20 Å long, 13 Å wide at the ends and 4 Å wide

at the waist) are filled with isonicotinamides. All measurements have been made from atom to atom hence the van der Waals radii have not been taken into account.

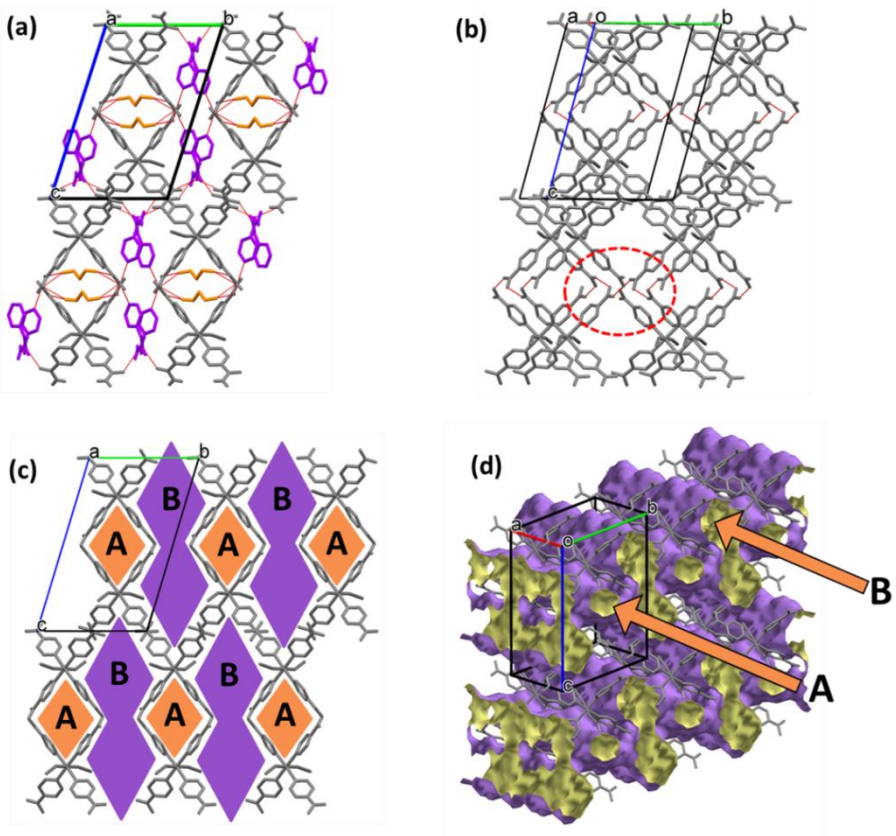

Figure 6.18 Packing down *a* of **H6•2INic•EtOH** with (a) the isonicotinamide (in purple) and ethanol (in orange) end-capped model; (b) the host packing offset from [100] to show the sheets of hosts bonded between planes by hydrogen bonds; (c) the host structure with the orange diamonds labelled A and hour-glass shaped channels in purple labelled B and (d) the void analysis of the structure with the orange arrows indicating the direction of channels A and B

Fig 6.18(d) shows the analysis of the voids in the structure with a void percentage of 34.6 % and volume of 773.57 Å. The direction of the channels down *a* are illustrated with orange arrows labelled A (diamond) and B (hour-glass) in the figure.

Table 6.10 Description of the values of interest in the closeness of packing in the **H6** clathrates

	H6•EtOH•0.4H2O	**H6•3H2O**	**H6•2INic•EtOH**
Space Group	*Pbcn*	*Pbcn*	$P\bar{1}$
Z	8	4	2
Cell Volume (Å^3)	6774.5	3147.5	2236.9
Guest Mol.Vol (Å^3) / cell	534.4	219.6	517.4
Host Mol Vol (Å^3) / cell	4058.4	2029.2	1014.6
Total Mol Vol (Å^3) / cell	4592.8	2248.8	1532.0
PF* (%)	67.8	71.5	68.5
Percentage Void	10.0	8.3	34.6
Void Volume (Å^3)	677.32	266.44	773.57

The packing data for the three **H6** clathrates is shown in Table 6.10. The packing factor (PF*) ranges from 67.8 to 71.5 % and this relates well to the majority of crystal packing coefficients. The percentage void has a larger range from 8.3 % in **H6•3H$_2$O** to 34.6 % in the case of **H6•2INic•EtOH.** Considering the figures 6.16(b), 6.17(c) and 6.18(d), this appears evident, as the spacing between the host and guests is relatively small in the first two cases (**H6•EtOH•0.4H2O** and **H6•3H$_2$O)** but much larger in the structure of **H6•2INic•EtOH**.

Crystal Structure of Mixed-ligand complex

Based on our findings in Chapter 5 regarding the mixed-ligand Werner complex which gave improved selectivity of isomers, we investigated the structure of the complex with a combination of the two ligands, nicotinamide and isonicotinamide, found in **H5** and **H6**. The mixed-ligand complex, containing both ligands, in *trans* pairs, called **H7**, is shown in Scheme 1. The crystallographic data for the structure of **H7•0.2MeOH•H$_2$O**, is given in Table 6.11. The compound crystallises in a general position in space group $P2_1/n$ with one host, one water and 0.2 methanols in the asymmetric unit.

Table 6.11 Crystallographic data of **H7** host with methanol and water guests

	H7•0.2MeOH•H_2O		
Chemical Formula	$Ni(NCS)_2(C_6H_6N_2O)_2(C_6H_6N_2O)_2•(CH_4O)_{0.2}•H_2O$		
Formula weight (g/mol.)	687.81	$D_{calc.}$/Mg m^{-3}	1.409
Temperature/K	173(2)	Radiation type	MoKα
Crystal System	$P2_1/c$	$F(000)$	1422
Space group (no.)	No.14	Crystal size/mm	0.41 x 0.36 x 0.26
a/Å	11.648(2)	Colour, Crystal form	Blue block
b/Å	20.508(4)	Total reflections	76030
c/Å	13.628(3)	Unique reflections	8040
α/°	90	$\Theta_{min-max}$/°	1.99 / 28.33
β/°	95.21(3)	$R[F^2>2\sigma(F^2)]$ $wR2(F^2)$ S	0.0306 0.0745 1.048
γ/°	90	Parameters / data	420 / 8040
V/$Å^3$	3242.0(11)	Res. Peak (max/min)/e$Å^{-3}$	0.562 / -0.390
Z'/Z	1 / 4		

Hydrogen Bonding

The format for the hydrogen bonding appeared complex, because the close packing and the attractive ligands in the host and guests, enabled hydrogen bonding to occur in many directions. A list of the H-bonds is given in Table 6.12.

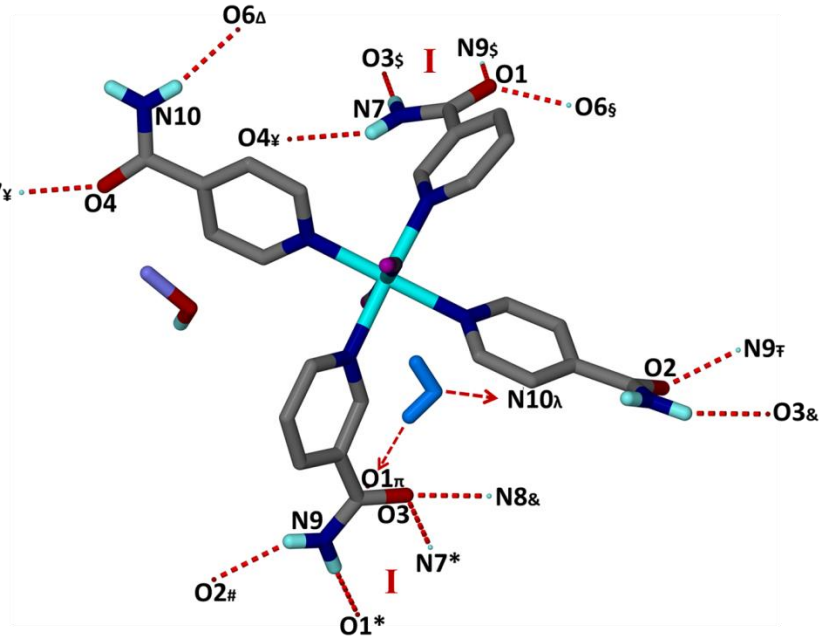

Figure 6.19 Hydrogen bonding sites in structure **H7•0.2MeOH•H_2O**, with label **I** showing the amide dimer groups between two hosts in each case. All other bonds are discrete and are addressed in the text.
(* -x+½, y-½, -z-½; [#] x-1, y, z; [$] -x+½, y+½, -z-½; [¥]-x, -y+2, -z; [&] -x+1, -y+1, -z; [Δ]-x+½, y+½, -z+½; [£]-x, -y+2, -z; [§]x+½, -y+3/2, z-½; [₸]1+x, y, z; [λ] ½-x, y-½, ½-z; [π] x-½, 3/2-y, ½+z)

The nicotinamide functional groups bond *via* amide dimers to two other host molecules. These are N7-H7AN···O3[$] and N9[$]-H9BN[$]···O1 and N9-H9BN···O1* and N7*-H7AN*···O3, both with graph sets $R_2^2(8)$. These groups are shown by label **I** in Fig 6.19. N7 is the donor in the bond between the host and water guest and the atoms involved are N7-H7BN···O4[¥]. In the case of isonicotinamide, the hydrogen bonds do not form amide dimers. They have a number of interactions such as the bonds between two different host molecules, N7[¥]-H7BN[¥]···O4 and N9[₸]- H9AN[₸]···O2. Secondly, the interaction between N10 and the water oxygen (N10-H10B···O6[Δ]) and thirdly, N10 donating the proton to the sulphur of a neighbouring host N10-H10A···S1[£]**.** The graph sets of the last discrete hydrogen bonds are all $D_1^1(3)$.

Table 6.12 Hydrogen bond parameters for the **H7** complex

	D-H / Å	H···A / Å	D···A / Å	< D-H···A / °
H7•0.2MeOH•H_2O				
N9-H9BN···O1*	0.88	2.12	2.981(2)	166.0
N9-H9AN···O2$^{\#}$	0.88	2.06	2.862(2)	151.8
N7-H7AN···O3$^{\$}$	0.88	1.99	2.872(2)	179.4
N7-H7BN···O4$^{¥}$	0.88	2.05	2.859(2)	151.8
N8-H8A···O3$^{\&}$	0.88	2.12	2.951(2)	157.0
N10-H10B···O6$^{\Delta}$	0.88	2.06	2.875(2)	154.5
N10-H10A···S1$^{£}$	0.88	2.71	3.557(2)	162.9
O6-H6B···O1$^{\pi}$	0.85	1.96	2.784(2)	164.3

Symmetry codes: * -x+½, y-½, -z-½; $^{\#}$ x-1, y, z; $^{\$}$ -x+½, y+½, -z-½; $^{¥}$-x, -y+2, -z; $^{\&}$ -x+1, -y+1, -z; $^{\Delta}$-x+½, y+½, -z+½; $^{£}$-x, -y+2, -z; §x+½, -y+3/2, z-½; ^{Ŧ}1+x, y, z; $^{\lambda}$ ½-x, y-½, ½-z; $^{\pi}$ x-½, 3/2-y, ½+z

Packing

Close packing of the hosts was found with the void analysis giving only 3.3% of unfilled space in the unit cell which translated to a volume of 108 Å^3. The MeOH (purple) and H_2O (blue) guests are shown in spacefill model in Fig. 6.20(a). Interactions between the hosts are shown in red in Fig. 6.20(b) with the combination of amide dimer groups and other discrete hydrogen bonds apparent in the figure.

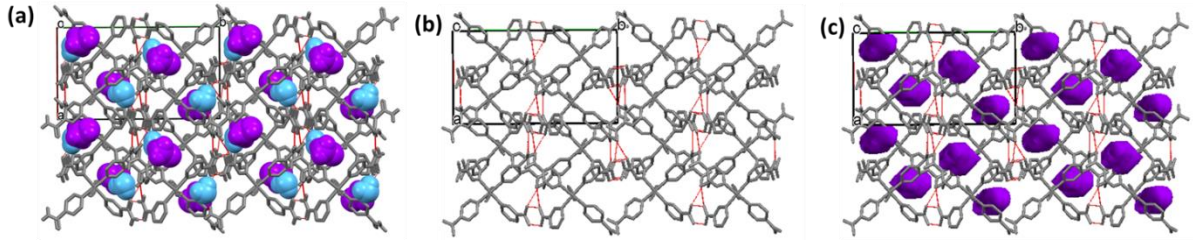

Figure 6.20 Packing of **H7•0.2MeOH•H_2O** shown down c, (a) with **MeOH** in purple and **H_2O** in blue spacefill model; (b) the host packing in the absence of the guest with the H-bonds shown in red; and (c) the void analysis

The network of the host arrangement is shown in Fig 6.21 with the hosts in different colours to clearly illustrate the 3-dimensional structure.

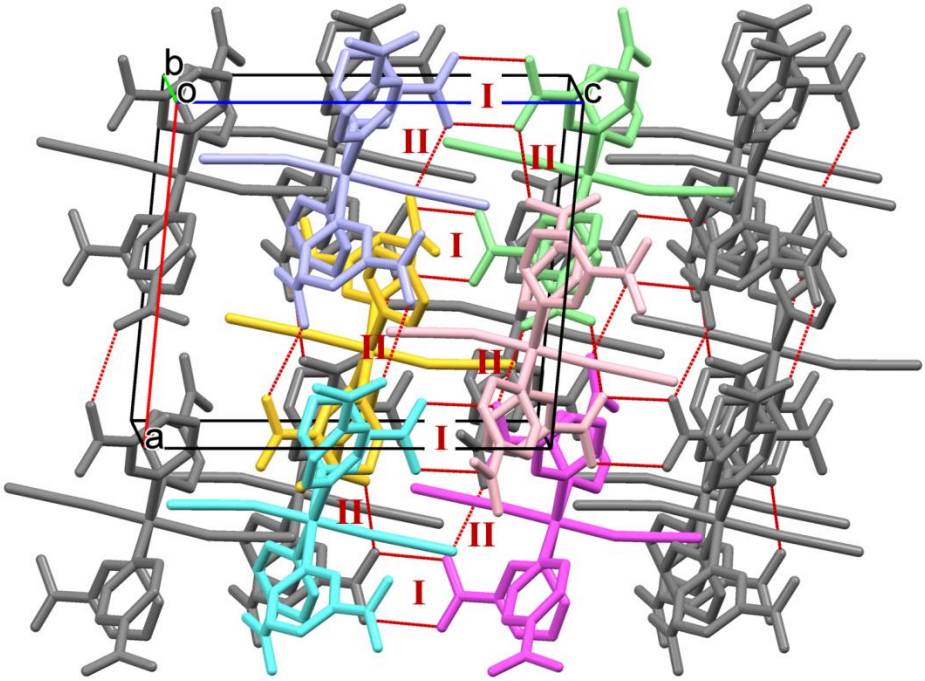

Figure 6.21 Packing of **H7** in **H7•0.2MeOH•H_2O** structure offset from the [010] view, showing the amide dimers between the nicotinamide ligands labelled with **I** and the amide H-bonds between nicotinamide and isonicotinamide labelled **II**. Host molecules are shown in different colours to emphasise the 3-D structure.

The packing factor was calculated from molecular host and guest volumes in each cell and was found to be 69.5 %. Apart from the low void percentage, this is a figure which agrees with other crystal structures. These values are listed in Table 6.13.

Table 6.13 **V**alues of interest in packing factor for **H7** clathrate

	H7•0.2MeOH•H_2O
Space Group	$P2_1/c$
Z	4
Cell Volume (Å^3)	3242.0
Guest Mol.Vol (Å^3) / cell	211.2
Host Mol Vol (Å^3) / cell	2041.6
Total Mol Vol (Å^3) / cell	2252.8
PF* (%)	69.5
Percentage Void	3.3
Void Volume (Å^3)	108.0

Selectivity

Differentiation for one guest over another by the Werner complex was considered for several pairs of guests with similar physical properties. Successful results were obtained in two cases, in which **H5** differentiated between two guests. The first was the selection of 1-butanol from a 50:50 mixture of 1-butanol and 2-pentanol. The properties of these two alcohols are similar and are shown in Table 6.14. The second observation was the selection of 4-methylcyclohexanone from a 50:50 mixture of 3- and 4-methylcyclohexanone. These organic isomers are used in the food industry as flavourants and occur naturally in peppermint and buchu oils. The properties of these two compounds are also shown in Table 6.14. The pairs of guests show similar, if not the same, boiling points and densities. Differentiation by classical means will not be suitable, hence the selectivity by the host **H5** is an interesting observation.

Table 6.14 Physical properties of compound of interest in selectivity

Organic guest	Chemical Formula	Molar mass (g/mol.)	Boiling Point (ºC)	Density ($g/cm^{3)}$
1-butanol	$C_4H_{10}O$	74.14	117.7	0.810
2-pentanol	$C_5H_{12}O$	88.15	119.3	0.812
3-methylcyclohexanone	$C_7H_{12}O$	112.17	169 - 170	0.914
4-methylcyclohexanone	$C_7H_{12}O$	112.17	169 - 171	0.914

The positive results for selectivity by **H5** for these compounds analysed adds a further advantage to the molecular architecture of this Werner clathrate and gives strength in our studies of clathrates with these characteristics.

Conclusion

Three Werner hosts with attractive or ‘sticky’ ligands were synthesised and inclusion compounds with selected alcohols, carbonyls and water were elucidated. The influence of hydrogen bond donor and acceptor groups on the molecular packing was investigated and the packing factors calculated.

In the first section, host **H5** was considered with a range of five alcohol guests (ethanol, 1- butanol, 1-pentanol, 2-methyl-1-propanol and 4-methylbenzoylalcohol) which all presented similar packing arrangements in the same space group $P\bar{1}$. The hosts form columns and interact through hydrogen bonding of the amides in pairs of dimers. Guests are positioned in voids between the columns and hydrogen bonding between the host nitrogen and the alcoholic guest oxygen are formed. They also display hydrogen bonds between the alcoholic functional group and thiocyanato sulphur. The structure with the aromatic alcohol **MeBeOH**, has the highest packing factor, probably due to its size and the flatness of its structure relative to the other aliphatic alcohols. However, it also demonstrates $\pi\cdots\pi$ interactions between the aromatic ring of **MeBeOH** with that of the nicotinamide ligand. The packing coefficients were in the range of 66.9 to 81.0 %.

Different packing arrangements were perceived for **H5** with the guests with carbonyl functional groups (dimethylformamide, 3-pentanone, 2-hexanone, pinacolone and 4-methylcyclohexanone). The hosts formed sheets of hydrogen bonded molecular bands. The host formed intercalate structure containing the guests in layers which showed hydrogen bonding between the carbonyl functional group and the amide host groups. No sulphur atoms were involved in hydrogen bonding and the packing factors ranged from 66.3 to 69.4 %. **H5•2HEX**, **H5•2PEN**, **H5•2PIN** and **H5•2MCH** were isomorphous and showed packing similarities. **H5•2DMF** in space group $P\bar{1}$, showed closer similarities to the structures of the **H5** with the alcohols.

The host in each of these two sets of structures forms a predictable hydrogen bonded design. This principle leads to architectures with analogous patterns. The physical properties between the structures with alcohol guests and those with carbonyl guests differ in their hydrogen bonding capabilities. Alcohols form H-bonds between oxygen and amide ligand and their hydrogen to thiocyanato sulphur. The carbonyls displayed only one hydrogen bond to the amide ligand. Thorough observations were made in the comparison of packing efficiency and intimacy of interactions. These were verified by the consideration of the difference between desolvation temperature and the guest's boiling point.

Host **H6** presented three different tubulate packing arrangements, with the guests occupying channels in the structure. These channels were the largest in the **H6•2INic•EtOH** compound as the isonicotinamide ligands occupied a large amount of space. The packing factor for the **H6** compounds ranged from 67.8 to 71.5 %. The volumes of the space available for the guests differed between the three structures with **H6•EtOH•0.4H_2O** and **H6•3H_2O** having similar space and **H6•2INicEtOH** having a large amount of space for the isonicotinamide and ethanol guests.

The final consideration in this chapter was to evaluate the performance of a mixed-ligand host, containing both nicotinamide and isonicotinamide ligands. Intermolecular hydrogen bonding between the amide groups, as well as H-bonds between the H_2O molecules occurred in these structures. Closer packing between the hosts was achieved, and this led to a low percentage of voids in the unit cell of 3.3 %, considerably less than that of the **H5** inclusion compounds.

In the **H6** and **H7** structures a network is formed through hydrogen bonding between carbonyl oxygens and amides as well as between host and guest. The use of metal centres gives the advantage of geometries which are not easily accessible in organic structures.

In two cases, selectivity was achieved for the separation of a pair of alcohols and a pair of carbonyls, both with physical properties so similar that other means of separation were not feasible. 1-butanol was selected from a 50:50 mixture of 1-butanol and 2-pentanol and 4-methylcyclohexanone from a 50:50 mixture of 3- and 4-methylcyclohexanone. The positive discrimination characteristics of host **H5** have given possibilities for future industrial prospects.

Hydrogen bonding of the ‘sticky’ ligands in Werner clathrates encourages a wide range of guests which hydrogen bond *via* their alcoholic or carbonyl functional groups. Their structures form supramolecular units which are a hydrogen bonded network of host and guest. The network of hosts

formed porous materials for inclusion, giving the advantage of 'tunability', and pores with different size and nature available to accommodate guest molecules and separate isomers.

Experimental Section

Preparation of Werner clathrates

The host compound, **H5**, bis (isothiocyanato) tetrakis (nicotinamide) nickel(II), was prepared by adding stoichiometric quantities of an ethanolic solution of nicotinamide (20 ml, 0.01 M) to an ethanolic solution of nickel-isothiocyanate (5 ml, 0.01 M) and stirring at room temperature for 2 hours. Blue crystals of $Ni(NCS)_2(C_6H_6N_2O)_4$ formed and were filtered and allowed to air dry overnight. **H6,** bis (isothiocyanato) tetrakis (isonicotinamide) nickel(II), and **H7,** bis (isothiocyanato) tetrakis bis (nicotinamide) bis (isonicotinamide) nickel(II) required stirring overnight at room temperature. Violet **H6** and blue/grey **H7** crystals were filtered and allowed to air dry overnight.

Enclathration of the guest/s was carried out by dissolving the host in the guest, stirring at 45 °C for 30 minutes, cooling and filtering. If solubility of the host in the selected guest was low, ethanol or methanol was added to improve dissolution of the host. Crystallisation occurred between 24 hours and fourteen days. Blue or violet crystals of the clathrates were formed.

Single crystal X-ray analysis

Intensity data of a selected single crystal for the compounds were collected on a Bruker DUO APEX II diffractometer[22] with graphite monochromated Mo $K_{\alpha 1}$ radiation (λ = 0.71073 Å) at 173 K using an Oxford Cryostream 700. Data reduction and cell refinement were performed using *SAINT-Plus.*[23] The space group was determined from systematic absences by *XPREP.*[24] The structure was solved using *SHELXS-97*[25] and refined using full matrix least squares methods in *SHELXL-97*[20] with the aid of the program *X-Seed.*[26] The hydrogen atoms bound to carbon atoms were placed at idealized positions and refined as riding atoms. Diagrams and publication material were generated using *PLATON,*[27] *X-Seed* and *Mercury (3.8).*[16] Crystal data and structure refinement parameters are given in Tables 6.1, 6.4, 6.7

and 6.10. In **H5•PeOH,** there was a higher level of disorder in the guest molecule and C18 was left isotropic. The structure was refined as far as possible for a chemically meaningful result. When we modelled the disorder in **H5•2PIN**, the minor disorder was under 10% and new geometries were not chemically meaningful to pursue. In **H5•PEN**, a 50:50 disorder of the sulphur was found. As the freely refined site occupancies gave a 50:50 disorder, we fixed that as the ratio.

Powder X-ray diffraction

Powder X-ray diffraction experiments were carried out on a Bruker D8 diffractometer using Cu K_α radiation. The sample was ground to a fine powder and loaded onto a silicon background plate in the instrument holder. The spectrum was run from 2θ values of 4 º to 40 º.

Thermogravimetric analysis

Thermal analyses were performed on a TA Q500 instrument from 25 to 400 °C at a heating rate of 10 ºC min^{-1} with a purge gas of dry nitrogen flowing at 60 ml min^{-1} for comparison of the percentage mass loss with the expected compound. All samples were dried on filter paper and placed in an open crucible for thermogravimetric analysis. Sample masses varied from 2 to 5 mg.

Competition experiments

The selectivity of the host for a particular isomer or compound was evaluated using crystal formation of the host with guest mixture using the same procedure mentioned above. Crystals were analysed by single crystal X-ray diffraction as mentioned above.

References

[1] C. Judson King, in *Separation Processes: 2nd Edition*, Dover Publications, **2013**, Ch. 14, 174

[2] L.R. Nassimbeni, in *Separations and Reactions in Organic Supramolecular Chemistry*, John Wiley & Sons, **2004**, Ch. 5, 123

[3] R.M. Barrer, *Zeolites and Clay Minerals as Solvents and Molecular Sieves*, Academic Press, London, **1978**

[4] J. Lipkowski, M. Pawlowska and D. Sybilska, *J. Chromatogr.*, **1979**, 176, 43

[5] A.M. Pivovar, K.T. Holman and M.D. Ward, *Chem. Mater.*, **2001**, 13, 3018

[6] W.D. Schaefer, W.S. Dorsey, D.A. Skinner and C.G. Christian, *J. Am. Chem. Soc.*, **1957**, 79, 5870

[7] C.A. Hunter and J.K.M. Sanders, *J. Am. Chem. Soc.*, **1990**, 112, 5525

[8] J. Lipkowski, in *Inclusion Compounds*, **1984**, Vol.1, Ch 3, 59

[9] (a) M.M. Moore, L.R. Nassimbeni, M.L. Niven and M.W. Taylor, *Inorganica Chimica Acta*, **1986**, 115, 211; (b) L. Lavelle and L.R. Nassimbeni, *J Incl.Phen.Mol.Rec.Chem.*, **1993**, 16, 25

[10] M.Lusi and L.J. Barbour, *Angew. Chem. Int. Ed*. 2012, 51, 3928.

[11] D.A. Köse, B. Öztürk, O. Şahin and O. Büyükgüngör, *J. Therm. Anal. Calorim.*, **2010**, 115, 1515

[12] C.B. Aakeröy, A.M. Beatty and D.S. Leinen, *Angew. Chem. Int. Ed.*, **1999**, 38, 1815

[13] P.Gilli and G. Gilli, in *Supramolecular Chemistry, From Molecules to Nanomaterials*, **2012**, 6, 2829

[14] M.C.Etter and J.C. MacDonald, *Acta Cryst.*, **1990**, B46, 256

[15] F.H. Allen, C.M. Bird, R.S. Rowland and P.R. Raithby, *Acta Cryst., Section B*, **1997a**, *53*, 680

[16] L. Pauling, *The Nature of the Chemical Bond*, **1939**, Cornell University Press, Ithaca, New York

[17] C. R. Groom, I. J. Bruno, M. P. Lightfoot and S. C. Ward, *Acta Cryst*., **2016**, B72, 171-179

[18] F. H. Allen, *Acta Cryst*., **2002**, B58, 380-388

[19] C.F. Macrae, I.J. Bruno, J.A. Chisholm, P.R. Edgington, P. McCabe, E. Pidcock, L. Rodriguez-Monge, R. Taylor, J. van de Streek P.A. and Wood, *J. Appl. Cryst*., **2008**, *41*, 466

[20] A.I. Kitaigorodskii, in *Organic Chemical Crystallography*, **1957**, 106

[21] Loots, L. and Barbour, L.J. in *The Importance of Pi-Interactions in Crystal Engineering*, **2012**, 112

[22] Bruker **2005**. APEX2. Version 1.0-27. Bruker AXS Inc., Madison, Wisconsin, USA.

[23] Bruker **2004**. SAINT-Plus (including XPREP). Version 7.12. Bruker AXS Inc., Madison, Wisconsin, USA.

[24] Bruker **2003**, XPREP2. Version 6.14. Bruker AXS Inc., Madison, Wisconsin, USA.

[25] G. M. Sheldrick, SHELXS-97 and SHELXL-97 Programs for crystal structure determination and refinement. University of Göttingen, **1997**.

[26] L. J. Barbour, *J. Supramol. Chem.*, **2001**, 1, 189.

[27] A. L. Spek, PLATON, A Multipurpose Crystallographic Tool, Utrecht University, Utrecht, The Netherlands, **2008**.

Chapter 7

Conclusion

Werner complexes have received considerable attention over many years due to their useful properties and have provided a platform on which to design materials with a range of characteristics such as non-covalent interactions. The use of metal centres gives the advantage of geometries which are not easily accessible in organic structures. The work presented in this thesis covers the preparation and characterisation of selected Werner complexes and their clathrates. Pyridine derivative ligands allowed interactions between the Werner host and the included guest of the type: π ···π, C-H···π and hydrogen bonding. In general the structural flexibility of the hosts during the enclathration process was established from the relative torsional angles of the ligands. When the 'sticky ligands' were used, i.e. ligands with hydrogen bonding functionalities, to form the Werner hosts, it was concluded that the hydrogen bonding parameters were reliant on the functional groups particular to each ligand. The inclusion compounds made were characterised using thermogravimetric (TGA), powder X-ray diffraction (PXRD) and Gas Chromatogaphy (GC) techniques. Structural elucidation was performed by single crystal X-ray diffraction. PXRD was used also to check the purity of the prepared materials. Kinetic studies were performed using non-isothermal TGA methods.

The importance of aromatic interactions of isoquinoline as the ligand in Werner clathrate $Ni(NCS)_2(isoquinoline)_4$, **H1**, was established as having a lesser effect on the selectivity of this host compared with that of the related host $Ni(NCS)_2(4\text{-phenylpyridine})_4$, **H2**. Due to the importance of the xylene isomers in the petroleum industry, discrimination of these guests was considered in this study. The success of the latter host was attributed to the torsional flexibility of the phenyl moieties in the ligands. In contrast, the isoquinoline ligands, although containing larger aromatic systems, have no such flexibility and their relative conformation is largely controlled by the steric hindrance between the *ortho*-hydrogens. The selectivity of **H1** towards the xylene isomers was determined using two methods, *viz.* solid vapour sorption and crystallisation from a liquid solution of host and a binary mixture of two of the guests. The results were analysed using headspace gas chromatography. No significant preference for one of the xylene isomers over the other two was found, showing poor selectivity of this host. However, the analysis of the fingerprint plots revealed the importance of the C-H···π interactions and unique C-H···S interactions were observed in the **H1•ox** structure. The

kinetics of thermal decomposition of the three inclusion compounds were analysed using the non-isothermal TGA method.

Green chemistry methods were used to enclathrate the environmental contaminants, polycyclic aromatic hydrocarbons (PAHs), using the Werner complex $Ni(NCS)_2(4\text{-vinylpyridine})_4$, **H3**. Single crystal structural analysis revealed two types of crystal arrangements. Indene, naphthalene and azulene yield isomorphous structures ($Pna2_1$) and the remaining inclusion compounds with anthracene, fluorene, phenanthrene and pyrene, all crystallised in $P\bar{1}$ space group with the guests located in channels along [010]. Different methods were employed to reach these compounds. Melting was unsuccessful. Grinding and slurrying obtained results that in some cases were successful. Diffusion as shown by the guests naphthalene and azulene led to the success of inclusion compound formation by grinding. The rate constant and half-life were determined for the reaction between the host with these two guests. Product formation with slurry methods with naphthalene, indene and azulene were successful at 25 ºC while with phenanthrene, fluorene and pyrene partial success was reached at 50 ºC. These guests all possessed minimal solubility in water at the corresponding temperatures to which the success of these experiments were related. It was shown that this selected Werner host gives equivalent products when the ways of crystal formations are changed.

The two different ligands *trans* coordinated to the $Ni(NCS)_2$ core and formed the host $Ni(NCS)_2(isoquinoline)_2(4\text{-phenylpyridine})_2$ which contained both the rigid isoquinoline and the flexible 4-phenylpyridine ligands. The arrangement of the ligands gave the host flexibility to pack *meta* xylene more intimately than the other two isomers, giving it the advantage of the favoured isomer in terms of selectivity hence the **mx** > **ox** > **px** outcome of this study. This finding was confirmed by Hirshfeld surface analysis as well as void spacing determination. The mixed ligand Werner complex, probed in this work, has the ability to differentiate between the four C8 aromatic compounds, in the order **mx** > **eb** > **ox** > **px**, a beneficial discovery in the selectivity of Werner inclusion compounds.

Hydrogen bonding of the 'sticky' ligands in Werner clathrates encourages a wide range of guests which hydrogen bond *via* their hydroxyl, amide or carbonyl functional groups. Their structures form supramolecular hydrogen bonded networks of hosts and guests. The network of hosts formed porous materials for inclusion, giving the advantage of 'tunability', and pores with different size and nature available to accommodate guest molecules and separate isomers. Three Werner hosts were synthesised and inclusion compounds with selected alcohols, carbonyls and water were elucidated. The influence of hydrogen bond donor and acceptor groups on the molecular packing was investigated and the packing factors calculated.

The host **H5,** $Ni(NCS)_2(nicotinamide)_4$, was considered with a range of five alcohol guests (ethanol, 1- butanol, 1-pentanol, 2-methyl-1-propanol and 4-methylbenzoylalcohol) which all presented similar packing arrangements in the same space group $P\bar{1}$. The hosts form columns and interact through hydrogen bonding of the amides in pairs of dimers. Guests are positioned in voids between the columns and hydrogen bonding between the host nitrogen and the hydroxyl guest oxygen are formed. They also display hydrogen bonds between the hydroxyl functional group and thiocyanato sulphur. The packing coefficients were in the range of 66.9 to 81.0 %. Different packing arrangements were perceived for **H5** with the guests with carbonyl functional groups (dimethylformamide, 3-pentanone, 2-hexanone, pinacolone and 4-methylcyclohexanone). The hosts formed sheets of hydrogen bonded molecular bands which contained the guests in layers which formed hydrogen bonding between the carbonyl functional group and the amide groups of the host. The packing factors ranged from 66.3 to 69.4 %.

A predictable hydrogen bonded design was observed in each of these two sets of structures. The physical properties between the structures with alcohol guests and those with carbonyl guests differ in their hydrogen bonding capabilities due to alcohols forming a second H-bond between alcoholic hydrogen and thiocyanato sulphur. In the comparison of packing efficiency and intimacy of interactions, the difference between desolvation temperature and the guest's boiling point showed a larger difference in the case of the alcohol structures.

In two cases, selectivity was achieved for the separation of a pair of alcohols and a pair of carbonyls, both with physical properties so similar that other means of separation were not feasible. 1-butanol was selected from a 50:50 mixture of 1-butanol and 2-pentanol and 4-methylcyclohexanone from a 50:50 mixture of 3- and 4-methylcyclohexanone. The positive discrimination characteristics of host **H5** have given possibilities for future industrial prospects.

Host **H6,** $Ni(NCS)_2(isonicotinamide)_4$ presented three different tubulate packing arrangements, with the guests occupying channels in the structure. Large spaces were evident in the compound which had self-included the ligand isonicotinamide. The packing factor for the **H6** compounds ranged from 67.8 to 71.5 %. The performance of a mixed-ligand host, **H7**, $Ni(NCS)_2(isonicotinamide)_2(isonicotinamide)_2$, demonstrated intermolecular hydrogen bonding between the amide groups, as well as H-bonds between the H_2O molecules in these structures. Closer packing between the hosts was achieved, and this led to a low percentage of voids in the unit cell of 3.3%, considerably less than that of the **H5** inclusion compounds. In the **H6** and **H7** structures a network is formed through hydrogen bonding between carbonyl oxygens and amides as well as between host and guest.

The primary objectives of the work were achieved, i.e. structural aspects of all the selected Werner complexes and their clathrates were analysed and characterised. Selectivity was performed on a variety of these complexes and was successful in three cases. At the same time the architecture of the structures were interpreted. Various crystallisation techniques were investigated and were largely successful.

A number of suggestions for future work have arisen and two of these will be mentioned here. Firstly, it is important to carry out further selectivity studies of the Werner complexes with attractive ligands as the design of the complexes leads to differently sized spaces for guest inclusion. Secondly, Werner

clathrates using other metal ions with different coordination geometries would broaden the scope of this study and lead to new opportunities of structural implications and selectivity.

The studies performed in this thesis have led to a greater fundamental understanding of Supramolecular Chemistry and Crystal Engineering and the vastness of their impacts on modern life as well as the implication of aspects already present in nature. The work also targeted current industrial problems (xylene separation) and concerning environmental issues (encapsulation of polyaromatic hydrocarbons), therefore represents a great example when fundamental basic research is successfully linked to current social economic issues.